UNIVERSITY OF OKLAHOMA

GRADUATE COLLEGE

A RECORD OF MID-LATITUDE DUSTINESS IN A CARBONIFEROUS-PERMIAN CARBONATE RAMP ON CENTRAL SPITSBERGEN

A THESIS

SUBMITTED TO THE GRADUATE FACULTY

in partial fulfillment of the requirements for the

Degree of

MASTER OF SCIENCE

BY

ANDREW OORDT
Norman, Oklahoma
2018

A RECORD OF MID-LATITUDE DUSTINESS IN A CARBONIFEROUS-PERMIAN CARBONATE RAMP ON CENTRAL SPITSBERGEN

A THESIS APPROVED FOR THE
CONOCOPHILLIPS SCHOOL OF GEOLOGY AND GEOPHYSICS

BY

Dr. Gerilyn S. Soreghan, Chair

Dr. Michael J. Soreghan

Dr. Lars Stemmerik

Acknowledgements

Funding for this thesis was provided by the National Science Foundation through EAR-1338331, with supplemental funding provided by the Eberly Fund (University of Oklahoma). Acknowledgement goes to Kathleen Miller, Thomas Givens and Nina McCollom for assistance in SMF extraction and grain size analysis, to Turin Haugen for providing field assistance and Baylee Kushner for her assistance in gathering zircon ages. I appreciate the help from Dr. Linda Hinov for her collaboration on quantitative cyclostratigraphy. Thank you to Dr. Lars Stemmerik for assistance with Svalbard stratigraphy and committee membership and to Dr. Michael Soreghan for serving on my committee and providing mentorship throughout this project. Finally, special thanks go to Dr. Gerilyn Soreghan for serving as my advisor, committee chair and mentor in the field of geology during my time at OU. Her guidance will remain with me throughout my career.

Table of Contents

List of Tables

List of Figures

Abstract

This study focuses on a mid-latitude dust record from the Wordiekammen Formation, a carbonate ramp on Spitsbergen. The ramp developed on the Northern Pangean margin in Moscovian (Carboniferous) through Sakmarian (Permian) time at a paleolatitude of 30-35°N. The study site on the Nordfjorden High was isolated from any source of fluvio-deltaic input, such that detrital material that occurs in this system experienced eolian transport, thus forming a proxy for atmospheric dustiness. We analyzed two intervals, of Moscovian (10m) and Asselian (26.8m) age, at 20 cm resolution, and identified five mid-ramp subtidal facies organized in upwardly shallowing, high-frequency sequences 3-5 m thick. High-frequency sequence boundaries commonly exhibit signs of subaerial exposure (e.g. *Microcodium*) developed atop subtidal facies, recording glacioeustatic falls (glacials), although the Moscovian section has a severe karst overprint at sequence boundaries attributable to prolonged exposure during this interval. Samples were processed to isolate the silicate mineral fraction (SMF), which includes both detrital silicates, and authigenic silica mostly in the form of (fine sand-sized) doubly terminated quartz crystals. Detrital cores within these crystals records recrystallization from fine-grained (<30 µm) dust.

Analysis of the dust record demonstrates that the Asselian had a significantly higher atmospheric dust load than the Moscovian. Within the Asselian interval, dust input varies commensurate with glacial interglacial cyclicity. Highest dust contents correspond to transgressive facies at sequence boundaries, indicating peak atmospheric dust loading at lowstand to incipient interglacial times. Provenance data from detrital zircon and whole rock geochemistry indicate two distinct source regions for the dust. Dust from the Moscovian and

lower Asselian intervals reflects a continental island arc signature consistent with sourcing from the basement of northeast Greenland. Dust from the upper Asselian interval is more consistent with recycling from Devonian and Carboniferous strata of the east Greenland Caledonides, likely deflated from fluvial systems draining this orogenic system, indicating an expansion of regions of eolian deflation.

Introduction

Dust deposits act as a high-resolution climate archive in the Cenozoic while also acting as an agent of climate change. Atmospheric dust influences global climate through its impacts on radiative forcing and affects primary production through nutrient delivery (e.g., Miller and Tegen, 1998; DeMott et al., 2003; Yoshioka et al., 2007, Coale et al., 1996; Mahowald, 2011). Pleistocene dust records such as those of the Chinese Loess Plateau as well as dust records extracted from ice and ocean sediment cores document significant variation in atmospheric dust deposition on a glacial-interglacial timescale (e.g., Rea, 1994; Muhs and Bettis, 2003). The variations in dust flux during glacial/interglacial intervals of the Pleistocene likely reflect increased aridity, decreased sea level, decreased vegetation, and stronger winds, in addition to increased supply of fines via glacial grinding (Rea, 1994; Muhs and Bettis, 2003; McGee et al., 2010). The strong radiative and biogeochemical effects and high temporal variability of atmospheric dust loading highlight the importance of considering these variables when constraining climate models.

Loess deposits are well recognized from the Pennsylvanian-Permian in western equatorial Pangaea (e.g., Johnson, 1989; Soreghan, 1992; Soreghan and Soreghan, 2002; Soreghan et al., 2008; Sweet et al., 2013; Foster et al., 2014). Additionally, equatorial records preserve evidence for high-resolution variations in dust flux on the glacial-interglacial scale (Sur et al., 2010a). This study is part of a larger effort to constrain volume and temporal variability of atmospheric dust flux at the paleo-mid-latitudes, focusing on dust delivery to carbonate strata of central Spitsbergen (Figure 1). These strata represent a carbonate ramp formed at a paleolatitude of 30-35°N and isolated from any source of fluvio-deltaic input (Stemmerik, 2000; Ahlborn and Stemmerik, 2015). Therefore any detrital material recovered from these strata should record eolian delivery, preserving a record of atmospheric dust influx.

The purpose of this study is to evaluate the amount, timing, and character (e.g. composition) of atmospheric dust delivered to the northern mid-latitudes during the late Carboniferous (Moscovian) and early Permian (Asselian). Our findings address the impact of a glacial-interglacial climate system on atmospheric dust loading in the northern mid-latitudes as well the system's response as climate change across the Carboniferous-Permian boundary. Additionally, detrital zircon and geochemical analysis provides evidence for potential dust source(s), with implications for wind direction and strength.

Geologic Setting

Present-day Spitsbergen is located on the western edge of the Barents Sea shelf and is the largest island on the Svalbard Archipelago. During the late Paleozoic, the Barents shelf formed along the Northern Pangaean margin (Figure 2). The region drifted north from ~20°N in the early Carboniferous (~350 Ma) to ~50°N by the late Permian (~260 Ma; Boucot et al., 2013). In early Carboniferous time, an extensional tectonic regime led to the formation of NW- SE oriented half-graben basins along the Northern Pangaean boundary (Johannessen and Steel, 1992; Stemmerik 2000). On Spitsbergen, two major fault blocks are recognized: the Nordfjorden High and the Ny Friesland High (Figure 1, Figure 3). Faulting during Serpukhovian-Bashkirian time resulted in the opening of the Billefjorden Trough and subsequent syntectonic infill by the Ebbadalen and Minkinfjellet Formations (Figure 3) (Johannessen and Steel, 1992). The Nordfjorden High remained a positive feature exposing rocks of the Devonian Andre Land Group (Critelli and Reed, 1999; Piepjohn and Dallman, 2014) that could have contributed sediment to local basins. By the late Carboniferous (Moscovian), tectonic activity along the Billefjorden fault had ceased and the shoreline transgressed across the Nordfjorden High, thus isolating this region from fluvio-deltaic clastic influx (Steel and Worsley, 1984). Minor uplift of the region during the Gzhelian resulted in a widespread discontinuity surface atop the Nordfjorden High (Figure 3; Ahlborn and Stemmerik, 2015; Steel and Worsley, 1984; Samuelsberg and Pickard, 1999). Renewed transgression resulted in the formation of a stable carbonate platform across the entire region with no thickness variations in the upper

Wordiekammen Formation over the Nordfjorden High by the early Permian (mid Asselian; Steel and Worsley, 1984).

Depositional environments reflect climatic shifts associated with the northern movement of Pangea. The climate of Spitsbergen shifted from warm and wet in the early Carboniferous, to warm and arid in the late Carboniferous to early Permian, and finally cool and arid by the late Permian (Stemmerik, 2000; Boucot et al., 2013). Development of carbonate platforms on Spitsbergen began during late Carboniferous (Moscovian) time (Cutbill and Chalinor, 1965; Pickard et al., 1996) in the semiarid climate zone at a paleolatitude of ~30-35°N (Stemmerik, 2008; Boucot et al., 2013). The Upper Palaeozoic strata display high-frequency cyclicity that characterizes marine strata from this time interval in many parts of the world (Stemmerik, 2008). The Carboniferous - Early Permian Earth hosted extensive continental glaciation at high southern latitudes (Crowell, 1978; Veevers and Powell, 1987; Fielding et al., 2008), and alpine glaciation has been hypothesized for elevated regions of even the equatorial latitudes (Soreghan et al., 2008, 2014). Some authors suggest that global ice volume pulsed in 1-8 My intervals of more-intense and less-intense glaciation (Isbell et al., 2003; Fielding et al., 2008; Montanez and Poulsen, 2013). In addition, Milankovitch-scale glacial-interglacial cyclicity has been documented within these longer pulses, well recognized in far-field records in particular (Heckel, 2002, 2008; Davydov et al., 2010; Van den Belt et al., 2015), and ascribed to glacioeustasy. Within basins on Spitsbergen, high-frequency cycles and numerous exposure surfaces reflect the glacioeustatic processes that played a role in controlling sedimentation in the region (Johannessen and Steel, 1992; Stemmerik, 2008).

The Gipsdalen Group consists of four formations that fill and overlie the Billefjorden Trough and Nordfjorden High, respectively (Figure 3). The upper Carboniferous (Bashkirian) Ebbadalen Formation is a siliciclastic- and evaporite-dominated synrift succession (Johannesen and Steel, 1992). The Devonian sediments of the Nordfjorden high sourced much of the siliciclastic material that interfingers with dolomitic and evaporitic strata that accumulated in restricted marine and sabkha environments within the basin (Steel and Worsley, 1984). The upper Carboniferous (Moscovian) Minkinfjellet Formation represents the transition to post-rift sedimentation (Pickard et al., 1996). The Minkinfjellet Formation comprises mixed clastic, carbonate and evaporite at the base, transitioning to entirely carbonate at the top, recording the shift from restricted to open-marine conditions and burial of relief as tectonic activity diminished in the Moscovian (Pickard et al., 1996; Eliassen and Talbot, 2003). The upper Carboniferous - lower Permian (Moscovian-Sakmarian) Wordiekammen Formation represents development of a widespread open-marine carbonate platform across the region, in which the entire region including former rift-margin highs were submerged. The top of the Minkinfjellet Formation correlates to the base of the Wordiekammen Formation and the boundary between the two is regionally diachronous, becoming younger westward (Pickard et al., 1996). The base of the Wordiekammen Formation consists of the Cadellfjellet Member (above the Minkinfjellet Formation), and the Kapitol Member, which rests directly on Devonian – Lower Carboniferous strata on the Nordfjorden High and records Moscovian transgression over the paleo-high (Figure 3) (Steel and Worsley, 1984). Deposition of the Kapitol Member ceased in the latest Carboniferous following uplift of the region, although deposition within the Cadellfjellet Member continued, indicating that uplift was related to continued movement along the

Billefjorden fault (Ahlborn, 2014). On the Nordfjorden High the Tyrellfjellet Member of the Wordiekammen Formation records renewed transgression over the Kapitol Sequences. Overlying the Wordiekammen Formation is the Sakmarian-Artinskian Gipshuken Formation, a succession of thick gypsum and carbonate that represent a change to a more restricted basin and coastal setting (Harland and Gedde, 1997; Samuelsberg and Pickard, 1999).

Methods

Field Work

We focused sampling on the Moscovian and Asselian intervals exposed in Asvindalen Canyon (Figure 4) in central Spitsbergen. Fusulinid biostratigraphy delineates the ages of the Wordiekammen Formation (Nilsson, 1993; Nilsson and Davydov, 1997). We measured (using a Jacob Staff) and logged the sections at cm scale, and collected samples at 20 cm intervals through the Moscovian (10 m thick) and Asselian (26 m thick) sections (181 samples total) for facies and other analyses. For detrital zircon analysis we collected samples from the Devonian sandstone exposed directly beneath our study section, the base of the Moscovian interval, and from a silt-rich carbonate 4.4 m above the top of the Asselian study section.

Petrography

Owing to pervasive and commonly fabric-destructive dolomitization, facies analysis at the hand-sample scale was challenging. To facilitate facies analysis, thin sections of 50 representative samples were made, stained with Alizarin Red-S (Dickson, 1965). For samples exhibiting pervasive and fabric-destructive dolomitization, Folk's (1987) "white card" technique was employed to better observe "ghosts" of recrystallized fossils and facies fabrics.

Extraction of the silicate mineral fraction (SMF)

Extraction of the SMF was accomplished following the process detailed in Sur et al. (2010b). Samples were first cleaned of exterior debris using distilled water, crushed to gravel size and re-washed with distilled water. Approximately 15 g of each sample was submerged in

2N HCl for 24 hours to remove carbonate, and the resultant insoluble residue was thoroughly rinsed, freeze-dried, and combusted at 500°C (15 hrs) to remove organic matter. The latter process also oxidizes any pyrite, and the resultant iron oxides are subsequently removed using the citrate-bicarbonate-dithionite (CBD) method (Mehra and Jackson, 1960). After rinsing and freeze-drying, this material represents the silicate mineral fraction (SMF), which is considered to comprise both eolian-delivered detrital material (dust) as well as possible authigenic silicate material. The SMF was then examined under reflected light, and found to contain small volumes of medium- to coarse sand-sized chert (microcrystalline quartz) debris in ~ 50% of samples. Where the chert is present it is typically a very small percentage of the SMF (~5%). Additionally, small volumes of silt- to very-fine-sand-sized doubly terminated quartz crystals also occur in the majority of samples. One interval within the greater Asselian section contains an unusually sandy carbonate, with clearly detrital grains interpreted as eolian (Ahlborn and Stemmerik, 2015) owing in part to the paleogeographic isolation of the platform (Larssen et al., 2005; Stemmerik and Worsley, 2005), and the texture (size, rounding) of the grains. Using the maximum grain size (~120 µm) of clearly detrital material in this unit, all samples of extracted SMF were sieved through 120 µm and 63 µm sieves. Material exceeding 120 µm is entirely authigenic (primarily chert and locally present doubly terminated quartz), albeit the source of the silica remains in question (further addressed below); hence, all material was retained, and the masses of all fractions were recorded.

Grain Size Analysis

Owing to the presence of both clearly authigenic and detrital silicate material, grain size analysis of the bulk fraction does not faithfully capture the detrital eolian signal. However, the granulometry of the <120 µm and < 63 µm fractions contains potentially useful information by virtue of the inclusion of original detrital material. Accordingly, we measured the grain size of the fine (<120 µm/ <63 µm) fractions using a Malvern Mastersizer 3000 laser particle size analyzer (LPSA).

ICP-MS

A subset of representative samples were assessed for whole-rock geochemical analysis to obtain major-oxide, trace element, and partial rare earth element chemical analyses. We selected three subintervals from the Asselian that span selected sequence boundaries, and four Moscovian samples (no relationship to sequence boundaries), as well as the Asselian and Moscovian detrital zircon samples. Samples were processed with 2N HCl to concentrate the SMF by removing carbonate minerals. A minimum of 1 g of acid-insoluble material was sent for analysis. Samples were pulverized to <75 µm before undergoing a four-acid digestion and subsequently analyzed by ICP-MS by an outside vendor.

Detrital Zircon Analysis

We collected three 5 kg samples from Devonian, Carboniferous (Moscovian) and Permian (Asselian) stratigraphic intervals in Asvindalen Canyon on Spitsbergen for detrital zircon analysis. The University of Arizona Laserchron facility processed the samples using techniques detailed in Gehrels et al. (2008). Briefly, the 5 kg samples were crushed, milled and sieved to sand size. To isolate the zircon grains the samples were separated into mineral fractions using a Wilfley table, methylene iodide density separation, and a Franz magnetic separator. A random selection of grains was mounted in epoxy with standard plutonic zircon grains. Cathode luminescence was used to select targets for 20 µm LA-ICPMS spots for 315 randomly selected grains for isotopic analysis, avoiding cracks, etc. The ages of the zircon grains were calculated using the $^{206}Pb/^{238}U$ and $^{207}Pb/^{235}U$ decay systems. Data points with >20% discordance or >5% reverse discordance were eliminated, and remaining concordant dates plotted on a probability density plot. Additionally, Kolmogorov-Smirnov (K-S) and overlap-similarity (O-S) tests were applied to evaluate statistical variation between and among samples.

Results

Sedimentary Facies

Bryozoan crinoid wackestone facies

Description: The Bryozoan crinoid wackestone facies consists of buff to light grey, medium bedded (15-25 cm) wackestone to packstone with a predominately heterozoan assemblage in a micritic matrix, and is commonly dolomitized (Figure 5). This facies occurs in 1.0-3.5 m thick intervals and contains common bryozoans, crinoids, and brachiopods. Fusulinids, ostracods and small forams occur rarely. Bioclasts are locally broken with minimal abrasion, and structures include extensive bioturbation with local disrupted laminae. This facies appears below the Palaeoaplysinid bioherms in the Asselian, and below the small foram packstone to grainstone facies in the Moscovian.

Interpretation: The presence of a normal-marine heterozoan fauna, minimal abrasion, and a bioturbated mud matrix indicates deposition in low-energy, open-marine conditions below both wave base and the photic zone.

Fusulinid wackestone

Description: This facies is a dark grey, medium-bedded calcitic to dolomitic wackestone with abundant fusulinids and occurs in intervals 1.0-2.0 m thick (Figure 5). This facies constitutes the "Brycebyen beds" (Cutbill and Chalinor, 1965), a distinctive unit present across much of central Spitsbergen and within the Asselian section at Asvindalen. Fusulinids typically appear as molds or calcite casts with little preservation of internal structure. The matrix consists of fine-grained dolomite with a relatively high organic content. Ahlborn and Stemmerik (2015) observed that the matrix is primarily mud in sections that are well preserved. Brachiopod, crinoid and bryozoan fragments compose a minor component of this facies. This facies appears in the study section below the Palaeoaplysinid bioherms.

Interpretation: Fusulinids record normal marine conditions, probably within the photic zone owing to their symbiosis with photosynthetic cyanobacteria (Hallock, 1985; Vachard et al., 2004). This facies appears in thin intervals at the base of the Palaeoaplysinid bioherms indicating an association with the initiation of mound growth.

Palaeoaplysinid boundstone

Description: This facies consists of medium to dark grey, massive calcitic to dolomitic boundstone in mounded lenses measuring 1-3 m thick and extending 50-70 m laterally, and occurs only in the Asselian section (Figure 5). Ahlborn and Stemmerik (2015) noted that the mounds form tabular buildups on the kilometer scale in the greater region. The binding organism is *Palaeoaplysina*, of problematic classification but possibly a hydrozoan encrusted by red coralline algae (Anderson and Beauchamp, 2014). *Palaeoaplysina* occurs as elongate, wavy, horizontal plates 4-30 cm long and 1-5 mm thick (Figure 5). The plates are preserved in life position (Huneke et al., 2001) and exhibit a distinctive internal cavity structure (Figure 5). Bryozoans, tubiphytes, and small forams commonly encrust the *Palaeoaplysina* plates. Fusulinids, crinoids and ostracod fragments occur in a lime mud matrix that fills interstitial spaces and internal cavities. This facies is associated with the Palaeoaplysinid floatstone facies.

Interpretation: The Palaeoaplysinid boundstone facies represents the carbonate buildups on the Nordfjorden High. *Palaeoaplysina* is thought to have grown in moderate- to low-energy environments below storm wave base (Skaug et al., 1982; Ahlborn and Stemmerik, 2015). This facies appears along the margins of the Nordfjorden High near the Billefjorden fault zone, indicating that the bioherms grew along paleo-topographic highs. Fusulinids and encrusting red algae indicate deposition within the photic zone. We interpret this facies as the core of *Palaeoaplysina* bioherms. Growth of this core was likely limited by storm wave base.

Palaeoaplysinid floatstone

Description: This facies consists of buff to dark grey, massive calcitic to dolomitic floatstone up to 1.0 m thick containing abundant fragments of both *Palaeoaplysina* and other biota (Figure 5). *Palaeoaplysina* plates occur fragmented within a peloidal and bioclastic wackestone to packstone matrix. Fusulinids, bryozoans, *Tubiphytes*, crinoids, brachiopods and ostracods commonly occur in various states of fragmentation as the bioclastic component. This facies is very similar to the Palaeoaplysinid boundstone facies and occurs above and on the flanks of the Palaeoaplysinid boundstone bioherms.

Interpretation: This facies records upward shallowing relative to the mound-core facies. The fragmentation and abrasion of the Palaeoaplysinid plates indicates relatively high energy as the *Palaeoaplysina* mounds were presumably impacted by storm wave base (Skaug et al., 1982; Ahlborn and Stemmerik, 2015). We interpret this facies to record mound-flank and mound-top environments.

Bioclastic packstone to grainstone

Description: This facies consists of grey, medium bedded (10-30 cm) calcitic packstone to grainstone occurring in intervals 0.5-3.0 m thick, and contain a diverse biotic assemblage (Figure 5). Biota include abundant *Beresella*, small forams, fusulinids, *Tubiphytes*, and less common highly fragmented crinoids, bryozoans and brachiopods. This facies occurs above the Bryozoan-Crinoid wackestone facies in the Moscovian interval, and independently in the Asselian interval.

Interpretation: The low mud content indicates deposition in a high-energy environment, consistent with photic-zone conditions recorded by dasycladacean algae, and the diverse, stenohaline assemblage indicates open-marine conditions. We interpret this facies to record a high energy, open-marine environment above fair weather wave base.

Indications of subaerial exposure

Microcodium

Description: *Microcodium* appears within both the Asselian and Moscovian intervals (Figure 6), typically hosted in either the *Palaeoaplysina* floatstone facies or foram grainstone facies. It presents as reddish-brown to black patches of recrystallized calcite along stratiform surfaces and penetrates ~0.4-1.5 m downward. In thin section, it exhibits a distinctive “corn-cob” texture (Figure 6).

Interpretation: Klappa (1978) described *Microcodium* as a mycorrhizal symbiont to living root systems while Kabanov (2008) inferred that a saprotrophic microorganism causes a biogenic mineralization of the *Microcodium* (Kabanov, 2008). In both interpretations, *Microcodium* results from plant colonization and thus exposure and subsequent soil formation. Its occurrence on subtidal facies indicates “abnormal” exposure in the sense that the carbonate system did not prograde fully prior to subaerial exposure (e.g. Wright, 1992; Dickson and Saller, 1995; Soreghan, 1997; Rankey et al., 1999). Accordingly, we interpret these surfaces to record glacio-eustatic sea-level fall.

Karst surfaces

Description: Distinctive karst surfaces appear in the upper Moscovian section (Figure 6). They are intervals ~1.5-2.0 m thick that contain abundant cavities and large pores. Cavities range in size from 1-400 mm across. *Microcodium* horizons occur at the tops of karst intervals. In thin section, samples show considerable fabric-destructive recrystallization of primary calcite to a sucrosic dolomite with abundant vuggy porosity (Figure 6).

Interpretation: Karst surfaces are indicative of prolonged subaerial exposure. Dissolution vugs and cavities form as a result of the groundwater table dissolving the rock during subaerial exposure.

Cyclo- and Sequence Stratigraphy

The studied sections within the Wordiekammen Formation contain two distinct facies stacking patterns that record upwardly shallowing successions (Figure 7). The Moscovian and Asselian facies stacking patterns closely resemble the Type-2 and Type-8 cycles of Ahlborn (2014) and Ahlborn and Stemmerik (2015).

In the Moscovian, the most common facies succession begins with the bryozoan crinoid wackestone facies, recording deposition in open-marine conditions below storm wave base. The bryozoan crinoid wackestone yields upwards to a thin interval of bioclastic packstone to grainstone facies indicating an upward shallowing of the cycle above fair weather wave base. In the Moscovian interval, three cycles occur ($M_{A,}$ M_B $M_{C)}$, with uniform thicknesses ranging from ~2.5- 3.0 m. Cycle M_B is missing the thin bioclastic packstone, but is interpreted as a cycle owing to the occurrence of *Microcodium* and karst (subaerial exposure) features developed atop subtidal facies.

The lower Kapitol Member is wedge shaped, and thickness varies across the ramp from 15 m in the down-dip regions to 1 m near the crest of the Nordfjorden block (Ahlborn and Stemmerik, 2015). Cycles are thin at the Asvindalen study section, presumably owing to deposition on the crest of the Nordfjorden High, a paleohigh. Ahlborn and Stemmerik (2015) observed ten exposure-capped cycles in the distal areas compared to the three we observe at Asvindalen. The well-developed (karst) evidence for subaerial exposure within the Moscovian section at Asvindalen likely reflects juxtaposition of multiple disconformities resulting in a section with large gaps and thus missing cycles in the sedimentary record. However, given this missing time, any deposition of atmospheric dust that affected this section would be concentrated on/proximal to exposure surfaces and recorded in the dust record. This negatively impacts our ability to reliably calculate dust flux at the high-frequency sequence scale within the Moscovian; however it does not preclude a comparison to the Asselian in terms of overall atmospheric dust loading recorded in the two intervals.

In the Asselian section, the typical facies succession begins with the open-marine bryozoan crinoid facies, recording deposition below storm wave base, superceded by the fusulinid wackestone. The Palaeoaplysinid boundstone facies overlies the wackestone, and represents the colonization phase and cores of the Palaeoaplysinid bioherms below storm wave base (Huneke et al., 2001). A transition to the Palaeoaplysinid floatstone facies records growth of the mounds into higher-energy environments above storm wave base. Seven complete cycles occur (A_A, A_B, A_C, A_D, A_E, A_F, A_G) in the Asselian study interval, with thicknesses of ~2.0-5.0 m. These intervals appear similar to the Type-8 cycles recorded by Ahlborn (2014) and Ahlborn and Stemmerik (2015). Cycle A_G does not show the same pattern as those below it being completely comprised of the bioclastic packstone-grainstone.

These cycles are dominated by upwardly shallowing subtidal facies capped by surfaces of subaerial exposure. These subaerial exposure surfaces atop subtidal facies are considered “abnormal” as the carbonate system did not fully prograde to peritidal conditions before exposure (Wright, 1992). Additionally, abrupt shifts to deeper-water facies occur immediately above exposure surfaces, recording relatively rapid transgression. The overprinting of subtidal facies by subaerial exposure surfaces subsequently capped by subtidal facies is consistent with the rapid sea level changes associated with glacioeustasy (Wright, 1992; Read, 1995; Dickson and Saller, 1995), commonly recorded in carbonate successions from the late Paleozoic (Soreghan, 1997; Stemmerik, 2008). Hence, these upwardly shallowing, esposure-capped facies successions are interpreted as high-frequency sequences driven by glacioeustasy.

Sedimentology and Stratigraphic Distribution of SMF

Because the Wordiekammen Formation represents a carbonate ramp setting far removed from potential sources of fluvio-deltaic sedimentation, we interpret all detrital siliciclastic material to record eolian, or atmospheric dust input. However, as noted in the methods, petrographic analysis of the silicate mineral fraction (SMF) revealed two distinct populations, one detrital and the other authigenic. The composition of the detrital component is primarily quartz, clay and minor muscovite. The authigenic material comprises chert and doubly terminated quartz crystals. Using the reasoning described in the methods, we used sieving as an initial means to separate the authigenic components from the detrital. The >120 µm component is predominately chert; however, doubly terminated quartz is also locally present in this size fraction immediately above Asselian sequence boundaries SB_{A7} and SB_{A8} (Figure 8). The material between 63-120 µm comprises both authigenic and detrital silica in the Moscovian and Asselian. In this size fraction, the authigenic mode consists almost entirely of doubly terminated quartz crystals with a minor (~5%) chert fraction. The <63 µm fraction is primarily detrital, however some doubly terminated quartz is present in local samples.

In thin section, some of the doubly terminated quartz crystals contain detrital cores of silt- to very fine sand-sized quartz grains (Figure 9), indicating they nucleated on a detrital grain. In such cases, the grain boundaries of the detrital cores appear highly corroded, consistent with silica dissolution and reprecipitation on the outer edges of these grains. Owing to high (initial) angularity, large surface-area-to volume ratios and a disordered crystal lattice produced by abrasion of eolian quartz, the fine-grained fraction (<30 µm) of mineral dust is highly soluble in an alkaline-rich environment such as seawater (Cecil et al., 2018). Sur et al (2010a) reported similar (doubly terminated quartz) grains which they also interpreted to reflect dissolution and reprecipitation of silica sourced from eolian dust. Additionally, grain-size histograms display an inverse relationship between the relative proportions of fine-grained (<30 µm) detrital material and doubly terminated quartz. Histograms of samples with minimal doubly terminated quartz have abundant fine (<30 µm) grains, whereas samples rich in doubly terminated quartz have minimal or no grains <30 µm (Figure 10). This result is similar to that of Sur et al. (2010a) who interpreted this to reflect preferential dissolution of the finest grains and local reprecipitation of the silica as coarser doubly terminated quartz. Thus we consider the doubly terminated quartz to have originated as eolian-sourced material. The relationship between chert and eolian silt is less clear; Cecil et al. (2018) hypothesize that chert also reflects silica sourced by eolian dust, but the evidence for this remains elusive.

The sieving procedures effectively separated the chert from the doubly terminated quartz at the 120 µm grain size with few exceptions. Samples located just above Asselian sequence boundaries SB_{A7} and SB_{A8} have significant volumes of doubly terminated quartz of sizes >120 µm and include no chert. Therefore we did not separate these samples at the 120 µm boundary, instead, the entire SMF is included in what we consider to reflect the detrital fraction. From this point forward, we use the term dust to refer to the <120 µm fraction and the entire SMF of samples located just above sequence boundaries SB_{A7} and SB_{A8}.

The Moscovian and Asselian dust records show different patterns with respect to both total volume of dust weight % (wt%) and glacial-interglacial variation (Figure 7). In order to quantify the volume of dust input to the Moscovian and Asselian sections, we compared the average amount of dust recovered per sample for each section (Appendix 2). The Moscovian section average is 1.29 wt%, while the total Asselian average is 2.26 wt%. However a significant increase in dust input to the Asselian occurs at SB_{A5}, indicating a change in overall dustiness at this boundary. The average dust volume below SB_{A5} is 1.45 wt % whereas above SB_{A5} it is 4.51 wt %. Additionally within the stratigraphic dust profile (Figure 7), significant intersample variation occurs through each section. For the Moscovian, dust amounts vary from 0.1 to 4.48 wt%, whereas Asselian values range from 0.03% to 23.46 wt%. As noted previously, the Moscovian section contains abundant and deeply penetrating unconformities (thick karst surfaces) reflecting deposition on a paleo-high, thus the Moscovian cycles are relatively thin, and incomplete in number.

Furthermore, within the Asselian interval, most (five of eight) sequences exhibit peaks in dust wt% immediately superjacent to subaerial exposure surfaces, then drop to background levels within ~0.2-1.0 m above the exposure surface. To further assess this, we averaged the dust wt% from all samples within the first meter above each exposure surface. In contrast to the Asselian, no significant pattern of dust wt% relative to cycle position occurs in the Moscovian interval. The average for the first meter of each cycle is 1.07 wt%, less than the section average of 1.29 wt%. In the Asselian section, average dust content in the first meter of each cycle is 5.18 wt%, more than double the average dust content of the overall section, 2.26 wt%. In the Asselian, a major shift occurs at SB_{A5}, with much higher values observed in the first meter of each cycle above SB_{A5}. Below SB_{A5} the 1st meter average is 2.26 wt % whereas values above SB_{A5} average 7.25 wt %. All the dust peaks in the Asselian occur in the first meter above sequence boundaries, although cycles A_B and A_D exhibit no significant peaks.

Geochemical Results

The geochemical results (ICP-MS; Table 1), are from three subintervals that represent dust input across sequence boundaries in the Asselian section, as well as selected Moscovian samples and the Moscovian and Asselian detrital zircon samples. The geochemical trends obtained from these data shed light on dust provenance.

Immobile trace elements such as La, Th, Sc and Zr can aid provenance characterization (Bahatia and Crook, 1983; Totten et al., 2000; Muhs, 2018). Enrichment in incompatible elements Th and La is associated with more felsic continental sources, whereas enrichment in compatible Sc tends to indicate more mafic sources. Accordingly, Th/Sc ≥ 1 typifies a continental felsic signature, whereas Th/Sc ratio <1 is more mafic (Totten et al., 2000; Sweet et al., 2013). Applying these ratios to our data produces clusters associated with stratigraphic intervals (Figure 11). The Asselian interval produces two distinct groupings: samples from below SB_{A7} and samples from above SB_{A7}. Asselian dust samples from below SB_{A7} generally exhibit a more mafic signature with Th/Sc ratios < 1. Moscovian samples, Asselian samples above SB_{A7} as well as both detrital zircon samples have Th/Sc ratios ≥1, associated with a more felsic source. A similar pattern is observed on the Th/Sc vs La/Sc diagram (Figure 11). Asselian samples from above SB_{A7} cluster around and above the value for upper continental crust (UCC) whereas samples from below SB_{A7} plot as more mafic and Moscovian samples cluster in between. Detrital zircons plot as more felsic than UCC.

Ternary diagrams of Th-La-Sc, and Sc-Th-Zr/10 can be used to discriminate tectonic setting (Bahatia and Crook, 1986; Muhs, 2018). Plotted on these ternary diagrams, samples cluster in groups similar to those discussed above (Figure 11). Asselian samples below SB_{A7} plot in the continental island arc field along with the Moscovian samples. The Asselian samples above SB_{A7} plot in both the continental island arc field and in the passive margin field trending towards the Asselian detrital zircon sample. The Moscovian detrital zircon sample plots in the continental island arc field whereas the Asselian detrital zircon sample plots in the passive margin field.

Ratios of chemically immobile elements such as Al, Ti and Zr also show variations in provenance of the dust source (Mason and Jacobs., 1998) reflected in the shifts in Ti/Zr and Al/Zr with depth (Figure 7). Variations in these ratios correspond with vertical changes in glacial-interglacial cyclicity, indicating a provenance shift that occurs above sequence boundaries. However, the direction of the provenance shift relative to dust peaks changes through the section. The dust peak above SB_{A1} exhibits positive excursions in Ti/Zr and Al/Zr, and positive excursions also occur associated with SB_{A4}, whereas negative excursions in Ti/Zr and Al/Zr occurs above SB_{A7} and SB_{A8}.

Detrital Zircon Results

The three samples collected for detrital zircon geochronology are from Devonian strata of the Nordfjorden high, Moscovian strata of the Kapitol Member and Asselian strata of the Tyrellfjellet Member, all sampled from Asvindalen Canyon. Figure 12 shows probability density plots of zircon ages, with detailed data in Appendix 2. Sample SVL-DZ-DEV is a medium-grained sandstone from the top of the Devonian Wood Bay Group, a 2900 m thick succession of continental (e.g. fluvial) siliciclastic strata (Critelli and Reed, 1999) unconformably subjacent to the Moscovian Kapitol Member of the Wordiekammen Formation. This sample yielded a dominate zircon population peak around 400-450 Ma, with a minor subpopulation of 911-1970 Ma, and single grains aged 2311 Ma and 2764 Ma (Figure 12). Sample SVL-DZ-M is from the basal-most sandy limestone of the Kapitol Member, ~10 cm above the unconformity surface with the Devonian Wood Bay Group (Figure 6). These strata capture the Moscovian transgression that drowned the Nordfjorden High (Stemmerik, 2000; Ahlborn and Stemmerik, 2015). The siliciclastic component comprises fine- to medium-grained sand (volume % mode ~250 µm), with rip-ups of Devonian strata, and is from the only siliciclastic-rich unit of the Moscovian section. This sample yields a dominant subpopulation at 400-450 Ma with minor populations at 600-700 Ma, 1000-2000 Ma and 2700-2900 Ma (Figure 12). The third sample (SVL-DZ-A) is from an especially siliclastic-rich limestone in the Tyrellfjellet Member, approximately 4.4 m above the detailed study interval of the Asselian section. The siliciclastic component comprises fine sand-sized (volume % mode ~132 µm) quartz that is moderately well sorted, with rounded, pitted and frosted sand-sized quartz as well as angular silt. This siliciclastic-rich limestone marks the base of the first of two wedge-shaped sand bodies documented by Ahlborn and Stemmerik (2015), and interpreted as eolian transported sand reworked during transgression (Stemmerik, pers. Commun., 2018). Ahlborn and Stemmerik (2015) noted that the abrupt appearance of significant sand in the Wordiekammen Formation is anomalous given that a large carbonate platform system covered the Barents sea region at this time (Larssen et al., 2005), but an eolian origin is consistent with the fine-grained, well-sorted texture. Detrital zircon ages in this sample yield dominant sub populations at 400-450 Ma, 950-2030 Ma, and 2650-2850 Ma (Figure 12).

Potential Detrital Zircon Source Regions

Palaeozoic (400-450 Ma)

Zircons of this age range make up 19% of all zircons found in this study and have ages that represent the Caledonides. The Caledonian orogeny occurred during the Ordovician to Devonian as a result of collision between Baltica and Laurentia, producing uplifts which subsequently contributed abundant sediment to circum-arctic basins (McClelland et al., 2016). Remnants of these uplifts are preserved across eastern Greenland, western Scandinavia, Svalbard and Scotland (McKerrow et al., 2000; Gee et al., 2008), and zircons of Palaeozoic age are known from these basement terranes, reflecting magmatic and metamorphic processes associated with the orogeny (Gee and Teben'Kov, 2004; Kalsbeek et al., 2008a; Bingen and Solli, 2009; Slama et al., 2011, Lundmark al., 2014). Grains of this age group occur in upper Carboniferous and Devonian strata throughout the circum-arctic region, demonstrating that Paleozoic grains formed an important source of sediment from various regions in the

Caledonides (Bingen and Solli, 2009; Slama et al., 2011, Schmidt et al., 2012; Lundmark et al., 2014; McClelland et al., 2016).

Neo-Paleoproterozoic (950-2000 Ma)

Zircons of Meso-Paleo Proterozoic age make up 60% of zircons from these samples. The broad spectrum of zircon ages indicates a large source area with multiple geological units as well as recycling of zircons from metasedimentary deposits. Zircons of ages 950-2000 Ma correlate to basement terranes and metasediments in Greenland, Scandinavia, and Arctic Canada (Cadwood et al., 2007; Bingen and Solli, 2009, Afinson et al., 2012; Kristoffersen et al., 2013). The Sveconorwegian belt contains a fairly complete record of Meso-Paleoproterozoic zircons ranging from 900-1800 with the only distinct gap in the record occurring at 1060-1130 Ma and comparatively few rocks aged 1800-2000 Ma (Bingen and Solli, 2009). In comparison the Scandinavian Caledonides have a relatively sparse Meso-Paleoproterozoic zircon record. Basement windows expose Transcandinavian igneous rocks (1600-1850 Ma) and minor amounts of Svecofennian (1800-2000 Ma) and Sveconorwegian (890-980 Ma, 1190-1240 Ma) rocks (Bingen and Solli, 2009). The basement of the East Greenland Caledonides contains abundant Paleoproterozoic rocks aged 1750-2000 Ma (Thrane, 2000; Kalsbeek et al., 2008b) as well as Neoproterozoic granites which yield ages 900-1000 Ma (Kalsbeek et al., 2008b). Primary magmatic rocks with Mezoproterozoic ages (1000-1200 Ma) do not occur in the east Greenland Caledonides, however Neoproterozoic metasediments of the Eleonore Bay Supergroup in eastern Greenland have abundant zircons with age peaks at 1000-1100 Ma as well as other significant populations 1400-1700 Ma. These Neoproterozoic sediments were recycled into circum-arctic sedimentary basins during Caledonide uplift (Slama et al., 2011; McClelland et al., 2016).

Archean (2650-2900 Ma)

Zircons in this age range constitute 5% of all zircons in this study. Archean basement terranes are known from the East Greenland Caledonides, the Scandinavian Caledonides, the Canadian Shield, and Scotland. (Thrane, 2002; Cadwood et al., 2007; Kalsbeek et al., 2008b; Holtta et al., 2008, Bingen and Solli, 2009). Archean grains have been used to determine provenance between Baltica and Laurentia (Bingen and Solli, 2009; Pedersen, 2011; Slama et al., 2011; Gasser and Andresen, 2013). While both cratons contain Archean basement rocks (Thrane, 2002; Cadwood et al., 2007; Holtta et al., 2008) exposure of this basement in the Caledonides varies. In eastern Greenland, Archean basement composes much of the craton and occurs in the southern part of the East Greenland Caledonides (Thrane, 2002; Holtta et al., 2008). During the Caledonian uplift abundant Archean zircons accumulated in Devonian and Carboniferous sedimentary basins (Slama et al., 2011; McClelland et al., 2016). In Scandinavia, Archean basement occurs in the Northern Caledonides and Eastern Scandinavian Shield (Holtta et al., 2008). Within the Northern Caledonides, Archean magmatic rocks as well as Proterozoic sedimentary rocks with Archean zircon components are exposed in basement windows, allowing for the possibility that Archean zircons were recycled during the Caledonian orogeny. However, these windows might or might not have been exposed during Paleozoic erosion of the Caledonides (Bingen and Solli, 2009). Ultimately, Archean zircons occur in limited quantity in sedimentary successions with known Scandinavian provenance (Kristoffersen et al., 2013) indicating that dominant Archean populations record a Greenland provenance.

Detrital Zircon Provenance Interpretation

The zircons in the Devonian sample (SVL-DZ-DEV) have a dominant Silurian-aged population as well as a minor subpopulation of ages 911-1970 Ma. This prevalence of Silurian zircons in the Devonian sample indicates a local source of Caledonian granitoids (Pettersson et al., 2009) transported directly into the basin. The remaining Mesoproterozoic subpopulation likely reflects recycling of local Neoproterozoic sediments uplifted during the Caledonian event (Gasser and Andresen, 2013).

Despite the presence of Devonian rip-up clasts in the Moscovian sample, the zircons from the Devonian and Moscovian samples are statistically different as noted by the K-S statistics. The zircons have a similar age profile as those found in the Carboniferous Billefjorden group that were derived from recycled Devonian sediments (Steel and Worsely, 1984; Gasser and Andresen, 2013). The basal Moscovian siliciclastic unit was likely locally sourced from other Devonian units (Piepjohn and Dallmann, 2014) that remained exposed until complete transgression of the region. Additional detrital zircon samples from the Devonian rocks of the Nordfjorden High are required in order to confirm this interpretation.

The ages of zircons in the Asselian sample (SVL-DZ-A) indicate that these eolian sediments were recycled from Devonian and Carboniferous sediments in the East Greenland Caledonides. The Paleozoic population reflects erosion of Caledonian granitoids common to eastern Greenland south of 76°N, and the Scandinavian Caledonides (Kalsbeek et al., 2008a; Bingen and Solli, 2009). The dominant Archean zircon population indicates a Greenland Caledonian provenance as opposed to a Scandinavian source (Bingen and Solli, 2009). It is likely that the Asselian sample was not sourced from primary basement, but instead from recycling of Devonian and Carboniferous sediments found in the east Greenland Caledonides, which have a near identical population as the Asselian sample (Slama et al., 2011). A similar zircon age population occurs in sediments sourced from the Pearya terrane (Kirkland et al., 2009; Afinson et al., 2012; Pozer Bue and Andresen, 2014), however these sedimentary deposits contain very little Caledonian-aged material and are ruled out as the source for the eolian material in Spitsbergen. Additionally we can eliminate the northeastern Greenland Caledonides as the distinctive 1700-1800 Ma and 1900-2000 Ma age peaks distinctive to this region (McClelland et al., 2016) are absent. Therefore, this sediment was not sourced from the nearest northeast Greenland location, reinforcing the interpretation that recycling of Devonian and Carboniferous fluvial sedimentary deposits from the east Greenland Caledonides form the most likely source for the Asselian detrital zircon sample (Figure 13).

Application of the Kolmogorov-Smirnov (K-S) test (Table) on detrital zircon age spectra show P values < 0.05 for all intersample comparisons, indicating rejection of the null hypothesis, and implying that each sample represents a distinct provenance (at >95% confidence level). However, application of the K-S test to detrital zircon data from Devonian and Carboniferous strata of Eastern Greenland (Slama et al., 2011) compared to the Spitsbergen Asselian sample reveals a P value of 0.171, (E. GL DEV; Table 2), indicating we cannot reject the null hypothesis that the two samples are from the same populations.

Additionally, results of the overlap-similarity (O-S) test (Table 2) reveal high values for overlap and similarity between the Asselian and Moscovian samples from Spitsbergen and the Devonian and Carboniferous samples from east Greenland

Discussion

Origin of the Silicate Mineral Fraction

The Wordiekammen Formation formed part of an extensive carbonate ramp that extended along the northern margin of Pangea (Beauchamp and Desrochers, 1997; Stemmerik and Worsley, 2005). This paleogeographic setting, together with the texture, grain size, and composition of the detrital silicate material recovered from the studied sections supports an eolian interpretation for transport of this material to the ramp. Authigenic silica (doubly terminated quartz) that co-occurs with detrital material is interpreted to have been dust-sourced (as detailed above). The relatively minor chert that occurs might have been similarly sourced from dust. Regardless, removal of the chert fraction does not significantly alter the observed trends in SMF through the section, and we interpret the observed patterns to reflect variations in loading of atmospheric dust.

Detrital zircon data for the Asselian sample implies transport from the eastern Greenland Caledonides to Spitsbergen (Figure 13), and thus moderately long transport distances (~1000 km; Stemmerik and Worsely, 2005). These fine-sand sized eolian sediments are larger (mode ~ 132 µm) than the silt-sized sediment we interpret as eolian-transported in the measured stratigraphic interval, but are within the feasible size of documented long-transport (>1000 km) eolian material (e.g. Betzer et. al., 1988; Beget et al., 1993; Middleton et al., 2001; Menendez et al., 2013; Jeong et al., 2014). During the Devonian, fluvial systems carried sediment from the East Greenland Caledonides to the Sverdrup basin (Afinson et al., 2012). These systems likely persisted during Carboniferous - early Permian uplift of the

Caledonides, recycling sediment from Devonian and Carboniferous basins onto these floodplains. Eolian input to the Asselian carbonate system likely reflects deflation of silt-sized material from these fluvial floodplains and implies a predominately southwesterly wind regime at this time (Figure 13).

Geochemical data from the dust fraction demonstrates a shifting dust provenance through the study interval. The Moscovian and lower Asselian exhibit a mafic continental island arc signature, possibly affiliated with basement arc terrains that were accreted onto the Laurentian craton during the Paleoproterozoic (Gasser, 2014) and exposed in northeast Greenland (McClelland et al., 2016). The provenance shift at SB_{A7} toward a more felsic passive margin setting has a similar geochemical character as the Asselian detrital zircon samples and is interpreted to record the introduction of recycled Devonian and Carboniferous sediments from the east Greenland Caledonides as an important source region. Variations in Ti/Zr and Al/Zr ratios of the mineral dust coupled with glacial-interglacial cyclicity records expansion of regions of eolian deflation during incipient interglacial times. The inversion of these excursions above SB_{A7} provides further evidence for a major change in source region in the upper Asselian interval. This change in provenance records an expansion of regions of eolian deflation from the northeast Greenland Caledonian basement to the drainage of recycled Devonian and Carboniferous sedimentary deposits in the east Greenland Caledonides (Figure 13).

Timing of Input

The average volume of dust preserved in the Asselian exceeds that of the Moscovian by a factor of ~2 for the overall average and ~5 for the first meter above sequence boundaries. However, the shift in dust input to the Asselian at SB_{A5} suggests that comparisons of overall dust averages may not be as meaningful as comparisons of averages above and below SB_{A5}. The lower Asselian section (below SB_{A5}) has overall dust values comparable to those of the Moscovian. However, the Moscovian section juxtaposes multiple deeply developed disconformities owing to deposition on a topographic high; given this, the Moscovian essentially records an artificially concentrated dust record, suggesting dustier atmospheric conditions during the Asselian. Furthermore, the upper Asselian section (above SB_{A5}) records substantially more dust (by ~3x) than the Moscovian and lower Asselian, consistent with increasing aridity of the northern Pangean margin from late Carboniferous to Permian time (Stemmerik, 2000; Boucot et al., 2013). These changes in aridity may relate to the increased intensity of the late Paleozoic icehouse in the Asselian (e.g., Isbell 2003; Fielding et al., 2008; Montanez and Poulsen, 2013), which should have enhanced global aridity. In equatorial Pangea, records of loess increase in prominence from the Moscovian to Asselian, reflecting increased continental aridity, and peak icehouse conditions (Soreghan et al., 2008). Presumably, these factors would impact regions outside of equatorial Pangea and contribute to a globally dusty atmosphere.

The increase in dust volume observed above SB_{A5} likely relates to the provenance shift that also occurs in the upper Asselian section, interpreted to record onset of peak icehouse conditions. Climate changes associated with peak icehouse conditions would include increased aridity, stronger winds, and decreased vegetation that would have influenced regional dustiness along the northern Pangean margin, causing expansion of regions of eolian deflation.

Relatively systematic variations in dust input occur through glacial-interglacial cycles in the Asselian. Dust typically increases directly above subaerial exposure surfaces, within basal transgressive intervals. This is similar to equatorial and southern mid-latitude studies on dust input to isolated carbonate settings (Stagner, 2008; Sur et al., 2010a; Carvajal et al., 2018) that document highest dust input during glacial and incipient interglacial conditions. The Asselian of Spitsbergen similarly records elevated dust preservation during incipient interglacials (Figure 14) indicating that dustiness in the northern hemisphere was controlled by conditions similar to those controlling dust variations in other latitudinal regions.

Conclusions

(1) The silicate mineral fraction within the Wordiekammen Formation provides a proxy for atmospheric dust in the northern mid-latitudes during the late Carboniferous and early Permian of Spitsbergen. Atmospheric dustiness serves as a climate indicator for aridity, atmospheric circulation and source area. Authigenic forms of silica appear in the SMF as (minor) chert and (locally abundant) doubly terminated quartz. The doubly terminated quartz preserves evidence for ultimate eolian derivation and is thus included in the dust fraction. The chert might also reflect recrystallization of fine dust, but the evidence for this remains elusive.

(2) Quantitative analysis of the dust demonstrates that, overall, the Asselian interval was significantly dustier than the Moscovian, particularly above SB_{A5}. This indicates increased aridity and gustiness of the source region due to the intensity of the late Paleozoic icehouse, which reached its maximum in the Asselian. The increase in dust input above SB_{A5} possibly records the onset of peak icehouse conditions.

(3) Three Moscovian sequences and seven Asselian sequences are identified in the study sections, recording high-frequency sequences capped by subaerial exposure surfaces and recording glacioeustasy. The position of the Moscovian section on a paleo-topographic high results in large amounts of missing time that precludes intracyclic analysis of dust input. The Asselian dust record varies with glacioeustatic cyclicity. Maximum dust input associated with transgressive facies suggests highest atmospheric

dust load and aridity in the northern mid-latitudes during glacial and incipient interglacial times.

(4) Provenance data suggests two distinct sources for the dust. The Moscovian and lower Asselian sections have a mafic continental island arc source interpreted to reflect derivation from Caledonian basement of northeastern Greenland, whereas the upper part of the Asselian section has a felsic passive margin provenance interpreted as reflecting derivation from recycled Devonian and Carboniferous strata from the east Greenland Caledonides. This indicates that an expansion of regions of eolian deflation occurred in conjunction with the onset of peak icehouse conditions.

References

ANFINSON, O.A., LEIER, A.L., EMBRY, A.F., AND DEWING, K., 2012, Detrital zircon geochronology provenance of the Neoproterozoic to Late Devonian Franklinian Basin, Canadian Arctic Islands: Geological Society of America Bulletin, v. 124, p. 415–430, doi: 10.1130/B30503.1.

AHLBORN, M. 2014: Carboniferous-Permian sedimentology and stratigraphy of the Nordfjorden High and Loppa spur, Arctic Norway. PhD thesis, University of Copenhagen, 127 pp.

AHLBORN, M., AND STEMMERIK, L., 2015, Depositional evolution of the Upper Carboniferous – Lower Permian Wordiekammen carbonate platform, Nordfjorden High, central Spitsbergen, Arctic Norway: Norwegian Journal of Geology, v. 95, p. 91-126

ANDERSON, K.D., AND BEAUCHAMP, B., 2014, Paleobiology and paleoecology of Palaeoaplysina and Eopalaeoaplysina new genus in Arctic Canada: Journal of Paleontology, v. 85(5), p. 1056-1071

BAHATIA, M.R., AND CROOK, K.A.W., 1986, Trace element characteristics of graywackes and tectonic setting discrimination of sedimentary basins: Contributions to Mineralogy and Petrology, v. 92, p. 181-193

BEAUCHAMP, B., AND DESROCHERS, A., 1997, Permian warm to very cold water carbonates and cherts in Northwest Pangea: *in* James, N.P., AND Clarke, J.A.D., eds., Cool-Water Carbonates: Society of Economic Paleontologists and Mineralogists Special Publication 56, p. 327–348.

BEGET, J.E., KESKINEN, M., AND SEVERIN, K., 1993, Mineral particles from Asia found in volcanic loess on the island of Hawaii; Sedimentary Geology, v.84, p. 189-197.

BETZER, P.R., CARDER, K.L., DUCE, R.A., MERRILL, J.T., TINDALE, N.W., UEMATSU, M., COSTELLO, D.K., YOUNG, R.W., FEELY, R.A., BRELAND, J.A., BERNSTEIN, R.E., AND GRECO, A.M., 1988, Long-range transport of giant mineral aerosol particles: Nature, v.336, p. 568-571.

BINGEN, B., AND SOLLI, A., 2009, Geochronology of magmatism in the Caledonian and Sveconorwegian belts of Baltica: synopsis for detrital zircon provenance studies: Norwegian Journal of Geology, v. 89 p. 267–290

BLOMEIER D., SCHEIBNER C., AND FORKE H., 2009, Facies arrangement and cyclostratigraphic architecture of a shallow-marine, warm-water carbonate platform: the Late Carboniferous Ny Friesland Platform in eastern Spitsbergen (Pyefjellet Beds, Wordiekammen Formation, Gipsdalen Group): Facies v. 55 p. 291–324

BOUCOT, A.J., CHEN. X., AND SCOTESE, C.R., 2013, Phanerozoic Paleoclimate: an Atlas of Lithological Indicators of Climate: SEPM Concepts in Sedimentology and Paleontology No. 11, p. 478.

CAWOOD, P.A., NEMCHIN, A.A., AND STRACHAN, R., 2007, Provenance record of Laurentian passive-margin strata in the northern Caledonides: Implications for paleodrainage and paleogeography: Geological Society of America Bulletin, v. 119, p. 993–1003.

COALE, K.H., JOHNSON, K.S., FITZWATER, S.E., GORDON, R.M., TANNER, S., CHAVEZ, F.P., FERIOLI, L., SAKAMOTO, C., ROGERS, P., MILLERO, F., STEINBERG, P., NIGHTINGALE, P., COOPER, D., COCHLAN, W.P., LANDRY, M.R., CONSTANTINOU, J., ROLLWAGEN, G., TRASVINA, A., AND KUDELA, R., 1996. A massive phytoplankton bloom induced by an ecosystem-scale iron fertilization experiment in the equatorial Pacific Ocean: Nature, v. 383, p. 495–501.

CECIL, C.B., HEMMINGWAY, B.S., AND DULONG, F.T., 2018, The chemistry of eolian quartz dust and the origin of chert: Journal of Sedimentary Research, v. 88, p. 743-752.

CROWELL, J.C., 1978, Godwanan Glaciation, Cyclothems, Continental Positioning, and Climate Change: American Journal of Science, v. 278, p. 1345-1372.

CRITELLII, S., AND REED, W.E., 1999, Provenance and stratigraphy of the Devonian (Old Red Sandstone) and Carboniferous sandstones of Spitsbergen, Svalbard: European Journal of Mineralogy, v. 11, p. 149-166.

CUTBILL, J., AND CHALINOR, A., 1965, Revision of the Stratigraphical Scheme for the Carboniferous and Permian Rocks of Spitsbergen and Bjornoya: Geological Magazine, v. 102, p. 418-439.

DAVYDOV, V., CROWLEY, J., SCHMITZ, M., AND POLETAEV, V., 2010, High-precision U-Pb zircon age calibration of the global Carboniferous time scale and Milankovitch band cyclicity in the Donets Basin, eastern Ukraine: Geochemistry Geophysics Geosystems, v. 11, p. 1–22, doi: 10.1029/2009GC002736.

DEMOTT, P.J., SASSEN, K., POELLOT, M.R., BAUMGARDNER, D., ROGERS, D.C., BROOKS, S.D., PRENNI, A.J., AND KREIDENWEIS, S.M., 2003. African dust aerosols as atmospheric ice nuclei: Geophysics Research Letters, v. 30 no. 14, 1732

DICKSON, J.A.D., 1965, A Modified Staining Technique for Carbonates in Thin Section: Nature, v. 205, p. 587.

DICKSON, J. A. D., AND SALLER, A. H., 1995, Identification of subaerial exposure surfaces and porosity preservation in Pennsylvanian and lower Permian shelf limestones, eastern

Central Basin Platform Texas, *i*n BUDD, D. A., SALLER, A. H., AND HARRIS, P. M., eds., Unconformities in carbonate shelf strata — their recognition and the significance of associated porosity: AAPG Memoir 57, p. 239–257.

ELIASSEN, A., AND TALBOT, M.R., 2003, Diagenesis of the mid-carboniferous Minkinfjellet Formation, central Spitsbergen, Svalbard: Norwegian Journal of Geology, v. 83, no. 4, p. 319–331.

FIELDING, C.R., FRANK, T.D., AND ISBELL, J.L., 2008, The late Paleozoic ice age; a review of current understanding and synthesis of global climate patterns *in* FIELDING, C.R., FRANK, T.D., AND ISBELL, J.L., eds., Resolving the Late Paleozoic Ice Age in Time and Space: Geological Society of America Special Paper, v. 441, no. 24, p. 343–354.

FOLK, R.L., 1987, Detection of organic matter in thin-sections of carbonate rocks using a white card: Sedimentary Geology, v. 54, p. 193–200.

FOSTER, T.M., SOREGHAN, G.S., SOREGHAN, M.J., BENISON, K.C., AND ELMORE, R.D., 2014, Climatic and paleogeographic significance of eolian sediment in the Middle Permian Dog Creek Shale (Midcontinent U.S.): Palaeogeography, Palaeoclimatology, Palaeoecology, v. 402, p 12-29.

GASSER, D., 2014 The Caledonides of Greenland, Svalbard and other Arctic areas: status of research and open questions: *in* CORFU, F., GASSER, D. AND CHEW, D. M. 2014. New Perspectives on the Caledonides of Scandinavia and Related Areas: Geological Society, London, Special Publications, v. 390, p. 93–129.

GASSER, D., AND ANDRESEN, A., 2013, Caledonian terrane amalgamation of Svalbard: Detrital zircon provenance of Mesoproterozoic to Carboniferous strata from Oscar II Land, western Spitsbergen: Geological Magazine, v. 150, p. 1103–1126, doi:10.1017/S0016756813000174 .

GEE, D.G., FOSSEN, H., HENRIKSEN, N. AND HIGGINS, A.K. 2008: From the early Paleozoic platforms of Baltica and Laurentia to the Caledonide orogen of Scandinavia and Greenland: Episodes, v. 31, p. 44-51.

GEE, D.G. AND TEBENKOV, A. M., 2004, Svalbard: a fragment of the Laurentian margin. *In* Gee D.G. and Pease V., eds., The Neoproterozoic Timanide Orogeny of Eastern Baltica: Geological Society, London, Memoirs, v. 30, p. 191–206.

GEHRELS, G.E., VALENCIA, V.A., AND RUIZ, J., 2008, Enhanced precision, accuracy, efficiency, and spatial resolution of U-Pb ages by laser ablation–multicollector– inductively coupled plasma–mass spectrometry: Geochemistry, Geophysics, Geosystems, v. 9, no. 3, p. 1-13. doi: 10.1029/2007GC001805.

HALLOCK, P., 1985, Why are Larger Foraminifera Large: Paleobiology, v. 11 No. 2, p 195-208.

HARLAND, W.B., AND GEDDES, I., 1997, Chapter 17- Carboniferous-Permian history of Svalbard: Geological Society of London Memoirs, v. 17, p. 310– 339.

HECKEL, P., 2002, Overview of Pennsylvanian cyclothems in midcontinent North America and brief summary of those elsewhere in the world: Canadian Society of Petroleum Geologists Memoir, v. 19, p. 79–98.

HECKEL, P.H., 2008, Pennsylvanian cyclothems in Midcontinent North America as far-field effects of waxing and waning of Gondwana ice sheets, *in* Fielding, C.R., Frank, T.D., Isbell, J.L., eds., Resolving the Late Paleozoic Ice Age in Time and Space: Geological Society of America Special Paper v. 441, p. 275-289.

HÖLTTÄ, P., BALAGANSKY, V., GARDE, A.A., MERTANEN, S., PELTONEN, P., SLABUNOV, A., SORJONEN-WARD, P. AND WHITEHOUSE, M, 2008, Archaean of Greenland and Fennoscandia: Episodes 31, p. 13-19.

HÜNEKE, H., JOACHIMSKI, M., BUGGISCH, W., AND LÜTZNER, H. 2001: Marine Carbonate facies in response to climate and nutrient level: The upper Carboniferous and Permian of Central Spitsbergen (Svalbard): Facies, v. 45, p. 93–136.

ISBELL, J.L., MILLER, M.F., WOLFE, K.L., AND LENAKER, P.A., 2003, Timing of late Paleozoic glaciation in Gondwana: Was glaciation responsible for the development of Northern Hemisphere cyclothems?: *in* CHAN, M.A., AND ARCHER, A.A., eds., Extreme Depositional Environments: Mega End Members in Geologic Time: Geological Society of America Special Papers, v. 370, p. 5–24.

JEONG, G.Y., KIM, J.Y., SEO, J., KIM, G.M., JIN, H.C., AND CHUN, Y., 2014, Long-range transport of giant particles in Asian dust identified by physical, mineralogical, and meteorological analysis: Atmospheric Chemistry and Physics, v. 14, p. 505-521.

JOHANNESSEN, E.P., AND STEEL, R.J., 1992, Mid-Carboniferous extension and rift-infill sequences in the Billefjorden Trough, Svalbard: Norwegian Journal of Geology, v. 72, p. 35–48.

JOHNSON, S.Y., 1989, Significance of loessite in the Maroon Formation (middle Pennsylvanian to lower Permian), Eagle Basin, northwest Colorado: Journal of Sedimentary Petrology, v. 59, no. 5, p. 782-791.

KABANOV, P., ANADON, P., AND KRUMBEIN, W.E., 2008, Microcodium: An extensive review and a proposed non-rhizogenic biologically induced origin for its formation: Sedimentary Geology, v. 205, p. 79-99.

KALSBEEK, F., HIGGINS, A.K., JEPSEN, H.F., FREI, R., AND NUTMAN, A.P., 2008a, Granites and granites in the East Greenland Caledonides, in Higgins, A.K., Gilotti, J.A., and Smith, M.P., eds., The Greenland Caledonides: Evolution of the Northeast Margin of Laurentia: Geological Society of America Memoir 202, p. 227–249.

KALSBEEK, F., THRANE, K., HIGGINS, A.K., JEPSEN, H., LESLIE, A.G., NUTMAN, A.P., AND FRIE, R., 2008b, Polyorogenic history of the East Greenland Caledonides, in Higgins, A.K., Gilotti, J.A., and Smith, M.P., eds., The Greenland Caledonides: Evolution of the Northeast Margin of Laurentia: Geological Society of America Memoir 202, p. 55–72.

KIRKLAND, C.L., Pease, V., Whitehouse, M.J., AND Ineson, J.R., 2009, Provenance record from Mesoproterozoic-Cambrian sediments of Peary Land, North Greenland: Implications for the ice-covered Greenland Shield and Laurentian palaeogeography, Precambrian Research, v. 170, p. 43-60.

KLAPPA, C.F., 1978. Biolithogenesis of Microcodium: elucidation: Sedimentology, v. 25, p. 489–522.

KRISTOFFERSEN, M., ANDERSEN, T., AND ANDRESEN, A., 2014, U-Pb age and Lu-Hf signatures of detrital zircon from Palaeozoic sandstones in the Oslo rift, Norway: Geological Magazine, v, 151, p. 816–829.

LARSSEN, G.B., ELVEBAKK, G., HENRIKSEN, L.B., KRISTENSEN, S.E., NILSSON, I., SAMUELSBERG, T.J., SVÅNÅ, T.A., STEMMERIK, L., AND WORSLEY, D., 2005, Upper Palaeozoic lithostratigraphy of the southern part of the Norwegian Barents Sea: Norges Geologiske Undersøkelse Bulletin v. 44, p. 1–43.

LUNDMARK, A.M., BUE, E.P., GABRIELSEN, R.H., FLAAT, K., STRAND, T., AND OHM, S.E., 2014, Provenance of late Palaeozoic terrestrial sediments on the northern flank of the Mid North Sea High: Detrital zircon geochronology and rutile geochemical constraints, *in* SCOTT, R.A., SMYTH, H.R., MORTON, A.C., AND RICHARDSON, N., eds., Sediment Provenance Studies in Hydrocarbon Exploration and Production: Geological Society, London, Special Publication 386, p. 243–259.

MAHOWALD, N., 2011, Aerosol indirect effect on biogeochemical cycles and climate: Science, v. 334, no. 6057, p. 794–796, doi: 10.1126/science.1207374.

MASON, J.A., AND JACOBS, P.M., 1998, Chemical and particle-size evidence for addition of fine dust to soils of the midwestern United States: Geology, v. 26, p. 1135-1138.

MCCLELLAND, W.C., GILOTTI, J.A., RAMARAO, T., STEMMERIK, L., AND DALHOFF, F., 2016, Carboniferous basin in Holm Land records local exhumation of the North-East Greenland

Caledonides: Implications for the detrital zircon signature of a collisional orogeny: Geosphere, v. 12, no. 3, p. 1-23.

MCGEE, D., BROECKER, W.S., AND WINCKLER, G., 2010, Gustiness: The driver of glacial dustiness?: Quaternary Science Reviews, v. 29, p. 2340-2350.

MCKERROW, W.S., MAC NIOCAILL, C.N., AND DEWEY, J.F., 2000, The Caledonian orogeny redefined: Journal of the Geological Society, London, v. 157, p. 1149–1154, doi: 10.1144/jgs.157.6.1149.

MEHRA, O.P., AND JACKSON, M.L., 1960, Iron oxide removal from soils and clays by a dithionite citrate system buffered with sodium bicarbonate: Clays and Clay Minerals, v. 7, p 313-317.

MENENDEZ, I., PEREZ-CHACON, E., MANGAS, J., TAULER, E., ENGELBRECHT, J.P., DERBYSHIRE, E., CANA, L., AND ALONSO, I., 2013, Dust deposits on La Graciosa Island (Canary Islands, Spain): Texture, mineralogy and a case study of recent dust plume transport: Catena, v. 117, p. 133-144.

MIDDLETON, N.J., BETZER, P.R., AND BULL, P.A., 2001, Long-range transport of ‘giant’ aeolian quartz grains: linkage with discrete sedimentary sources and implications for protective particle transfer: Marine Geology, v. 177, p. 411-417.

MILLER, R.L., AND TEGEN, I., 1998. Climate response to soil dust aerosols: Journal of Climate, v. 11, p. 3247–3267.

MONTAÑEZ, I.P., AND POULSEN, C.J., 2013, The Late Paleozoic ice age: An evolving paradigm: Annual Review of Earth and Planetary Sciences, v. 41, no. 1, p. 629–656.

MUHS D.R., 2013, Loess and its Geomorphic, Stratigraphic, and Paleoclimatic Significance in the Quaternary, *in* SHRODER, J.F., LANCASTER, N., SHERMAN, D.J., AND BAAS, A.C.W., Treatise on Geomorphology, v. 11, p. 149-183.

MUHS, D.R., 2018, The geochemistry of loess: Asian and North American deposits compared: Journal of Asian Earth Sciences: v. 155, p. 81-115.

MUHS, D.R., AND BETTIS, E.A., 2003, Quaternary loess-paleosol sequences as an example of climatic extremes: *in* CHAN, M.A., AND ARCHER, A.W., eds., Extreme depositional environments: Mega end members in geologic time: Boulder, Colorado,Geological Society of America Special Publication 370, p. 53-74.

NILSSON, I. 1993, Upper Paleozoic fusulinid stratigraphy of the Barents Shelf and surrounding areas [PhD thesis]: University of Tromsø, Tromsø Norway, 538 p.

NILSSON, I., AND DAVYDOV, V.I., 1997, Fusulinid biostratigraphy in Upper Carboniferous (Gzhelian) and Lower Permian (Asselian-Sakmarian) successions of Spitsbergen, Arctic Norway: Permophiles, v. 30, p. 18–24.

PEDERSEN, L.E., 2011. Zircon provenance of Devonian deposits in Western Norway: MSc. thesis, Department of Earth Science, University of Bergen, Bergen Norway.

PETTERSSON, C.H., TEBENKOV, A.M., LARIONOV, A.N., ANDRESEN, A., AND PEASE, V., Timing of migmatization and granite genesis in the Northwestern Terrane of Svalbard, Norway: implications for regional correlations in the Arctic Caledonides: Journal of the Geological Society, London, v. 166, p. 147-158.

PICKARD, N.A.H., EILERTSEN, F., HANKEN, N., JOHANSEN, T.A., LØNØY, A., NAKREM, H.A., NILSSON, I., SAMUELSBERG, T.J., AND SOMERVILLE, I. A.N.D., 1996, Stratigraphic framework of Upper Carboniferous (Moscovian - Kasimovian) strata In Bünsow Land , central Spitsbergen : palaeogeographic implications: Norwegian Journal of Geology, v. 76, p. 169-185.

PIEPJOHN, K., AND DALLMANN, W., 2014, Stratigraphy of the uppermost Old Red Sandstone of Svalbard (Mimerdalen Subgroup): Polar Research, v.33, 19998, http://dx.doi.org/10.3402/polar.v33.19998

POZER BUE, E., AND ANDRESEN, A., 2014, Constraining depositional models in the Barents Sea region using detrital zircon U–Pb data from Mesozoic sediments in Svalbard, *in* SCOTT, R. A., SMYTH, H. R., MORTON, A. C. AND RICHARDSON, N. eds, Sediment provenance studies in hydrocarbon exploration and production: Geological Society, London, Special Publications v. 386 p. 261–279.

RANKEY, E.C., BATCHEL, S.L., AND KAUFMAN, J., 1999, Controls on stratigraphic architecture of icehouse mixed carbonate-siliciclastic systems: A case study from the Holder Formation (Pennsylvanian, Virgilian), Sacramento Mountains, New Mexico: Advances in Carbonate Sequence Stratigraphy: Application to reservoirs, outcrops and models, SEPM Special Publication, No. 63, p. 127-150.

REA, D.K., 1994, The paleoclimatic record provided by eolian deposition in the deep sea; the geologic history of wind: Reviews of Geophysics, v. 32, p. 159-195.

READ, J.F., 1995, Overview of carbonate platform sequences, cycle stratigraphy and reservoirs in greenhouse and ice-house worlds, *in* Read, J.F., eds., Milankovitch Sea-Level Changes, Cycles, and Reservoirs on Carbonate Platforms in Greenhouse and Icehouse Worlds. SEPM Short Course 35, p. 1-102.

SAMUELSBERG, T.J., AND Pickard, N.A.H., 1999, Upper Carboniferous to Lower Permian transgressive - regressive sequences of central Spitsbergen, Arctic Norway: Geological Journal, v. 34, p. 393–411.

SCHMIDT, A.S., MORTON, A.C., NICHOLS, G.J., AND FANNING, C.M., 2012, Interplay of proximal and distal sources in Devonian–Carboniferous sandstones of the Clair Basin, west of Shetland, revealed by detrital zircon U-Pb ages: Journal of the Geological Society, London, v. 169, p. 691–702, doi: 10.1144/jgs2011-148.

SKAUG, M., DONS, C.E., LAURITZEN, Ø. AND WORSLEY, D. 1982: Lower Permian paleoaplysinid bioherm and associated sediments from central Spitsbergen: Polar Research v. 2, p. 57–74.

SLAMA, J., WALDERHAUG, O., FONNELAND, H., KOSLER, J., AND PEDERSEN, R.B., 2011, Provenance of Neoproterozoic to Upper Cretaceous sedimentary rocks, eastern Greenland: Implications for recognizing the sources of sediments in the Norwegian Sea: Sedimentary Geology, v. 238, p. 254–267, doi: 10 .1016 /j .sedgeo .2011 .04 .018.

SOREGHAN, G.S., 1992. Preservation and paleoclimatic significance of eolian dust in the Ancestral Rocky Mountains province: Geology v. 20, p. 1111–1114.

SOREGHAN, G.S., 1997. Walther's Law, climate change, and Upper Paleozoic cyclostratigraphy in the Ancestral Rocky Mountains: Journal of Sedimentary Research, v. 67, p. 1001–1004.

SOREGHAN, G.S., AND SOREGHAN, M.J., 2002, Atmospheric dust and algal dominance in the late Paleozoic: A hypothesis: Journal of Sedimentary Research, v. 72, p. 457-461.

SOREGHAN, G.S., SOREGHAN, M.J., AND HAMILTON, M.A., 2008, Origin and paleoclimatic significance of tropical silt in the Late Paleozoic icehouse: Palaeogeography, Palaeoclimatology, Palaeoecology, v. 268, p. 234-259.

SOREGHAN, G. S., SWEET, D. E., AND HEAVENS, N. G., 2014, Upland glaciation in tropical Pangaea: Geologic evidence and implications for late Paleozoic climate modeling: Journal of Geology, v.122, p. 137–163. http://doi.org/10.1086/675255.

STAGNER, A.F., 2008, Eolian silt in upper Paleozoic carbonates of the Bird Spring Formation (Arrow Canyon, Nevada): Implications for climate controlled sedimentation: Masters Thesis, University of Oklahoma, 115 p.

STEEL, R.J., AND WORSLEY, D., 1984, Svalbard's post-Caledonian strata - An atlas of sedimentational patterns and palaeogeo- graphic evolution, *in* Spencer, A.M., Holter, E., Johnsen, S.O., Mørk, A., Nysæther, E., Songstand, P., Spinnangr, P., Petroleum geology of the north European margin: Norwegian Petroleum Society, London, Graham & Trotman, p. 109–135.

STEMMERIK, L., 2000, Late Palaeozoic evolution of the North Atlantic margin of Pangea: Palaeogeography, Palaeoclimatology, Palaeoecology, v. 161, p. 95–126.

STEMMERIK, L., 2008, Influence of late Paleozoic Gondwana glaciations on the depositional evolution of the northern Pangean shelf, North Greenland, Svalbard, and the Barents Sea: *in* FIELDING, C.R., FRANK, T.D., AND ISBELL, J.L., eds., Resolving the Late Paleozoic Ice Age in Time and Space: Geological Society of America Special Paper 441, no. 14, p. 205–217.

STEMMERIK, L., AND WORSLEY, D., 2005, 30 years on: Arctic Upper Palaeozoic stratigraphy, depositional evolution and hydrocarbon prospectivity: Norwegian Journal of Geology, v. 85, p. 151–168.

SUR, S., SOREGHAN, G.S., SOREGHAN, M.J., YANG, W., AND SALLER, A., 2010a, A record of glacial aridity and Milankovitch-scale fluctuations in atmospheric dust from the Pennsylvanian tropics: Journal of Sedimentary Research, v. 80, p. 1046-1067.

SUR, S., SOREGHAN, G.S., SOREGHAN, M.J., AND STAGNER, A., 2010b, Extracting the silicate mineral fraction from ancient carbonate: Assessing the geologic record of dust: Journal of Sedimentary Research, v. 80, p. 763-769.

SWEET, A.C., SOREGHAN, G.S., SWEET, D.E., SOREGHAN, M.J., AND MADDEN, A.S., 2013, Permian dust in Oklahoma: Source and origin for Middle Permian (Flowerpot-Blaine) redbeds in Western Tropical Pangaea: Sedimentary Geology, v. 284-285, p. 181-196.

THRANE, K., 2002, Relationships between Archean and Paleoproterozoic crystalline basement complexes in the southern part of the East Greenland Caledonides: An ion microprobe study: Precambrian Research, v. 113, p. 19–42, doi: 10.1016/S0301-9268(01)00198-X.

TOTTEN, M.W., HANAN, M.A., AND WEAVER, B.L., 2000, Beyond whole-rock geochemistry of shales: The importance of assessing mineralogic controls for revealing tectonic discriminants of multiple sediment sources for the Ouachita mountain flysch deposits: Geological Scociety of America Bulletin, v. 112, no. 7, p. 1012-1022.

VACHARD, D., MUNNECKE, A., AND SERVAIS, T., 2004, New SEM observations of keriothecal walls: Implications for the evolution of Fusulinida: Journal of Formainiferal Research, v. 34, no. 3, p. 232-242.

VAN DEN BELT, F.J.G., VAN HOOF, T.B., AND PAGNIER, H.J.M., 2015, Revealing the hidden Milankovitch record from Pennsylvanian cyclothem successions and implications regarding late Paleozoic chronology and terrestrial-carbon (coal) storage: Geosphere, v. 11, no. 4, p. 1062–1076.

VEEVERS, J.J., AND POWELL, C.M., 1987, Late Paleozoic glacial episodes in Gondwanaland reflected in transgressive-regressive depositional sequences in Euramerica: Geological Society of America Bulletin, v. 98, p. 475–487.

WRIGHT, V.P., 1992, Speculations on the controls on cyclic peritidal carbonates: ice-house versus greenhouse eustatic controls: Sedimentary Geology, v. 76, p. 1-5.

YOSHIOKA, M., MAHOWALD, N.M., CONLEY, A.J., COLLINS, W.D., FILLMORE, D.W., ZENDER, C.S., AND COLEMAN, D.B., 2007, Impact of desert dust radiative forcing on sahel precipitation: Relative importance of dust compared to sea surface temperature variations, vegetation changes, and greenhouse gas warming: Journal of Climate, v. 20, p. 1445-1467.

Appendix 1: Tables and Figures

Table 1: ICP-MS results

Sample	Ti (wt%)	Al (wt%)	K (wt%)	Zr (ppm)	La (ppm)	Sc (ppm)	Th (ppm)
M4.6	0.131	2.65	0.72	84.3	4.5	3.7	2.67
M6.2	0.071	0.93	0.35	39.7	1.7	1.4	1.82
M6.8	0.151	1.9	0.82	91	3.6	3.8	3.48
M8.2	0.078	1.17	0.44	45.5	1.9	1.6	1.41
M9.8	0.059	0.73	0.26	32.5	1.2	0.9	0.8
A0.8	0.21	4.11	2.61	57.7	2.9	3.3	2.5
A1.0	0.295	6.07	3.87	84.1	5.8	5.3	3.54
A1.2	0.262	4.93	3.07	81	4.9	4	3.22
A1.4	0.215	3.87	2.31	66	4.3	3.4	2.37
A1.6	0.272	6.22	3.94	88.5	7.5	5.6	3.9
A1.8	0.185	3.44	1.93	92.2	4.4	3.9	3.06
A2.0	0.228	4.7	2.59	95.6	5.3	4.7	3.61
A2.2	0.261	5.77	3.36	107	4.6	4.9	3.36
A2.4	0.301	5.52	3.41	111.5	5.4	6	2.93
A2.6	0.343	5.78	3.26	146	7.1	6.8	4.25
A3.0	0.138	2.38	1.22	55.1	5.6	3.7	2.05
A5.0	0.345	5.38	2.42	122	22.5	7.1	6.25
A10.2	0.219	4.19	2.28	106.5	2.7	4.4	3.56
A11.0	0.32	5.37	3.17	174	4.3	6	4.39
A11.4	0.36	5.39	3.13	167.5	4.5	6.9	5.94
A11.8	0.289	5.25	3.14	111	4.6	5.5	3.93
A12.2	0.326	4.98	2.88	109.5	5.3	5.7	3.98
A12.6	0.232	4.18	2.63	89.8	3.8	4.3	3.06
A13.0	0.212	4.52	2.72	74.2	4.1	4.5	2.39
A13.2	0.077	1.71	1	43.7	1.6	1.5	0.83
A13.4	0.142	3.1	1.92	42.8	2.4	3	1.15
A13.6	0.15	2.95	1.7	55	2.9	3.1	1.8
A14.0	0.11	1.64	0.88	36.8	1.9	1.9	1
A14.4	0.088	1.17	0.49	35.8	2.6	1.6	1
A14.6	0.176	3.05	1.69	70.6	2.5	3.7	1.99
A15.8	0.048	0.82	0.42	34.7	0.8	0.9	0.54
A19.2	0.251	4.76	2.8	97.9	9.5	6	3.35
A19.6	0.246	4.5	2.84	91	6.8	5.3	2.64
A20.0	0.187	3.95	2.57	66.9	6.6	4.3	2.03
A20.6	0.293	5.84	3.81	97	9.8	6.7	3.31

A21	0.306	5.76	3.53	100	8.1	6.8	3.22
A21.4	0.221	4.03	2.4	85.7	6.1	4.2	2.01
A21.8	0.078	1.36	0.76	26.6	2.6	1.5	0.91
A22.0	0.202	3.7	2.07	74.9	7.7	4.2	2.23
A22.2	0.109	2.31	1.32	40.2	3.5	2.8	1.25
A22.6	0.155	2.69	1.82	65.1	6.6	2.4	2.2
A22.8	0.312	5.03	3.5	147	14.3	4.8	5.13
A23.0	0.097	1.1	0.78	64.5	5.8	0.7	2.2
A23.2	0.064	0.87	0.63	55.3	2.9	0.6	1.47
A23.4	0.06	0.73	0.47	42.5	2.3	0.6	0.92
A23.8	0.068	1.21	0.69	41.2	2.2	1	0.84
A24.2	0.081	1.47	0.9	47.2	2.5	1.1	1.1
A24.6	0.053	1	0.58	32.6	1.6	0.7	0.67
A25.0	0.107	2.06	1.26	54	2.9	1.5	1.23
A25.4	0.115	2.31	1.56	56.3	2.7	1.7	1.59
A25.6	0.128	2.56	1.61	54.3	2.9	2.2	1.65
A25.8	0.168	3.41	2.11	61.8	3.7	3.3	1.73
A26.0	0.161	3.41	2.16	67.5	5.3	3	2.28
A26.2	0.167	2.27	1.81	106	8	1.8	3.89
A26.4	0.154	3.02	2.03	65.9	4.5	2.8	2.02
DZ A	0.088	1.19	1.01	48.3	3	0.7	1.15
DZ M	0.101	1.72	0.82	26.2	4.7	1.5	1.9

Table 2: K-S and O-S test results

K-S P-values using error in the CDF					
	SVL-DZ-DEV	SVL-DZ-M	SVL-DZ-A	E. GL DEV	E. GL Carb
SVL-DZ-DEV		0.000	0.000	0.000	0.000
SVL-DZ-M	0.000		0.001	0.005	0.001
SVL-DZ-A	0.000	0.001		**0.171**	0.044
E. GL DEV	0.000	0.005	**0.171**		0.000
E. GL Carb	0.000	0.001	0.044	0.000	

Overlap					
	SVL-DZ-DEV	SVL-DZ-M	SVL-DZ-A	E. GL DEV	E. GL Carb
SVL-DZ-DEV					
SVL-DZ-M	0.750				
SVL-DZ-A	0.735	0.864			
E. GL DEV	0.695	0.856	0.835		
E. GL Carb	0.638	0.795	0.804	0.935	

Similarity					
	SVL-DZ-DEV	SVL-DZ-M	SVL-DZ-A	E. GL DEV	E. GL Carb
SVL-DZ-DEV					
SVL-DZ-M	0.758				
SVL-DZ-A	0.656	0.869			
E. GL DEV	0.716	0.889	0.910		
E. GL Carb	0.681	0.834	0.864	0.873	

Figure 1: Map of Spitsbergen

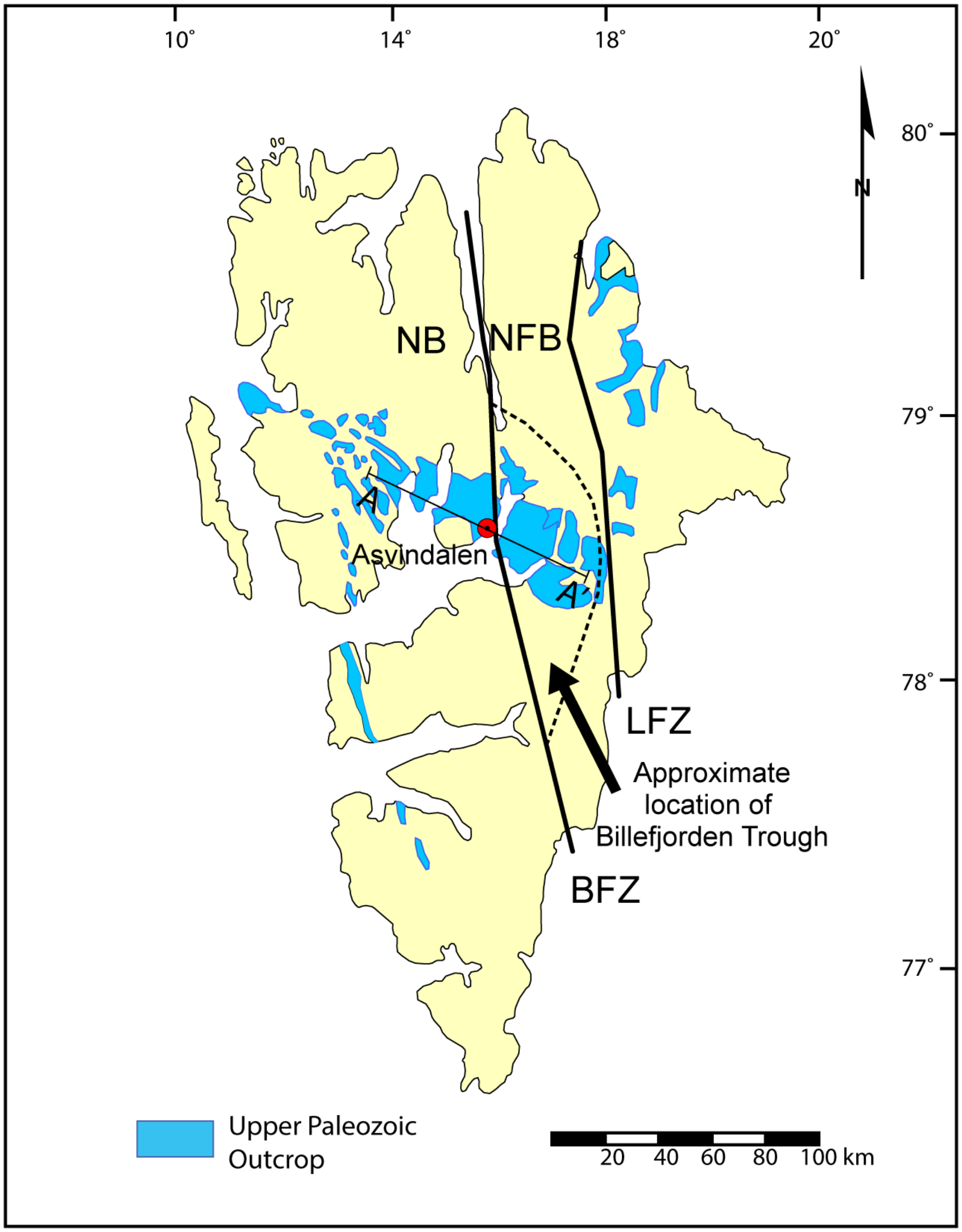

Map of Spitsbergen showing structural elements and upper Paleozoic outcrops. Abbreviations: NB- Nordfjorden Block, NFB – Ny Friesland Block, BFZ – Billefjorden Fault Zone, LFZ- Lomfjorden Fault Zone. Modified from Pickard et al. (1996).

Figure 2: Paleogeographic Map

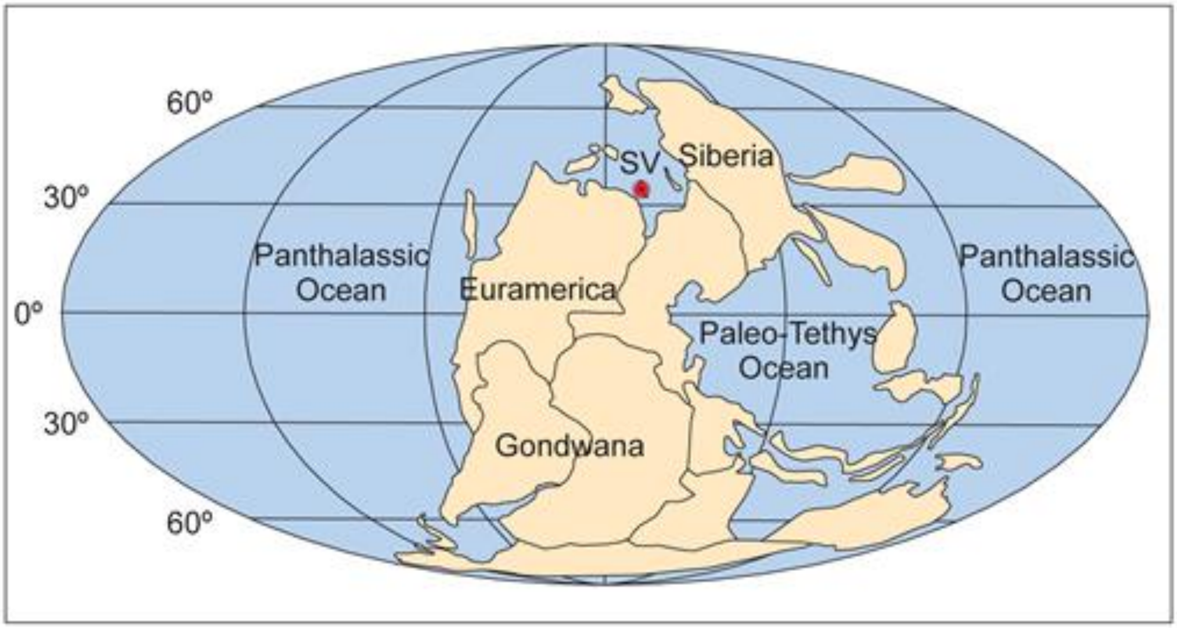

Position of the continents during the late Paleozoic. Svalbard (SV) was located at approximately 30-35°N (Stemmerik, 2008). Modified from Boucot et al. (2013).

Figure 3: Spitsbergen Cross Section

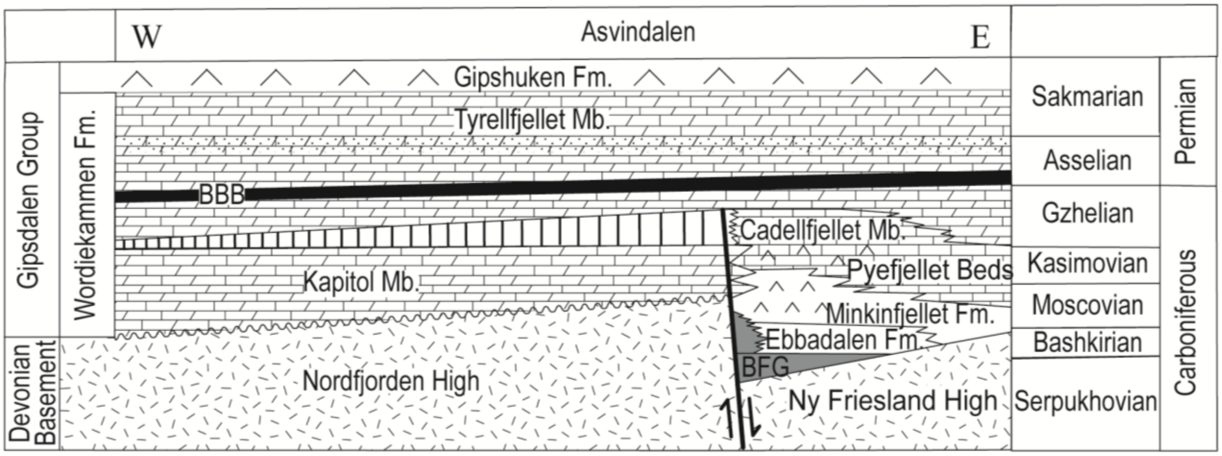

Late Paleozoic correlations from central Spitsbergen. BBB- Brucebyen Beds; BFG- Billefjorden Group; Modified from Samuelsberg and Pickard (1999) and Ahlborn et al. (2015).

Figure 4: Asvindalen Location Map

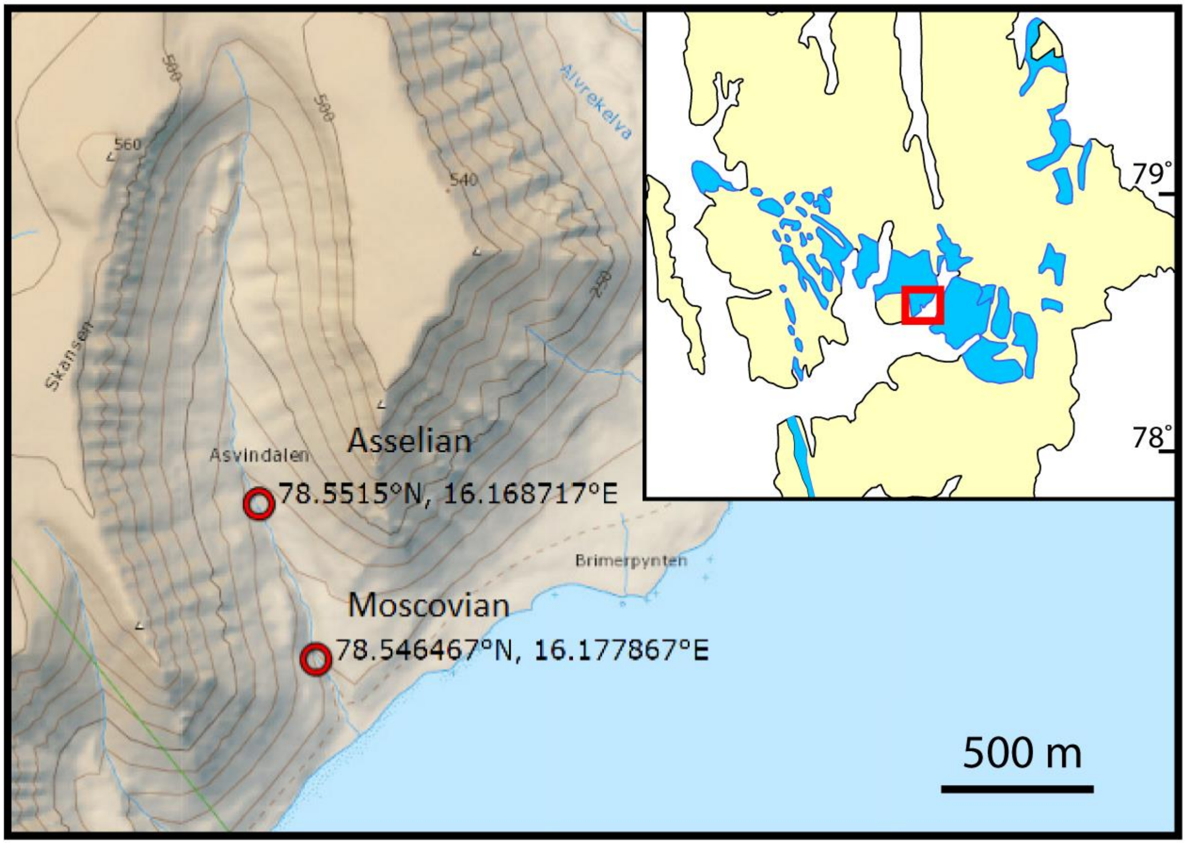

Location of Asvindalen Canyon in Central Spitsbergen. Coordinates mark the base of each study section. This figure is constructed from a map from http://toposvalbard.npolar.no/, small scale map modified from Pickard et al. (1996).

Figure 5: Plate 1

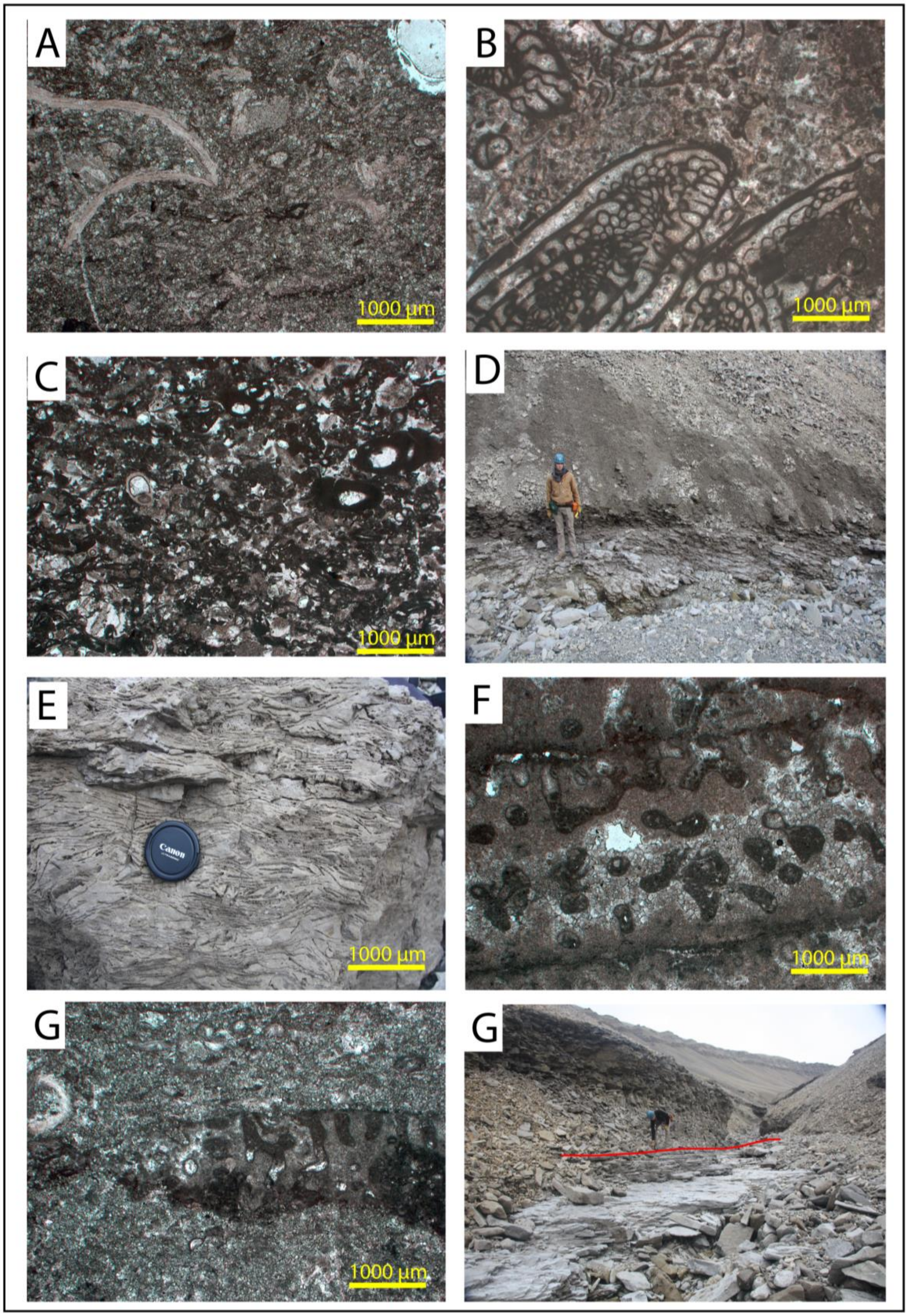

Plate 1: (A) Photomicrographs of Bryozoan Crinoid Wackestone Facies (B) Fusulinid Wackestone Facies (C) Small Foram Wackestone to Grainstone (D,E) Outcrop photos of Palaeoaplysinid boundstone facies (F) Photomicrographs of Palaeoaplysinid boundstone facies (G) Photomicrograph of Palaeoaplysinid floatstone facies

Figure 6: Plate 2

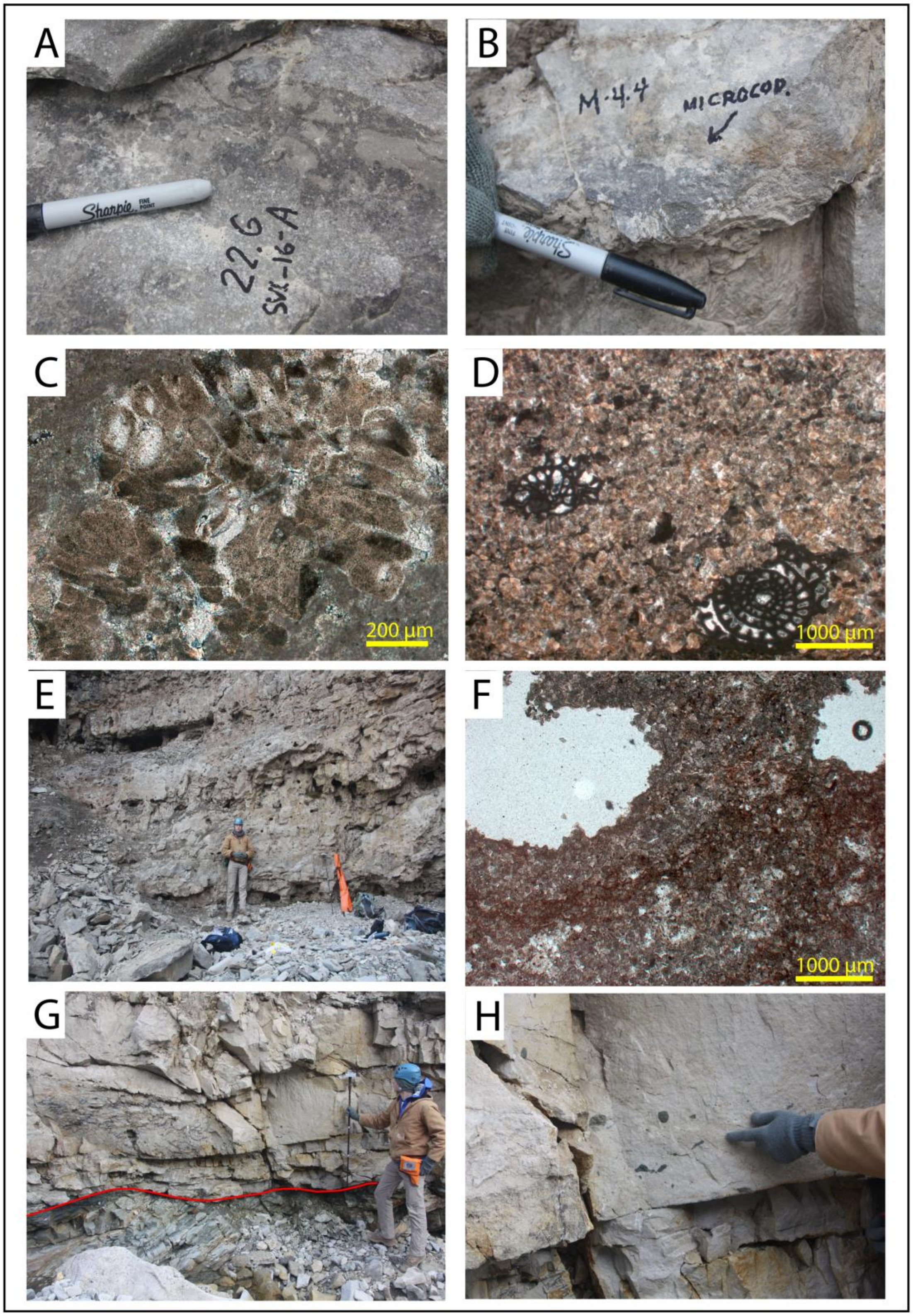

Plate 2: (A,B) Outcrop photos of Microcodium overprint (C) Photomicrograph displaying the "corncob" texture of Microcodium. (D) Photomicrograph displaying Microcodium overprint facies. (E) Outcrop photo of the Moscovian section, note the large karst cavities. (F) Photomicrograph of the karst overprint facies. (G) Base of the Moscovian interval. Contact with the Devonian Nordfjorden block is marked in red. (H) Devonian rip up clasts at the base of the Moscovian interval.

Figure 7: Stratigraphic section, dust profiles and chemical ratios

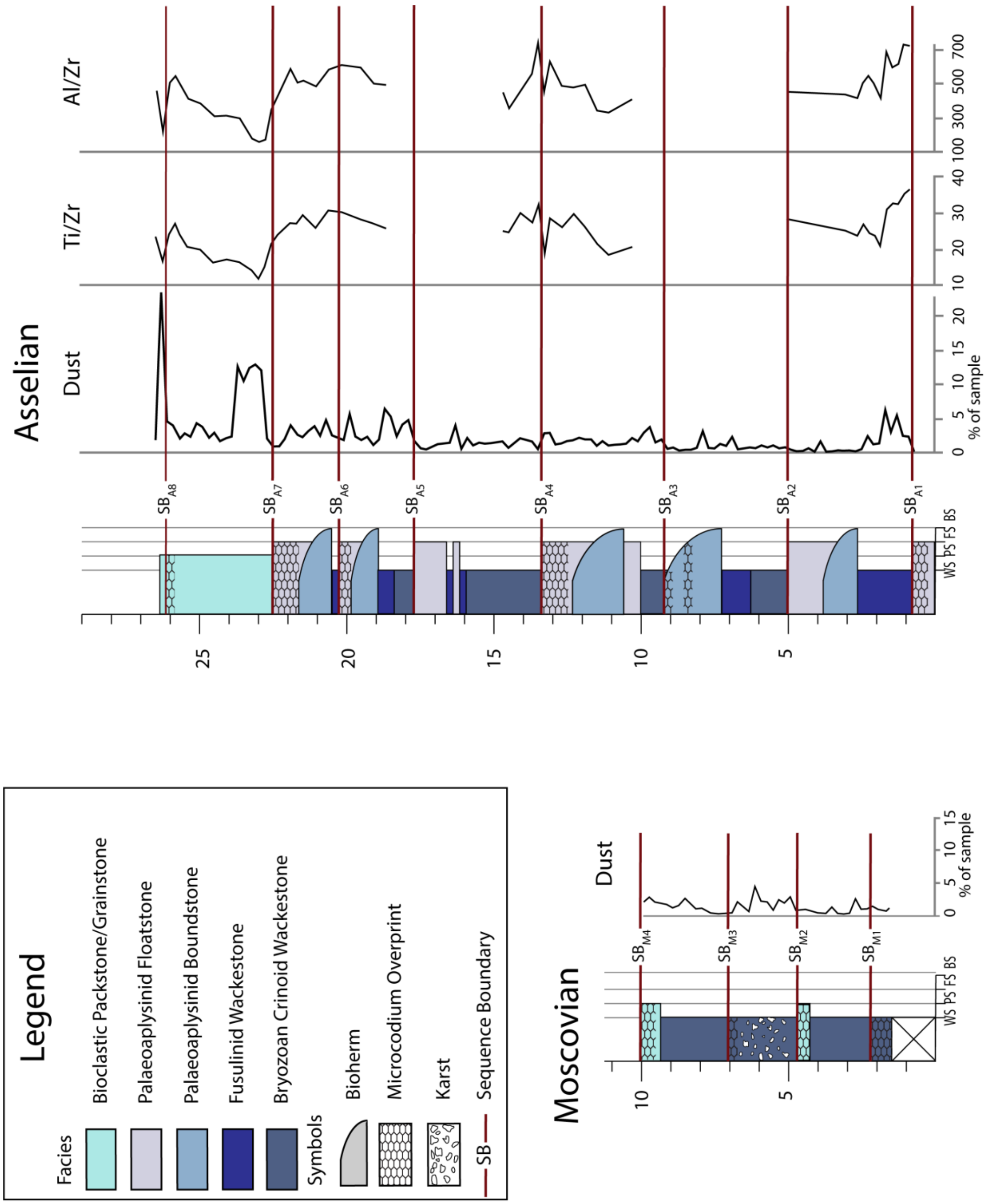

Stratigraphic section with facies interpretation of Moscovian and Asselian intervals. Dust record and geochemical ratios are plotted alongside stratigraphy.

Figure 8: Sieved fraction photos

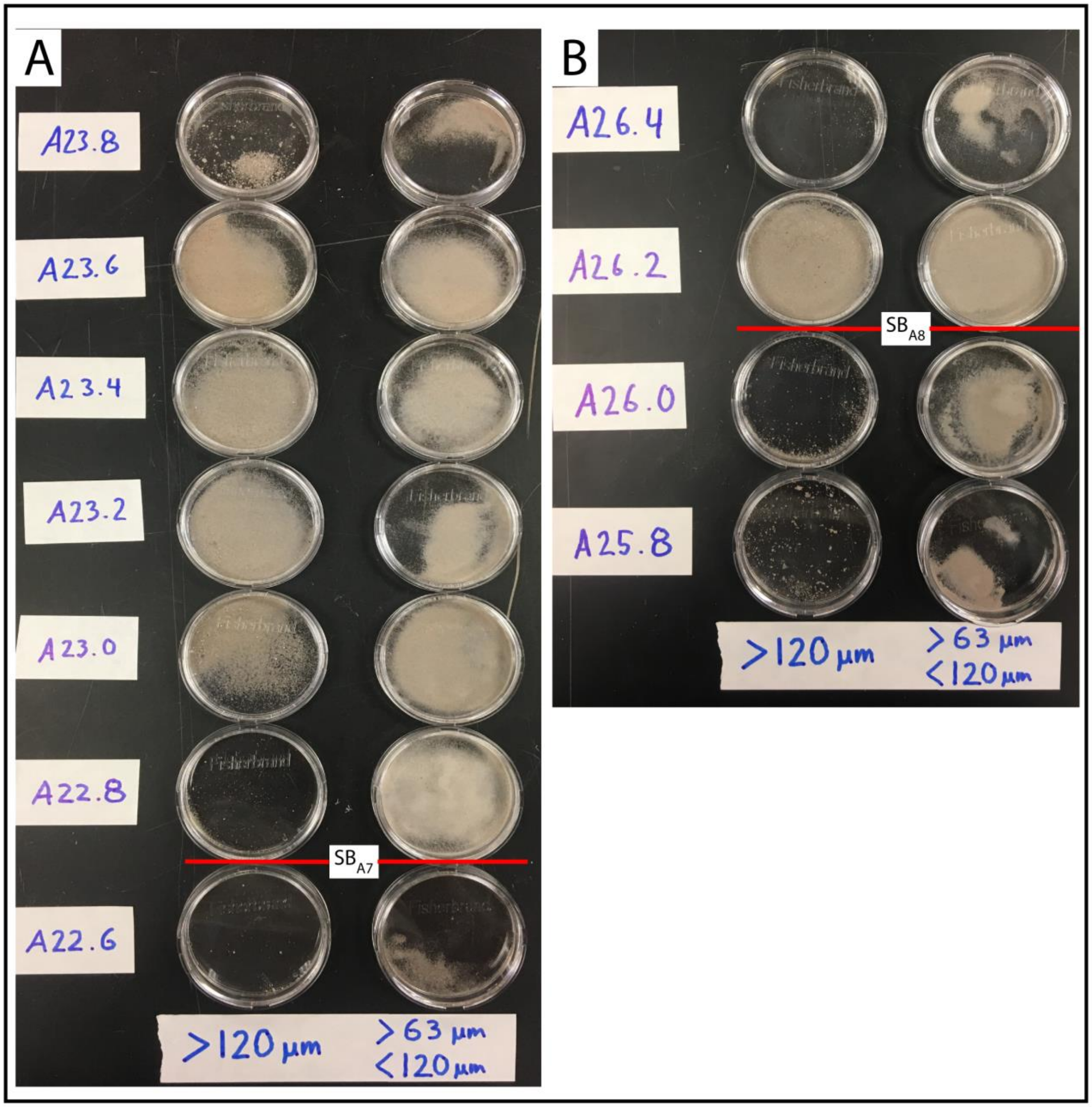

Photos of the sieved fractions of the SMF. Note the sudden appearance of large amounts of authigenic quartz above sequence boundaries SB_{A7} (A) and SB_{A8}(B).

Figure 9: Detrital Core photos

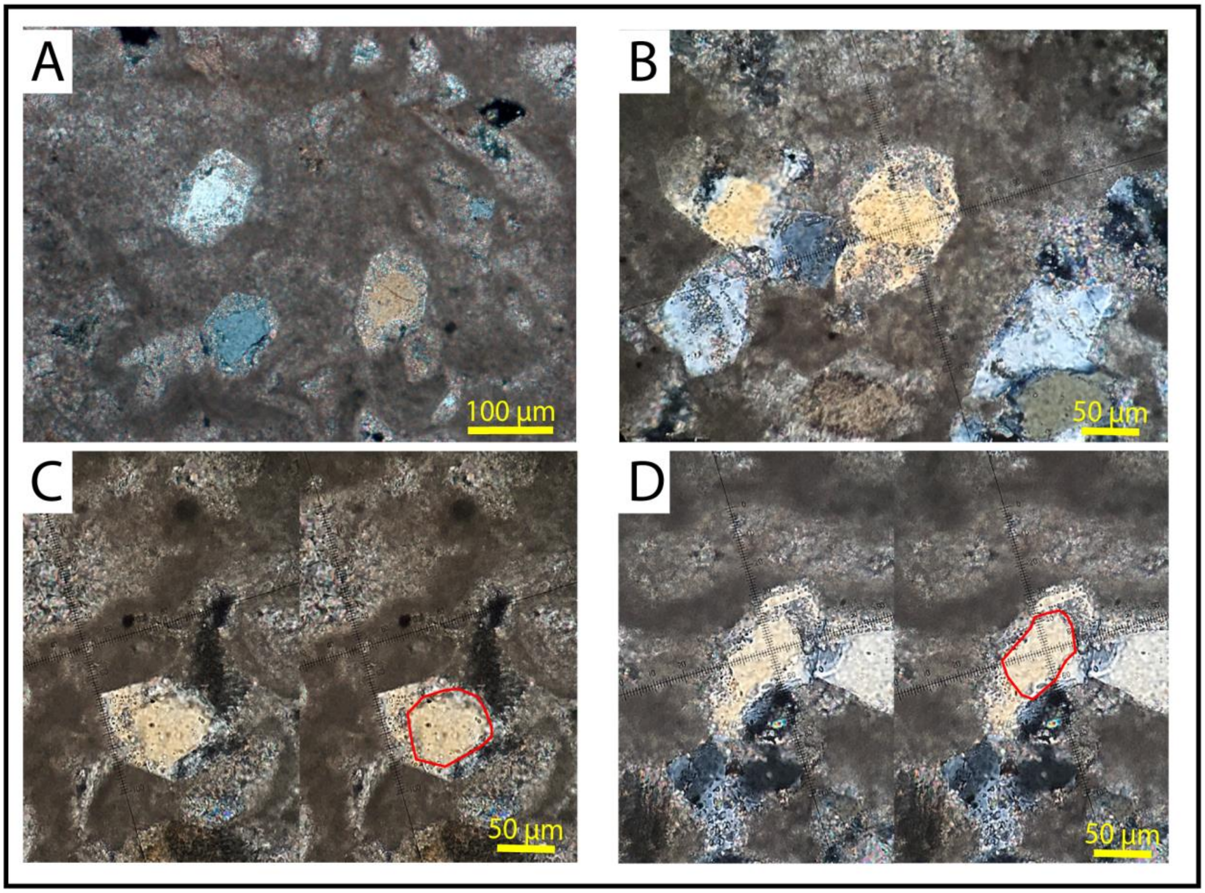

Detrital Cores at the center of authigenic quartz grains. Corrosion is visible along the edges of the detrital grains. In plate C and D, grains are displayed with the detrital core outlined in red on the right side of the image.

Figure 10: Histograms

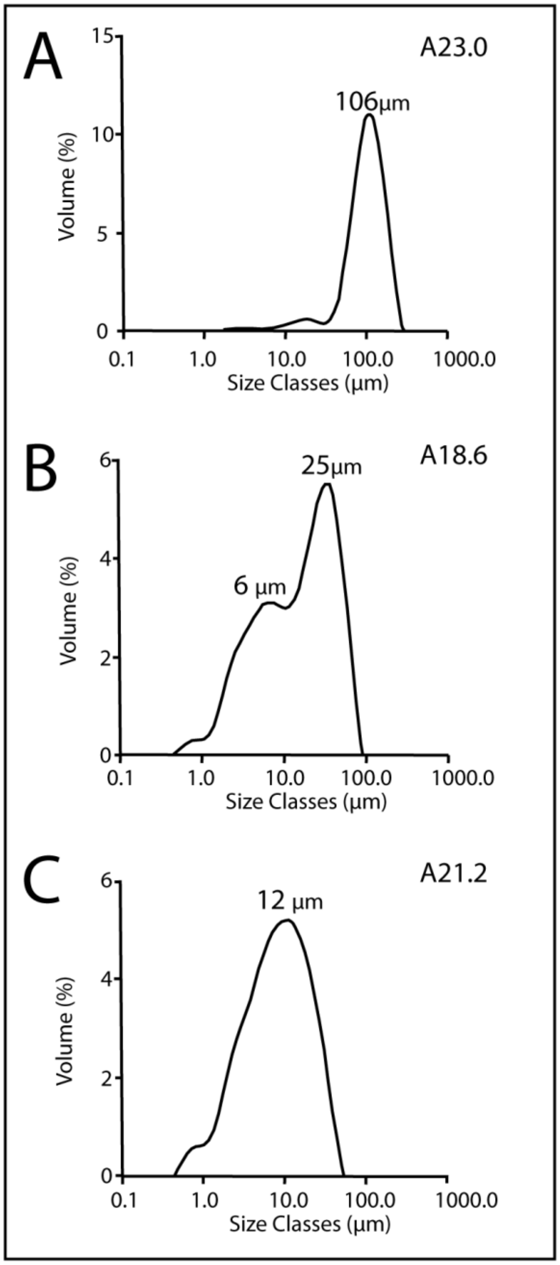

Histograms with large volumes of doubly terminated quartz crystals have small volumes of grains < 30 µm. (A) Sample 23.0 has abundant doubly terminated quartz and a very small volume of grains <30 µm. (B) Sample 18.6 has a smaller fraction of doubly terminated quartz and retains a fraction <30 µm. (C) Sample 21.2 has no double terminated quartz and the grain size distribution is entirely <30 µm. Note the grain size modes above individual peaks.

Figure 11: Geochemical data plots

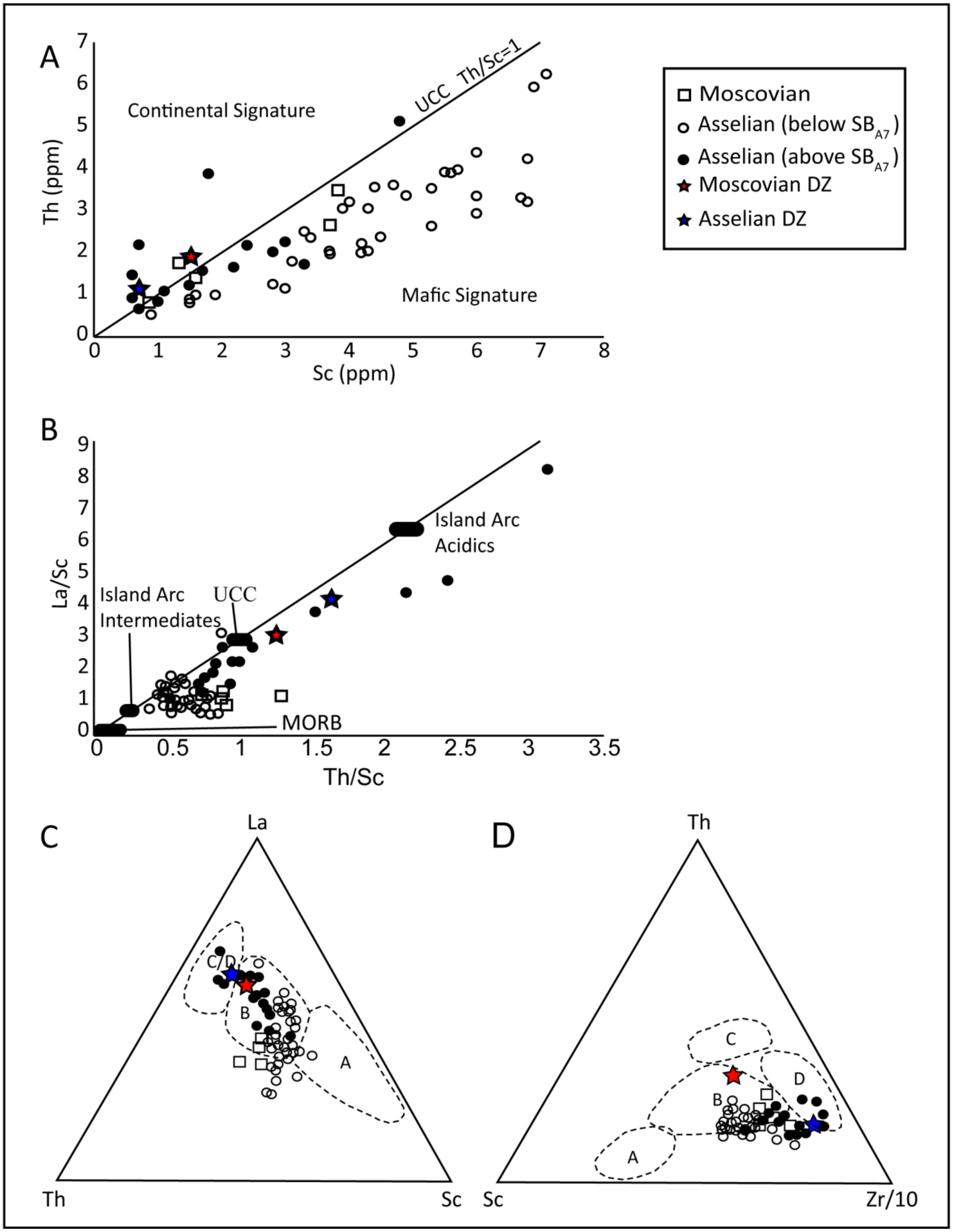

(A) Th vs Sc cross plot (B) La/Sc vs Th/Sc plot (from Totten et al., 2000). See test for detailed description (C) La-Th-Sc and (D) Th-Sc-Zr/10 ternary diagrams show fields that discriminate tectonic environment: A- Oceanic Island Arc; B- Continental Island Arc; C- Active Continental Margins; D- Passive Margins (from Bahatia and Crook, 1986).

Figure 12: Probability density plots

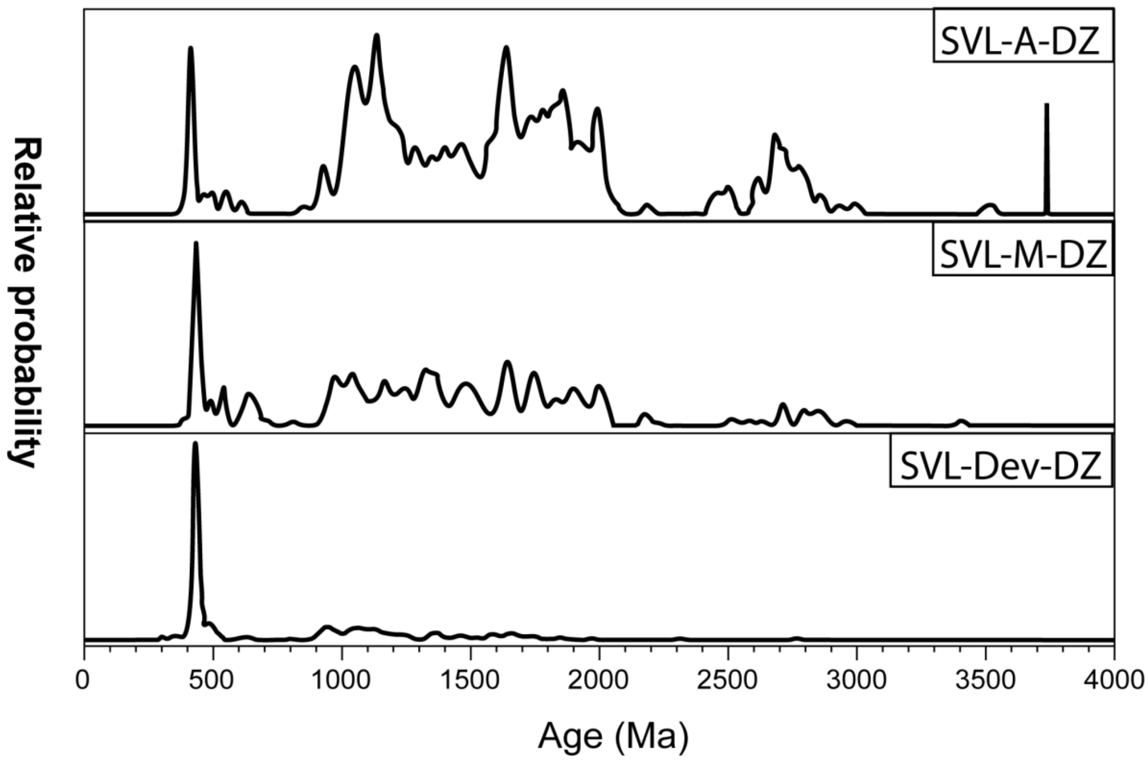

Probability Density Plots of Detrital Zircon Data. (SVL-DEV-DZ) Devonian detrital zircon sample, (SVL-M-DZ) Moscovian detrital zircon sample, (SVL-A-DZ) Asselian detrital zircon sample.

Figure 13: Detrital Zircon Map

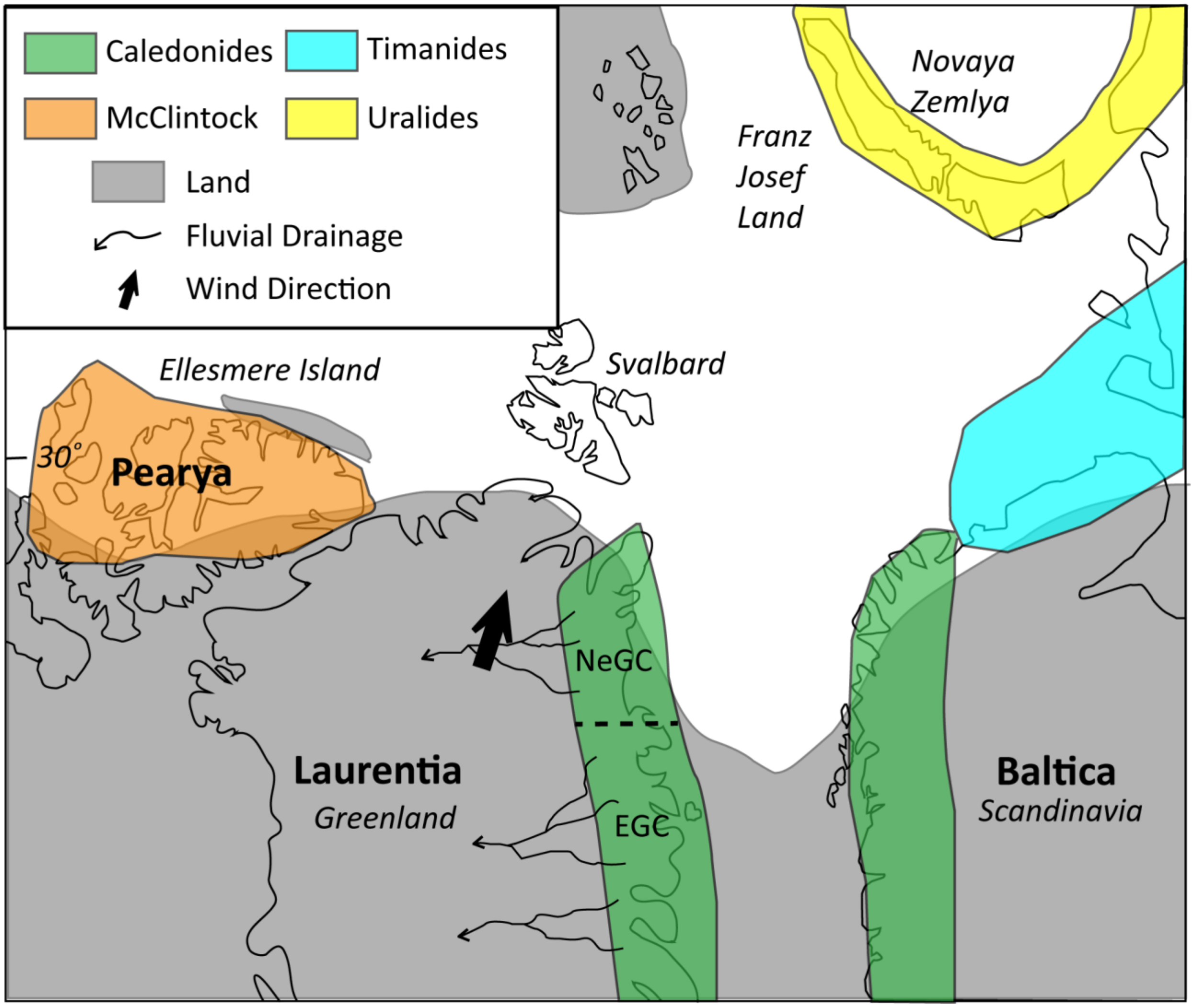

Paleogeographic reconstruction of the Barents Sea region during the late Paleozoic. The northeast Greenland Caledonides (NeGC, north of modern 78°N) were all uplifted basement while in the East Greenland Caledonides (EGC) uplifted Devonian and Carboniferous Strata were uplifted and recycled along with basement. Modified from Stemmerik and Worsely (2005) and Pozer Bue and Andresen (2014).

Figure 14: Schematic of Dust Timing

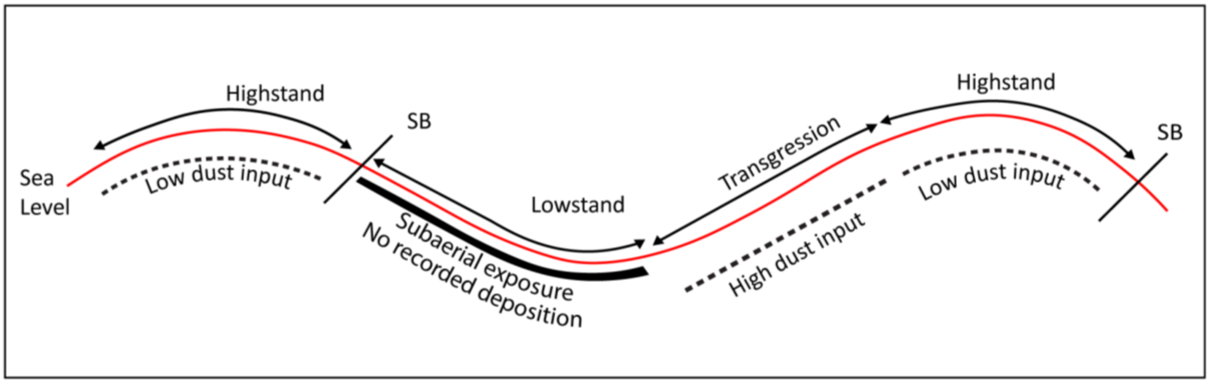

Schematic of dust timing. Highest dust input during transgressive intervals indicates highest dustiness during incipient interglacials. Modified from Carvajal et al. (2018).

Appendix 2: Field and Laboratory Supplements

Field Notes

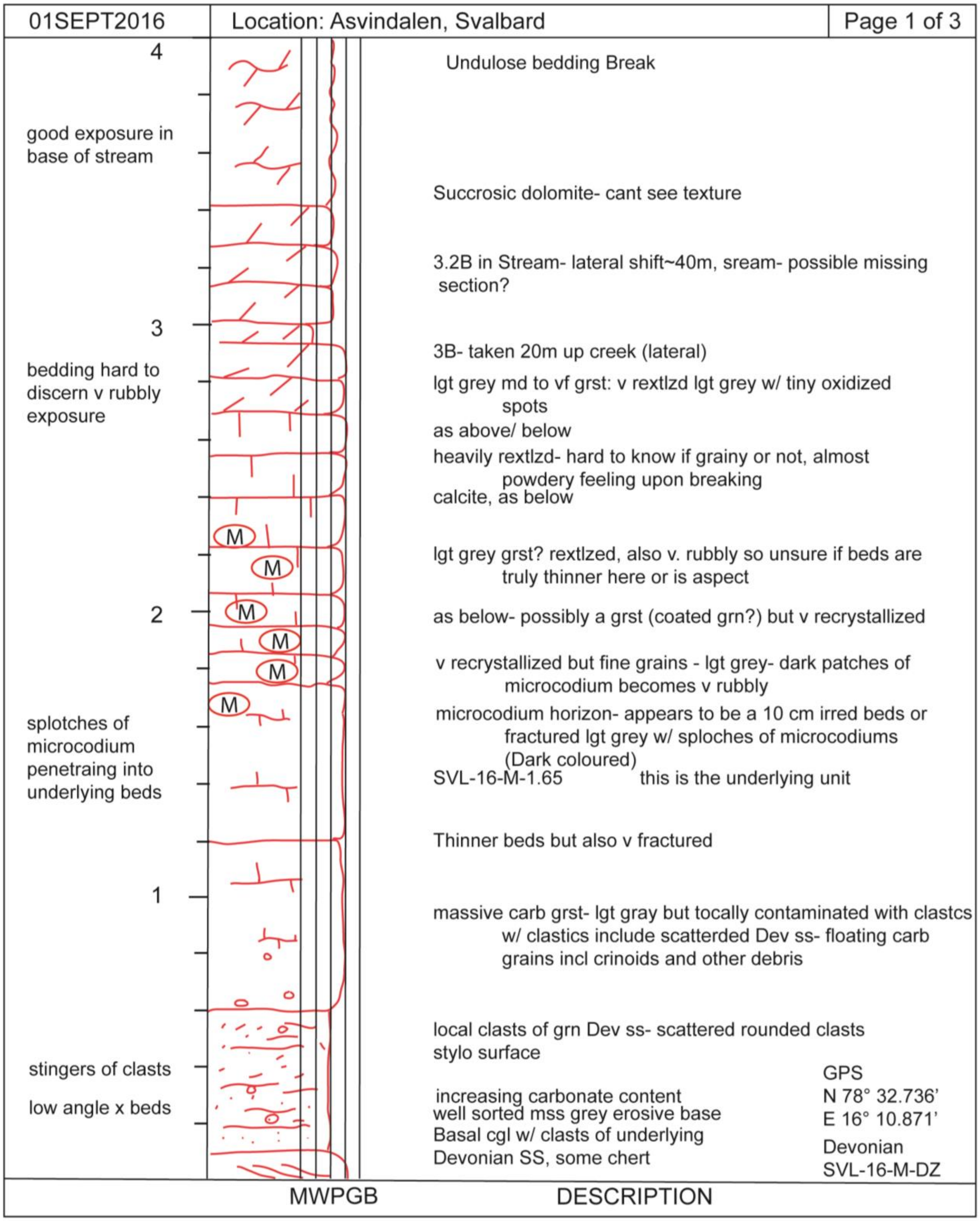

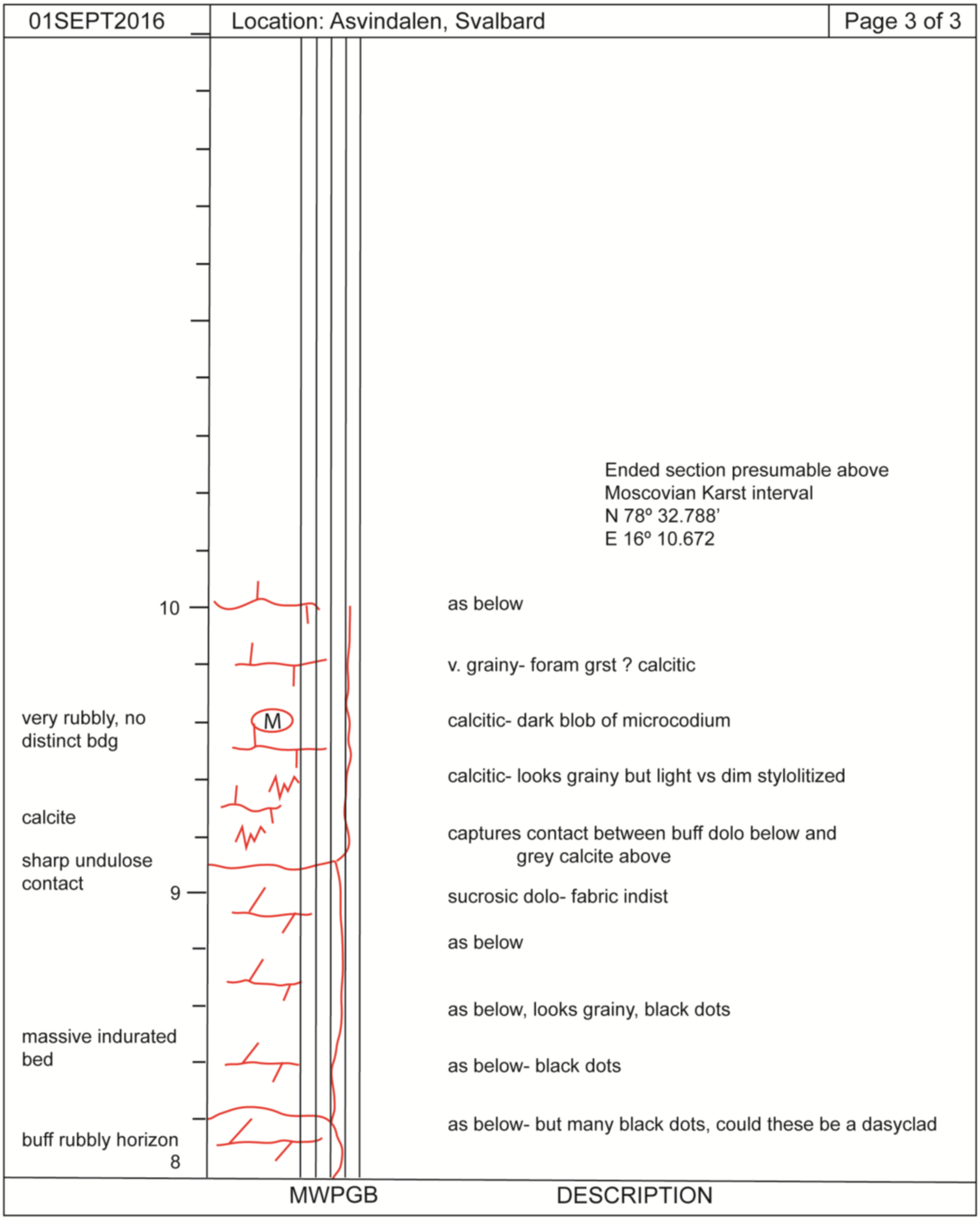
01SEPT2016
Location: Asvindalen, Svalbard
Page 3 of 3
Ended section presumable above
Moscovian Karst interval
N 78º 32.788’
E 16º 10.672
10
as below
v. grainy- foram grst ? calcitic
very rubbly, no
distinct bdg
M
calcitic- dark blob of microcodium
calcitic- looks grainy but light vs dim stylolitized
calcite
captures contact between buff dolo below and
grey calcite above
sharp undulose
contact
9
sucrosic dolo- fabric indist
as below
as below, looks grainy, black dots
massive indurated
bed
as below- black dots
as below- but many black dots, could these be a dasyclad
buff rubbly horizon
8
MWPGB
DESCRIPTION

01SEPT2016	Location: Asvindalen, Svalbard	Page 2 of 3

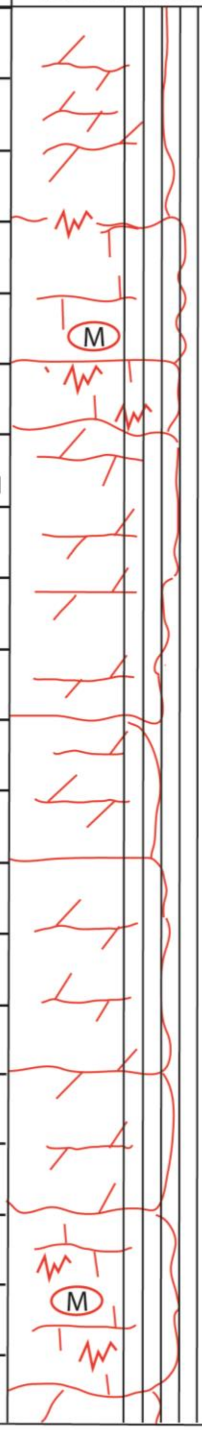

Notes	Depth	Description
	8	as below
		as below but starting to see small black dots
rubbly difficult to sample		dolo- sucrosic, fabric unclear
good bdg plane		Moved upstream to sample but traced beds hard, grst- lmst, faint sylos
		Hard- singer-grst, see small brach
stylos 20 cm ampl	7	hard- possible grst, poss microcodium ? calcitic
dolo reddish on weathered surface		possibly finely grained, sucrosic dolo as above
skattered karst holes		a bit harder than below impossible to tell grst/pkst/wkst
		cavities
karst holes	6	laterally along this horizon lrg karst cavities
		as below - sucrosic but also crushes into powder easily so weathered! all of this sucrosic dolo is also v porous.
		as below
		as bekow vf. sucrosic buff dolo
starting to see karst holes		massiv bdg but with karst cavities up to 10 cm
	5	k.f. grainstone- dolomitized, fairly massive
buff		sucrosic xtlln dolo- possibly tiny grains
microkarst holes		back to sucrosic xtlln dolo
grayish		grey calcitic, appears v. crainy- coated grst, small forams? stylos of ~15cm amplitude
		grey -w/ crinoids - poss pkst texture but still hard to see
stylos 15cm	4	buff
	MWPGB	DESCRIPTION

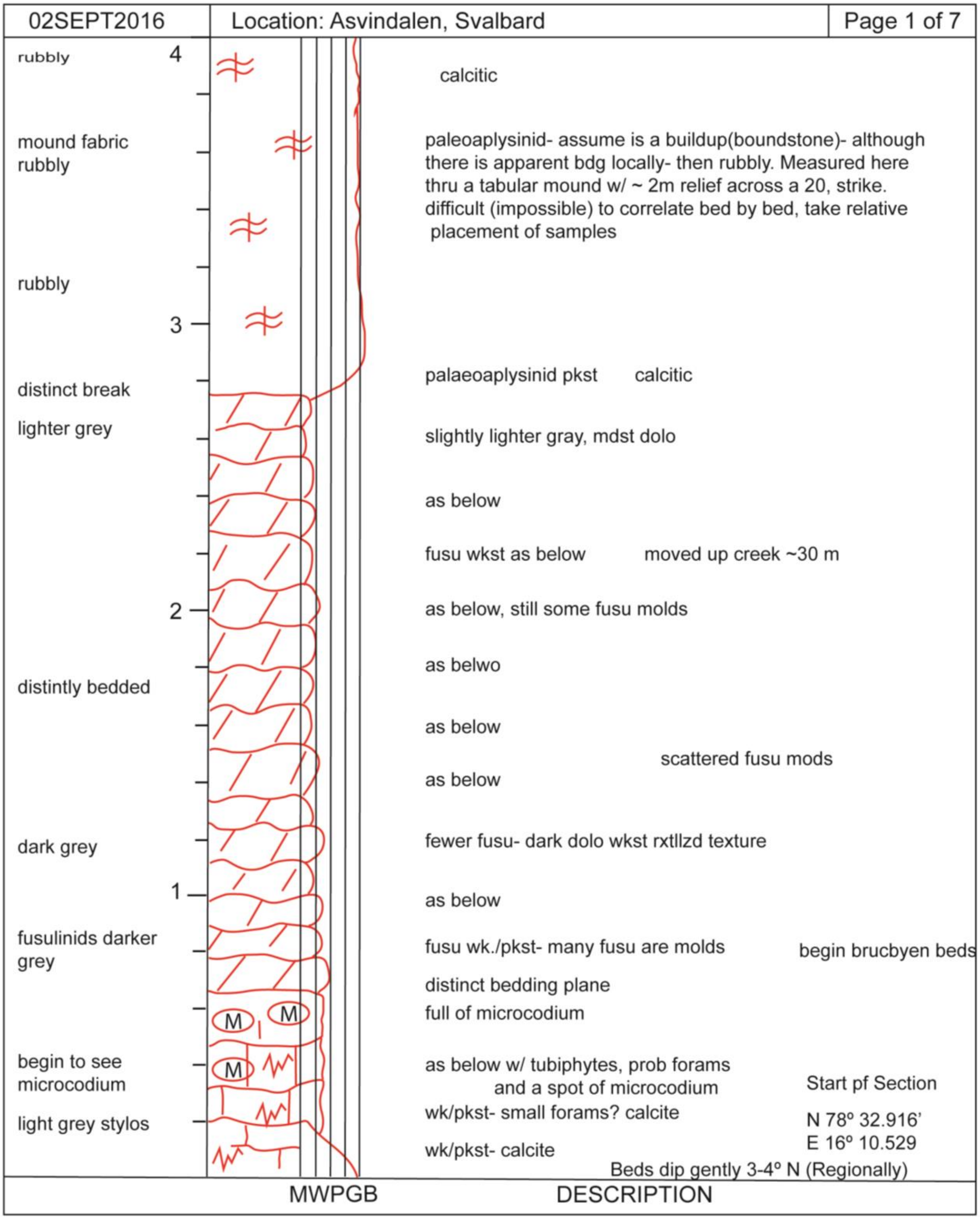
02SEPT2016
Location: Asvindalen, Svalbard
Page 1 of 7
rubbly
4
calcitic
mound fabric
rubbly
paleoaplysinid- assume is a buildup(boundstone)- although there is apparent bdg locally- then rubbly. Measured here thru a tabular mound w/ ~ 2m relief across a 20, strike. difficult (impossible) to correlate bed by bed, take relative placement of samples
rubbly
3
distinct break
palaeoaplysinid pkst calcitic
lighter grey
slightly lighter gray, mdst dolo
as below
fusu wkst as below
moved up creek ~30 m
2
as below, still some fusu molds
distintly bedded
as belwo
as below
scattered fusu mods
as below
dark grey
fewer fusu- dark dolo wkst rxtllzd texture
1
as below
fusulinids darker grey
fusu wk./pkst- many fusu are molds
begin brucbyen beds
distinct bedding plane
full of microcodium
M
M
M
begin to see microcodium
as below w/ tubiphytes, prob forams and a spot of microcodium
Start pf Section
light grey stylos
wk/pkst- small forams? calcite
N 78º 32.916'
E 16º 10.529
wk/pkst- calcite
Beds dip gently 3-4º N (Regionally)
MWPGB
DESCRIPTION

02SEPT2016	Location: Asvindalen, Svalbard	Page 2 of 7

Notes	m	Description
	8	
		palaeoaplysinid bdst check inf dolo in lab (out of acid)
transition into rubbly mound		transition into rubbly mound
		as below
buff - lgt grey as below		rextllzd
bedded	7	dolo- rextllzd - check for possibl calcrete or microcodium
		dolomitic- rextllzd
lgt grey		as above
bedded		fusulinid wkst - molds, changes to dolo
15cm amp stylos		palaeoaplysinids- a lot
stylos ~ 2-3 cm amplitude	6	begin to see small palaeoaplysinid pkst
		calcite, poss microcodium splotch, poss pkst texture
		calcite
15-25 cm beds		xtlln texture
buff		
top of mounded interval		dolomitic texture uncertain
v. rubbly outcrop	5	dolomitic
		foram pkst
dk grey		calcite
		tubiphytes, foram pkst
v. rubbly		palaeoaplysinids

MWPGB DESCRIPTION

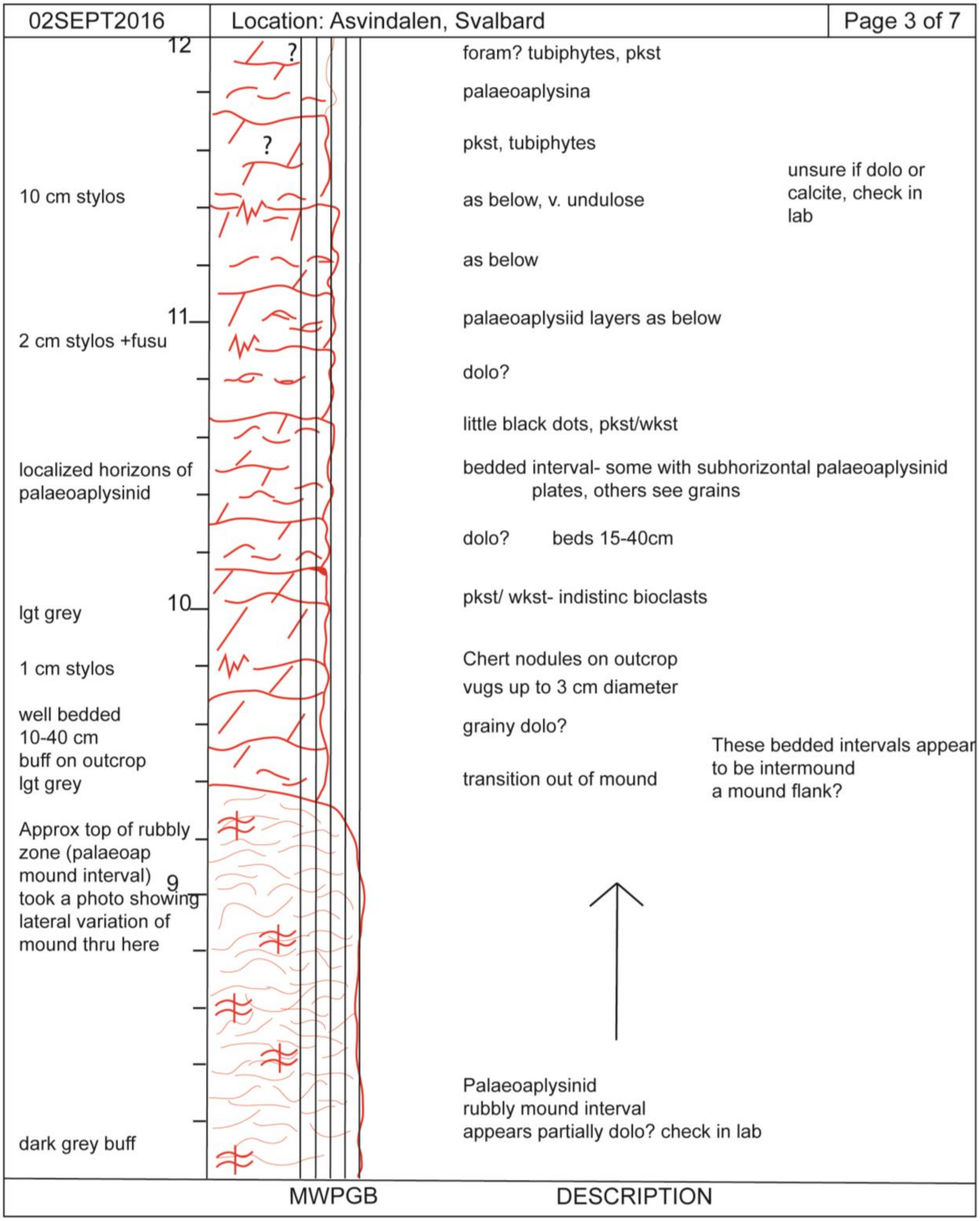
02SEPT2016
Location: Asvindalen, Svalbard
Page 3 of 7
12
foram? tubiphytes, pkst
palaeoaplysina
pkst, tubiphytes
unsure if dolo or calcite, check in lab
10 cm stylos
as below, v. undulose
as below
11
palaeoaplysiid layers as below
2 cm stylos +fusu
dolo?
little black dots, pkst/wkst
localized horizons of palaeoaplysinid
bedded interval- some with subhorizontal palaeoaplysinid plates, others see grains
dolo? beds 15-40cm
10
lgt grey
pkst/ wkst- indistinc bioclasts
1 cm stylos
Chert nodules on outcrop
vugs up to 3 cm diameter
well bedded
10-40 cm
buff on outcrop
lgt grey
grainy dolo?
These bedded intervals appear to be intermound a mound flank?
transition out of mound
Approx top of rubbly zone (palaeoap mound interval)
9
took a photo showing lateral variation of mound thru here
dark grey buff
Palaeoaplysinid
rubbly mound interval
appears partially dolo? check in lab
MWPGB
DESCRIPTION

02SEPT2016	Location: Asvindalen, Svalbard	Page 4 of 7

Notes	m	Description	Remarks
	16	fusu	
		can't see	
lgt grey		as below	
buff		as below	
buff grey bedded		vaguely grainy but xtlln	back to buff bedding succession like below the microcodium A13.4
	15	xtlln texture	
		check for microcodium	
		as below	GPS coord N 78º 33.003' E 16º 10.310'
		xtalln texture, fusu molds	
		am drawing as dolo but check	
	14	palaeoaplysinid	
		apparent grst pkstt, foram, grainy, fusu	
buff grey beds		as above	
dk grey		palaeoaplysina horizon	
		microcod ends here	
dk grey and rubbly			
up on hill	13	microcod horizon	
lgt grey buff			check for dolo v calcite
bedded as below		palaeoaplysina layer?	bedded as below
		palaeoaplysina	
2 cm stylo		fenestrate bryozoan fusu donezella?	
		palaeoaplysinid hash	
		MWPGB	DESCRIPTION

02SEPT2016	Location: Asvindalen, Svalbard	Page 5 of 7

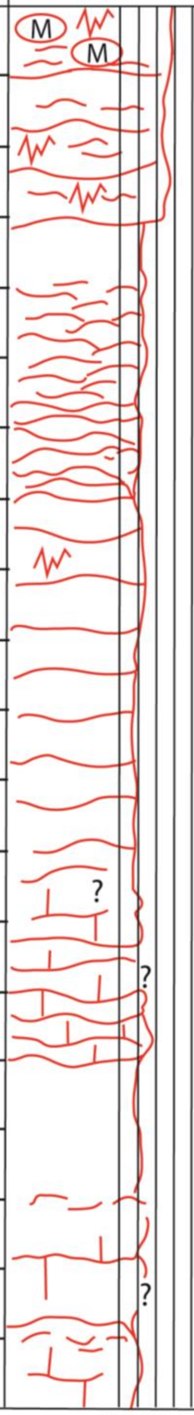

1 cm stylos	20	microcodium
		palaeoaplysinids + other grains, pkst
bedded 10-20 cm		
4 cm stylos		palaeoaplysinids
dk grey v. rubbly outcrop (overhand) w/ gypsum infilling (rextllzd)		fusu wkst
	19	same is this a mound
		dk greu wkst
smakk stylo		stopped 02SEPT @ 4 PM
med grey		insert description and dolo vs calcite later in lab
dk grey	18	
dk grey		
dk grey		
dk grey		fusu wkst- thicker bed than below
dk grey		v rubbly, dug out late on 02SEPT
	17	
lgt grey		
		palaeoaplysinids
lgt grey		
		palaeoaplysinids
dk grey		fusu molds, calcite

MWPGB   DESCRIPTION

03SEPT2016	Location: Asvindalen, Svalbard	Page 6 of 7

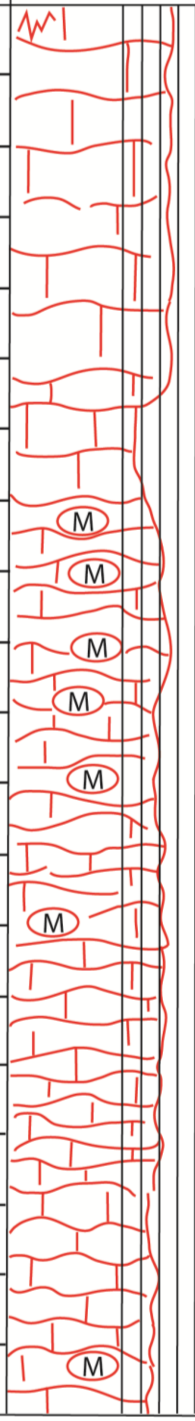

3 cm stylo	24	tubi foram pkst/grst
		as below poss rextllzed
lgt grey buff as below		as below
prob 10-30 cm beds		tubiphyres foram pkst/grst
	23	v tiny grains tubi forams
lgt grey buff		mudst?? or recrystallzd
v. distinct break		microcod/ laminar calcrete
		tubiphytes fusu pkst
patchy microcod thru here		tubiphytes fusu pkst/grst
	22	microcod tubi palaeoap
		abundant microcod
grey		palaeoaply tubi pkst
poss thinner bdg 5-10 cm undulose		microcod
		as below
	21	palaeoaply tubi pkst
med grey		tubiphytes fusu pkst
undulose thin bedding		palaeoaplysinid wkst
med grey		tubiphytes fusu pkst
stylos		palaeoaplysinids tubi poss microcod

MWPGB DESCRIPTION

03SEPT2016	Location: Asvindalen, Svalbard	Page 7 of 7

28

Asselian 117
samples + 1 DZ

From 26.6 it is another roughly 4.4 m to the siltstone with DZ sampples (assuming zero dip) so only an estimate. Could be 5-6 m?
GPS N 78º 33.090'
E 16º 10.123'

27

End of section
GPS N 78º 33.050'
E 16º 10.195'

tubiphyres foram pkst

dark grey in
fresh

26

microcodium a bit

4 cm stylo

as below

10 cm ampl
stylo

25

tubiphytes foram grst/pkst

small stylo

tubyphytes foram pkst/grst

4 cm ampl stylo

as belwo but w/ stylos

bdg as below

tubiphytes pkst grst

as below

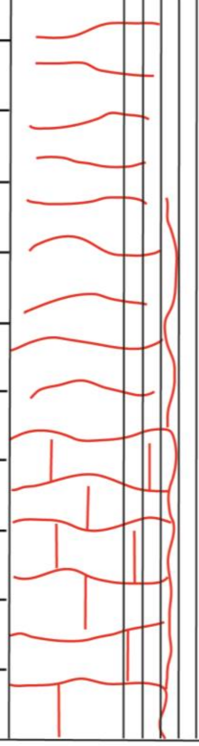

MWPGB

DESCRIPTION

Comprehensive Dust Data

Sample (m)	Section	Facies	SMF wt %	<120 µm wt %	>120 um wt %	63<x<120 wt %	<63 um wt %	"Dust"	Dx (10) µm	Dx (50) µm	Dx (90) µm	Mode (µm)	Volume Below 2.5 µm	Vol Between 2.5-10 µm	Vol Below 10 um	Volume Below 20 um	Volume Below 63 um
1.65	Moscovian	BC WS	1.16	1.07	0.10	0.08	0.99	1.07	3.43 µm	21.0 µm	83.2 µm	34.2	5.94%	24.98%	30.92%	48.68%	83.00%
1.75	Moscovian	BC WS	0.88	0.55	0.33	0.00	0.55	0.55	4.29 µm	41.1 µm	118 µm	75.9	4.62%	17.32%	21.94%	33.38%	64.88%
2	Moscovian	BC WS	0.86	0.85	0.01	0.05	0.80	0.85	2.87 µm	15.8 µm	67.2 µm	34.9	7.95%	30.11%	38.05%	56.32%	88.28%
2.2	Moscovian	BC WS	5.05	1.28	3.77	0.13	1.14	1.28	4.89 µm	37.1 µm	107 µm	65.2	4.20%	15.47%	19.67%	33.06%	69.65%
2.4	Moscovian	BC WS	1.14	0.98	0.16	0.11	0.87	0.98	3.29 µm	21.2 µm	88.4 µm	43.5	6.62%	23.96%	30.58%	48.37%	81.00%
2.6	Moscovian	BC WS	0.99	0.94	0.06	0.08	0.85	0.94	3.58 µm	20.5 µm	85.0 µm	31.4	5.67%	24.88%	30.55%	49.29%	82.32%
2.8	Moscovian	BC WS	2.61	2.61	0.00	6.81	0.14	2.61	4.26 µm	17.3 µm	56.4 µm	19	4.76%	25.52%	30.28%	55.50%	92.30%
3	Moscovian	BC WS	0.56	0.38	0.17	0.00	0.38	0.38	3.91 µm	23.4 µm	110 µm	27	4.78%	23.70%	28.48%	45.84%	75.86%
3.2	Moscovian	BC WS	0.40	0.15	0.25	0.00	0.15	0.15	5.47 µm	27.6 µm	108 µm	67.7	2.32%	20.33%	22.66%	41.18%	73.74%
3.4	Moscovian	BC WS	0.33	0.23	0.10	0.00	0.23	0.23	2.07 µm	10.3 µm	102 µm	5.22	13.52%	35.95%	49.47%	61.43%	80.00%
3.6	Moscovian	BC WS	1.55	1.30	0.24	0.06	1.24	1.30	3.81 µm	18.1 µm	63.1 µm	24.8	5.47%	25.36%	30.83%	53.41%	89.80%
3.8	Moscovian	BC WS	0.43	0.37	0.06	0.01	0.36	0.37	3.28 µm	15.9 µm	56.3 µm	19.8	6.91%	27.46%	34.37%	58.42%	91.94%
4	Moscovian	BC WS	0.44	0.41	0.03	0.02	0.39	0.41	2.71 µm	12.2 µm	50.5 µm	17	8.71%	35.16%	43.87%	64.91%	93.90%
4.2	Moscovian	B PS/CS	0.54	0.54	0.00	0.01	0.53	0.54	2.70 µm	7.31 µm	25.1 µm	6.22	7.99%	55.53%	63.52%	85.36%	98.77%
4.4	Moscovian	B PS/CS	0.87	0.82	0.06	0.05	0.77	0.82	2.53 µm	8.63 µm	41.1 µm	7.24	9.79%	45.71%	55.51%	76.39%	94.78%
4.6	Moscovian	BC WS	1.01	0.93	0.07	0.03	0.91	0.93	3.85 µm	11.3 µm	38.6 µm	10.8	5.39%	38.28%	43.67%	75.44%	94.79%
4.8	Moscovian	BC WS	0.95	0.75	0.20	0.05	0.70	0.75	5.00 µm	15.3 µm	82.4 µm	12.5	3.67%	27.70%	31.38%	60.54%	85.48%
5	Moscovian	BC WS	2.96	2.83	0.13	0.13	2.71	2.83	2.39 µm	8.70 µm	32.8 µm	7.66	10.87%	44.37%	55.23%	77.69%	99.01%
5.2	Moscovian	BC WS	1.86	1.79	0.08	0.09	1.70	1.79	2.51 µm	14.1 µm	54.5 µm	32.1	9.96%	31.22%	41.18%	59.59%	93.11%
5.4	Moscovian	BC WS	2.84	2.47	0.37	0.13	2.34	2.47	2.83 µm	11.2 µm	44.3 µm	8.84	7.97%	38.11%	46.07%	68.66%	95.77%
5.6	Moscovian	BC WS	0.78	0.74	0.04	0.03	0.72	0.74	3.22 µm	15.9 µm	65.2 µm	23.5	6.69%	29.53%	36.22%	56.91%	89.06%
5.8	Moscovian	BC WS	2.26	2.13	0.13	0.12	2.01	2.13	3.70 µm	15.0 µm	58.2 µm	13.2	5.44%	30.19%	35.63%	59.92%	91.40%
6	Moscovian	BC WS	2.33	2.18	0.15	0.18	2.00	2.18	4.02 µm	15.0 µm	78.6 µm	12.4	4.83%	29.89%	34.72%	60.12%	85.72%
6.2	Moscovian	BC WS	9.50	4.48	5.03	0.95	3.53	4.48	4.35 µm	14.7 µm	51.1 µm	13.3	3.50%	30.98%	34.48%	62.02%	93.58%
6.4	Moscovian	BC WS	0.62	0.48	0.13	0.00	0.48	0.48	4.78 µm	22.9 µm	84.1 µm	38.4	3.63%	21.91%	25.55%	45.81%	82.18%
6.6	Moscovian	BC WS	1.47	1.40	0.07	0.07	1.33	1.40	3.86 µm	14.8 µm	60.1 µm	11.7	4.92%	30.95%	35.86%	60.10%	90.78%
6.8	Moscovian	BC WS	4.94	2.01	2.93	0.12	1.88	2.01	3.22 µm	13.2 µm	84.2 µm	8.22	6.04%	35.60%	41.63%	60.67%	83.25%
7	Moscovian	BC WS	0.50	0.36	0.14	0.05	0.32	0.36	3.82 µm	28.2 µm	113 µm	71.7	4.91%	22.83%	27.74%	42.09%	72.12%
7.2	Moscovian	BC WS	0.39	0.38	0.01	0.01	0.37	0.38	4.07 µm	19.8 µm	65.4 µm	31.6	4.48%	24.97%	29.46%	50.38%	88.86%
7.4	Moscovian	BC WS	0.20	0.20	0.00	0.07	0.13	0.20	3.27 µm	15.4 µm	56.0 µm	29	6.26%	30.75%	37.01%	58.10%	92.50%
7.6	Moscovian	BC WS	0.10	0.10	0.00	0.00	0.10	0.10	2.57 µm	11.1 µm	47.3 µm	7.24	9.53%	37.26%	46.79%	67.01%	94.97%
7.8	Moscovian	BC WS	0.44	0.44	0.00	0.01	0.43	0.44	2.83 µm	13.6 µm	51.4 µm	20.9	8.27%	32.24%	40.50%	62.58%	93.48%
8	Moscovian	BC WS	1.21	1.13	0.08	0.06	1.07	1.13	3.36 µm	13.3 µm	49.8 µm	10.8	6.44%	33.26%	39.70%	63.89%	94.03%
8.2	Moscovian	BC WS	1.05	1.05	0.00	0.02	1.03	1.05	6.05 µm	15.9 µm	43.6 µm	15.3	3.17%	23.16%	26.32%	61.78%	95.99%
8.4	Moscovian	BC WS	1.73	1.73	0.00	0.21	1.51	1.73	5.93 µm	16.3 µm	63.2 µm	14.3	3.20%	23.55%	26.74%	59.54%	89.84%
8.6	Moscovian	BC WS	2.68	2.62	0.06	0.15	2.47	2.62	6.11 µm	16.2 µm	53.6 µm	14.1	2.41%	24.08%	26.49%	59.86%	92.69%
8.8	Moscovian	BC WS	1.53	1.51	0.02	0.07	1.43	1.51	5.27 µm	17.0 µm	51.5 µm	16.7	3.76%	23.34%	27.10%	57.46%	93.62%
9	Moscovian	BC WS	1.18	1.12	0.06	0.07	1.05	1.12	5.01 µm	17.9 µm	67.5 µm	15.2	3.93%	23.54%	27.48%	54.31%	88.35%

Sample (m)	Section	Facies	SMF wt %	<120 µm wt %	>120 um wt %	63<x<120 wt %	<63 um wt %	"Dust"	Dx (10) µm	Dx (50) µm	Dx (90) µm	Mode (µm)	Volume Below 2.5 µm	Vol Between 2.5-10 µm	Vol Below 10 um	Volume Below 20 um	Volume Below 63 um
9.2	Moscovian	BC WS	1.85	1.77	0.08	0.13	1.63	1.77	4.74 µm	15.7 µm	74.8 µm	13.2	4.02%	27.15%	31.18%	59.33%	87.08%
9.4	Moscovian	BC WS	2.08	1.87	0.21	0.15	1.72	1.87	4.13 µm	17.0 µm	77.3 µm	12.7	4.49%	27.67%	32.17%	55.16%	85.54%
9.6	Moscovian	B PS/CS	2.19	2.03	0.16	0.13	1.90	2.03	4.20 µm	21.4 µm	91.3 µm	26.6	4.22%	24.28%	28.51%	47.95%	80.83%
9.8	Moscovian	B PS/CS	2.97	2.72	0.25	0.34	2.38	2.72	4.42 µm	20.6 µm	77.9 µm	28.9	4.49%	23.30%	27.79%	49.13%	84.36%
10	Moscovian	B PS/CS	2.16	1.97	0.18	0.15	1.83	1.97	6.02 µm	26.6 µm	78.0 µm	38.1	3.20%	16.42%	19.61%	39.74%	83.30%
0	Asselian	Palaeo F	0.04	0.04	0.00	0.00	0.04	0.04	40.00	3.71 µm	22.5 µm	81.0 µm	4.83%	25.36%	30.20%	46.78%	83.42%
0.2	Asselian	Palaeo F	0.06	0.06	0.00	0.00	0.06	0.06	-	-	-	-	-	-	-	-	-
0.4	Asselian	Palaeo F	0.03	0.03	0.00	0.00	0.03	0.03	-	-	-	-	-	-	-	-	-
0.6	Asselian	Palaeo F	0.06	0.06	0.00	0.00	0.06	0.06	37.30	4.35 µm	24.6 µm	88.0 µm	3.79%	21.80%	25.59%	43.53%	81.51%
0.8	Asselian	Fusu WS	2.42	2.42	0.00	0.05	2.37	2.42	17.10	2.71 µm	10.8 µm	34.1 µm	8.44%	38.80%	47.25%	72.64%	99.08%
1	Asselian	Fusu WS	2.63	2.53	0.10	0.05	2.47	2.53	6.99	2.37 µm	7.77 µm	25.6 µm	11.30%	48.38%	59.69%	83.36%	99.95%
1.2	Asselian	Fusu WS	5.62	5.52	0.10	0.09	5.43	5.52	25.00	2.94 µm	15.5 µm	49.1 µm	7.45%	29.27%	36.72%	58.91%	94.91%
1.4	Asselian	Fusu WS	3.83	3.08	0.74	0.19	2.90	3.08	17.50	2.81 µm	11.8 µm	35.7 µm	7.91%	36.08%	43.99%	70.32%	98.77%
1.6	Asselian	Fusu WS	7.82	6.33	1.49	0.13	6.20	6.33	19.50	2.62 µm	10.4 µm	36.9 µm	9.08%	39.78%	48.87%	71.42%	98.58%
1.8	Asselian	Fusu WS	1.47	1.43	0.04	0.02	1.41	1.43	62.50	3.62 µm	27.1 µm	92.7 µm	5.49%	22.92%	28.41%	43.10%	76.24%
2	Asselian	Fusu WS	1.30	1.30	0.00	0.01	1.29	1.30	9.61	2.61 µm	10.4 µm	36.5 µm	9.14%	39.41%	48.55%	71.68%	98.81%
2.2	Asselian	BC WS	2.52	2.52	0.00	0.33	2.19	2.52	6.20	2.55 µm	8.96 µm	42.0 µm	9.57%	44.04%	53.60%	72.97%	96.15%
2.4	Asselian	BC WS	0.59	0.59	0.00	0.04	0.55	0.59	7.04	2.77 µm	12.7 µm	59.4 µm	8.13%	35.38%	43.51%	62.10%	90.99%
2.6	Asselian	BC WS	0.28	0.28	0.00	0.01	0.27	0.28	6.91	2.60 µm	11.3 µm	49.2 µm	9.25%	37.15%	46.40%	65.98%	94.49%
2.8	Asselian	Palaeo B	0.44	0.42	0.02	0.02	0.40	0.42	59.10	6.06 µm	41.3 µm	105 µm	3.54%	12.23%	15.78%	27.29%	68.74%
3	Asselian	Palaeo B	0.59	0.35	0.24	0.03	0.32	0.35	30.70	2.26 µm	20.7 µm	135 µm	11.49%	24.63%	36.13%	49.30%	74.26%
3.2	Asselian	Palaeo B	0.42	0.42	0.00	0.09	0.33	0.42	30.40	3.06 µm	16.8 µm	74.7 µm	7.18%	28.83%	36.02%	54.75%	86.11%
3.4	Asselian	Palaeo B	0.29	0.29	0.00	0.01	0.27	0.29	27.30	2.92 µm	14.7 µm	56.4 µm	7.70%	31.11%	38.81%	59.33%	92.20%
3.6	Asselian	Palaeo B	0.23	0.23	0.00	0.00	0.22	0.23	27.20	2.02 µm	11.4 µm	52.6 µm	13.62%	32.92%	46.55%	64.59%	93.34%
3.8	Asselian	Palaeo B	1.75	1.72	0.03	0.02	1.70	1.72	28.40	2.04 µm	16.8 µm	46.1 µm	12.54%	23.50%	36.04%	56.21%	97.09%
4	Asselian	Palaeo F	0.47	0.19	0.28	0.00	0.00	0.19	38.00	3.56 µm	24.3 µm	66.5 µm	6.64%	18.93%	25.56%	43.30%	88.00%
4.2	Asselian	Palaeo F	1.70	0.73	0.97	0.00	0.73	0.73	26.50	2.81 µm	16.4 µm	47.7 µm	8.57%	26.05%	34.62%	57.41%	96.21%
4.4	Asselian	Palaeo F	0.33	0.33	0.00	0.00	0.33	0.33	25.60	2.46 µm	12.0 µm	50.4 µm	10.30%	34.54%	44.83%	64.49%	94.20%
4.6	Asselian	Palaeo F	0.28	0.28	0.00	0.00	0.28	0.28	7.75	2.31 µm	10.7 µm	46.6 µm	11.41%	36.72%	48.13%	68.01%	95.21%
4.8	Asselian	Palaeo F	0.63	0.53	0.10	0.01	0.52	0.53	32.00	1.89 µm	12.7 µm	58.1 µm	14.25%	30.02%	44.27%	61.47%	91.52%
5	Asselian	Palaeo F	0.86	0.86	0.00	0.04	0.82	0.86	19.30	1.70 µm	10.4 µm	40.7 µm	16.07%	32.83%	48.90%	70.01%	96.79%
5.2	Asselian	BC WS	0.76	0.71	0.04	0.05	0.67	0.71	40.90	3.39 µm	21.5 µm	72.0 µm	6.14%	24.39%	30.53%	47.89%	86.00%
5.4	Asselian	BC WS	1.13	1.13	0.00	0.10	1.03	1.13	37.50	3.34 µm	20.2 µm	64.3 µm	6.22%	25.17%	31.38%	49.65%	89.17%
5.6	Asselian	BC WS	0.85	0.85	0.00	0.13	0.72	0.85	42.20	3.71 µm	23.5 µm	71.2 µm	5.37%	22.58%	27.95%	45.10%	85.97%
5.8	Asselian	BC WS	1.19	1.13	0.05	0.13	1.00	1.13	41.80	4.71 µm	26.0 µm	75.1 µm	4.12%	18.85%	22.97%	41.21%	84.06%
6	Asselian	BC WS	0.73	0.73	0.00	0.06	0.67	0.73	47.00	4.14 µm	26.8 µm	80.6 µm	4.86%	19.95%	24.81%	41.24%	81.61%
6.2	Asselian	BC WS	0.84	0.84	0.00	0.03	0.81	0.84	5.00	3.10 µm	15.6 µm	64.5 µm	7.05%	29.40%	36.45%	57.68%	89.31%
6.4	Asselian	Fusu WS	0.70	0.70	0.00	0.15	0.56	0.70	69.60	4.25 µm	39.5 µm	101 µm	5.01%	17.90%	22.91%	35.47%	68.28%

Sample (m)	Section	Facies	SMF wt %	<120 µm wt %	>120 um wt %	63<x<120 wt %	<63 um wt %	"Dust"	Dx (10) µm	Dx (50) µm	Dx (90) µm	Mode (µm)	Volume Below 2.5 µm	Vol Between 2.5-10 µm	Vol Below 10 um	Volume Below 20 um	Volume Below 63 um
6.6	Asselian	Fusu WS	0.58	0.58	0.00	0.13	0.45	0.58	72.50	5.13 µm	42.3 µm	106 µm	3.47%	17.44%	20.91%	34.15%	65.68%
6.8	Asselian	Fusu WS	2.37	2.37	0.00	0.47	1.91	2.37	62.80	3.80 µm	35.3 µm	92.0 µm	5.54%	21.06%	26.61%	38.61%	73.15%
7	Asselian	Fusu WS	1.07	1.07	0.00	0.19	0.88	1.07	49.90	3.73 µm	24.2 µm	82.3 µm	5.59%	22.34%	27.92%	44.78%	81.47%
7.2	Asselian	Fusu WS	1.37	1.36	0.01	0.18	1.18	1.36	28.50	2.92 µm	14.1 µm	52.7 µm	7.56%	32.49%	40.05%	60.58%	93.66%
7.4	Asselian	Palaeo B	0.71	0.71	0.00	0.06	0.65	0.71	44.60	2.85 µm	17.8 µm	70.8 µm	8.01%	28.20%	36.21%	52.91%	86.62%
7.6	Asselian	Palaeo B	0.78	0.77	0.00	0.06	0.71	0.77	19.30	2.25 µm	11.3 µm	42.0 µm	11.75%	34.54%	46.29%	68.27%	96.97%
7.8	Asselian	Palaeo B	3.21	3.21	0.00	0.51	2.70	3.21	18.30	1.55 µm	9.31 µm	30.7 µm	17.79%	34.30%	52.09%	75.79%	99.73%
8	Asselian	Palaeo B	0.88	0.80	0.08	0.10	0.70	0.80	30.80	2.62 µm	15.6 µm	63.0 µm	9.35%	28.76%	38.11%	57.08%	89.83%
8.2	Asselian	Palaeo B	0.62	0.51	0.11	0.04	0.47	0.51	28.10	2.63 µm	16.7 µm	60.1 µm	9.33%	26.34%	35.68%	55.73%	90.87%
8.4	Asselian	Palaeo B	0.50	0.50	0.01	0.02	0.48	0.50	25.10	2.69 µm	14.8 µm	52.9 µm	8.98%	29.42%	38.40%	59.73%	93.54%
8.6	Asselian	Palaeo B	0.40	0.39	0.01	0.02	0.37	0.39	30.50	3.09 µm	19.0 µm	57.5 µm	7.45%	23.97%	31.42%	51.72%	92.05%
8.8	Asselian	Palaeo B	0.86	0.83	0.03	0.04	0.79	0.83	30.70	3.44 µm	22.0 µm	77.3 µm	6.39%	21.93%	28.32%	46.93%	84.75%
9	Asselian	Palaeo B	0.71	0.66	0.06	0.03	0.63	0.66	30.90	3.46 µm	20.0 µm	60.1 µm	5.99%	23.73%	29.72%	49.95%	90.94%
9.2	Asselian	Palaeo B	2.04	2.00	0.05	0.19	1.81	2.00	35.00	4.60 µm	26.7 µm	63.6 µm	4.43%	15.90%	20.33%	37.88%	89.42%
9.4	Asselian	BC WS	1.97	1.58	0.39	0.15	1.43	1.58	14.30	2.64 µm	11.7 µm	39.8 µm	9.17%	35.17%	44.34%	69.84%	97.05%
9.6	Asselian	BC WS	3.98	3.81	0.17	0.43	3.38	3.81	26.00	3.25 µm	18.8 µm	50.7 µm	6.85%	23.10%	29.95%	52.49%	94.63%
9.8	Asselian	BC WS	3.09	2.97	0.12	0.16	2.81	2.97	13.00	2.15 µm	8.79 µm	27.9 µm	13.05%	41.59%	54.64%	79.84%	99.90%
10	Asselian	BC WS	1.78	1.75	0.03	0.52	1.23	1.75	9.88	2.19 µm	8.33 µm	26.5 µm	12.71%	44.46%	57.17%	82.39%	99.60%
10.2	Asselian	Palaeo F	2.23	2.22	0.01	0.07	2.15	2.22	7.10	1.98 µm	6.36 µm	18.3 µm	15.88%	53.21%	69.09%	92.29%	100.00%
10.4	Asselian	Palaeo F	1.39	1.39	0.00	0.05	1.33	1.39	7.29	1.94 µm	7.04 µm	23.7 µm	15.71%	47.48%	63.20%	85.77%	99.96%
10.6	Asselian	Palaeo F	1.28	1.28	0.00	0.03	1.25	1.28	7.00	2.19 µm	9.13 µm	37.5 µm	12.68%	40.18%	52.86%	73.21%	98.36%
10.8	Asselian	Palaeo B	1.23	1.23	0.00	0.07	1.17	1.23	9.33	2.19 µm	8.45 µm	27.5 µm	12.65%	43.56%	56.21%	80.69%	99.91%
11	Asselian	Palaeo B	1.11	1.11	0.00	0.05	1.07	1.11	8.44	2.16 µm	8.07 µm	26.6 µm	13.07%	44.98%	58.05%	82.14%	99.92%
11.2	Asselian	Palaeo B	1.77	1.77	0.00	0.06	1.71	1.77	8.64	2.16 µm	8.35 µm	28.1 µm	13.02%	43.50%	56.53%	80.29%	99.89%
11.4	Asselian	Palaeo B	1.11	1.08	0.03	0.07	1.01	1.08	10.20	2.57 µm	10.6 µm	37.9 µm	9.49%	38.51%	48.00%	71.40%	98.22%
11.6	Asselian	Palaeo B	1.99	1.99	0.00	0.20	1.79	1.99	28.30	2.90 µm	15.4 µm	57.8 µm	7.92%	29.69%	37.61%	58.04%	91.71%
11.8	Asselian	Palaeo B	2.10	2.01	0.09	0.15	1.86	2.01	10.70	2.24 µm	9.65 µm	34.3 µm	12.02%	39.21%	51.22%	74.46%	98.97%
12	Asselian	Palaeo B	2.29	2.25	0.04	0.11	2.13	2.25	14.00	2.24 µm	10.0 µm	36.4 µm	11.99%	37.85%	49.84%	72.56%	98.57%
12.2	Asselian	Palaeo B	1.89	1.89	0.00	0.15	1.74	1.89	7.64	2.25 µm	8.95 µm	35.3 µm	12.14%	41.58%	53.71%	75.42%	98.15%
12.4	Asselian	Palaeo B	1.79	1.79	0.00	0.06	1.73	1.79	8.10	2.19 µm	7.78 µm	26.7 µm	13.01%	46.76%	59.78%	82.97%	99.72%
12.6	Asselian	Palaeo F	1.42	1.42	0.00	0.08	1.35	1.42	8.02	2.18 µm	8.10 µm	32.9 µm	12.93%	44.92%	57.85%	79.96%	97.30%
12.8	Asselian	Palaeo F	1.29	1.29	0.00	0.07	1.23	1.29	25.10	2.45 µm	12.3 µm	47.7 µm	10.32%	33.72%	44.05%	64.59%	95.34%
13	Asselian	Palaeo F	2.96	2.96	0.00	0.03	2.94	2.96	9.90	2.18 µm	8.19 µm	23.6 µm	12.67%	45.68%	58.35%	85.17%	100.00%
13.2	Asselian	Palaeo F	5.11	2.88	2.23	0.64	2.24	2.88	24.00	2.63 µm	13.3 µm	42.8 µm	9.27%	31.29%	40.55%	64.87%	96.79%
13.4	Asselian	BC WS	0.81	0.57	0.23	0.04	0.53	0.57	21.50	2.83 µm	15.1 µm	46.2 µm	8.43%	27.45%	35.88%	60.73%	95.80%
13.6	Asselian	BC WS	1.76	1.70	0.07	0.40	1.30	1.70	22.70	3.68 µm	19.7 µm	89.5 µm	5.83%	23.88%	29.70%	50.56%	83.21%
13.8	Asselian	BC WS	2.04	1.95	0.09	0.34	1.61	1.95	20.60	2.78 µm	14.0 µm	49.2 µm	8.50%	30.57%	39.07%	62.40%	94.20%
14	Asselian	BC WS	2.32	2.17	0.15	0.62	1.55	2.17	27.00	3.96 µm	22.6 µm	91.9 µm	5.25%	21.57%	26.83%	46.15%	81.17%

Sample (m)	Section	Facies	SMF wt %	<120 µm wt %	>120 um wt %	63<x<120 wt %	<63 um wt %	"Dust"	Dx (10) µm	Dx (50) µm	Dx (90) µm	Mode (µm)	Volume Below 2.5 µm	Vol Between 2.5-10 µm	Vol Below 10 um	Volume Below 20 um	Volume Below 63 um
14.4	Asselian	BC WS	1.02	0.80	0.22	0.19	0.61	0.80	24.90	4.91 µm	23.3 µm	88.0 µm	3.98%	19.57%	23.55%	44.76%	81.81%
14.6	Asselian	BC WS	2.05	1.72	0.33	0.14	1.57	1.72	25.80	2.94 µm	16.8 µm	68.5 µm	7.85%	27.48%	35.34%	55.27%	87.98%
15	Asselian	BC WS	1.59	1.48	0.12	0.13	1.34	1.48	9.67	2.33 µm	10.3 µm	38.4 µm	11.24%	37.76%	49.00%	71.06%	98.16%
15.2	Asselian	BC WS	1.43	1.39	0.03	0.23	1.17	1.39	23.70	2.71 µm	12.7 µm	48.2 µm	8.72%	33.85%	42.57%	63.99%	95.09%
15.4	Asselian	BC WS	1.54	1.54	0.00	0.08	1.46	1.54	12.80	2.65 µm	11.2 µm	38.2 µm	9.07%	36.86%	45.93%	70.89%	97.68%
15.6	Asselian	BC WS	1.17	1.14	0.03	0.06	1.08	1.14	18.80	2.74 µm	12.4 µm	42.1 µm	8.58%	34.33%	42.91%	66.78%	96.95%
15.8	Asselian	BC WS	5.17	2.26	2.91	0.25	2.01	2.26	29.00	3.05 µm	19.4 µm	57.7 µm	7.89%	22.14%	30.04%	51.08%	91.89%
16	Asselian	Fusu WS	1.10	0.66	0.45	0.03	0.62	0.66	44.00	7.96 µm	35.7 µm	87.9 µm	2.64%	10.15%	12.80%	26.93%	77.24%
16.2	Asselian	Palaeo F	4.78	4.04	0.74	0.57	3.47	4.04	58.80	11.7 µm	48.8 µm	100 µm	1.68%	6.93%	8.61%	16.31%	65.21%
16.4	Asselian	Palaeo F	1.64	1.52	0.12	0.02	1.50	1.52	31.00	3.51 µm	18.1 µm	52.6 µm	5.83%	26.11%	31.96%	53.48%	94.36%
16.8	Asselian	Palaeo F	1.40	1.32	0.09	0.00	1.31	1.32	6.33	2.23 µm	7.28 µm	27.1 µm	12.59%	49.54%	62.13%	82.88%	99.88%
17	Asselian	Palaeo F	0.99	0.98	0.01	0.01	0.97	0.98	12.70	2.84 µm	11.7 µm	40.1 µm	8.00%	36.30%	44.29%	69.37%	97.25%
17.2	Asselian	Palaeo F	0.62	0.60	0.02	0.00	0.59	0.60	11.80	2.65 µm	10.9 µm	39.1 µm	9.04%	37.77%	46.81%	72.34%	96.33%
17.4	Asselian	Palaeo F	0.75	0.74	0.01	0.01	0.73	0.74	13.80	2.91 µm	12.0 µm	40.0 µm	7.70%	35.62%	43.31%	68.70%	97.52%
17.6	Asselian	Palaeo F	1.74	1.74	0.00	0.01	1.73	1.74	6.70	2.22 µm	7.59 µm	31.3 µm	12.56%	47.83%	60.39%	80.80%	98.65%
17.8	Asselian	BC WS	4.82	4.82	0.00	0.05	4.77	4.82	7.70	1.94 µm	7.35 µm	24.8 µm	15.29%	46.26%	61.54%	84.40%	100.00%
18	Asselian	BC WS	4.16	4.16	0.00	0.05	4.12	4.16	5.90	1.82 µm	6.32 µm	23.6 µm	17.71%	49.04%	66.74%	86.42%	99.91%
18.2	Asselian	BC WS	2.45	2.45	0.00	0.00	2.45	2.45	7.40	2.01 µm	7.50 µm	26.9 µm	14.63%	46.04%	60.68%	82.84%	99.76%
18.4	Asselian	BC WS	5.32	5.32	0.00	0.06	5.26	5.32	8.20	2.08 µm	7.71 µm	26.4 µm	14.00%	45.91%	59.90%	83.13%	99.72%
18.6	Asselian	BC WS	6.93	6.46	0.47	0.57	5.88	6.46	32.30	2.73 µm	15.9 µm	46.2 µm	8.55%	30.11%	38.66%	56.83%	97.58%
18.8	Asselian	Palaeo B	2.00	2.00	0.00	0.02	1.97	2.00	11.00	2.24 µm	8.38 µm	23.2 µm	12.14%	45.23%	57.38%	85.24%	100.00%
19	Asselian	Palaeo B	1.16	1.16	0.00	0.50	0.66	1.16	13.70	2.58 µm	10.5 µm	32.5 µm	9.43%	38.73%	48.15%	74.60%	99.38%
19.2	Asselian	Palaeo B	2.43	2.43	0.00	0.02	2.40	2.43	7.70	2.00 µm	6.52 µm	17.1 µm	14.99%	54.74%	69.72%	93.93%	100.00%
19.4	Asselian	Palaeo B	1.92	1.92	0.00	0.15	1.77	1.92	11.60	2.34 µm	9.65 µm	32.3 µm	11.25%	40.01%	51.26%	75.77%	99.38%
19.6	Asselian	Palaeo B	2.53	2.43	0.11	0.03	2.39	2.43	13.50	2.22 µm	9.55 µm	29.8 µm	12.14%	39.55%	51.68%	77.35%	99.96%
19.8	Asselian	Palaeo B	5.81	5.71	0.10	0.08	5.63	5.71	7.50	1.88 µm	7.38 µm	25.4 µm	16.07%	44.76%	60.83%	83.46%	100.00%
20	Asselian	Palaeo F	1.92	1.92	0.00	0.07	1.85	1.92	10.70	2.39 µm	8.98 µm	27.0 µm	10.89%	43.38%	54.27%	80.83%	99.95%
20.4	Asselian	Fusu WS	2.61	2.61	0.00	0.11	2.49	2.61	11.50	2.44 µm	9.39 µm	27.1 µm	10.45%	42.17%	52.62%	80.63%	99.78%
20.6	Asselian	Palaeo B	4.86	4.82	0.04	0.01	4.81	4.82	8.10	2.14 µm	7.48 µm	22.5 µm	13.28%	48.66%	61.94%	86.84%	100.00%
20.8	Asselian	Palaeo B	2.74	2.50	0.24	0.09	2.41	2.50	15.20	2.51 µm	11.6 µm	38.6 µm	9.95%	34.86%	44.80%	70.26%	97.34%
21	Asselian	Palaeo B	4.19	3.99	0.21	2.18	1.80	3.99	12.00	2.34 µm	9.41 µm	28.1 µm	11.21%	41.17%	52.39%	79.30%	99.91%
21.2	Asselian	Palaeo B	3.25	3.21	0.04	0.01	3.20	3.21	10.00	2.15 µm	8.21 µm	24.2 µm	12.99%	44.96%	57.95%	84.27%	100.00%
21.4	Asselian	Palaeo B	2.55	2.17	0.38	0.14	2.04	2.17	10.00	2.24 µm	8.49 µm	26.5 µm	12.08%	44.65%	56.73%	82.74%	97.90%
21.6	Asselian	Palaeo B	2.88	2.78	0.10	0.06	2.72	2.78	12.20	2.55 µm	11.6 µm	47.1 µm	9.67%	35.45%	45.12%	68.24%	94.34%
21.8	Asselian	Palaeo F	7.97	4.05	3.92	1.92	2.13	4.05	114.00	4.00 µm	67.6 µm	164 µm	5.25%	17.03%	22.28%	32.88%	47.98%
22	Asselian	Palaeo F	2.73	2.07	0.66	0.08	2.00	2.07	10.70	2.52 µm	9.29 µm	27.3 µm	9.86%	43.24%	53.10%	80.82%	99.56%
22.2	Asselian	Palaeo F	1.56	0.96	0.60	0.10	0.85	0.96	16.20	3.40 µm	19.0 µm	98.3 µm	6.61%	24.46%	31.07%	51.58%	79.65%
22.4	Asselian	Palaeo F	1.88	1.00	0.89	0.10	0.90	1.00	15.50	3.24 µm	17.6 µm	87.8 µm	6.97%	26.05%	33.01%	53.82%	82.64%

Sample (m)	Section	Facies	SMF wt %	<120 µm wt %	>120 um wt %	63<x<120 wt %	<63 um wt %	"Dust"	Dx (10) µm	Dx (50) µm	Dx (90) µm	Mode (µm)	Volume Below 2.5 µm	Vol Between 2.5-10 µm	Vol Below 10 um	Volume Below 20 um	Volume Below 63 um
22.6	Asselian	Palaeo F	2.22	2.14	0.08	0.28	1.86	2.14	62.00	10.9 µm	50.5 µm	107 µm	2.11%	7.14%	9.25%	17.02%	62.41%
22.8	Asselian	B PS/CS	12.03	11.95	0.09	2.44	9.51	12.03	88.50	36.3 µm	81.5 µm	141 µm	0.86%	3.46%	4.32%	7.11%	30.19%
23	Asselian	B PS/CS	12.89	8.34	4.55	4.48	3.86	12.89	106.00	48.5 µm	99.1 µm	170 µm	0.27%	1.28%	1.55%	4.24%	18.37%
23.2	Asselian	B PS/CS	12.39	6.68	5.71	2.97	3.71	12.39	113.00	57.6 µm	108 µm	183 µm	0.00%	0.23%	0.23%	2.32%	12.93%
23.4	Asselian	B PS/CS	10.00	4.92	5.08	2.28	2.64	10.00	112.00	45.8 µm	104 µm	179 µm	0.48%	1.85%	2.33%	5.52%	17.64%
23.6	Asselian	B PS/CS	12.60	5.41	7.19	3.75	1.67	12.60	109.00	32.1 µm	98.6 µm	171 µm	0.64%	2.81%	3.45%	7.19%	21.36%
23.8	Asselian	B PS/CS	3.00	2.43	0.56	0.69	1.74	2.43	34.80	3.67 µm	27.3 µm	109 µm	5.94%	19.34%	25.28%	41.21%	74.51%
24	Asselian	B PS/CS	2.66	2.18	0.48	0.67	1.51	2.18	30.70	3.35 µm	20.7 µm	69.3 µm	6.72%	22.54%	29.27%	48.80%	87.51%
24.2	Asselian	B PS/CS	2.08	1.76	0.32	0.69	1.08	1.76	97.00	7.95 µm	60.8 µm	146 µm	2.46%	10.05%	12.51%	23.00%	51.10%
24.4	Asselian	B PS/CS	4.26	2.98	1.28	0.92	2.05	2.98	29.00	4.46 µm	29.0 µm	113 µm	4.85%	17.31%	22.16%	38.97%	72.77%
24.6	Asselian	B PS/CS	3.54	2.13	1.40	0.00	2.13	2.13	34.00	5.28 µm	27.3 µm	90.1 µm	3.72%	16.87%	20.59%	39.08%	80.09%
24.8	Asselian	B PS/CS	4.61	3.84	0.77	2.00	1.84	3.84	97.00	7.10 µm	54.4 µm	146 µm	2.76%	11.09%	13.86%	24.99%	54.79%
25	Asselian	B PS/CS	4.63	4.37	0.26	1.51	2.86	4.37	36.00	3.38 µm	22.1 µm	63.9 µm	6.66%	21.70%	28.36%	46.65%	89.33%
25.2	Asselian	B PS/CS	2.20	2.16	0.04	0.63	1.54	2.16	41.00	5.12 µm	28.5 µm	77.1 µm	3.77%	16.58%	20.35%	37.32%	83.03%
25.4	Asselian	B PS/CS	3.23	3.04	0.19	1.09	1.95	3.04	77.00	7.27 µm	51.3 µm	119 µm	2.94%	10.57%	13.51%	24.25%	59.05%
25.6	Asselian	B PS/CS	2.10	1.94	0.16	0.35	1.59	1.94	69.00	4.76 µm	30.7 µm	107 µm	4.29%	17.01%	21.30%	37.63%	72.51%
25.8	Asselian	B PS/CS	4.22	4.04	0.18	0.89	3.15	4.04	33.60	3.34 µm	21.7 µm	67.0 µm	6.75%	21.65%	28.40%	47.20%	88.08%
26	Asselian	B PS/CS	4.77	4.64	0.13	1.76	2.88	4.64	29.30	3.35 µm	20.7 µm	71.4 µm	6.85%	22.29%	29.15%	48.93%	86.83%
26.2	Asselian	B PS/CS	23.46	21.08	2.38	4.89	16.19	23.46	101.00	59.1 µm	98.4 µm	153 µm	0.54%	1.89%	2.42%	3.92%	12.64%
26.4	Asselian	B PS/CS	2.32	2.23	0.09	0.97	1.26	2.32	97.00	6.26 µm	64.4 µm	143 µm	3.50%	11.61%	15.11%	25.31%	48.81%

Comprehensive Geochemical Data

SAMPLE	Ag	Al	As	Ba	Be	Bi	Ca	Cd	Ce	Co	Cr
	ppm	%	ppm	ppm	ppm	ppm	%	ppm	ppm	ppm	ppm
0.8	0.96	4.11	25.6	130	0.99	0.09	7.87	160.5	4.8	2.9	100
1	1.94	6.07	55.8	190	1.43	0.09	2.52	2.02	8.14	7	161
1.2	1.6	4.93	24.2	190	1.13	0.1	1.4	0.2	6.62	4.4	154
1.4	0.91	3.87	29.3	180	0.79	0.1	3.52	0.24	7.01	5.1	109
1.6	1.26	6.22	38.7	170	1.68	0.05	0.41	0.12	8.98	5.6	159
1.8	0.62	3.44	30.9	190	0.64	0.07	0.75	0.12	7.94	4	114
2	0.73	4.7	35.6	270	1.23	0.1	0.56	0.12	9.32	5.4	164
2.2	0.2	5.77	44.1	220	1.43	0.12	1.16	0.11	7.13	4.9	257
2.4	0.34	5.52	24.9	280	1.54	0.11	0.47	0.14	9.72	6	157
2.6	1.23	5.78	65.5	290	1.89	0.95	0.25	169.5	13.65	16.5	162
3	0.35	2.38	22.2	110	0.68	0.08	0.26	0.68	9.47	6.6	91
5	0.18	5.38	17.5	240	1.5	0.1	1.01	0.17	37.1	11.1	136
10.2	0.12	4.19	19.9	170	1.3	0.1	0.18	0.09	4.62	7.9	162
11	0.05	5.37	17	230	1.46	0.09	0.45	0.05	7.49	5.9	161
11.4	0.05	5.39	62.1	220	1.48	0.26	0.52	0.18	7.23	25.3	209
11.8	0.05	5.25	15.6	210	1.31	0.14	0.59	0.22	8.41	10.7	81
12.2	0.07	4.98	30.4	250	1.2	0.11	4.8	0.08	9.35	9.7	96
12.6	0.05	4.18	17	190	0.94	0.09	0.84	0.1	6.82	6.5	56
13	0.09	4.52	27.6	190	1.05	0.1	0.79	0.11	6.8	9.7	70
13.2	0.21	1.71	9.5	80	0.46	0.05	0.14	0.02	2.67	3.3	33
13.4	0.05	3.1	15.8	120	0.71	0.07	0.21	0.08	3.99	6.8	100
13.6	0.06	2.95	16.1	140	0.73	0.04	0.49	0.05	5.17	6.4	142
14	0.04	1.64	6.1	80	0.43	0.02	3.86	0.08	3.44	4.1	66
14.4	0.07	1.17	13.8	90	0.32	0.03	6.24	0.07	4.47	6.2	69
14.6	0.08	3.05	17.5	140	0.82	0.05	0.13	0.27	4.47	10.4	70
15.8	0.09	0.82	1.5	50	0.26	0.02	0.1	0.07	1.36	1.7	31
19.2	4.64	4.76	10.9	200	1.33	0.14	2.39	1.83	13.5	15.7	88
19.6	0.04	4.5	14.3	180	1.16	0.12	0.64	0.11	9.69	12.9	78
20	0.04	3.95	7.4	150	0.95	0.08	6.67	0.26	8.88	7.6	55
20.6	0.06	5.84	19.5	210	1.51	0.12	0.51	0.15	12	13.5	110
21	0.06	5.76	15.1	210	1.52	0.17	0.5	0.37	11.4	19.8	113
21.4	0.04	4.03	9.4	170	0.86	0.1	0.52	0.13	8.65	6	78
21.8	0.02	1.36	3.5	60	0.41	0.04	1.61	0.27	3.61	3.5	34
22	0.09	3.7	6.9	140	1.01	0.1	1.12	0.25	10.2	7.6	72
22.2	0.04	2.31	9.6	100	0.55	0.06	0.76	1.16	4.99	5.3	93
22.6	0.06	2.69	9	150	0.53	0.11	1.51	0.27	9.93	3.4	77
22.8	0.03	5.03	5.4	290	0.98	0.05	0.25	0.13	22.7	4.3	64
23	0.02	1.1	2.9	140	0.15	0.03	0.63	0.08	10.6	1.1	25
23.2	0.11	0.87	1	100	0.19	0.02	1.56	0.22	5.07	0.5	16
23.4	0.02	0.73	2.2	100	0.15	0.02	7.01	0.17	3.67	0.9	23
23.8	0.04	1.21	7.8	100	0.21	0.03	1.25	0.37	3.75	5.4	139
24.2	0.05	1.47	6.8	110	0.28	0.03	2.6	0.99	4.44	2.7	90
24.6	0.03	1	3.4	80	0.18	0.02	1.01	0.68	2.8	1.9	66
25	0.05	2.06	6.4	140	0.36	0.03	0.82	0.21	4.88	3	120
25.4	0.07	2.31	4.4	130	0.46	0.06	0.41	0.22	5.04	3.6	85
25.6	0.08	2.56	6	130	0.6	0.07	0.44	1.46	5.37	5	147
25.8	0.04	3.41	6.2	170	0.92	0.05	0.47	1.25	5.59	3.5	171
26	0.05	3.41	5.8	180	0.74	0.05	0.35	0.29	8.54	3.4	154
26.2	0.05	2.27	4.1	250	0.48	0.06	0.15	0.2	14.25	2.4	64
26.4	0.04	3.02	7.3	160	0.7	0.06	0.54	0.11	6.69	3.2	130
DZ A	0.04	1.19	1.8	180	0.26	0.03	0.06	0.34	4.96	1.8	59
DZ M	0.09	1.72	3	90	0.52	0.06	0.06	0.08	9.34	4	130
M4.6	0.09	2.65	32.5	80	0.91	0.08	0.73	0.23	6.43	3.8	137
M6.2	0.16	0.93	19.6	40	0.27	0.03	0.05	0.42	2.48	2.2	32
M6.8	0.07	1.9	27.6	90	0.64	0.04	0.73	0.17	5.16	1.7	59
M8.2	0.11	1.17	60.4	50	0.38	0.05	5.17	0.25	3.2	1.9	67
M9.8	0.08	0.73	11.4	30	0.27	0.02	1.06	0.19	2.08	1.4	80

SAMPLE	Ag	Al	As	Ba	Be	Bi	Ca	Cd	Ce	Co	Cr
	ppm	%	ppm	ppm	ppm	ppm	%	ppm	ppm	ppm	ppm
0.8	0.96	4.11	25.6	130	0.99	0.09	7.87	160.5	4.8	2.9	100
1	1.94	6.07	55.8	190	1.43	0.09	2.52	2.02	8.14	7	161
1.2	1.6	4.93	24.2	190	1.13	0.1	1.4	0.2	6.62	4.4	154
1.4	0.91	3.87	29.3	180	0.79	0.1	3.52	0.24	7.01	5.1	109
1.6	1.26	6.22	38.7	170	1.68	0.05	0.41	0.12	8.98	5.6	159
1.8	0.62	3.44	30.9	190	0.64	0.07	0.75	0.12	7.94	4	114
2	0.73	4.7	35.6	270	1.23	0.1	0.56	0.12	9.32	5.4	164
2.2	0.2	5.77	44.1	220	1.43	0.12	1.16	0.11	7.13	4.9	257
2.4	0.34	5.52	24.9	280	1.54	0.11	0.47	0.14	9.72	6	157
2.6	1.23	5.78	65.5	290	1.89	0.95	0.25	169.5	13.65	16.5	162
3	0.35	2.38	22.2	110	0.68	0.08	0.26	0.68	9.47	6.6	91
5	0.18	5.38	17.5	240	1.5	0.1	1.01	0.17	37.1	11.1	136
10.2	0.12	4.19	19.9	170	1.3	0.1	0.18	0.09	4.62	7.9	162
11	0.05	5.37	17	230	1.46	0.09	0.45	0.05	7.49	5.9	161
11.4	0.05	5.39	62.1	220	1.48	0.26	0.52	0.18	7.23	25.3	209
11.8	0.05	5.25	15.6	210	1.31	0.14	0.59	0.22	8.41	10.7	81
12.2	0.07	4.98	30.4	250	1.2	0.11	4.8	0.08	9.35	9.7	96
12.6	0.05	4.18	17	190	0.94	0.09	0.84	0.1	6.82	6.5	56
13	0.09	4.52	27.6	190	1.05	0.1	0.79	0.11	6.8	9.7	70
13.2	0.21	1.71	9.5	80	0.46	0.05	0.14	0.02	2.67	3.3	33
13.4	0.05	3.1	15.8	120	0.71	0.07	0.21	0.08	3.99	6.8	100
13.6	0.06	2.95	16.1	140	0.73	0.04	0.49	0.05	5.17	6.4	142
14	0.04	1.64	6.1	80	0.43	0.02	3.86	0.08	3.44	4.1	66
14.4	0.07	1.17	13.8	90	0.32	0.03	6.24	0.07	4.47	6.2	69
14.6	0.08	3.05	17.5	140	0.82	0.05	0.13	0.27	4.47	10.4	70
15.8	0.09	0.82	1.5	50	0.26	0.02	0.1	0.07	1.36	1.7	31
19.2	4.64	4.76	10.9	200	1.33	0.14	2.39	1.83	13.5	15.7	88
19.6	0.04	4.5	14.3	180	1.16	0.12	0.64	0.11	9.69	12.9	78
20	0.04	3.95	7.4	150	0.95	0.08	6.67	0.26	8.88	7.6	55
20.6	0.06	5.84	19.5	210	1.51	0.12	0.51	0.15	12	13.5	110
21	0.06	5.76	15.1	210	1.52	0.17	0.5	0.37	11.4	19.8	113
21.4	0.04	4.03	9.4	170	0.86	0.1	0.52	0.13	8.65	6	78
21.8	0.02	1.36	3.5	60	0.41	0.04	1.61	0.27	3.61	3.5	34
22	0.09	3.7	6.9	140	1.01	0.1	1.12	0.25	10.2	7.6	72
22.2	0.04	2.31	9.6	100	0.55	0.06	0.76	1.16	4.99	5.3	93
22.6	0.06	2.69	9	150	0.53	0.11	1.51	0.27	9.93	3.4	77
22.8	0.03	5.03	5.4	290	0.98	0.05	0.25	0.13	22.7	4.3	64
23	0.02	1.1	2.9	140	0.15	0.03	0.63	0.08	10.6	1.1	25
23.2	0.11	0.87	1	100	0.19	0.02	1.56	0.22	5.07	0.5	16
23.4	0.02	0.73	2.2	100	0.15	0.02	7.01	0.17	3.67	0.9	23
23.8	0.04	1.21	7.8	100	0.21	0.03	1.25	0.37	3.75	5.4	139
24.2	0.05	1.47	6.8	110	0.28	0.03	2.6	0.99	4.44	2.7	90
24.6	0.03	1	3.4	80	0.18	0.02	1.01	0.68	2.8	1.9	66
25	0.05	2.06	6.4	140	0.36	0.03	0.82	0.21	4.88	3	120
25.4	0.07	2.31	4.4	130	0.46	0.06	0.41	0.22	5.04	3.6	85
25.6	0.08	2.56	6	130	0.6	0.07	0.44	1.46	5.37	5	147
25.8	0.04	3.41	6.2	170	0.92	0.05	0.47	1.25	5.59	3.5	171
26	0.05	3.41	5.8	180	0.74	0.05	0.35	0.29	8.54	3.4	154
26.2	0.05	2.27	4.1	250	0.48	0.06	0.15	0.2	14.25	2.4	64
26.4	0.04	3.02	7.3	160	0.7	0.06	0.54	0.11	6.69	3.2	130
DZ A	0.04	1.19	1.8	180	0.26	0.03	0.06	0.34	4.96	1.8	59
DZ M	0.09	1.72	3	90	0.52	0.06	0.06	0.08	9.34	4	130
M4.6	0.09	2.65	32.5	80	0.91	0.08	0.73	0.23	6.43	3.8	137
M6.2	0.16	0.93	19.6	40	0.27	0.03	0.05	0.42	2.48	2.2	32
M6.8	0.07	1.9	27.6	90	0.64	0.04	0.73	0.17	5.16	1.7	59
M8.2	0.11	1.17	60.4	50	0.38	0.05	5.17	0.25	3.2	1.9	67
M9.8	0.08	0.73	11.4	30	0.27	0.02	1.06	0.19	2.08	1.4	80

SAMPLE	Cs	Cu	Fe	Ga	Ge	Hf	In	K	La	Li	Mg
	ppm	ppm	%	ppm	ppm	ppm	ppm	%	ppm	ppm	%
0.8	5.17	29.3	0.96	9.92	0.14	1.6	0.017	2.61	2.9	47.6	1.13
1	7.28	199	4.38	14.85	0.21	2.3	0.019	3.87	5.8	75.1	1.61
1.2	5.4	41.1	2.14	11.75	0.13	2.2	0.014	3.07	4.9	58.5	1.12
1.4	4.3	75.5	3.02	9.3	0.13	1.8	0.018	2.31	4.3	47.8	0.77
1.6	6.82	24.5	1.34	16.5	0.27	2.4	0.021	3.94	7.5	83.5	1.18
1.8	2.83	120	3.36	7.47	0.2	2.5	0.014	1.93	4.4	39.3	0.6
2	4.34	71.8	3.11	10.9	0.28	2.6	0.022	2.59	5.3	53.5	0.77
2.2	4.76	68.3	2.37	13.15	0.16	2.6	0.025	3.36	4.6	63.3	1.1
2.4	4.8	118.5	3.54	12.5	0.29	3	0.027	3.41	5.4	76.5	0.82
2.6	4.93	228	5.21	18.4	0.45	3.4	0.043	3.26	7.1	105	0.95
3	3.04	117	3.34	5.72	0.14	1.5	0.011	1.22	5.6	36.1	0.29
5	13.65	37.3	2.64	13.65	0.14	3.2	0.034	2.42	22.5	73.5	0.64
10.2	3.77	94.4	1.11	11.1	0.13	2.4	0.017	2.28	2.7	83.6	0.66
11	5.27	25	1.77	13.2	0.12	3.9	0.024	3.17	4.3	79.5	0.71
11.4	5.1	62.9	2.75	12.85	0.11	3.9	0.036	3.13	4.5	77.9	0.72
11.8	5.13	46.9	1.77	12.8	0.12	2.7	0.027	3.14	4.6	79	0.77
12.2	5.1	45.1	3.08	12.15	0.11	2.7	0.031	2.88	5.3	62.8	0.65
12.6	3.63	39.4	1.48	9.3	0.11	2.4	0.021	2.63	3.8	62	0.52
13	4.02	43.5	2.63	10.5	0.12	1.9	0.025	2.72	4.1	83.6	0.63
13.2	1.52	191.5	0.54	4.26	0.12	1	0.019	1	1.6	44.7	0.24
13.4	2.59	48	1.32	6.97	0.12	1.2	0.015	1.92	2.4	57.4	0.41
13.6	2.43	43	2.94	7.03	0.09	1.7	0.021	1.7	2.9	52.9	0.36
14	1.38	20.3	0.97	3.85	0.11	1	0.01	0.88	1.9	39.3	0.17
14.4	0.93	29.7	3.44	3.1	0.08	1	0.018	0.49	2.6	29.5	0.12
14.6	2.43	36.3	1.54	7.82	0.1	1.9	0.017	1.69	2.5	56.7	0.4
15.8	0.64	34.8	0.12	1.98	0.13	0.8	<0.005	0.42	0.8	23.8	0.09
19.2	5.99	47.5	3.03	12.05	0.13	2.7	0.024	2.8	9.5	133	0.92
19.6	5.05	40.6	2.33	10.45	0.13	2.5	0.023	2.84	6.8	114	0.67
20	4.11	19.6	1.4	8.8	0.13	1.8	0.019	2.57	6.6	85.1	0.56
20.6	6.62	75.4	2.3	13.6	0.13	2.7	0.031	3.81	9.8	134.5	0.91
21	7.45	45.1	2.31	13.85	0.13	2.9	0.03	3.53	8.1	142	0.98
21.4	5.01	99.8	1.98	8.59	0.11	1.7	0.022	2.4	6.1	87.8	0.58
21.8	1.93	9.6	1.31	3.65	0.05	0.6	0.009	0.76	2.6	39.1	0.22
22	5.31	26	1.06	9.57	0.13	1.9	0.016	2.07	7.7	117	0.82
22.2	2.45	41.3	2.53	5.3	0.07	1.2	0.015	1.32	3.5	57	0.34
22.6	2.36	58.6	1.5	5.14	0.08	1.6	0.013	1.82	6.6	38.6	0.27
22.8	4.24	16.7	1.7	9.85	0.12	3.9	0.023	3.5	14.3	68.2	0.71
23	0.5	8	1.4	1.75	0.05	1.7	0.006	0.78	5.8	20.2	0.05
23.2	0.43	3	0.2	1.48	0.11	1.6	<0.005	0.63	2.9	33.8	0.05
23.4	0.5	7	0.83	1.29	<0.05	1.1	0.007	0.47	2.3	25.8	0.06
23.8	0.9	29.2	12.1	3.6	0.08	1.1	0.011	0.69	2.2	29.7	0.14
24.2	0.9	27.6	3.36	2.94	<0.05	1.3	0.019	0.9	2.5	27.3	0.15
24.6	0.57	18	2.17	1.95	0.05	0.8	0.007	0.58	1.6	30.4	0.09
25	1.36	23.9	2.89	4.17	0.05	1.3	0.024	1.26	2.9	37.1	0.23
25.4	1.47	80.5	2.98	4.09	0.06	1.6	0.008	1.56	2.7	48.7	0.26
25.6	1.8	72.6	3.98	5.01	0.06	1.5	0.013	1.61	2.9	51.9	0.34
25.8	3.04	41.8	2.31	7.31	0.08	1.8	0.016	2.11	3.7	70.1	0.49
26	2.64	41.4	2.6	6.63	0.08	1.9	0.012	2.16	5.3	54.8	0.45
26.2	1.59	32.5	1.74	4.3	0.07	2.9	0.011	1.81	8	30.2	0.22
26.4	2.46	56.2	2.09	5.95	0.08	1.9	0.016	2.03	4.5	51.5	0.4
DZ A	0.69	20.5	3.55	2.41	<0.05	1.2	<0.005	1.01	3	17.5	0.08
DZ M	1.92	77.8	6.54	4.41	0.07	0.8	0.009	0.82	4.7	104	1.38
M4.6	2.94	45.2	0.84	7.27	0.09	1.7	0.01	0.72	4.5	341	3.67
M6.2	1.08	10.5	0.27	2.58	0.08	1	0.008	0.35	1.7	81.7	0.53
M6.8	2.53	22.1	0.39	5.48	0.11	2.1	0.01	0.82	3.6	128.5	1.22
M8.2	1.42	44.6	1.05	3.3	0.06	1	<0.005	0.44	1.9	120.5	0.96
M9.8	0.7	6.1	0.27	2.07	0.09	0.8	0.005	0.26	1.2	76	0.58

SAMPLE	Mn	Mo	Na	Nb	Ni	P	Pb	Rb	Re	S	Sb
	ppm	ppm	%	ppm	ppm	ppm	ppm	ppm	ppm	%	ppm
0.8	38	135.5	0.25	6.2	61.1	10	174.5	92	1.685	6.87	3.63
1	346	237	0.33	8.6	116.5	80	1160	132.5	1.875	1.79	5.72
1.2	175	198.5	0.29	7.7	80.7	50	47	104	3.33	1.05	2.85
1.4	245	120.5	0.24	6.3	74.3	50	34	81.2	2.3	3.27	2.93
1.6	42	83.1	0.3	8.8	109.5	40	26.6	140.5	0.349	0.66	3.43
1.8	278	49	0.43	5.3	57.1	60	54	63.2	0.963	0.96	1.3
2	217	68.8	0.44	6.9	95.8	100	44.8	88.4	1.235	1.29	2.52
2.2	187	35.2	0.44	7.6	77.6	50	21.2	113.5	1.24	1.06	1.87
2.4	286	28.4	0.61	10.1	96.4	30	18.8	111.5	1.16	0.96	1.16
2.6	387	128	0.51	11.8	202	120	484	113.5	1.465	1.39	4.9
3	251	18.2	0.2	4.4	73.4	70	15.3	46.7	0.552	0.69	0.66
5	71	22.3	0.19	10.7	71.3	220	10.3	110.5	0.138	0.22	1.21
10.2	35	6.62	0.32	7.5	110	60	7.8	88.4	0.052	0.17	1.18
11	124	11.1	0.42	12	50.4	50	7.7	109.5	0.073	0.46	1.66
11.4	101	25.6	0.52	13.5	173.5	110	18.1	105.5	0.031	0.38	2.59
11.8	103	10.65	0.41	10.2	69.9	80	9.6	111.5	0.074	0.39	1.31
12.2	253	6.04	0.36	11.3	49.1	140	15.1	104.5	0.047	0.2	1.16
12.6	94	5.01	0.4	7.8	40.7	60	10.1	83.9	0.022	0.18	1.04
13	208	6.96	0.43	7.3	48.4	100	19.2	88.4	0.022	0.26	1.32
13.2	18	2.95	0.19	2.6	31	20	78.4	35.1	0.011	0.15	0.8
13.4	80	8.64	0.29	5	50.7	30	9.7	59.8	0.217	0.53	1
13.6	277	3.76	0.26	4.7	30.4	70	19.5	56.1	0.048	0.27	0.82
14	79	2.03	0.19	3.4	27.8	50	5.1	34.1	0.042	0.19	0.37
14.4	332	3.39	0.16	2.7	30.9	90	18.7	21.1	0.035	0.33	0.54
14.6	114	4.69	0.3	5.8	75.9	40	8.3	60.3	0.055	0.29	1.6
15.8	6	0.55	0.12	1.7	15.8	10	7.9	14.3	0.013	0.07	0.6
19.2	234	2.48	0.38	9.5	91.6	50	9.3	101.5	0.135	1.75	1.31
19.6	164	2.77	0.35	8.7	62.3	90	13	94.6	0.054	0.28	1.55
20	87	0.95	0.33	6.7	55.9	30	6.1	80.3	0.038	6.07	1.08
20.6	135	1.87	0.47	10.5	117.5	60	12.8	126	0.025	1.1	2.02
21	128	1.01	0.44	10.8	154.5	30	10.4	131	0.031	1.73	1.81
21.4	152	1.35	0.31	7.4	46.8	40	10.6	82.8	0.02	0.75	1.02
21.8	119	0.88	0.11	2.6	15.8	20	2.9	30.7	0.005	0.29	0.45
22	54	0.73	0.29	7.1	69.6	30	4.1	86.7	0.01	0.82	1.15
22.2	237	1.87	0.24	3.7	36.4	40	10.9	45.5	0.013	0.75	0.99
22.6	110	0.72	0.3	5	65.9	20	10.9	52.4	0.011	1.3	2.61
22.8	131	1.48	0.34	9.3	40.3	40	7.7	99.8	0.004	0.79	1.67
23	142	0.6	0.24	2.6	7.5	20	3.8	19.1	0.002	0.18	0.45
23.2	16	0.16	0.18	1.9	3.8	20	2.3	16.9	<0.002	0.07	0.2
23.4	80	0.69	0.11	1.7	6	50	3.4	13.8	0.002	1.5	0.26
23.8	1240	4.65	0.16	2.2	38.8	40	5.4	20.7	0.007	0.27	1.16
24.2	336	2.37	0.26	2.3	20.7	40	11.4	23.1	0.008	0.66	0.61
24.6	215	1.11	0.19	1.6	16.9	10	3.8	16.2	0.006	0.42	0.51
25	287	2.09	0.31	3	23.1	30	10.7	35.1	0.006	0.29	0.68
25.4	268	2.8	0.37	3.3	37.8	20	9.5	40.8	0.018	0.43	0.69
25.6	358	4.16	0.38	3.7	52.7	20	11.7	46	0.037	0.89	0.82
25.8	187	1.55	0.38	5	43.9	20	5.3	68.3	0.008	0.65	0.86
26	227	1.84	0.45	4.7	36.6	20	5.7	64.2	0.007	0.48	0.74
26.2	154	1.39	0.27	4.3	33.1	30	8.6	52.7	0.007	0.36	0.89
26.4	170	1.63	0.31	4.4	44.5	20	8.3	61	0.008	0.49	0.99
DZ A	357	2.3	0.18	2.1	12.2	120	6.1	28.4	0.002	0.02	0.36
DZ M	642	4.26	0.22	2.9	26.9	360	11.1	34.7	0.002	0.03	0.74
M4.6	41	5.56	0.04	4.3	128.5	50	14.1	41.8	0.01	0.09	1.46
M6.2	10	1.15	0.03	2.2	39.6	10	6.8	18.2	0.002	0.09	0.74
M6.8	14	3.37	0.04	5.1	42.3	30	11.3	43.2	0.004	0.13	1.23
M8.2	104	7.65	0.03	2.4	79.2	60	8.6	20.3	0.009	0.09	1.77
M9.8	12	4.84	0.02	1.8	20.6	10	4.3	12.8	0.004	0.2	0.65

SAMPLE	Sc	Se	Sn	Sr	Ta	Te	Th	Ti	Tl	U	V
	ppm	ppm	ppm	ppm	ppm	ppm	ppm	%	ppm	ppm	ppm
0.8	3.3	40	1.3	134.5	0.45	0.06	2.5	0.21	3.36	26.9	65
1	5.3	67	3.6	45.3	0.59	0.1	3.54	0.295	3.4	34.8	108
1.2	4	30	1.9	30.8	0.55	0.06	3.22	0.262	3.05	27.7	147
1.4	3.4	36	2.1	72.8	0.45	<0.05	2.37	0.215	1.59	20.9	117
1.6	5.6	55	1.6	23.7	0.62	0.05	3.9	0.272	2.73	31.9	289
1.8	3.9	48	2.5	27.3	0.3	0.05	3.06	0.185	1.69	20.9	61
2	4.7	87	2.3	36	0.48	0.09	3.61	0.228	2.54	44.5	90
2.2	4.9	42	2.4	38	0.51	0.06	3.36	0.261	1.01	37.7	109
2.4	6	96	3	31.8	0.65	0.06	2.93	0.301	2.15	41.9	82
2.6	6.8	163	5.2	32.1	0.7	0.22	4.25	0.343	5.29	139	102
3	3.7	40	1.9	21.6	0.07	<0.05	2.05	0.138	1.15	18	64
5	7.1	14	1.8	63.9	0.71	<0.05	6.25	0.345	1.02	13.4	116
10.2	4.4	14	1.6	17.7	0.48	0.07	3.56	0.219	0.71	44.3	82
11	6	11	2.1	28.2	0.68	0.06	4.39	0.32	0.77	46.3	87
11.4	6.9	12	2.6	194.5	0.77	0.13	5.94	0.36	0.89	50.7	146
11.8	5.5	7	2	27.1	0.62	0.09	3.93	0.289	0.75	41.4	79
12.2	5.7	5	1.9	38	0.68	0.08	3.98	0.326	0.68	27.7	83
12.6	4.3	6	1.5	23.5	0.52	0.05	3.06	0.232	0.52	19.8	67
13	4.5	7	1.7	28.8	0.44	<0.05	2.39	0.212	0.55	22.4	74
13.2	1.5	4	59	12.3	0.16	<0.05	0.83	0.077	0.34	12.9	41
13.4	3	18	1.2	16.2	0.28	<0.05	1.15	0.142	0.5	16.9	88
13.6	3.1	5	1.3	867	0.31	<0.05	1.8	0.15	0.43	14.3	66
14	1.9	4	0.7	18.2	0.21	<0.05	1	0.11	0.26	7.2	33
14.4	1.6	4	0.7	287	0.07	<0.05	1	0.088	0.24	5	28
14.6	3.7	14	1.3	17.4	0.35	0.05	1.99	0.176	0.49	40.2	57
15.8	0.9	2	6	8.8	0.11	<0.05	0.54	0.048	0.16	11.7	15
19.2	6	7	1.8	78.3	0.62	0.09	3.35	0.251	0.67	15.6	105
19.6	5.3	4	2.7	45	0.54	0.14	2.64	0.246	0.55	10.1	73
20	4.3	6	1.3	2380	0.44	0.06	2.03	0.187	0.59	6.7	50
20.6	6.7	13	2.2	40.5	0.66	0.11	3.31	0.293	0.74	9.9	86
21	6.8	8	1.9	91.3	0.7	0.09	3.22	0.306	1.03	8.8	86
21.4	4.2	7	1.6	31.6	0.45	0.06	2.01	0.221	0.45	7	66
21.8	1.5	2	0.6	40.9	0.16	<0.05	0.91	0.078	0.2	3.9	35
22	4.2	4	1.3	43.4	0.47	<0.05	2.23	0.202	0.48	9.4	93
22.2	2.8	7	0.9	27.9	0.22	0.05	1.25	0.109	0.3	9.3	76
22.6	2.4	9	1.1	26.3	0.32	0.18	2.2	0.155	0.44	10.3	87
22.8	4.8	3	1.6	37.2	0.63	<0.05	5.13	0.312	0.59	9.5	84
23	0.7	2	0.4	26.5	0.18	<0.05	2.2	0.097	0.17	2.7	12
23.2	0.6	1	0.4	27.9	0.13	<0.05	1.47	0.064	0.1	2.3	12
23.4	0.6	1	0.3	71.3	0.11	<0.05	0.92	0.06	0.1	2.1	14
23.8	1	3	1.2	21.3	0.14	0.07	0.84	0.068	0.17	3	36
24.2	1.1	4	0.8	33.8	0.15	<0.05	1.1	0.081	0.18	4.2	39
24.6	0.7	5	0.6	150	0.11	<0.05	0.67	0.053	0.14	2.6	21
25	1.5	3	0.9	26.8	0.2	<0.05	1.23	0.107	0.25	4.4	53
25.4	1.7	3	1.8	24.2	0.22	<0.05	1.59	0.115	0.26	6.6	68
25.6	2.2	6	1.7	23.2	0.25	<0.05	1.65	0.128	0.44	8.6	97
25.8	3.3	6	1.4	27.4	0.35	<0.05	1.73	0.168	0.45	8.4	119
26	3	7	1.3	30.2	0.33	<0.05	2.28	0.161	0.39	7.2	91
26.2	1.8	2	0.9	40.9	0.31	<0.05	3.89	0.167	0.38	10.4	38
26.4	2.8	3	1.3	43.9	0.32	<0.05	2.02	0.154	0.41	18.9	74
DZ A	0.7	<1	0.6	29.2	0.14	<0.05	1.15	0.088	0.18	2.7	19
DZ M	1.5	1	2.2	11	0.24	<0.05	1.9	0.101	0.3	2.1	74
M4.6	3.7	2	1	9.6	0.25	0.05	2.67	0.131	0.85	27.3	112
M6.2	1.4	1	0.5	5.9	0.13	<0.05	1.82	0.071	0.31	9.7	19
M6.8	3.8	2	1.1	8.3	0.32	<0.05	3.48	0.151	0.57	17.1	44
M8.2	1.6	3	0.5	8.9	0.15	<0.05	1.41	0.078	0.77	5.6	39
M9.8	0.9	2	0.5	7.6	0.1	<0.05	0.8	0.059	0.31	7.6	46

SAMPLE	W ppm	Y ppm	Zn ppm	Zr ppm	Zr %
0.8	1.4	4.6	7970	57.7	0.00577
1	2.2	7.3	447	84.1	0.00841
1.2	1.8	6.3	54	81	0.0081
1.4	1.4	4.9	83	66	0.0066
1.6	2	6.1	91	88.5	0.00885
1.8	1.8	5	94	92.2	0.00922
2	2.4	6.7	96	95.6	0.00956
2.2	1.6	6.2	156	107	0.0107
2.4	2.7	7.1	97	111.5	0.01115
2.6	13.8	11.5	7760	146	0.0146
3	3.3	3.4	164	55.1	0.00551
5	1.2	9.3	143	122	0.0122
10.2	1.1	8.6	46	106.5	0.01065
11	21.8	17.2	17	174	0.0174
11.4	23.3	17.3	307	167.5	0.01675
11.8	29.1	11.6	62	111	0.0111
12.2	16.9	15.3	26	109.5	0.01095
12.6	32.5	7.7	29	89.8	0.00898
13	17.1	7.3	64	74.2	0.00742
13.2	1.2	2.2	72	43.7	0.00437
13.4	33.8	3.7	38	42.8	0.00428
13.6	16.2	4.2	34	55	0.0055
14	37.5	3	14	36.8	0.00368
14.4	46.4	4.3	23	35.8	0.00358
14.6	76.7	4.8	49	70.6	0.00706
15.8	0.5	1.8	24	34.7	0.00347
19.2	1.1	8.3	195	97.9	0.00979
19.6	16.8	7.3	42	91	0.0091
20	27.9	6	23	66.9	0.00669
20.6	9.8	9.1	40	97	0.0097
21	59.4	9.1	36	100	0.01
21.4	6.9	5.8	21	85.7	0.00857
21.8	27.2	2.4	18	26.6	0.00266
22	1	6.7	27	74.9	0.00749
22.2	12.1	3.4	57	40.2	0.00402
22.6	5.7	4.4	14	65.1	0.00651
22.8	4.2	7.1	12	147	0.0147
23	7	2.3	7	64.5	0.00645
23.2	0.3	2	27	55.3	0.00553
23.4	2.7	2.3	7	42.5	0.00425
23.8	30.2	1.7	28	41.2	0.00412
24.2	22.9	2.4	46	47.2	0.00472
24.6	23.5	1.3	33	32.6	0.00326
25	27.5	2.3	45	54	0.0054
25.4	1	2.3	69	56.3	0.00563
25.6	5.6	2.4	116	54.3	0.00543
25.8	1.1	3	67	61.8	0.00618
26	1.1	3.1	35	67.5	0.00675
26.2	2	3.8	28	106	0.0106
26.4	1.4	3.3	39	65.9	0.00659
DZ A	0.6	1.8	24	48.3	0.00483
DZ M	1	2.3	64	26.2	0.00262
M4.6	0.7	10.3	144	84.3	0.00843
M6.2	0.3	3	46	39.7	0.00397
M6.8	0.7	8.4	62	91	0.0091
M8.2	0.5	4.9	192	45.5	0.00455
M9.8	0.4	2.2	38	32.5	0.00325

Detrital Zircon Data

Devonian raw detrital zircon data

		Apparent ages (Ma)						
206Pb* 238U*	± (Ma)	207Pb* 235U	± (Ma)	206Pb* 207Pb*	± (Ma)	Best age (Ma)	± (Ma)	Conc (%)
306.3	7.1	537.3	14.3	1696.5	45.9	306.3	7.1	NA
331.5	15.5	417.7	18.7	927.4	53.2	331.5	15.5	NA
352.7	8.5	411.8	9.6	759.1	28.7	352.7	8.5	NA
369.1	10.0	587.9	14.3	1558.6	29.7	369.1	10.0	NA
386.1	16.1	424.6	15.9	640.5	33.3	386.1	16.1	NA
402.4	10.2	416.0	10.8	493.3	40.1	402.4	10.2	81.6
403.9	11.5	407.9	10.7	431.5	26.1	403.9	11.5	93.6
414.9	8.8	418.4	8.4	438.7	23.6	414.9	8.8	94.6
417.7	10.5	421.5	9.5	443.2	21.0	417.7	10.5	94.3
418.8	9.6	417.7	8.8	412.8	22.8	418.8	9.6	101.5
419.6	8.7	423.8	8.1	447.4	21.7	419.6	8.7	93.8
421.2	9.8	431.2	9.4	485.9	26.2	421.2	9.8	86.7
423.4	12.1	424.5	10.9	431.1	24.1	423.4	12.1	98.2
424.2	9.0	433.3	8.5	482.8	22.5	424.2	9.0	87.9
424.3	11.6	429.2	10.8	456.8	27.4	424.3	11.6	92.9
424.5	10.4	434.5	9.7	489.1	22.3	424.5	10.4	86.8
424.6	10.7	429.5	9.8	456.8	23.1	424.6	10.7	92.9
424.8	12.5	429.8	11.1	457.7	19.9	424.8	12.5	92.8
424.9	9.2	431.6	8.8	468.6	24.0	424.9	9.2	90.7
425.1	9.6	432.3	9.0	471.8	22.9	425.1	9.6	90.1
425.3	9.9	430.0	9.4	456.5	26.1	425.3	9.9	93.2
425.6	8.6	430.2	7.9	456.0	19.8	425.6	8.6	93.3
426.9	8.1	433.8	7.9	471.7	23.6	426.9	8.1	90.5
427.0	8.6	429.4	8.4	442.8	26.5	427.0	8.6	96.4
427.4	11.4	437.9	10.7	494.4	25.6	427.4	11.4	86.4
428.2	12.2	432.6	11.0	457.2	21.8	428.2	12.2	93.7
428.6	8.9	428.5	8.3	429.3	22.5	428.6	8.9	99.8
428.8	8.6	429.2	8.3	432.4	26.1	428.8	8.6	99.2
428.9	7.2	434.4	8.4	464.4	36.3	428.9	7.2	92.3
429.7	11.2	426.5	10.0	410.5	22.7	429.7	11.2	104.7
429.7	11.9	433.5	10.8	454.7	24.2	429.7	11.9	94.5
429.7	9.9	428.8	9.3	424.5	26.1	429.7	9.9	101.2
429.8	12.2	430.8	10.8	437.2	20.4	429.8	12.2	98.3
430.0	10.5	443.2	10.1	513.0	26.3	430.0	10.5	83.8
430.1	11.8	433.8	10.8	454.6	25.5	430.1	11.8	94.6
430.3	9.8	430.8	9.4	434.5	28.6	430.3	9.8	99.0

430.5	13.2	428.3	11.8	417.1	25.5	430.5	13.2	103.2
430.8	8.2	446.9	7.8	531.4	19.9	430.8	8.2	81.1
431.0	9.8	442.9	9.2	506.3	23.0	431.0	9.8	85.1
431.3	10.1	430.3	9.2	425.9	23.0	431.3	10.1	101.3
431.6	13.0	440.7	12.0	489.2	27.8	431.6	13.0	88.2
431.6	8.8	432.0	8.1	435.0	21.0	431.6	8.8	99.2
431.7	9.6	439.4	9.1	481.2	24.6	431.7	9.6	89.7
431.8	10.0	434.7	9.1	451.3	21.0	431.8	10.0	95.7
432.4	8.5	434.9	8.0	449.0	22.1	432.4	8.5	96.3
432.5	10.5	432.6	9.9	434.0	27.8	432.5	10.5	99.6
432.6	11.2	439.6	10.6	477.2	29.5	432.6	11.2	90.7
432.6	10.7	431.0	9.7	423.3	24.0	432.6	10.7	102.2
432.8	9.9	431.5	9.3	425.5	26.2	432.8	9.9	101.7
432.8	12.0	436.3	11.1	456.2	28.6	432.8	12.0	94.9
432.8	9.8	448.9	9.2	532.8	20.8	432.8	9.8	81.2
433.0	10.3	438.9	9.3	470.5	18.9	433.0	10.3	92.0
433.1	11.7	431.0	10.2	421.1	18.0	433.1	11.7	102.8
433.3	8.5	431.1	7.9	420.3	22.7	433.3	8.5	103.1
433.3	9.0	434.7	8.2	443.2	18.1	433.3	9.0	97.8
433.4	8.9	430.8	8.6	418.2	27.7	433.4	8.9	103.6
433.6	10.9	432.8	9.7	429.2	19.4	433.6	10.9	101.0
433.7	8.3	435.0	7.7	442.9	20.4	433.7	8.3	97.9
433.8	9.7	435.4	8.9	445.0	22.1	433.8	9.7	97.5
434.2	9.3	442.1	8.9	484.8	24.6	434.2	9.3	89.5
434.3	12.9	437.2	11.4	453.8	21.7	434.3	12.9	95.7
434.4	8.3	432.3	7.7	422.0	20.7	434.4	8.3	102.9
434.5	11.4	434.8	10.3	437.3	22.8	434.5	11.4	99.3
434.5	11.2	437.8	10.3	456.5	25.5	434.5	11.2	95.2
434.6	12.8	435.0	11.3	437.9	21.4	434.6	12.8	99.3
435.0	10.3	432.8	9.3	422.0	22.3	435.0	10.3	103.1
435.2	10.2	436.8	9.4	446.2	23.7	435.2	10.2	97.5
435.3	9.9	434.1	9.1	428.3	23.7	435.3	9.9	101.6
435.9	10.1	450.6	9.4	527.0	20.7	435.9	10.1	82.7
436.1	10.5	436.3	9.5	438.5	22.2	436.1	10.5	99.4
436.1	11.3	436.8	10.3	441.2	24.8	436.1	11.3	98.9
436.2	11.8	439.9	11.1	460.1	29.8	436.2	11.8	94.8
436.3	10.2	436.0	9.3	435.6	22.1	436.3	10.2	100.2
436.5	9.2	438.5	8.6	449.6	23.5	436.5	9.2	97.1
436.6	12.4	435.9	11.1	433.1	24.4	436.6	12.4	100.8
436.6	12.8	435.9	11.5	432.9	25.3	436.6	12.8	100.9
436.8	9.5	438.0	8.7	445.2	21.5	436.8	9.5	98.1
436.8	8.7	434.2	8.4	421.5	26.1	436.8	8.7	103.6
436.9	11.0	434.5	10.4	422.7	30.8	436.9	11.0	103.3
437.2	9.9	448.8	9.8	509.7	29.3	437.2	9.9	85.8
437.7	12.1	441.6	11.2	463.5	28.2	437.7	12.1	94.4
438.1	8.3	437.5	7.8	435.8	21.1	438.1	8.3	100.5
438.2	14.3	438.7	13.1	442.0	33.3	438.2	14.3	99.2

438.3	13.3	438.2	11.7	438.6	22.0	438.3	13.3	99.9
438.3	12.7	439.2	11.5	444.6	26.6	438.3	12.7	98.6
438.5	9.6	440.8	9.0	454.0	24.7	438.5	9.6	96.6
438.5	12.1	437.7	10.8	434.6	23.0	438.5	12.1	100.9
438.5	11.3	439.4	10.5	445.2	26.5	438.5	11.3	98.5
439.0	10.3	436.2	9.4	422.3	23.2	439.0	10.3	103.9
439.4	13.0	441.0	11.7	450.5	25.0	439.4	13.0	97.5
439.4	11.1	448.2	10.1	494.2	20.3	439.4	11.1	88.9
439.5	11.9	446.0	10.6	480.7	19.2	439.5	11.9	91.4
440.4	11.1	441.8	10.1	450.1	23.4	440.4	11.1	97.8
440.8	9.8	444.5	9.3	464.6	25.1	440.8	9.8	94.9
440.9	10.2	440.6	9.3	439.9	22.4	440.9	10.2	100.2
441.0	10.5	449.8	10.1	496.5	27.3	441.0	10.5	88.8
441.0	10.3	438.5	9.5	426.1	25.4	441.0	10.3	103.5
441.2	10.7	439.5	9.5	431.7	20.5	441.2	10.7	102.2
441.4	11.0	441.0	10.5	439.6	30.4	441.4	11.0	100.4
441.6	13.0	442.3	11.6	446.9	24.8	441.6	13.0	98.8
442.2	11.0	442.2	10.0	442.9	23.2	442.2	11.0	99.8
442.3	13.0	441.2	11.3	436.5	19.4	442.3	13.0	101.3
442.5	10.9	442.6	9.9	443.9	23.6	442.5	10.9	99.7
443.2	10.3	439.9	9.4	423.7	23.5	443.2	10.3	104.6
443.5	10.9	442.7	9.8	439.4	22.3	443.5	10.9	100.9
443.6	10.2	446.4	9.7	461.7	27.1	443.6	10.2	96.1
443.7	10.8	459.6	10.1	540.8	22.9	443.7	10.8	82.0
444.1	10.7	445.1	9.6	451.5	20.1	444.1	10.7	98.4
444.2	11.4	445.8	10.6	454.9	28.5	444.2	11.4	97.7
444.6	13.3	448.8	12.2	471.4	28.8	444.6	13.3	94.3
445.4	10.2	444.9	9.2	443.5	21.8	445.4	10.2	100.4
445.5	8.8	448.5	8.3	464.8	22.6	445.5	8.8	95.9
445.7	11.1	444.8	9.8	441.0	19.5	445.7	11.1	101.1
446.5	11.0	447.3	10.4	452.7	28.8	446.5	11.0	98.6
448.5	9.6	451.8	8.9	469.1	23.6	448.5	9.6	95.6
449.3	11.0	447.9	9.9	441.9	22.2	449.3	11.0	101.7
450.0	13.3	448.3	11.9	440.5	27.3	450.0	13.3	102.2
450.4	12.6	449.0	11.9	442.3	34.4	450.4	12.6	101.8
451.7	8.6	450.1	8.6	442.9	29.0	451.7	8.6	102.0
457.9	11.8	463.2	11.2	490.6	30.4	457.9	11.8	93.3
471.4	10.3	475.3	9.6	494.9	24.6	471.4	10.3	95.2
474.3	11.5	470.4	10.2	452.8	22.3	474.3	11.5	104.7
479.6	12.0	480.8	10.5	487.2	19.0	479.6	12.0	98.4
481.6	11.1	485.0	10.9	502.1	33.9	481.6	11.1	95.9
488.5	11.0	487.8	9.6	485.3	17.8	488.5	11.0	100.7
491.9	12.4	496.7	11.3	520.0	26.6	491.9	12.4	94.6
494.0	9.6	494.4	8.9	497.3	23.0	494.0	9.6	99.3
494.2	11.2	492.8	9.8	487.2	19.7	494.2	11.2	101.4
494.4	13.6	495.6	11.7	502.3	18.6	494.4	13.6	98.4
495.5	9.9	494.8	9.0	492.3	21.8	495.5	9.9	100.7

498.0	12.6	510.4	11.3	567.2	21.2	498.0	12.6	87.8
510.4	10.6	520.5	9.8	566.0	23.5	510.4	10.6	90.2
521.0	11.6	525.8	10.5	547.3	23.8	521.0	11.6	95.2
522.0	12.0	529.1	10.8	560.9	22.8	522.0	12.0	93.1
524.0	14.6	521.2	13.3	510.1	32.7	524.0	14.6	102.7
601.7	14.5	620.6	12.6	691.5	21.6	601.7	14.5	87.0
632.7	17.8	630.2	14.6	621.9	21.2	632.7	17.8	101.7
641.0	14.3	641.9	13.4	646.0	33.7	641.0	14.3	99.2
804.9	16.9	813.2	13.8	836.9	22.1	804.9	16.9	96.2
909.5	20.6	909.8	16.0	911.5	22.5	911.5	22.5	99.8
898.2	19.5	904.6	15.5	921.1	23.4	921.1	23.4	97.5
966.0	28.8	953.2	20.8	924.5	20.5	924.5	20.5	104.5
958.3	21.8	947.9	16.9	925.0	25.4	925.0	25.4	103.6
932.8	21.0	932.6	16.1	932.8	21.8	932.8	21.8	100.0
961.3	19.5	952.9	15.2	934.3	23.1	934.3	23.1	102.9
942.0	21.9	940.4	16.6	937.5	21.1	937.5	21.1	100.5
927.4	23.2	930.3	17.5	937.9	20.5	937.9	20.5	98.9
958.0	24.7	953.8	18.3	945.0	21.3	945.0	21.3	101.4
976.3	20.0	966.6	15.3	945.6	21.5	945.6	21.5	103.3
963.4	23.0	958.1	17.3	946.8	21.6	946.8	21.6	101.7
952.6	19.8	950.7	15.3	947.2	21.9	947.2	21.9	100.6
939.9	25.1	945.0	18.8	957.8	21.6	957.8	21.6	98.1
923.3	18.2	934.9	14.3	963.0	20.5	963.0	20.5	95.9
951.0	22.8	955.8	16.9	968.0	18.0	968.0	18.0	98.2
945.4	22.4	952.9	17.5	971.1	25.0	971.1	25.0	97.3
941.4	21.5	953.5	16.1	982.5	17.8	982.5	17.8	95.8
899.4	22.4	925.2	17.3	988.0	20.4	988.0	20.4	91.0
1006.5	20.0	1001.2	14.8	990.4	17.9	990.4	17.9	101.6
1038.6	31.2	1030.5	22.5	1014.1	24.5	1014.1	24.5	102.4
1014.5	20.2	1017.3	14.9	1024.3	17.3	1024.3	17.3	99.0
1029.7	19.7	1029.2	14.6	1029.1	18.7	1029.1	18.7	100.1
1034.7	22.2	1034.0	16.1	1033.4	17.4	1033.4	17.4	100.1
1056.2	17.9	1050.3	13.6	1038.9	19.4	1038.9	19.4	101.7
997.9	20.8	1012.2	16.3	1044.1	24.0	1044.1	24.0	95.6
1093.1	28.5	1077.9	20.0	1048.2	20.6	1048.2	20.6	104.3
983.2	21.3	1004.6	16.2	1052.3	20.1	1052.3	20.1	93.4
1036.6	23.2	1042.9	16.9	1057.0	18.9	1057.0	18.9	98.1
1084.1	26.5	1075.1	18.8	1058.0	20.0	1058.0	20.0	102.5
923.7	17.9	967.0	14.7	1067.9	22.1	1067.9	22.1	86.5
1100.9	21.5	1090.2	16.4	1069.6	24.6	1069.6	24.6	102.9
1072.6	25.0	1071.9	18.3	1071.4	22.5	1071.4	22.5	100.1
1052.5	24.0	1059.9	18.1	1076.1	24.5	1076.1	24.5	97.8
1112.1	21.2	1102.0	15.7	1082.9	21.1	1082.9	21.1	102.7
1103.2	27.8	1096.4	19.4	1083.6	18.3	1083.6	18.3	101.8
1130.7	31.3	1117.1	21.3	1091.7	17.2	1091.7	17.2	103.6
1066.9	25.3	1076.6	18.6	1097.0	22.2	1097.0	22.2	97.3
1073.7	22.9	1086.3	17.0	1112.4	21.3	1112.4	21.3	96.5

1028.8	24.9	1056.7	18.5	1115.9	20.9	1115.9	20.9	92.2
952.7	22.6	1004.1	20.0	1118.9	36.4	1118.9	36.4	85.1
1094.5	25.5	1103.0	18.2	1120.6	18.8	1120.6	18.8	97.7
1129.8	26.6	1126.8	19.4	1121.8	24.7	1121.8	24.7	100.7
1111.1	23.5	1116.6	17.0	1128.3	19.5	1128.3	19.5	98.5
1131.7	29.1	1130.6	20.9	1129.5	24.4	1129.5	24.4	100.2
1112.5	23.2	1119.6	16.9	1134.2	20.2	1134.2	20.2	98.1
1190.8	23.5	1170.9	16.0	1135.1	15.4	1135.1	15.4	104.9
1178.8	17.7	1168.9	14.4	1151.3	25.2	1151.3	25.2	102.4
1192.9	27.6	1182.7	19.4	1165.1	22.2	1165.1	22.2	102.4
1119.2	27.9	1136.1	20.2	1169.4	23.4	1169.4	23.4	95.7
1160.8	24.7	1166.3	17.7	1177.6	20.6	1177.6	20.6	98.6
1146.8	29.3	1159.1	21.0	1183.0	23.7	1183.0	23.7	96.9
1056.4	22.9	1099.8	17.7	1187.4	23.3	1187.4	23.3	89.0
1226.4	24.1	1214.2	18.2	1193.5	27.4	1193.5	27.4	102.8
1261.9	30.2	1243.4	19.7	1212.4	14.9	1212.4	14.9	104.1
1209.5	28.7	1214.4	20.2	1224.0	22.7	1224.0	22.7	98.8
1231.3	24.8	1235.1	17.3	1242.6	19.3	1242.6	19.3	99.1
1259.1	25.0	1253.0	17.3	1243.4	19.7	1243.4	19.7	101.3
1224.1	26.7	1235.3	18.7	1255.7	20.2	1255.7	20.2	97.5
1084.6	27.8	1143.6	20.7	1258.2	22.2	1258.2	22.2	86.2
1305.1	20.0	1319.2	14.3	1343.0	18.4	1343.0	18.4	97.2
1332.2	31.7	1340.8	20.8	1355.3	17.8	1355.3	17.8	98.3
1340.1	24.7	1347.3	17.7	1359.5	23.4	1359.5	23.4	98.6
1250.7	33.6	1291.4	22.9	1360.4	20.3	1360.4	20.3	91.9
1282.7	26.3	1313.4	18.6	1364.7	21.7	1364.7	21.7	94.0
1337.9	27.1	1352.9	18.1	1377.6	17.7	1377.6	17.7	97.1
1375.9	24.4	1376.5	16.7	1378.3	19.5	1378.3	19.5	99.8
1377.8	31.2	1379.9	20.7	1383.9	20.9	1383.9	20.9	99.6
1426.0	28.9	1425.2	18.9	1424.8	19.0	1424.8	19.0	100.1
1470.3	28.8	1462.9	18.7	1453.0	19.2	1453.0	19.2	101.2
1389.7	28.5	1415.9	18.8	1456.3	17.5	1456.3	17.5	95.4
1490.2	38.2	1481.4	24.0	1469.6	21.2	1469.6	21.2	101.4
1438.4	28.6	1453.7	18.8	1476.9	19.2	1476.9	19.2	97.4
1482.8	27.1	1492.6	18.4	1507.3	21.6	1507.3	21.6	98.4
1528.2	30.9	1527.2	18.9	1526.4	14.0	1526.4	14.0	100.1
1584.8	36.0	1578.6	21.6	1571.2	16.2	1571.2	16.2	100.9
1564.7	35.9	1569.6	22.1	1577.0	18.4	1577.0	18.4	99.2
1597.7	27.7	1593.2	17.3	1588.0	16.5	1588.0	16.5	100.6
1331.9	29.0	1433.8	19.7	1589.3	16.2	1589.3	16.2	83.8
1618.7	35.7	1608.4	21.8	1595.7	19.3	1595.7	19.3	101.4
1553.4	36.6	1582.8	22.6	1622.9	17.8	1622.9	17.8	95.7
1640.9	37.2	1635.9	22.7	1630.4	20.6	1630.4	20.6	100.6
1618.4	34.7	1632.9	21.1	1652.3	17.4	1652.3	17.4	97.9
1652.1	20.7	1652.0	13.7	1652.6	16.5	1652.6	16.5	100.0
1656.4	37.0	1655.4	22.3	1655.0	18.9	1655.0	18.9	100.1
1679.7	38.4	1672.8	22.6	1665.0	16.7	1665.0	16.7	100.9

1689.2	39.9	1682.8	24.3	1675.6	22.7	1675.6	22.7	100.8
1760.9	34.5	1727.6	20.3	1688.3	18.3	1688.3	18.3	104.3
1583.8	32.2	1631.7	20.3	1694.9	18.3	1694.9	18.3	93.4
1749.3	29.9	1738.2	18.3	1725.7	18.5	1725.7	18.5	101.4
1759.2	33.2	1745.1	19.4	1728.9	16.0	1728.9	16.0	101.8
1725.9	42.1	1736.9	24.2	1750.9	15.9	1750.9	15.9	98.6
1761.6	38.8	1761.4	22.6	1762.0	17.9	1762.0	17.9	100.0
1796.6	36.2	1804.7	21.6	1814.8	20.2	1814.8	20.2	99.0
1870.8	38.7	1861.0	21.1	1850.9	12.2	1850.9	12.2	101.1
1872.6	43.9	1873.8	26.2	1875.8	26.2	1875.8	26.2	99.8
1913.9	39.7	1940.9	21.6	1970.5	12.7	1970.5	12.7	97.1
2297.4	43.0	2304.6	22.1	2311.7	16.6	2311.7	16.6	99.4
2700.1	61.3	2736.7	27.6	2764.5	14.5	2764.5	14.5	97.7

Moscovian detrital zircon raw data

		Apparent ages (Ma)						
206Pb*	±	207Pb*	±	206Pb*	±	Best age	±	Conc
238U*	(Ma)	235U	(Ma)	207Pb*	(Ma)	(Ma)	(Ma)	(%)
388.3	11.3	414.1	10.9	561.4	24.3	388.3	11.3	NA
416.4	10.1	431.8	9.5	515.8	21.2	416.4	10.1	80.7
423.8	7.6	434.8	7.4	494.6	21.3	423.8	7.6	85.7
425.4	9.7	432.0	9.2	468.3	25.4	425.4	9.7	90.8
426.2	9.7	441.0	9.3	519.9	25.3	426.2	9.7	82.0
427.6	8.6	430.1	7.9	444.0	19.4	427.6	8.6	96.3
430.2	12.3	433.4	11.0	451.6	22.9	430.2	12.3	95.3
430.4	9.6	431.3	8.9	436.7	22.5	430.4	9.6	98.6
430.9	8.1	437.9	7.9	476.0	24.1	430.9	8.1	90.5
431.2	8.8	437.0	8.6	468.8	26.1	431.2	8.8	92.0
432.5	11.5	439.6	10.2	477.5	18.7	432.5	11.5	90.6
432.6	11.5	436.4	10.3	457.7	20.1	432.6	11.5	94.5
433.0	8.9	436.6	8.6	456.6	25.9	433.0	8.9	94.8
435.6	9.9	434.3	9.0	428.6	21.5	435.6	9.9	101.6
435.9	9.7	438.5	8.9	453.0	21.7	435.9	9.7	96.2
435.9	8.2	437.3	7.6	445.8	20.0	435.9	8.2	97.8
436.1	13.1	441.5	11.8	470.4	25.1	436.1	13.1	92.7
436.3	11.3	435.0	10.0	428.8	19.9	436.3	11.3	101.8
436.5	11.5	439.6	10.3	457.0	21.1	436.5	11.5	95.5
436.8	9.1	437.7	8.3	443.1	20.2	436.8	9.1	98.6
437.8	10.7	434.7	9.7	419.0	24.3	437.8	10.7	104.5
438.4	11.4	439.4	10.3	445.7	24.3	438.4	11.4	98.4
438.8	9.5	440.6	8.7	451.1	22.3	438.8	9.5	97.3

439.4	7.4	444.4	7.3	471.3	23.0	439.4	7.4	93.2
441.3	10.0	444.7	9.3	463.5	23.1	441.3	10.0	95.2
442.6	10.7	445.2	9.8	459.6	23.8	442.6	10.7	96.3
446.6	9.6	444.4	8.6	433.6	19.6	446.6	9.6	103.0
448.7	13.7	451.1	12.2	464.4	24.7	448.7	13.7	96.6
450.3	10.3	449.6	9.4	446.8	22.6	450.3	10.3	100.8
453.7	9.7	460.0	8.9	492.6	21.0	453.7	9.7	92.1
462.9	7.8	465.3	7.4	478.0	20.4	462.9	7.8	96.9
482.5	12.0	484.9	11.4	497.3	32.0	482.5	12.0	97.0
492.6	12.9	495.3	11.2	508.9	18.6	492.6	12.9	96.8
494.5	11.3	491.3	10.1	477.5	23.4	494.5	11.3	103.6
496.4	9.1	498.2	8.7	507.6	24.0	496.4	9.1	97.8
531.9	13.6	536.6	12.2	557.8	26.3	531.9	13.6	95.4
532.0	11.7	543.2	10.4	591.2	19.8	532.0	11.7	90.0
536.8	13.2	543.7	11.6	573.7	22.1	536.8	13.2	93.6
541.1	10.5	550.6	9.8	591.2	24.4	541.1	10.5	91.5
542.0	9.8	538.9	9.2	526.8	25.1	542.0	9.8	102.9
542.2	10.8	541.8	9.5	541.3	19.7	542.2	10.8	100.2
605.6	10.1	612.1	9.7	637.0	26.0	605.6	10.1	95.1
631.9	15.7	632.6	13.7	636.1	27.7	631.9	15.7	99.3
635.6	15.7	630.3	13.6	612.1	28.1	635.6	15.7	103.8
636.5	11.0	643.8	9.6	670.5	18.6	636.5	11.0	94.9
639.3	13.7	658.4	11.9	725.3	20.4	639.3	13.7	88.1
641.2	14.0	655.7	12.0	706.8	20.5	641.2	14.0	90.7
658.1	15.4	662.3	12.7	677.5	18.6	658.1	15.4	97.1
662.2	15.3	665.5	13.0	677.3	23.8	662.2	15.3	97.8
672.4	15.0	675.7	12.9	687.7	24.5	672.4	15.0	97.8
707.5	15.4	735.5	13.5	822.8	24.4	707.5	15.4	86.0
810.4	20.1	806.3	15.4	796.0	17.8	810.4	20.1	101.8
968.3	20.8	954.9	15.0	925.2	15.0	925.2	15.0	104.7
910.3	19.7	920.5	15.4	945.9	21.5	945.9	21.5	96.2
993.1	24.6	979.0	17.9	948.5	20.5	948.5	20.5	104.7
955.2	21.8	955.6	16.2	957.3	18.1	957.3	18.1	99.8
963.9	16.7	963.4	12.8	963.4	17.9	963.4	17.9	100.1
971.4	21.7	969.0	16.2	964.4	19.5	964.4	19.5	100.7
903.4	23.5	921.2	17.8	965.2	19.2	965.2	19.2	93.6
1000.7	26.5	990.5	19.1	968.8	19.6	968.8	19.6	103.3
930.7	17.8	942.7	13.5	971.9	16.1	971.9	16.1	95.8
949.7	21.3	957.1	16.3	975.1	21.3	975.1	21.3	97.4
974.3	20.5	976.1	15.1	981.0	17.1	981.0	17.1	99.3
935.8	23.5	951.0	18.2	987.3	24.7	987.3	24.7	94.8
895.4	16.3	922.4	13.6	988.5	22.7	988.5	22.7	90.6
1007.6	24.7	1001.9	18.0	990.2	20.2	990.2	20.2	101.8
939.7	22.5	955.8	17.2	994.2	20.9	994.2	20.9	94.5
951.9	24.1	965.6	18.2	997.6	21.4	997.6	21.4	95.4
1051.7	22.9	1037.2	16.5	1007.6	19.1	1007.6	19.1	104.4
1030.9	16.3	1023.7	12.5	1009.1	18.8	1009.1	18.8	102.2

983.8	21.1	994.6	16.1	1019.4	20.8	1019.4	20.8	96.5
1012.9	22.9	1016.5	16.9	1025.1	19.7	1025.1	19.7	98.8
1070.3	23.4	1055.4	17.0	1025.5	21.3	1025.5	21.3	104.4
1004.9	28.2	1014.8	20.0	1037.2	15.3	1037.2	15.3	96.9
1031.4	22.5	1033.7	15.9	1039.6	13.5	1039.6	13.5	99.2
1012.1	24.7	1020.6	18.3	1039.8	21.1	1039.8	21.1	97.3
1056.4	20.5	1052.4	15.1	1045.1	19.4	1045.1	19.4	101.1
1028.5	24.0	1034.1	17.3	1046.8	17.0	1046.8	17.0	98.3
1058.0	21.9	1054.6	15.6	1048.6	15.5	1048.6	15.5	100.9
1013.0	19.8	1024.5	15.0	1050.0	19.2	1050.0	19.2	96.5
1063.6	24.9	1059.2	17.9	1051.3	20.3	1051.3	20.3	101.2
1007.0	22.7	1023.2	16.9	1058.9	19.3	1058.9	19.3	95.1
1085.4	23.7	1080.3	17.1	1070.7	19.8	1070.7	19.8	101.4
1074.4	22.9	1073.8	16.9	1073.6	21.2	1073.6	21.2	100.1
1089.1	23.0	1086.5	16.1	1082.2	15.5	1082.2	15.5	100.6
1060.1	23.4	1068.9	17.6	1087.7	23.0	1087.7	23.0	97.5
1094.9	22.5	1096.9	16.7	1101.5	22.2	1101.5	22.2	99.4
1038.9	21.0	1059.4	15.9	1102.8	20.3	1102.8	20.3	94.2
949.5	18.5	1001.3	14.9	1117.4	20.6	1117.4	20.6	85.0
1081.8	23.7	1095.4	17.0	1123.5	17.7	1123.5	17.7	96.3
994.6	19.1	1038.8	16.9	1133.9	31.2	1133.9	31.2	87.7
1166.8	23.5	1156.6	16.3	1138.5	16.8	1138.5	16.8	102.5
1135.1	21.0	1137.4	15.2	1142.7	18.2	1142.7	18.2	99.3
1190.0	25.0	1173.6	17.5	1144.4	20.3	1144.4	20.3	104.0
1160.4	28.4	1156.5	20.0	1150.1	22.4	1150.1	22.4	100.9
1133.9	23.3	1141.2	16.8	1156.0	19.5	1156.0	19.5	98.1
1105.4	19.7	1123.9	14.6	1160.7	18.4	1160.7	18.4	95.2
1146.9	24.8	1152.5	17.8	1163.8	20.5	1163.8	20.5	98.6
1013.7	22.5	1062.8	17.1	1165.8	19.6	1165.8	19.6	87.0
1180.2	22.5	1177.9	15.4	1174.5	14.6	1174.5	14.6	100.5
1179.2	26.5	1177.6	18.7	1175.6	21.0	1175.6	21.0	100.3
1184.8	23.5	1182.2	16.5	1178.2	18.5	1178.2	18.5	100.6
1166.1	25.7	1172.6	17.9	1185.4	18.2	1185.4	18.2	98.4
1192.3	24.1	1190.2	16.9	1187.2	18.7	1187.2	18.7	100.4
1160.8	29.2	1171.0	21.0	1190.7	24.5	1190.7	24.5	97.5
1102.4	27.5	1139.2	20.0	1210.8	21.3	1210.8	21.3	91.0
1249.8	33.5	1235.9	22.1	1212.7	18.4	1212.7	18.4	103.1
989.9	23.3	1063.8	18.9	1219.6	26.3	1219.6	26.3	81.2
1141.4	29.0	1170.6	20.3	1226.0	18.1	1226.0	18.1	93.1
1235.5	27.5	1232.4	19.0	1227.8	20.7	1227.8	20.7	100.6
1015.8	23.6	1088.2	18.4	1237.1	22.3	1237.1	22.3	82.1
1271.0	24.2	1258.5	16.7	1238.1	18.9	1238.1	18.9	102.7
1210.9	23.3	1223.2	16.3	1245.9	17.4	1245.9	17.4	97.2
1221.1	33.6	1231.7	22.6	1251.2	18.5	1251.2	18.5	97.6
1222.4	30.5	1232.8	20.5	1251.9	16.3	1251.9	16.3	97.6
1157.4	29.5	1191.9	20.3	1256.0	15.8	1256.0	15.8	92.1
1264.1	28.3	1260.9	19.5	1256.2	21.5	1256.2	21.5	100.6

1243.5	24.3	1256.4	16.7	1279.4	16.5	1279.4	16.5	97.2
1265.8	22.6	1276.0	16.0	1294.1	19.5	1294.1	19.5	97.8
1241.4	28.0	1260.5	18.6	1294.1	12.8	1294.1	12.8	95.9
1305.3	29.3	1303.3	19.7	1300.8	19.7	1300.8	19.7	100.3
1325.3	29.6	1315.9	19.7	1301.3	19.4	1301.3	19.4	101.8
1334.8	31.5	1324.2	20.5	1307.9	18.1	1307.9	18.1	102.1
1302.9	34.7	1308.5	22.9	1318.7	19.3	1318.7	19.3	98.8
1348.9	27.9	1337.1	18.3	1319.0	17.7	1319.0	17.7	102.3
1319.0	32.9	1318.8	21.5	1319.3	17.9	1319.3	17.9	100.0
1371.1	27.5	1351.6	18.3	1321.6	19.6	1321.6	19.6	103.7
1293.8	29.2	1305.1	19.9	1324.7	20.3	1324.7	20.3	97.7
1317.0	32.1	1320.7	20.8	1327.7	15.3	1327.7	15.3	99.2
1305.2	22.6	1313.5	15.5	1328.0	16.6	1328.0	16.6	98.3
1326.3	36.3	1327.8	24.1	1331.1	22.5	1331.1	22.5	99.6
1348.0	32.7	1341.2	21.4	1331.3	19.5	1331.3	19.5	101.2
1257.4	25.6	1285.4	18.2	1333.4	21.1	1333.4	21.1	94.3
1309.3	24.4	1323.5	16.8	1347.3	18.3	1347.3	18.3	97.2
1325.4	28.5	1335.4	19.2	1352.3	19.4	1352.3	19.4	98.0
1390.4	28.0	1377.8	18.2	1359.1	17.4	1359.1	17.4	102.3
1408.9	24.5	1389.7	16.0	1361.0	16.4	1361.0	16.4	103.5
1288.6	30.2	1316.2	20.5	1362.3	19.7	1362.3	19.7	94.6
1301.5	26.3	1324.7	18.6	1363.1	22.2	1363.1	22.2	95.5
1328.7	26.8	1343.1	18.7	1366.9	22.1	1366.9	22.1	97.2
1240.0	32.8	1287.1	22.0	1367.4	15.1	1367.4	15.1	90.7
1407.0	25.9	1391.0	16.7	1367.4	15.8	1367.4	15.8	102.9
1389.2	25.4	1381.1	16.8	1369.3	17.6	1369.3	17.6	101.5
1363.2	35.8	1371.3	23.1	1384.8	18.4	1384.8	18.4	98.4
1247.9	32.6	1301.9	22.1	1392.7	17.0	1392.7	17.0	89.6
1397.5	28.5	1395.7	18.3	1393.9	16.0	1393.9	16.0	100.3
1377.9	31.7	1390.3	20.2	1410.2	14.7	1410.2	14.7	97.7
1156.7	31.5	1250.6	23.7	1417.0	27.0	1417.0	27.0	81.6
1418.0	26.6	1426.9	17.5	1441.0	17.8	1441.0	17.8	98.4
1415.3	31.1	1426.2	19.9	1443.3	16.7	1443.3	16.7	98.1
1279.7	25.7	1342.1	17.9	1443.9	18.0	1443.9	18.0	88.6
1416.8	37.7	1430.1	24.0	1450.9	19.3	1450.9	19.3	97.6
1381.5	34.5	1411.5	23.0	1457.9	22.1	1457.9	22.1	94.8
1438.1	26.4	1446.7	16.9	1460.3	14.8	1460.3	14.8	98.5
1419.8	28.8	1439.2	18.4	1468.9	14.9	1468.9	14.9	96.7
1496.9	34.4	1485.1	21.4	1469.2	18.1	1469.2	18.1	101.9
1463.1	29.9	1467.0	19.0	1473.4	16.3	1473.4	16.3	99.3
1329.9	30.9	1387.7	20.8	1478.4	18.2	1478.4	18.2	90.0
1519.7	35.5	1507.6	21.5	1491.6	15.0	1491.6	15.0	101.9
1452.4	27.7	1468.9	17.9	1493.6	16.8	1493.6	16.8	97.2
1518.3	38.9	1507.9	23.8	1494.0	18.3	1494.0	18.3	101.6
1468.3	37.0	1480.8	24.0	1499.6	23.4	1499.6	23.4	97.9
1444.4	29.3	1467.5	18.9	1501.9	16.9	1501.9	16.9	96.2
1443.7	33.8	1467.4	21.8	1502.5	19.4	1502.5	19.4	96.1

1510.5	27.7	1514.4	17.2	1520.6	13.8	1520.6	13.8	99.3
1377.3	25.1	1435.8	17.2	1524.3	18.0	1524.3	18.0	90.4
1526.7	42.0	1526.1	26.3	1526.1	23.5	1526.1	23.5	100.0
1486.7	28.8	1503.9	18.7	1529.0	18.6	1529.0	18.6	97.2
1504.3	30.0	1515.0	19.4	1530.7	19.8	1530.7	19.8	98.3
1487.6	29.8	1508.5	19.3	1538.8	18.7	1538.8	18.7	96.7
1462.0	35.5	1494.6	22.4	1541.9	17.3	1541.9	17.3	94.8
1613.9	35.2	1588.6	20.7	1556.0	14.1	1556.0	14.1	103.7
1607.2	34.4	1601.4	21.1	1594.6	18.6	1594.6	18.6	100.8
1609.9	33.3	1605.1	20.5	1599.7	18.9	1599.7	18.9	100.6
1615.1	35.3	1610.3	21.3	1604.8	17.2	1604.8	17.2	100.6
1623.9	35.8	1617.1	21.6	1609.1	17.9	1609.1	17.9	100.9
1622.8	31.3	1619.9	19.0	1616.8	16.5	1616.8	16.5	100.4
1638.1	31.6	1630.2	19.6	1620.8	19.1	1620.8	19.1	101.1
1546.2	37.4	1579.9	23.1	1626.0	17.5	1626.0	17.5	95.1
1701.4	43.5	1668.1	25.6	1627.3	21.1	1627.3	21.1	104.6
1635.1	33.2	1632.3	19.8	1629.6	15.4	1629.6	15.4	100.3
1563.0	35.1	1592.2	21.6	1632.0	17.0	1632.0	17.0	95.8
1563.8	39.4	1593.7	23.9	1634.3	16.6	1634.3	16.6	95.7
1630.1	37.7	1631.6	22.7	1634.4	18.2	1634.4	18.2	99.7
1593.0	28.6	1612.1	17.6	1637.9	14.9	1637.9	14.9	97.3
1616.1	23.5	1627.3	15.7	1642.7	19.2	1642.7	19.2	98.4
1631.4	38.6	1636.0	23.0	1642.7	17.3	1642.7	17.3	99.3
1639.9	28.9	1642.8	18.2	1647.4	18.8	1647.4	18.8	99.5
1579.5	36.4	1610.8	22.3	1652.7	17.1	1652.7	17.1	95.6
1607.4	33.4	1627.3	20.3	1654.0	15.9	1654.0	15.9	97.2
1372.8	30.5	1487.6	20.7	1656.1	18.3	1656.1	18.3	82.9
1627.9	33.2	1640.3	19.8	1656.9	14.1	1656.9	14.1	98.3
1640.6	36.4	1647.7	21.8	1657.6	17.2	1657.6	17.2	99.0
1604.4	41.2	1636.2	24.5	1678.2	15.5	1678.2	15.5	95.6
1574.6	26.4	1619.3	17.6	1678.8	19.6	1678.8	19.6	93.8
1653.3	29.9	1680.1	18.8	1714.5	18.9	1714.5	18.9	96.4
1722.1	30.5	1719.7	18.0	1717.5	14.4	1717.5	14.4	100.3
1703.2	31.1	1711.0	18.7	1721.2	16.1	1721.2	16.1	99.0
1583.6	30.8	1645.4	19.4	1726.0	16.8	1726.0	16.8	91.8
1733.1	27.5	1730.8	16.8	1728.8	16.3	1728.8	16.3	100.2
1663.9	39.2	1694.0	22.8	1732.1	13.6	1732.1	13.6	96.1
1774.6	36.4	1757.7	20.8	1738.5	15.2	1738.5	15.2	102.1
1715.2	34.2	1725.6	19.6	1739.1	12.3	1739.1	12.3	98.6
1717.3	29.3	1728.5	17.9	1742.9	17.3	1742.9	17.3	98.5
1728.8	50.6	1736.5	29.2	1746.6	19.7	1746.6	19.7	99.0
1723.0	41.0	1734.2	24.0	1748.5	18.0	1748.5	18.0	98.5
1693.2	33.5	1720.1	20.6	1753.7	19.3	1753.7	19.3	96.5
1771.6	37.4	1764.3	21.6	1756.4	16.3	1756.4	16.3	100.9
1684.6	32.5	1717.7	18.9	1759.1	11.7	1759.1	11.7	95.8
1581.2	28.1	1660.0	17.5	1762.0	13.7	1762.0	13.7	89.7
1707.6	41.8	1737.7	25.1	1775.0	21.4	1775.0	21.4	96.2

1724.2	35.1	1748.6	20.9	1778.6	17.2	1778.6	17.2	96.9
1734.1	32.3	1755.6	19.7	1782.2	18.6	1782.2	18.6	97.3
1680.0	44.1	1730.3	27.3	1792.5	25.5	1792.5	25.5	93.7
1777.4	37.9	1793.1	21.7	1812.3	15.4	1812.3	15.4	98.1
1466.2	33.1	1618.5	21.9	1823.4	18.0	1823.4	18.0	80.4
1607.9	45.9	1705.3	28.2	1828.0	19.9	1828.0	19.9	88.0
1553.9	30.3	1674.0	19.4	1828.8	16.3	1828.8	16.3	85.0
1827.7	30.2	1830.2	17.8	1833.8	16.6	1833.8	16.6	99.7
1836.4	44.2	1840.2	24.7	1845.2	16.3	1845.2	16.3	99.5
1935.2	34.8	1900.0	20.0	1862.5	18.8	1862.5	18.8	103.9
1909.7	35.8	1890.6	20.3	1870.4	17.5	1870.4	17.5	102.1
1890.5	39.6	1880.9	22.7	1871.1	19.4	1871.1	19.4	101.0
1890.4	35.7	1883.0	20.6	1875.6	18.4	1875.6	18.4	100.8
1912.6	34.3	1901.1	19.7	1889.3	17.9	1889.3	17.9	101.2
1886.3	36.1	1889.6	20.1	1894.1	14.1	1894.1	14.1	99.6
1916.5	44.0	1906.8	23.6	1897.0	12.5	1897.0	12.5	101.0
1777.3	40.2	1834.8	23.4	1901.4	17.2	1901.4	17.2	93.5
1918.1	38.0	1913.7	21.2	1909.6	15.9	1909.6	15.9	100.4
1886.6	48.3	1899.4	26.6	1914.2	16.5	1914.2	16.5	98.6
1980.9	46.9	1949.0	26.1	1916.0	22.0	1916.0	22.0	103.4
1901.6	36.5	1913.8	20.7	1927.9	16.5	1927.9	16.5	98.6
1773.5	40.0	1845.7	23.7	1928.9	18.5	1928.9	18.5	91.9
1981.6	31.8	1960.2	17.8	1938.4	14.9	1938.4	14.9	102.2
1795.4	39.0	1866.5	23.0	1947.3	18.5	1947.3	18.5	92.2
1966.9	40.6	1968.8	22.1	1971.4	15.4	1971.4	15.4	99.8
1922.3	41.5	1949.2	23.4	1978.6	18.1	1978.6	18.1	97.2
1956.6	47.7	1968.7	26.0	1982.3	17.1	1982.3	17.1	98.7
2004.8	39.4	1995.6	21.2	1986.8	14.7	1986.8	14.7	100.9
2011.8	41.7	2001.9	23.2	1992.5	19.6	1992.5	19.6	101.0
1954.5	43.0	1976.8	23.5	2000.8	15.9	2000.8	15.9	97.7
2014.4	48.5	2007.4	26.3	2001.0	19.2	2001.0	19.2	100.7
1804.5	32.2	1898.4	19.4	2003.5	16.9	2003.5	16.9	90.1
2009.7	35.3	2007.6	20.1	2006.2	18.5	2006.2	18.5	100.2
1834.2	43.6	1916.6	25.4	2007.7	19.8	2007.7	19.8	91.4
1794.1	45.4	1895.3	26.0	2008.8	15.2	2008.8	15.2	89.3
2178.1	41.5	2173.8	21.1	2170.4	12.3	2170.4	12.3	100.4
2218.0	40.7	2195.8	21.3	2176.0	16.8	2176.0	16.8	101.9
2033.8	42.1	2124.5	24.5	2214.3	23.0	2214.3	23.0	91.8
2204.0	38.1	2360.2	20.5	2498.8	15.4	2498.8	15.4	88.2
2516.9	46.9	2523.3	23.1	2529.2	17.6	2529.2	17.6	99.5
2525.9	47.8	2554.0	23.0	2577.0	15.5	2577.0	15.5	98.0
2499.2	48.8	2570.2	24.2	2627.5	17.6	2627.5	17.6	95.1
2744.9	46.6	2721.5	22.0	2704.9	16.8	2704.9	16.8	101.5
2680.9	52.3	2696.2	24.3	2708.4	15.9	2708.4	15.9	99.0
2528.7	41.2	2629.8	19.9	2709.3	12.8	2709.3	12.8	93.3
2648.1	56.6	2682.8	25.8	2709.7	13.8	2709.7	13.8	97.7
2607.8	44.2	2708.4	20.8	2785.1	12.5	2785.1	12.5	93.6

2533.6	59.9	2676.0	28.4	2786.1	15.5	2786.1	15.5	90.9
2768.7	39.4	2787.0	19.2	2801.0	16.6	2801.0	16.6	98.8
2781.8	57.1	2802.7	26.2	2818.5	17.8	2818.5	17.8	98.7
2359.3	51.0	2625.7	25.7	2838.7	14.7	2838.7	14.7	83.1
2739.9	51.6	2799.7	24.3	2843.7	17.6	2843.7	17.6	96.3
2747.1	57.9	2814.6	27.3	2864.0	19.9	2864.0	19.9	95.9
2925.4	48.1	2894.1	22.0	2873.1	16.9	2873.1	16.9	101.8
2925.1	58.0	2942.9	25.4	2955.8	15.3	2955.8	15.3	99.0
2918.6	66.5	3208.3	29.1	3395.5	15.0	3395.5	15.0	86.0

Asselian detrital zircon raw data

		Apparent ages (Ma)						
206Pb*	±	207Pb*	±	206Pb*	±	Best age	±	Conc
238U*	(Ma)	235U	(Ma)	207Pb*	(Ma)	(Ma)	(Ma)	(%)
395.6	12.4	394.7	10.9	389.8	19.5	395.6	12.4	NA
415.9	8.7	418.5	8.2	433.9	21.9	415.9	8.7	95.8
417.0	8.7	427.9	8.4	487.6	23.1	417.0	8.7	85.5
421.3	8.4	430.6	8.2	481.4	24.3	421.3	8.4	87.5
423.5	10.6	424.0	10.0	427.4	28.3	423.5	10.6	99.1
423.6	8.6	430.9	8.2	470.9	23.5	423.6	8.6	90.0
425.8	10.9	429.9	10.1	452.7	25.2	425.8	10.9	94.1
425.8	9.5	433.6	9.0	475.8	24.7	425.8	9.5	89.5
426.7	10.0	429.7	9.5	447.1	26.2	426.7	10.0	95.4
429.3	9.3	433.1	8.6	454.4	20.8	429.3	9.3	94.5
433.7	11.7	435.0	10.5	442.5	23.2	433.7	11.7	98.0
436.5	10.4	436.9	9.8	440.0	28.0	436.5	10.4	99.2
473.8	13.6	477.1	12.2	494.1	26.7	473.8	13.6	95.9
489.2	15.1	504.7	13.4	576.6	22.4	489.2	15.1	84.8
511.9	9.7	535.5	10.2	638.2	31.2	511.9	9.7	80.2
560.0	13.0	565.5	11.9	588.3	27.5	560.0	13.0	95.2
567.5	16.3	575.9	14.2	609.9	26.4	567.5	16.3	93.0
624.7	13.1	637.0	11.3	682.0	19.7	624.7	13.1	91.6
863.9	23.0	873.6	17.9	899.0	23.4	863.9	23.0	96.1
894.7	18.0	906.2	13.8	935.0	16.2	935.0	16.2	95.7
899.1	19.6	909.7	15.2	936.5	19.6	936.5	19.6	96.0
950.2	19.9	946.8	15.2	939.7	20.3	939.7	20.3	101.1
954.0	22.6	950.2	16.8	942.2	19.3	942.2	19.3	101.2
932.4	23.3	936.2	17.5	945.8	20.4	945.8	20.4	98.6
991.4	22.3	981.4	17.7	959.7	29.0	959.7	29.0	103.3
1021.5	17.7	1016.2	13.4	1005.9	18.9	1005.9	18.9	101.5
1042.2	21.5	1030.9	16.2	1007.9	23.2	1007.9	23.2	103.4

972.4	24.7	984.9	18.0	1013.9	16.5	1013.9	16.5	95.9
1033.6	18.3	1031.1	14.3	1026.5	22.1	1026.5	22.1	100.7
1031.3	21.5	1031.3	16.0	1032.3	20.2	1032.3	20.2	99.9
1032.4	17.0	1035.7	13.2	1043.7	19.4	1043.7	19.4	98.9
1059.2	24.2	1054.5	17.1	1045.7	16.7	1045.7	16.7	101.3
1075.4	23.3	1066.6	16.8	1049.6	19.3	1049.6	19.3	102.5
1048.0	22.8	1048.8	16.7	1051.3	20.4	1051.3	20.4	99.7
1055.2	24.6	1053.8	17.7	1051.9	19.5	1051.9	19.5	100.3
1028.7	22.1	1036.0	16.8	1052.4	22.6	1052.4	22.6	97.7
1004.5	21.7	1019.7	16.4	1053.4	20.6	1053.4	20.6	95.4
1016.7	19.6	1028.2	15.6	1053.7	24.1	1053.7	24.1	96.5
1071.9	24.6	1066.1	17.7	1055.3	20.2	1055.3	20.2	101.6
1029.4	23.3	1037.7	17.6	1056.2	23.2	1056.2	23.2	97.5
1071.5	21.2	1067.9	15.5	1061.4	18.9	1061.4	18.9	100.9
1067.1	28.0	1066.2	19.6	1065.2	17.0	1065.2	17.0	100.2
1036.6	21.8	1046.5	16.0	1068.1	17.8	1068.1	17.8	97.0
980.2	22.4	1009.2	17.4	1073.5	23.3	1073.5	23.3	91.3
1088.2	21.8	1083.1	15.6	1073.9	17.1	1073.9	17.1	101.3
1060.5	20.0	1066.5	18.0	1079.7	36.1	1079.7	36.1	98.2
1018.5	21.5	1038.2	16.1	1080.7	19.7	1080.7	19.7	94.2
1070.8	21.3	1074.3	15.4	1082.3	17.7	1082.3	17.7	98.9
1088.9	27.7	1087.8	21.2	1086.6	31.3	1086.6	31.3	100.2
975.3	25.3	1010.2	18.8	1087.5	17.7	1087.5	17.7	89.7
1078.9	20.3	1084.9	16.9	1097.8	29.9	1097.8	29.9	98.3
1064.6	19.7	1076.9	14.6	1102.6	17.8	1102.6	17.8	96.6
941.9	22.0	991.7	17.2	1104.4	20.4	1104.4	20.4	85.3
1077.2	23.5	1087.2	18.8	1108.1	30.5	1108.1	30.5	97.2
1165.0	25.3	1147.6	17.8	1115.9	20.7	1115.9	20.7	104.4
1097.7	20.1	1104.5	14.5	1118.8	16.1	1118.8	16.1	98.1
1078.0	25.6	1091.8	18.7	1120.2	21.3	1120.2	21.3	96.2
1128.1	23.2	1126.1	16.8	1123.0	20.3	1123.0	20.3	100.5
1129.2	26.6	1128.7	18.4	1128.6	17.3	1128.6	17.3	100.1
1100.4	28.5	1109.7	19.9	1128.7	16.9	1128.7	16.9	97.5
1154.9	29.5	1147.5	20.0	1134.3	17.0	1134.3	17.0	101.8
1144.9	25.8	1142.6	18.0	1139.1	17.9	1139.1	17.9	100.5
1159.7	23.5	1152.3	16.5	1139.2	18.5	1139.2	18.5	101.8
958.3	21.2	1015.0	16.8	1140.3	21.7	1140.3	21.7	84.0
1161.0	23.9	1153.5	16.9	1140.4	19.5	1140.4	19.5	101.8
986.3	21.8	1035.6	16.7	1142.2	19.4	1142.2	19.4	86.3
1165.9	23.4	1158.0	16.5	1144.0	19.1	1144.0	19.1	101.9
1157.4	21.1	1154.2	16.5	1149.0	26.6	1149.0	26.6	100.7
1182.4	25.3	1170.6	17.4	1149.6	17.5	1149.6	17.5	102.9
1107.0	22.2	1121.6	16.3	1150.9	20.1	1150.9	20.1	96.2
1119.0	31.0	1129.8	21.5	1151.4	18.0	1151.4	18.0	97.2
1132.8	29.9	1138.9	20.8	1151.5	18.8	1151.5	18.8	98.4
1118.6	20.0	1130.2	14.9	1153.3	19.5	1153.3	19.5	97.0
1180.5	26.5	1170.7	18.0	1153.4	16.4	1153.4	16.4	102.4

1071.1	27.1	1098.8	22.5	1155.0	38.0	1155.0	38.0	92.7
1167.8	28.7	1164.4	19.9	1159.0	20.5	1159.0	20.5	100.8
1146.7	19.9	1151.5	14.7	1161.5	19.4	1161.5	19.4	98.7
1173.2	27.7	1173.3	19.7	1174.5	22.8	1174.5	22.8	99.9
1128.4	20.4	1146.1	14.3	1180.5	13.5	1180.5	13.5	95.6
1130.6	31.3	1148.0	22.0	1181.9	21.2	1181.9	21.2	95.7
1122.8	22.2	1144.8	16.1	1187.6	18.2	1187.6	18.2	94.5
983.2	26.6	1050.4	20.2	1193.7	20.1	1193.7	20.1	82.4
1163.2	26.8	1174.4	18.9	1195.9	20.1	1195.9	20.1	97.3
1192.9	28.6	1197.5	19.6	1206.8	18.0	1206.8	18.0	98.8
1175.9	24.1	1186.7	17.2	1207.2	20.1	1207.2	20.1	97.4
1151.4	27.2	1171.5	19.4	1209.7	20.6	1209.7	20.6	95.2
1185.8	26.1	1195.5	18.0	1213.8	16.6	1213.8	16.6	97.7
1236.5	25.9	1230.2	17.8	1220.0	18.7	1220.0	18.7	101.4
1154.7	26.0	1177.9	21.4	1221.8	36.3	1221.8	36.3	94.5
1195.2	26.7	1208.5	18.3	1233.3	16.2	1233.3	16.2	96.9
1066.7	21.9	1124.2	16.0	1237.9	14.8	1237.9	14.8	86.2
1136.6	28.8	1172.8	20.6	1241.1	21.1	1241.1	21.1	91.6
1215.0	28.4	1225.0	19.6	1243.4	19.9	1243.4	19.9	97.7
1221.1	27.2	1229.0	18.8	1243.7	19.0	1243.7	19.0	98.2
1206.6	27.4	1223.7	19.3	1254.7	21.5	1254.7	21.5	96.2
1277.0	30.2	1274.3	20.1	1270.7	17.9	1270.7	17.9	100.5
1231.0	30.7	1248.5	21.0	1279.7	19.8	1279.7	19.8	96.2
1253.4	21.4	1266.7	14.4	1290.1	12.8	1290.1	12.8	97.1
1308.6	21.4	1305.2	14.7	1300.5	16.8	1300.5	16.8	100.6
1257.8	21.9	1273.5	15.7	1301.0	19.2	1301.0	19.2	96.7
1323.7	35.4	1315.0	23.4	1301.7	22.2	1301.7	22.2	101.7
1341.5	25.3	1328.5	17.0	1308.3	18.8	1308.3	18.8	102.5
1313.4	28.3	1311.5	18.5	1309.3	16.0	1309.3	16.0	100.3
1342.1	25.7	1338.9	17.6	1334.6	20.5	1334.6	20.5	100.6
1290.0	27.7	1308.3	18.7	1339.4	18.2	1339.4	18.2	96.3
1264.1	27.2	1295.0	18.9	1347.4	19.9	1347.4	19.9	93.8
1384.5	27.9	1370.6	19.1	1349.7	23.4	1349.7	23.4	102.6
1344.2	29.3	1349.9	19.3	1359.6	18.0	1359.6	18.0	98.9
1339.0	25.4	1347.5	16.5	1361.9	13.0	1361.9	13.0	98.3
1242.5	23.5	1293.3	16.4	1379.6	16.1	1379.6	16.1	90.1
1356.9	32.6	1368.7	21.5	1387.9	19.7	1387.9	19.7	97.8
1342.7	29.8	1362.5	20.6	1394.5	23.3	1394.5	23.3	96.3
1336.9	31.3	1363.1	21.4	1405.4	22.8	1405.4	22.8	95.1
1427.1	34.7	1418.7	21.7	1407.0	16.4	1407.0	16.4	101.4
1389.3	26.2	1397.8	17.1	1411.5	15.9	1411.5	15.9	98.4
1318.7	29.7	1354.4	20.0	1412.1	18.5	1412.1	18.5	93.4
1421.6	38.3	1421.6	24.3	1422.4	19.9	1422.4	19.9	99.9
1405.8	35.1	1412.6	23.3	1423.8	24.2	1423.8	24.2	98.7
1479.2	26.5	1466.5	17.3	1448.9	18.6	1448.9	18.6	102.1
1449.2	35.3	1449.4	22.8	1450.6	21.7	1450.6	21.7	99.9
1341.9	30.0	1384.4	19.9	1451.4	16.7	1451.4	16.7	92.5

1452.8	29.5	1453.8	19.3	1456.1	20.1	1456.1	20.1	99.8
1430.4	26.2	1446.0	17.5	1469.7	19.1	1469.7	19.1	97.3
1305.6	41.5	1369.0	27.4	1470.0	18.7	1470.0	18.7	88.8
1445.0	42.0	1457.9	26.2	1477.5	18.6	1477.5	18.6	97.8
1488.9	32.5	1487.1	19.9	1485.3	13.2	1485.3	13.2	100.2
1376.6	31.6	1420.2	20.8	1486.9	17.7	1486.9	17.7	92.6
1456.3	27.8	1470.7	18.4	1492.4	19.8	1492.4	19.8	97.6
1501.9	28.3	1506.4	18.9	1513.5	21.6	1513.5	21.6	99.2
1450.8	24.2	1476.9	15.9	1515.4	15.6	1515.4	15.6	95.7
1461.2	38.4	1484.6	24.0	1519.0	17.4	1519.0	17.4	96.2
1474.9	29.5	1495.8	19.5	1526.3	20.7	1526.3	20.7	96.6
1568.2	33.6	1561.6	20.7	1553.6	18.1	1553.6	18.1	100.9
1353.0	36.9	1433.9	25.3	1556.9	24.3	1556.9	24.3	86.9
1614.0	35.1	1596.9	21.6	1575.2	20.4	1575.2	20.4	102.5
1527.3	24.9	1547.6	16.1	1576.2	16.3	1576.2	16.3	96.9
1572.6	39.4	1574.8	23.7	1578.7	16.9	1578.7	16.9	99.6
1595.0	27.9	1589.4	17.3	1582.7	16.1	1582.7	16.1	100.8
1484.8	29.7	1529.2	19.0	1591.9	16.3	1591.9	16.3	93.3
1616.9	32.1	1607.2	19.6	1595.3	17.3	1595.3	17.3	101.4
1519.3	36.2	1554.1	23.1	1602.5	21.2	1602.5	21.2	94.8
1663.2	29.5	1643.9	18.4	1620.2	18.9	1620.2	18.9	102.7
1613.6	31.5	1616.3	19.8	1620.7	19.8	1620.7	19.8	99.6
1645.1	40.6	1634.9	23.8	1622.7	15.9	1622.7	15.9	101.4
1617.3	27.7	1619.4	17.2	1622.8	16.6	1622.8	16.6	99.7
1641.9	34.7	1635.8	21.0	1628.8	18.1	1628.8	18.1	100.8
1606.2	28.2	1615.7	17.6	1628.8	16.4	1628.8	16.4	98.6
1580.2	36.2	1601.5	22.2	1630.5	17.8	1630.5	17.8	96.9
1576.4	35.6	1601.0	22.1	1634.3	19.3	1634.3	19.3	96.5
1622.2	34.4	1629.3	21.1	1639.3	18.7	1639.3	18.7	99.0
1613.5	29.1	1625.7	18.6	1642.3	19.3	1642.3	19.3	98.2
1587.5	27.2	1612.5	17.9	1646.0	20.2	1646.0	20.2	96.4
1639.2	34.1	1642.3	20.9	1647.0	19.2	1647.0	19.2	99.5
1630.0	37.3	1637.3	23.5	1647.4	23.9	1647.4	23.9	98.9
1592.1	28.4	1616.3	17.2	1648.6	12.7	1648.6	12.7	96.6
1637.6	33.8	1642.5	20.3	1649.4	16.0	1649.4	16.0	99.3
1551.8	41.5	1593.6	25.4	1650.1	17.8	1650.1	17.8	94.0
1605.7	31.4	1625.2	19.1	1651.4	15.2	1651.4	15.2	97.2
1607.8	34.5	1626.8	21.7	1652.2	21.3	1652.2	21.3	97.3
1606.1	28.4	1626.3	18.3	1653.2	19.6	1653.2	19.6	97.2
1532.1	34.6	1585.0	21.7	1656.9	17.2	1656.9	17.2	92.5
1670.8	40.8	1664.4	24.1	1657.2	18.0	1657.2	18.0	100.8
1716.7	36.4	1698.3	21.1	1676.6	16.0	1676.6	16.0	102.4
1577.1	37.2	1621.9	23.1	1681.2	19.1	1681.2	19.1	93.8
1686.3	33.1	1684.3	20.9	1682.7	22.7	1682.7	22.7	100.2
1685.4	33.9	1683.9	20.2	1682.9	16.6	1682.9	16.6	100.1
1626.1	36.4	1653.7	22.2	1689.7	18.3	1689.7	18.3	96.2
1663.5	44.1	1678.0	26.9	1697.1	24.1	1697.1	24.1	98.0

1736.7	30.9	1719.1	18.5	1698.5	17.1	1698.5	17.1	102.3
1490.6	36.3	1582.4	23.3	1707.6	18.3	1707.6	18.3	87.3
1703.3	36.1	1707.1	21.6	1712.6	18.2	1712.6	18.2	99.5
1607.2	30.8	1660.1	19.6	1728.5	18.9	1728.5	18.9	93.0
1748.7	40.3	1741.5	23.2	1733.6	16.5	1733.6	16.5	100.9
1768.2	42.1	1753.0	24.6	1735.6	20.5	1735.6	20.5	101.9
1705.0	39.5	1720.2	24.2	1739.6	22.8	1739.6	22.8	98.0
1729.4	37.7	1733.8	22.1	1739.9	17.4	1739.9	17.4	99.4
1570.7	34.4	1644.1	22.5	1740.1	22.6	1740.1	22.6	90.3
1700.2	33.7	1718.0	20.1	1740.6	16.5	1740.6	16.5	97.7
1663.4	35.1	1700.0	21.7	1746.2	19.7	1746.2	19.7	95.3
1679.3	39.6	1713.6	23.7	1756.5	18.5	1756.5	18.5	95.6
1851.2	71.2	1810.6	41.0	1765.0	36.4	1765.0	36.4	104.9
1623.2	46.0	1686.0	28.1	1765.8	21.8	1765.8	21.8	91.9
1621.2	35.9	1685.6	22.4	1767.5	19.6	1767.5	19.6	91.7
1638.8	31.6	1697.9	19.7	1772.3	17.5	1772.3	17.5	92.5
1736.4	32.5	1753.9	19.5	1775.6	17.6	1775.6	17.6	97.8
1696.5	38.6	1734.1	23.6	1780.6	21.5	1780.6	21.5	95.3
1790.0	32.6	1787.9	18.9	1786.2	15.4	1786.2	15.4	100.2
1748.7	29.9	1767.9	17.6	1791.5	14.1	1791.5	14.1	97.6
1498.3	34.3	1624.6	22.2	1793.0	17.6	1793.0	17.6	83.6
1811.8	31.7	1803.7	18.5	1795.1	15.7	1795.1	15.7	100.9
1790.0	36.8	1794.1	21.0	1799.7	15.3	1799.7	15.3	99.5
1534.4	39.1	1655.5	25.2	1813.6	20.7	1813.6	20.7	84.6
1773.2	36.6	1791.6	21.9	1813.9	20.0	1813.9	20.0	97.8
1691.1	35.5	1747.5	21.3	1816.4	16.3	1816.4	16.3	93.1
1853.2	38.3	1836.8	21.9	1819.0	18.2	1819.0	18.2	101.9
1835.9	32.3	1832.0	18.7	1828.3	16.0	1828.3	16.0	100.4
1758.0	23.9	1790.6	14.7	1829.5	14.7	1829.5	14.7	96.1
1802.7	27.6	1816.5	16.4	1833.2	14.9	1833.2	14.9	98.3
1807.7	37.1	1821.2	21.1	1837.5	14.6	1837.5	14.6	98.4
1845.9	44.5	1844.6	25.0	1843.8	17.4	1843.8	17.4	100.1
1851.8	52.2	1848.9	29.5	1846.4	22.1	1846.4	22.1	100.3
1781.2	43.4	1811.1	25.0	1846.5	17.9	1846.5	17.9	96.5
1810.4	45.9	1833.8	25.9	1861.2	16.4	1861.2	16.4	97.3
1833.4	26.6	1847.6	15.6	1864.4	13.6	1864.4	13.6	98.3
1706.4	33.2	1778.3	20.5	1864.6	18.5	1864.6	18.5	91.5
1770.8	42.4	1814.1	24.4	1865.0	16.6	1865.0	16.6	95.0
1917.9	39.8	1893.0	22.3	1866.5	17.8	1866.5	17.8	102.8
1647.7	33.9	1746.5	26.2	1867.7	38.1	1867.7	38.1	88.2
1848.1	37.7	1859.3	22.1	1872.6	19.8	1872.6	19.8	98.7
1860.9	42.1	1866.7	24.1	1874.0	19.2	1874.0	19.2	99.3
1878.3	30.0	1876.1	16.9	1874.4	13.0	1874.4	13.0	100.2
1811.1	40.2	1840.4	22.3	1874.5	11.9	1874.5	11.9	96.6
1848.1	31.5	1861.1	18.5	1876.5	16.5	1876.5	16.5	98.5
1861.2	47.3	1880.8	26.2	1903.2	16.1	1903.2	16.1	97.8
1814.8	34.5	1859.1	20.5	1909.7	18.0	1909.7	18.0	95.0

1790.3	37.9	1846.9	21.9	1912.1	15.4	1912.1	15.4	93.6
1933.6	39.2	1926.4	22.4	1919.3	19.7	1919.3	19.7	100.7
1848.0	29.8	1883.0	17.7	1922.6	16.2	1922.6	16.2	96.1
1928.4	42.5	1926.4	23.5	1925.0	17.0	1925.0	17.0	100.2
1882.4	38.5	1909.2	22.5	1939.2	20.3	1939.2	20.3	97.1
1938.5	40.3	1941.1	22.4	1944.6	16.9	1944.6	16.9	99.7
1809.9	35.8	1875.9	21.1	1950.6	17.2	1950.6	17.2	92.8
1825.7	34.5	1885.4	20.5	1952.5	17.9	1952.5	17.9	93.5
1863.9	41.7	1905.9	23.9	1952.8	18.9	1952.8	18.9	95.4
1952.6	40.0	1956.7	22.8	1961.7	20.1	1961.7	20.1	99.5
1996.3	35.1	1988.9	19.9	1981.9	17.8	1981.9	17.8	100.7
1940.0	40.2	1961.6	22.4	1985.3	17.1	1985.3	17.1	97.7
1955.1	41.8	1971.9	22.9	1990.3	15.8	1990.3	15.8	98.2
1647.8	38.8	1806.8	24.0	1996.3	17.3	1996.3	17.3	82.5
1884.0	40.8	1938.3	23.9	1997.6	20.9	1997.6	20.9	94.3
1884.2	49.6	1940.4	27.9	2001.7	19.0	2001.7	19.0	94.1
1872.2	30.6	1934.1	17.5	2001.9	13.2	2001.9	13.2	93.5
2006.5	43.3	2006.4	23.6	2007.1	17.7	2007.1	17.7	100.0
2014.2	35.8	2011.2	19.8	2008.8	16.2	2008.8	16.2	100.3
1915.9	47.4	1961.6	26.5	2011.0	18.9	2011.0	18.9	95.3
1958.9	27.0	1984.0	16.3	2011.0	17.3	2011.0	17.3	97.4
1945.7	39.8	1977.4	22.0	2011.6	15.7	2011.6	15.7	96.7
2054.8	42.5	2047.9	22.7	2041.8	16.1	2041.8	16.1	100.6
1947.3	49.0	2005.5	27.0	2066.7	18.0	2066.7	18.0	94.2
2056.8	40.9	2125.6	22.6	2193.4	17.8	2193.4	17.8	93.8
2440.7	43.0	2447.2	21.2	2453.3	15.1	2453.3	15.1	99.5
2353.3	52.5	2416.4	25.9	2470.7	15.2	2470.7	15.2	95.2
2525.5	59.7	2511.8	28.9	2501.4	20.5	2501.4	20.5	101.0
2450.5	52.5	2479.8	25.8	2504.7	17.7	2504.7	17.7	97.8
2411.8	39.8	2468.3	20.1	2515.8	15.2	2515.8	15.2	95.9
2592.1	45.9	2607.4	21.9	2620.1	15.0	2620.1	15.0	98.9
2543.0	46.7	2587.4	23.1	2623.0	18.1	2623.0	18.1	97.0
2438.1	57.5	2541.7	28.4	2626.3	18.8	2626.3	18.8	92.8
2658.1	57.2	2646.3	26.3	2638.0	15.9	2638.0	15.9	100.8
2616.5	49.2	2650.6	22.9	2677.5	13.4	2677.5	13.4	97.7
2675.1	47.6	2678.3	22.3	2681.4	15.7	2681.4	15.7	99.8
2522.2	54.8	2613.7	25.9	2686.2	14.3	2686.2	14.3	93.9
2572.0	46.6	2636.5	22.4	2687.1	15.2	2687.1	15.2	95.7
2521.4	55.9	2615.3	27.0	2689.6	17.1	2689.6	17.1	93.7
2167.6	38.0	2448.0	20.5	2690.6	13.2	2690.6	13.2	80.6
2350.6	67.4	2538.2	33.2	2692.4	16.3	2692.4	16.3	87.3
2572.5	43.8	2650.2	20.8	2710.7	13.3	2710.7	13.3	94.9
2723.8	44.0	2723.0	20.2	2723.0	13.1	2723.0	13.1	100.0
2597.0	44.9	2668.9	21.4	2724.5	14.0	2724.5	14.0	95.3
2736.0	53.8	2730.6	24.5	2727.3	15.5	2727.3	15.5	100.3
2771.6	48.1	2745.9	22.4	2727.8	16.7	2727.8	16.7	101.6
2703.2	52.3	2730.0	24.9	2750.5	18.9	2750.5	18.9	98.3

2568.1	47.1	2671.8	22.7	2752.0	15.1	2752.0	15.1	93.3
2671.4	66.7	2719.5	30.1	2756.1	15.2	2756.1	15.2	96.9
2760.2	57.1	2771.5	25.4	2780.4	13.3	2780.4	13.3	99.3
2753.2	53.6	2771.1	24.5	2784.8	15.8	2784.8	15.8	98.9
2690.4	49.0	2745.6	23.5	2787.1	17.9	2787.1	17.9	96.5
2800.3	52.2	2796.5	24.2	2794.5	17.9	2794.5	17.9	100.2
2792.1	65.8	2804.6	29.1	2814.4	15.6	2814.4	15.6	99.2
2787.3	48.7	2804.1	22.2	2817.0	14.8	2817.0	14.8	98.9
2681.0	76.0	2784.3	34.3	2860.8	16.3	2860.8	16.3	93.7
2791.3	52.5	2837.4	24.1	2871.0	16.3	2871.0	16.3	97.2
2847.1	57.7	2902.6	26.5	2942.1	19.0	2942.1	19.0	96.8
2902.7	57.7	2959.7	25.6	2999.4	16.1	2999.4	16.1	96.8
3412.4	62.4	3482.2	25.7	3523.3	17.7	3523.3	17.7	96.9
3501.7	66.0	3654.2	24.1	3739.5	1.5	3739.5	1.5	93.6

Grain size Histograms

Detrital Zircon Histograms

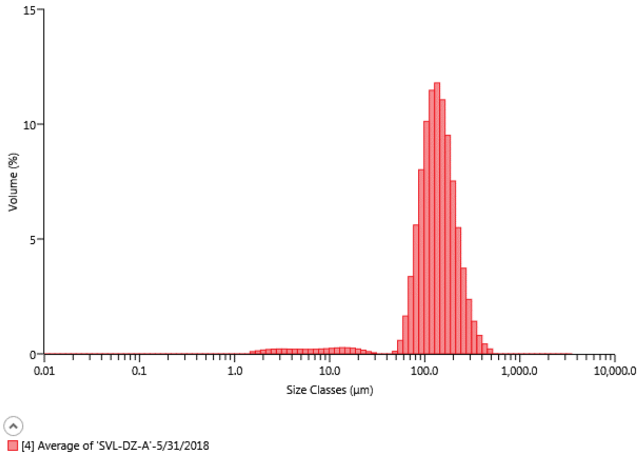

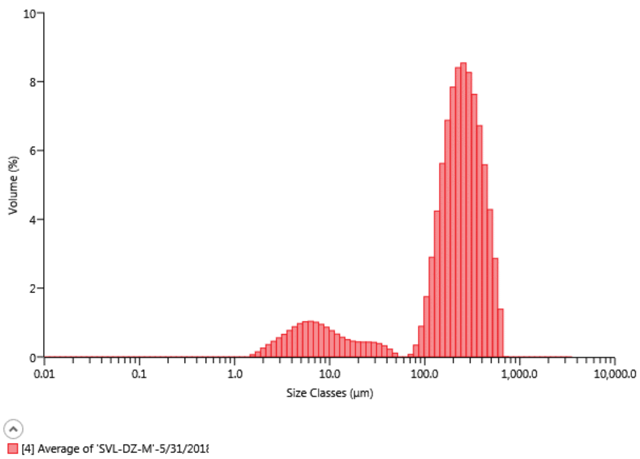

Moscovian Grain Size Histograms

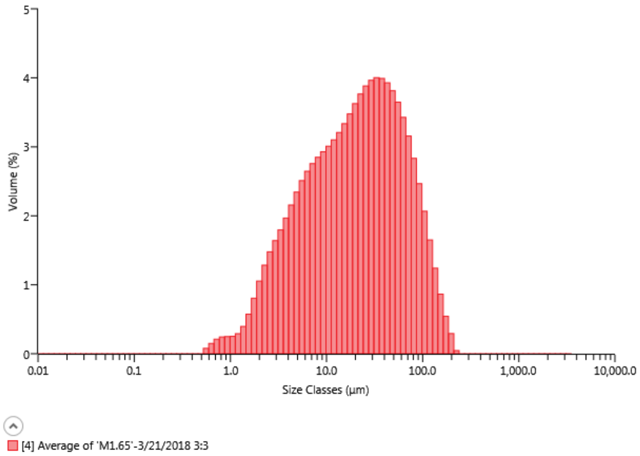

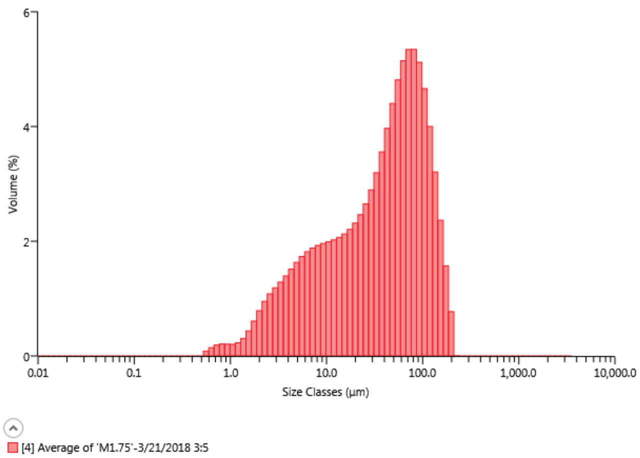

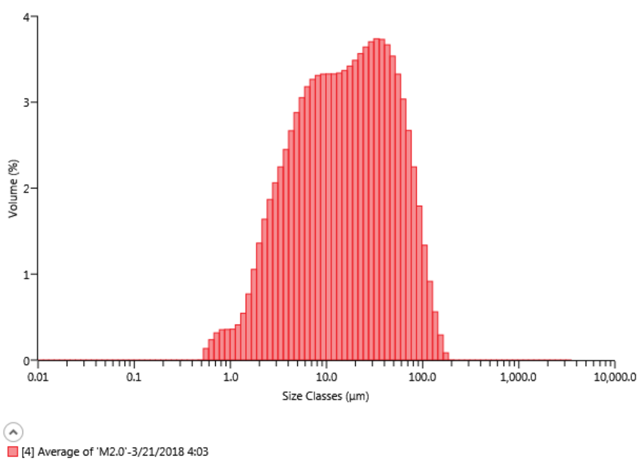

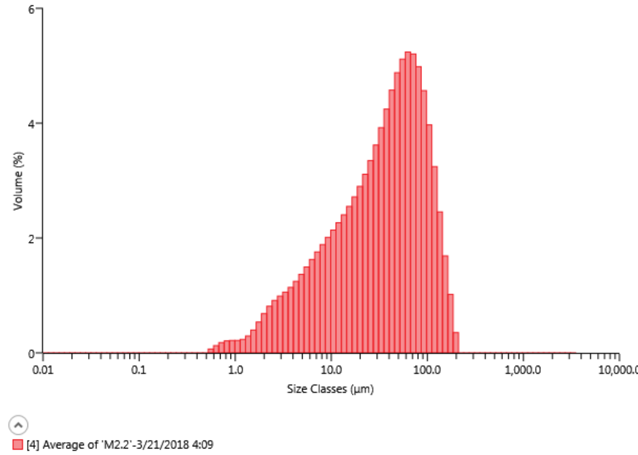

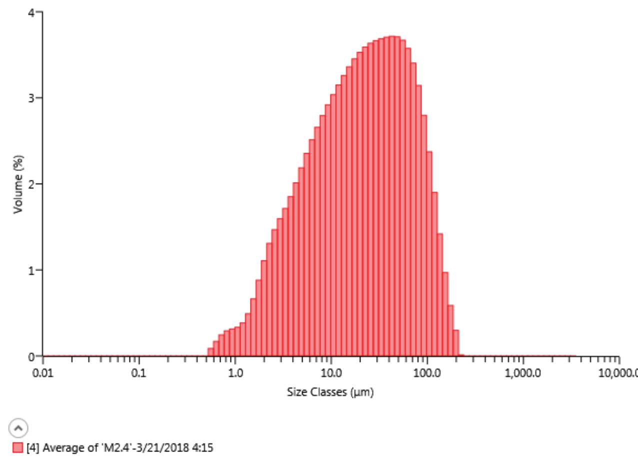

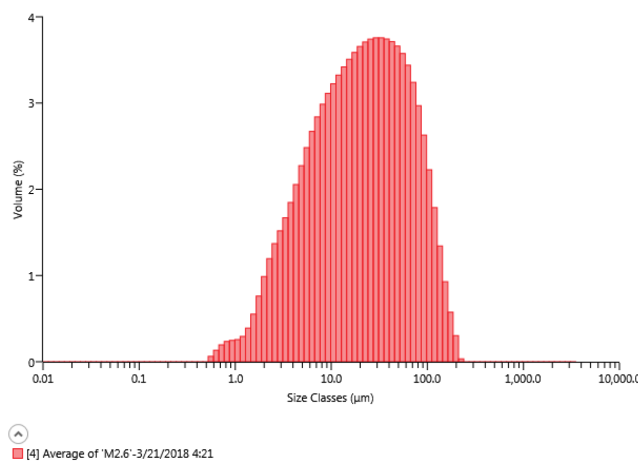

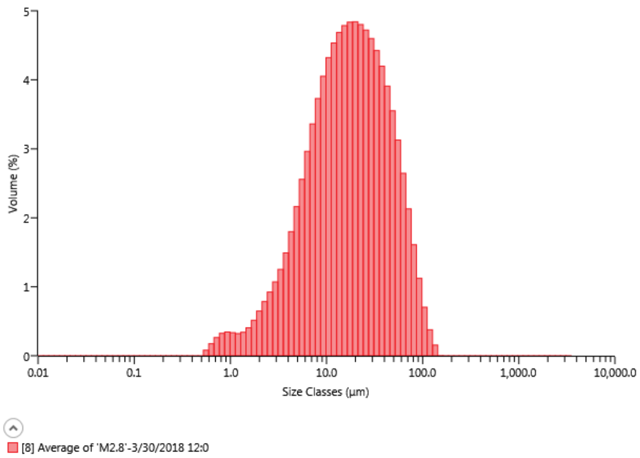
Volume (%)
Size Classes (µm)
[8] Average of 'M2.8'-3/30/2018 12:0

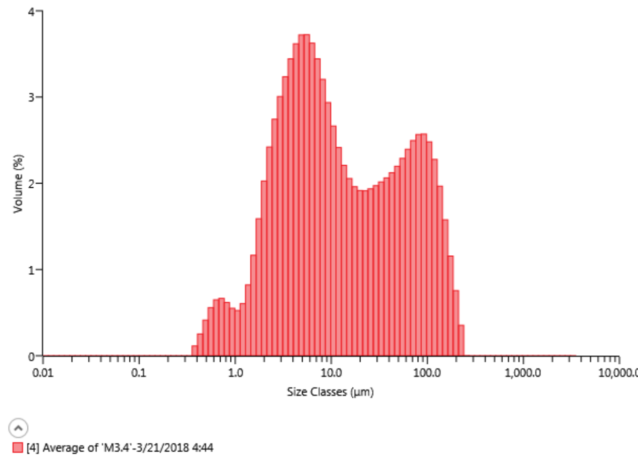
Volume (%)
Size Classes (µm)
[4] Average of 'M3.4'-3/21/2018 4:44

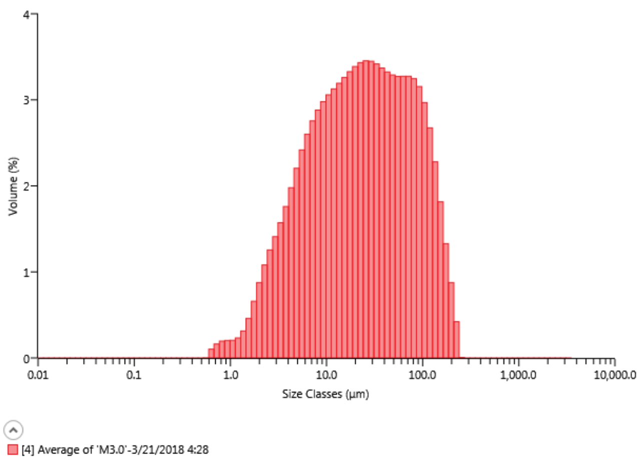
Volume (%)
Size Classes (µm)
[4] Average of 'M3.0'-3/21/2018 4:28

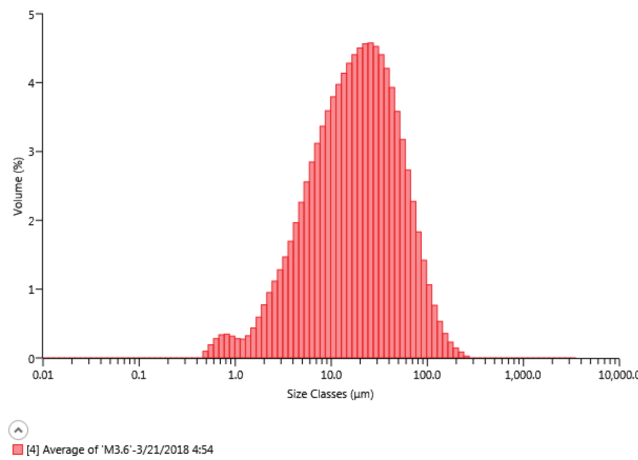
Volume (%)
Size Classes (µm)
[4] Average of 'M3.6'-3/21/2018 4:54

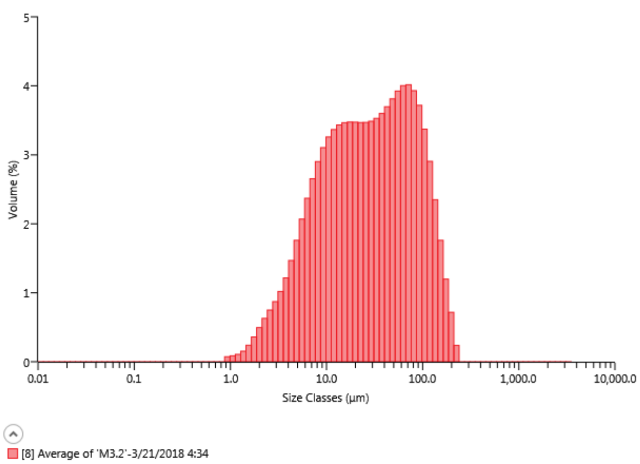
Volume (%)
Size Classes (µm)
[8] Average of 'M3.2'-3/21/2018 4:34

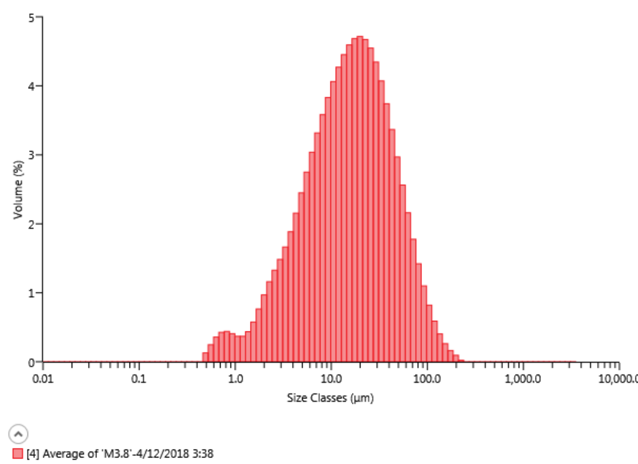
Volume (%)
Size Classes (µm)
[4] Average of 'M3.8'-4/12/2018 3:38

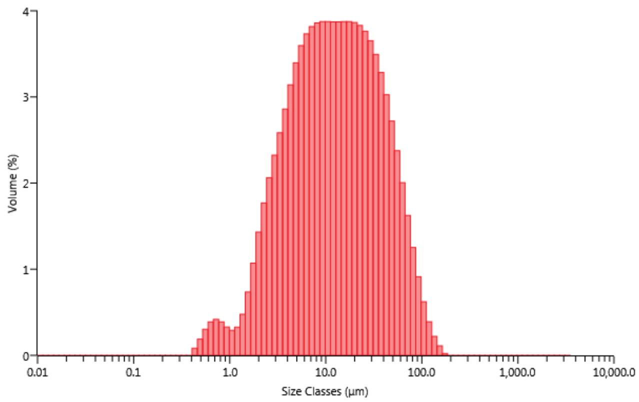

[4] Average of 'M4.0'-4/12/2018 3:44

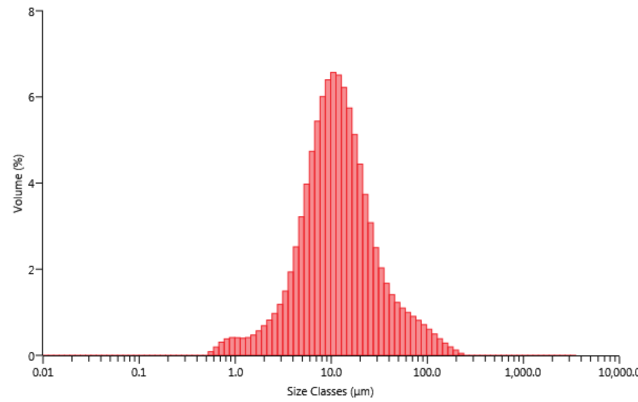

[4] Average of 'M4.6'-3/21/2018 5:16

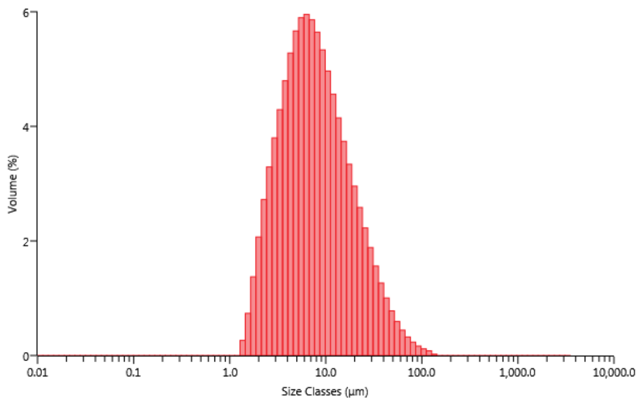

[4] Average of 'M4.2'-3/21/2018 5:02

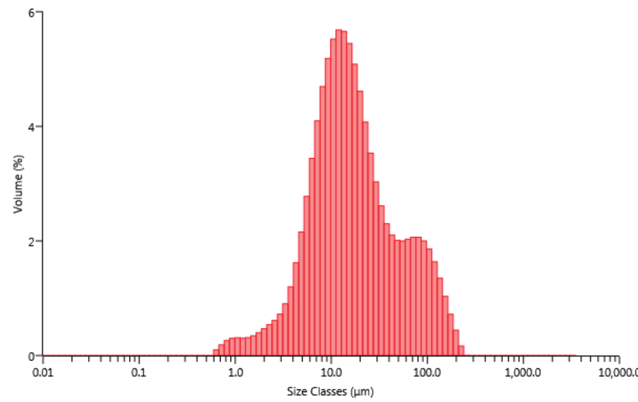

[4] Average of 'M4.8'-3/21/2018 5:23

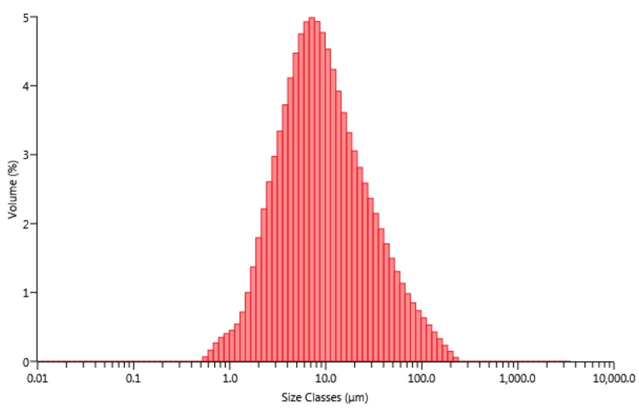

[4] Average of 'M4.4'-3/21/2018 5:11

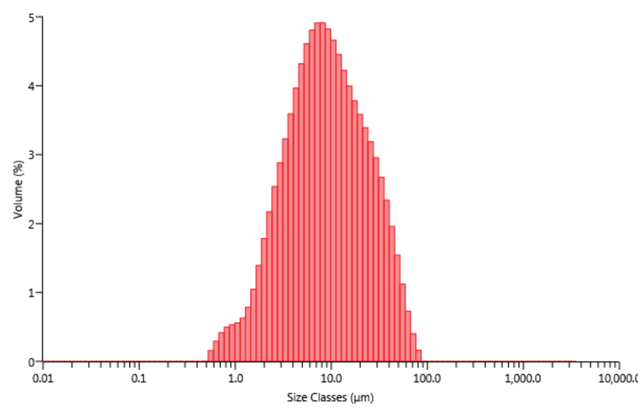

[4] Average of 'M5.0'-3/27/2018 10:2

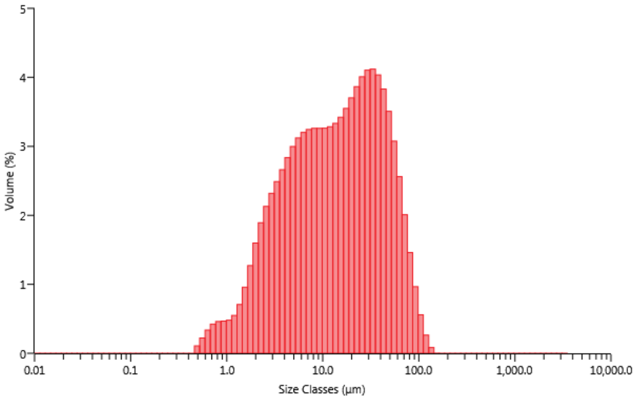

[4] Average of 'M5.2'-3/27/2018 10:3

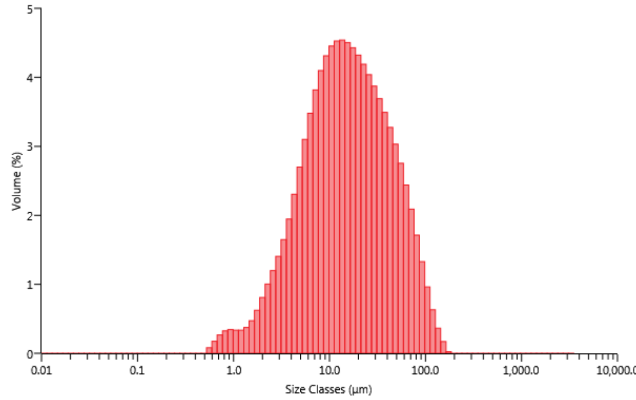

[4] Average of 'M5.8'-3/27/2018 10:4

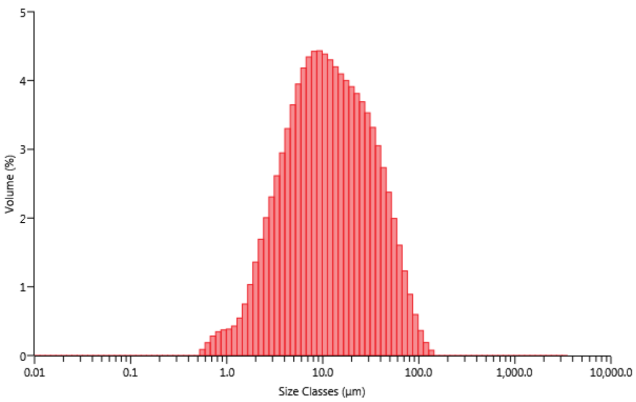

[4] Average of 'M5.4'-3/27/2018 10:3

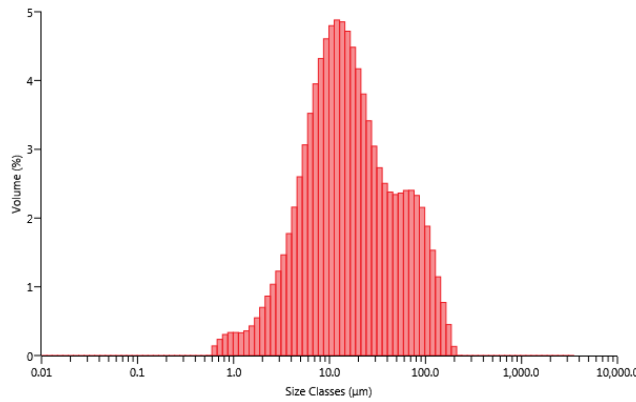

[4] Average of 'M6.0'-3/27/2018 10:5

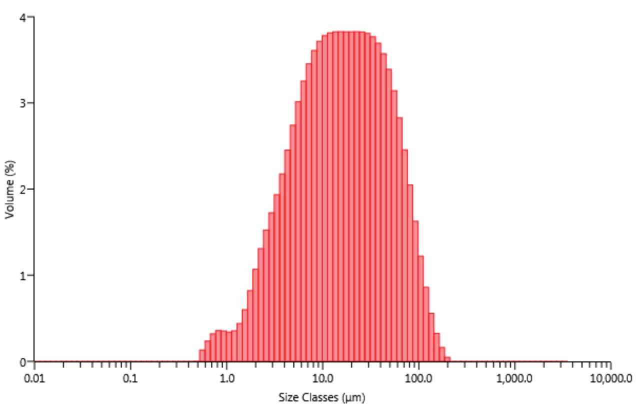

[4] Average of 'M5.6'-3/27/2018 10:4

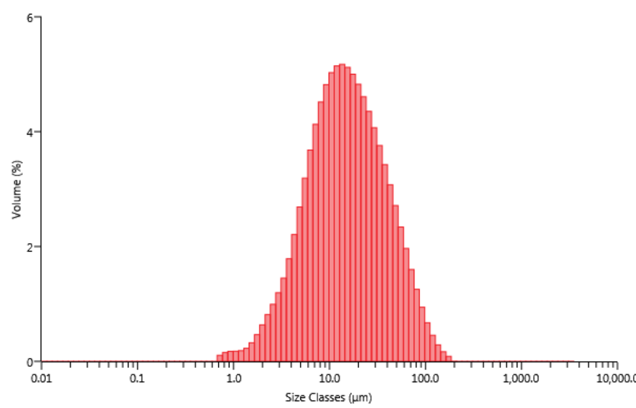

[4] Average of 'M6.2'-3/27/2018 10:5

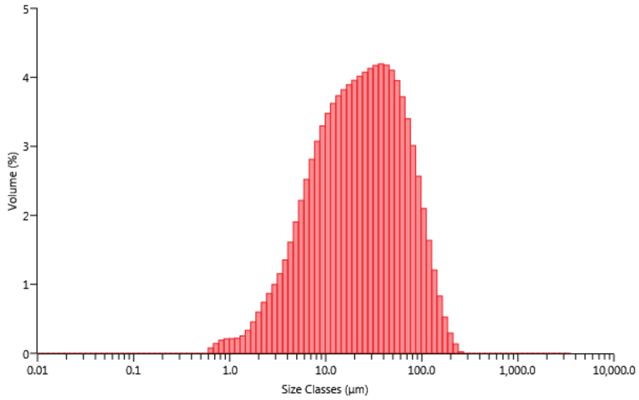

[4] Average of 'M6.4'-3/27/2018 11:0

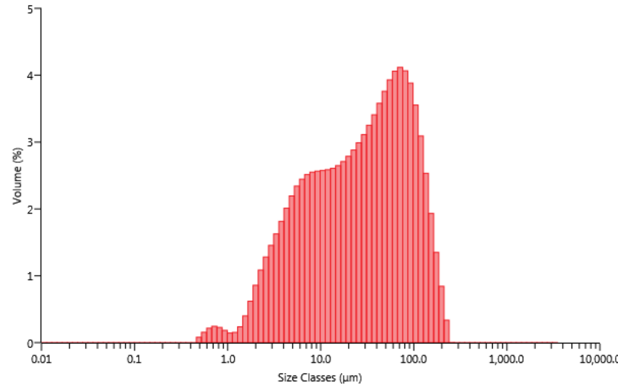

[8] Average of 'M7.0
'-3/27/2018 11:13:22 AM

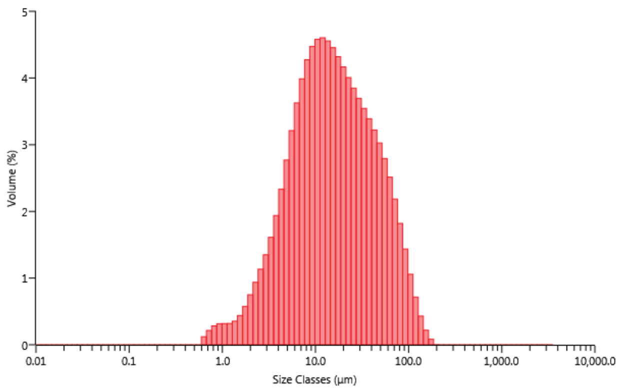

[4] Average of 'M6.6
'-3/27/2018 11:06:20 AM

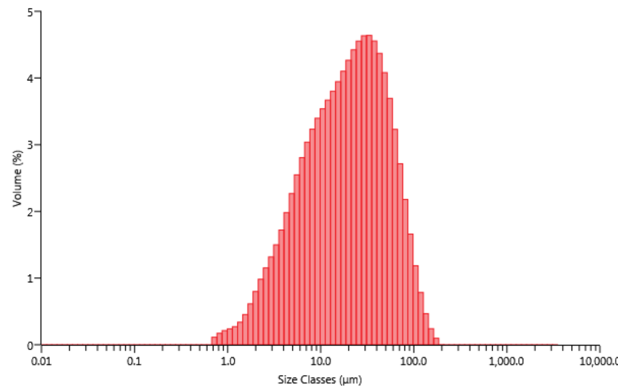

[4] Average of 'M7.2
'-3/27/2018 11:25:12 AM

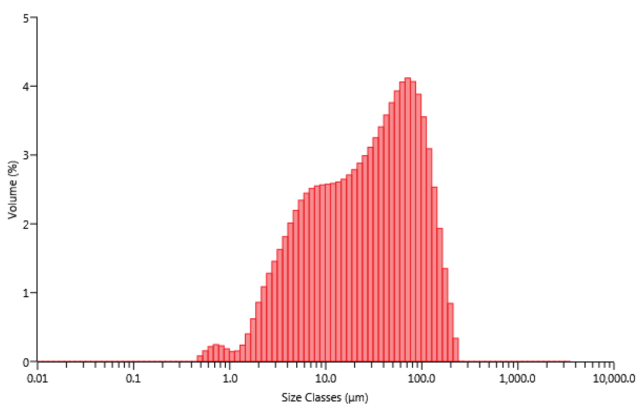

[4] Average of 'M6.8'-3/27/2018 11:1

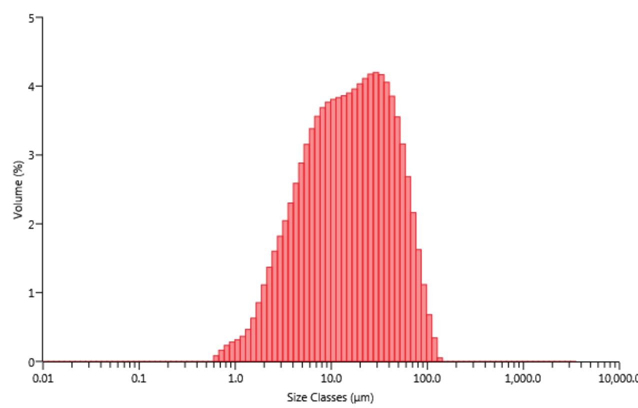

[4] Average of 'M7.4'-3/27/2018 11:3

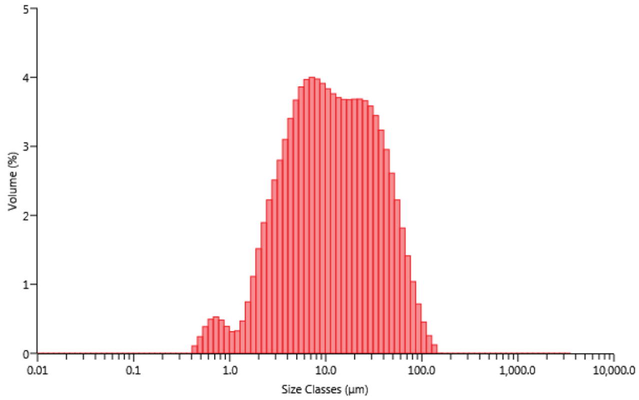

[4] Average of 'M7.6'-3/27/2018 11:3

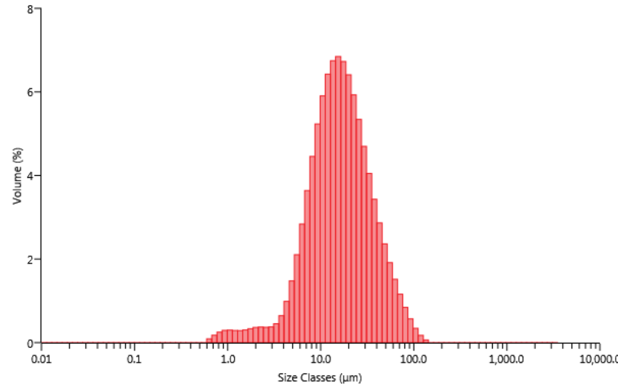

[8] Average of 'M8.2
'-3/27/2018 11:51:03 AM

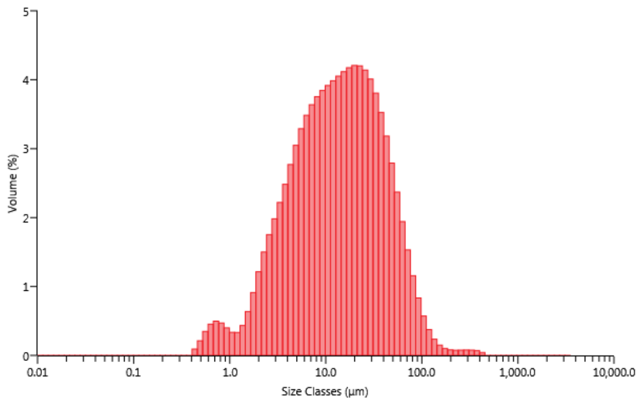

[4] Average of 'M7.8'-3/27/2018 11:4

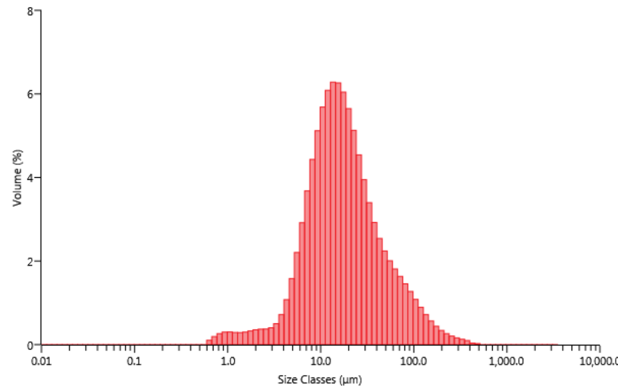

[4] Average of 'M8.4
'-3/27/2018 12:01:55 PM

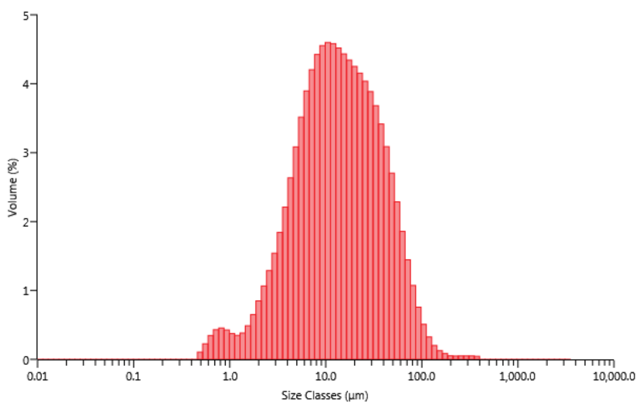

[4] Average of 'M8.0'-4/12/2018 3:58

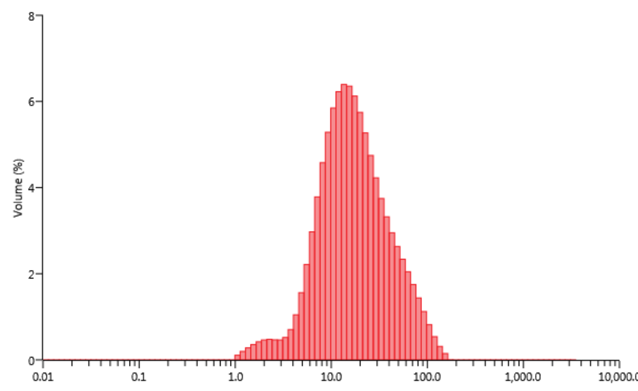

[4] Average of 'M8.6'-3/27/2018 12:0

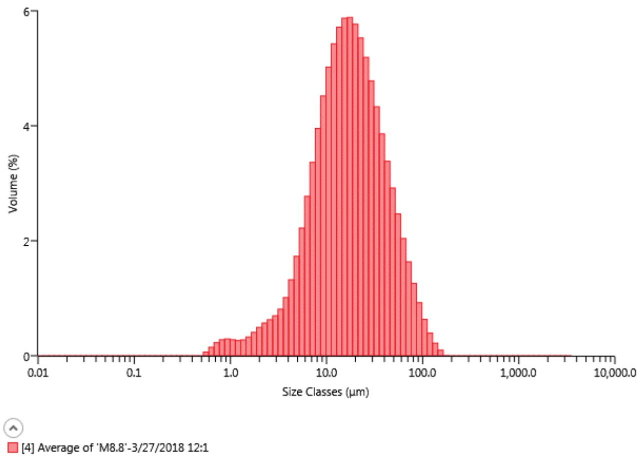
Volume (%)
Size Classes (µm)
[4] Average of 'M8.8'-3/27/2018 12:1

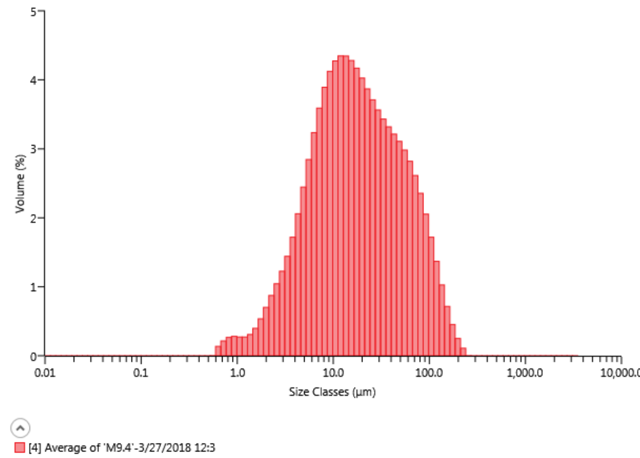
Volume (%)
Size Classes (µm)
[4] Average of 'M9.4'-3/27/2018 12:3

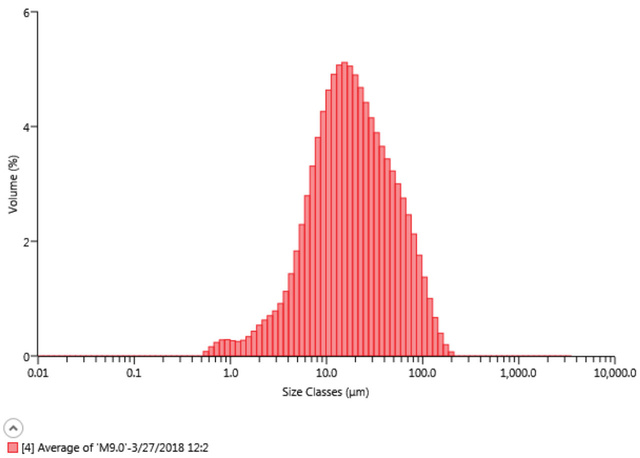
Volume (%)
Size Classes (µm)
[4] Average of 'M9.0'-3/27/2018 12:2

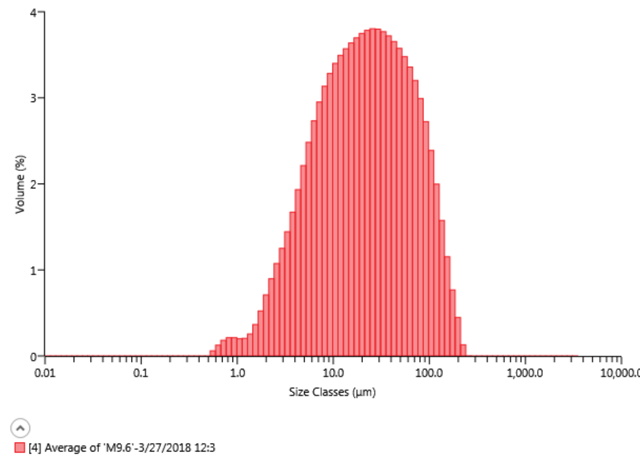
Volume (%)
Size Classes (µm)
[4] Average of 'M9.6'-3/27/2018 12:3

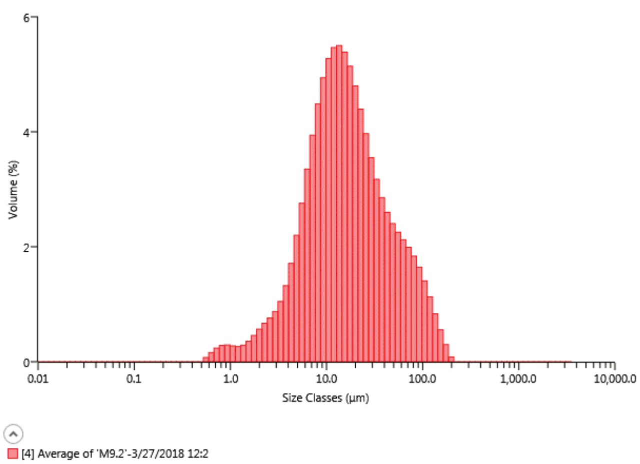
Volume (%)
Size Classes (µm)
[4] Average of 'M9.2'-3/27/2018 12:2

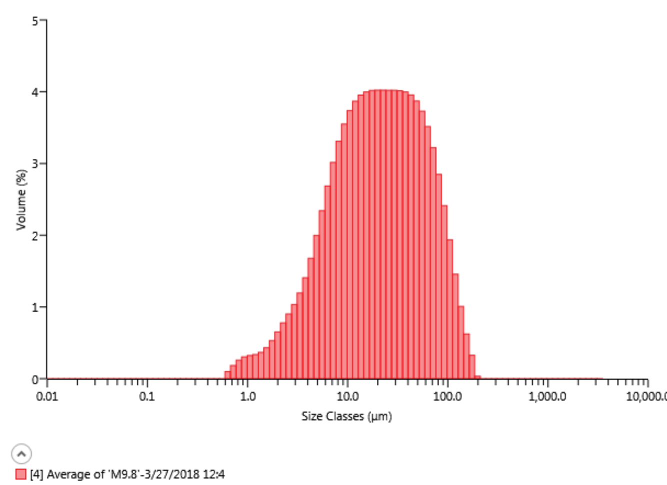
Volume (%)
Size Classes (µm)
[4] Average of 'M9.8'-3/27/2018 12:4

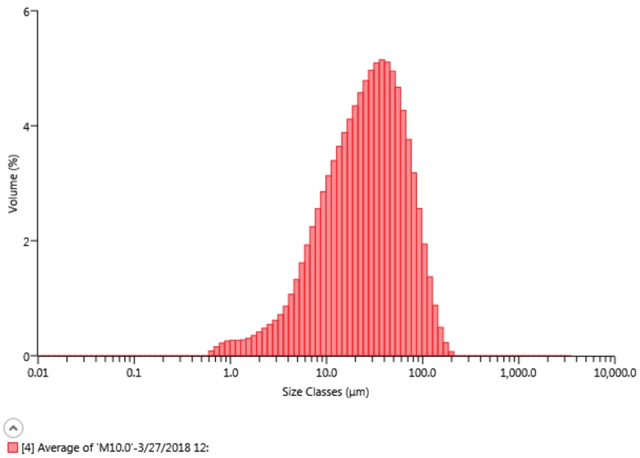

6
4
2
0
Volume (%)
0.01
0.1
1.0
10.0
100.0
1,000.0
10,000.0
Size Classes (μm)
[4] Average of 'M10.0'-3/27/2018 12:

Asselian Grain Size Histograms

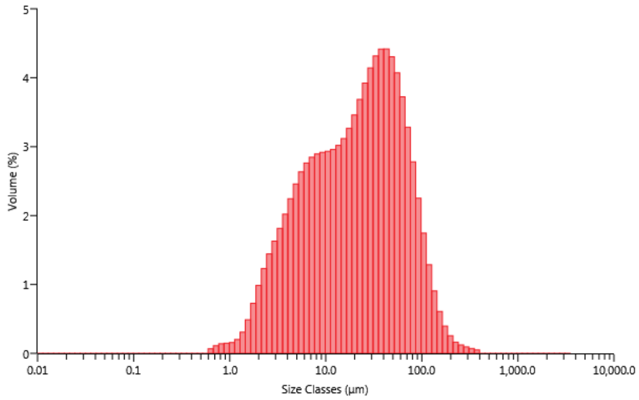

[4] Average of 'A0.0 '-3/11/2018 2:13

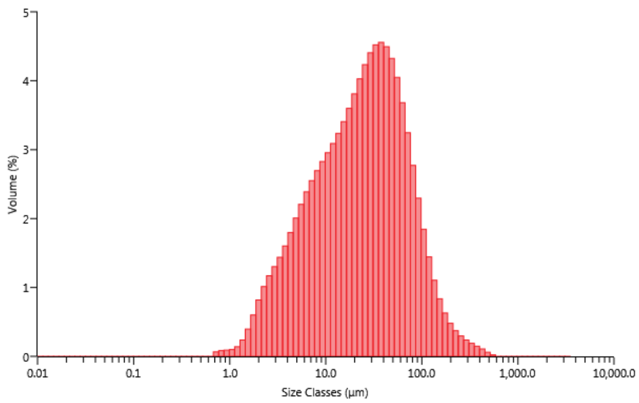

[4] Average of 'A0.6'-3/11/2018 2:44:

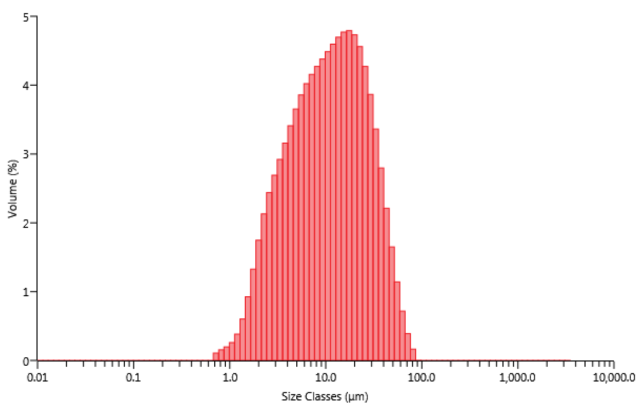

[4] Average of 'A0.8'-3/11/2018 2:25:

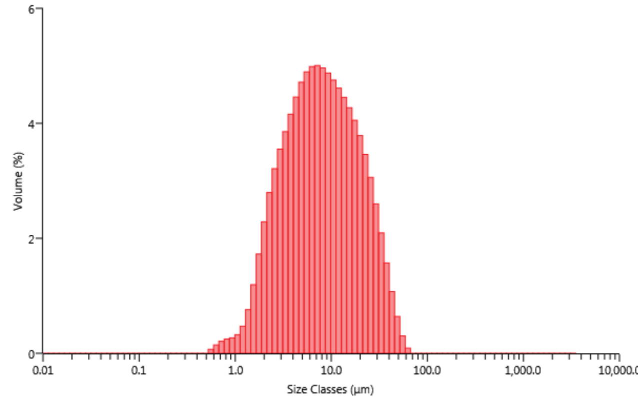

[4] Average of 'A1.0'-3/11/2018 2:51:

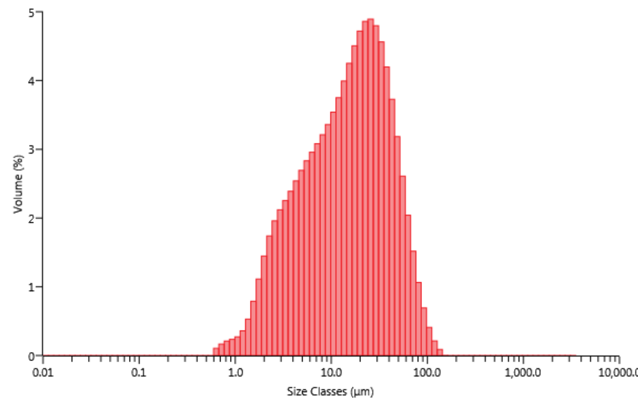

[4] Average of 'A1.2'-3/11/2018 2:58:

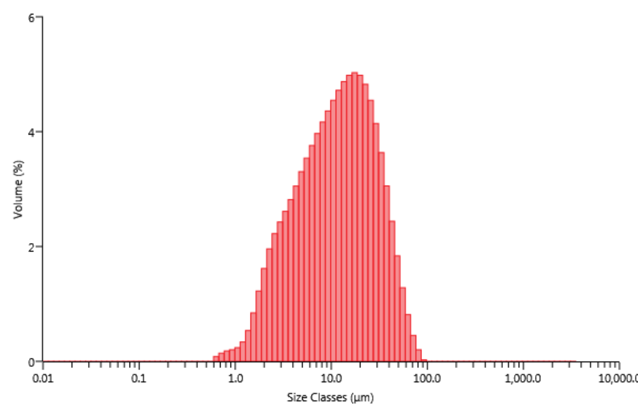

[4] Average of 'A1.4'-3/11/2018 3:05:

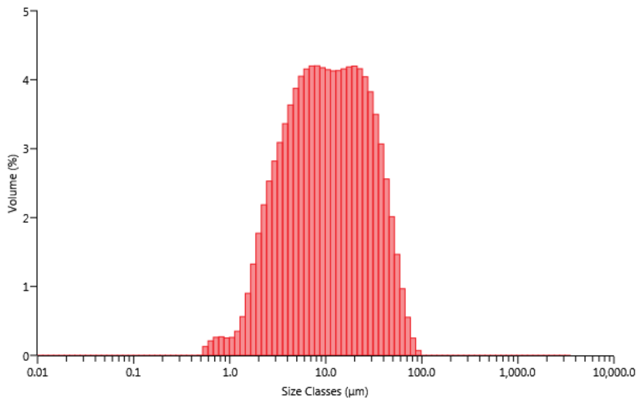

[4] Average of 'A1.6'-3/11/2018 3:11:

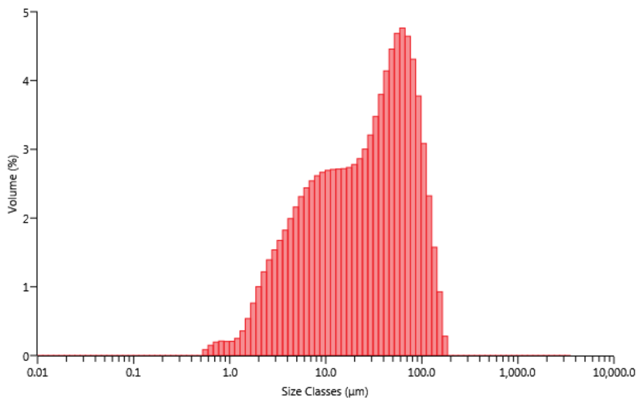

[4] Average of 'A1.8'-3/11/2018 3:17:

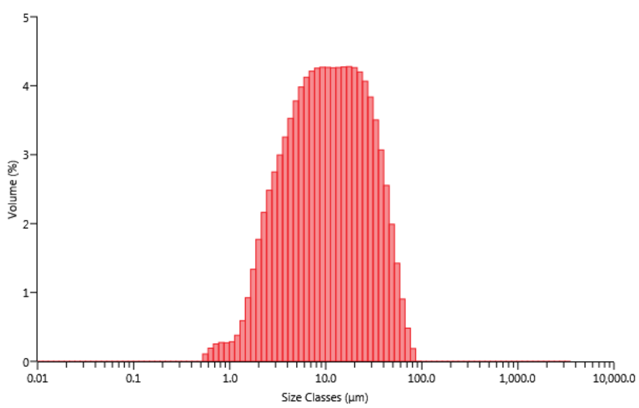

[4] Average of 'A2.0'-3/11/2018 3:23:

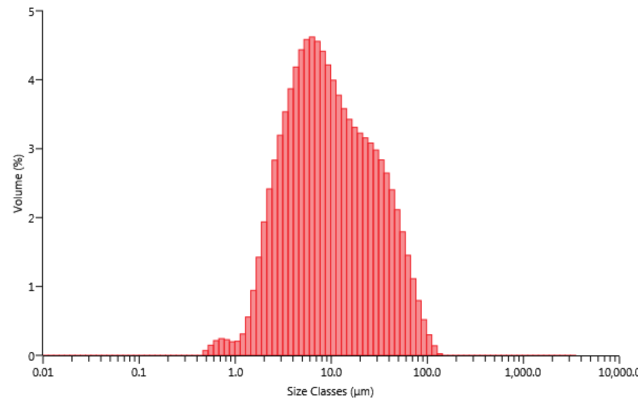

[4] Average of 'A2.2'-3/11/2018 3:29:

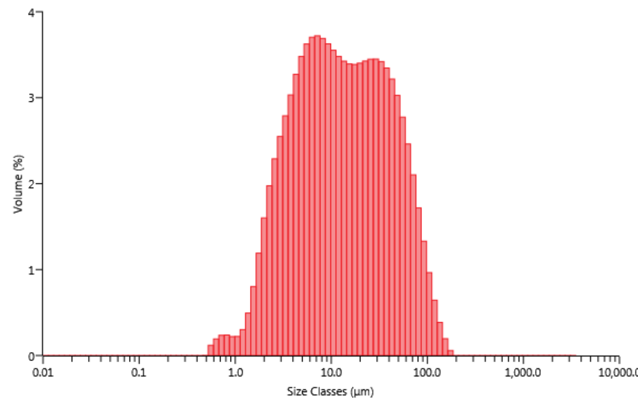

[4] Average of 'A2.4'-3/11/2018 3:34:

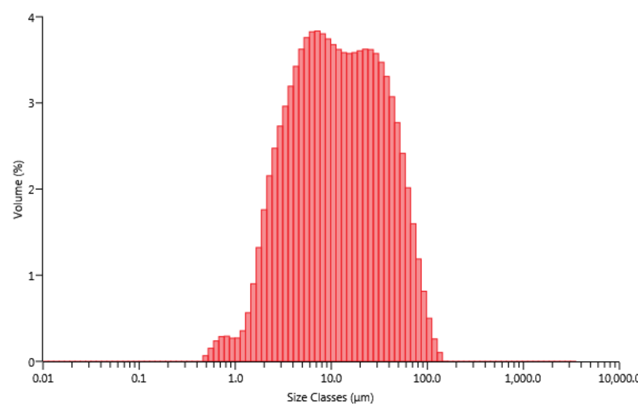

[4] Average of 'A2.6'-3/11/2018 3:41:

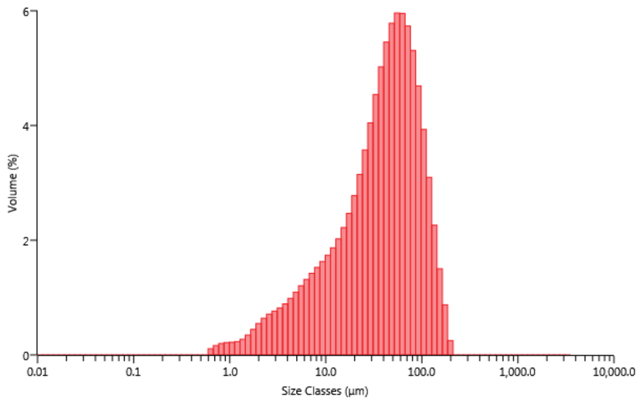

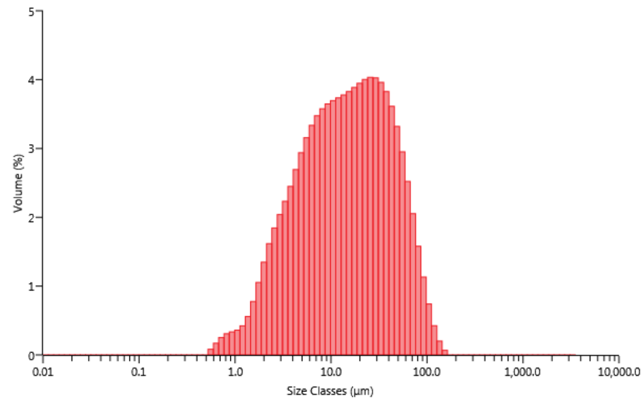

[4] Average of 'A2.8'-3/11/2018 3:49:

[4] Average of 'A3.4'-3/11/2018 4:12:

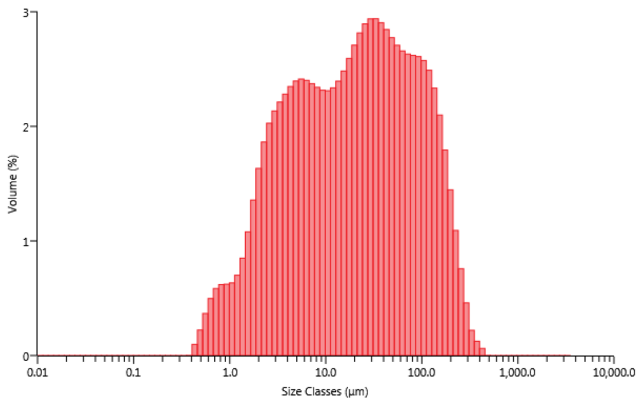

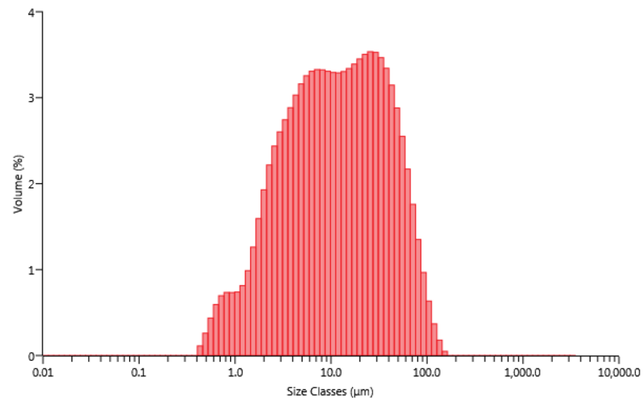

[4] Average of 'A3.0'-3/11/2018 3:57:

[4] Average of 'A3.6'-3/11/2018 4:18:

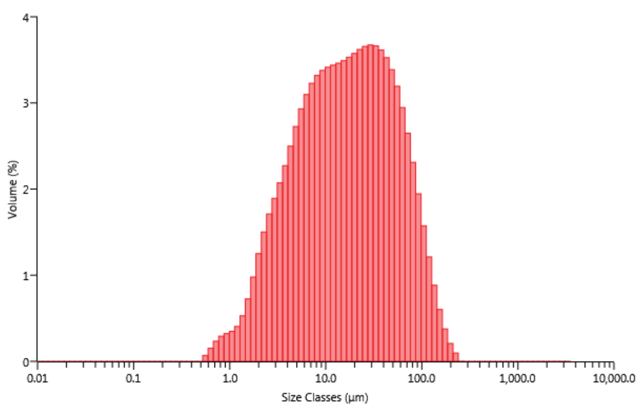

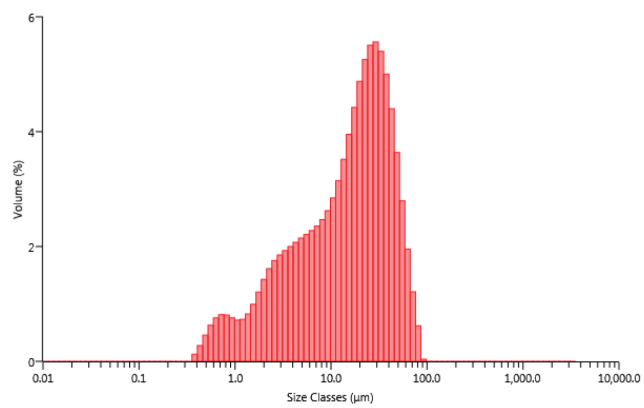

[4] Average of 'A3.2'-3/11/2018 4:05:

[4] Average of 'A3.8'-3/11/2018 4:24:

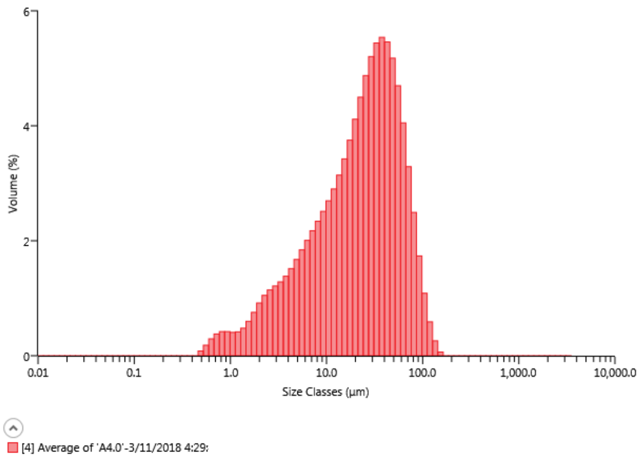
6
4
2
0
Volume (%)
0.01
0.1
1.0
10.0
100.0
1,000.0
10,000.0
Size Classes (μm)
[4] Average of 'A4.0'-3/11/2018 4:29:

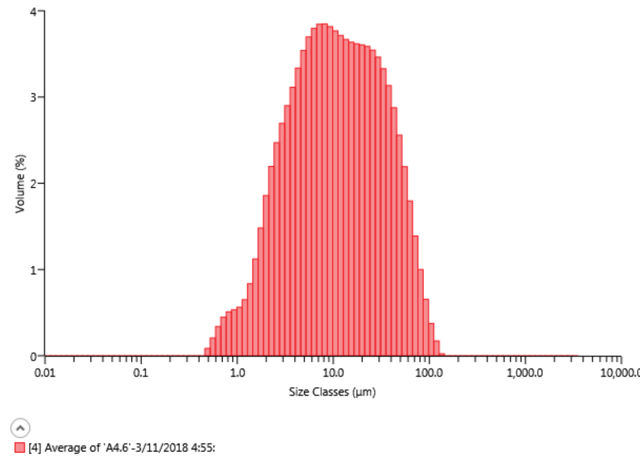
4
3
2
1
0
Volume (%)
0.01
0.1
1.0
10.0
100.0
1,000.0
10,000.0
Size Classes (μm)
[4] Average of 'A4.6'-3/11/2018 4:55:

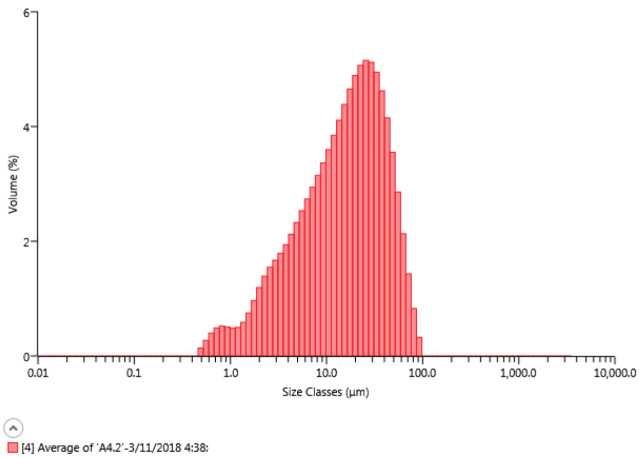
6
4
2
0
Volume (%)
0.01
0.1
1.0
10.0
100.0
1,000.0
10,000.0
Size Classes (μm)
[4] Average of 'A4.2'-3/11/2018 4:38:

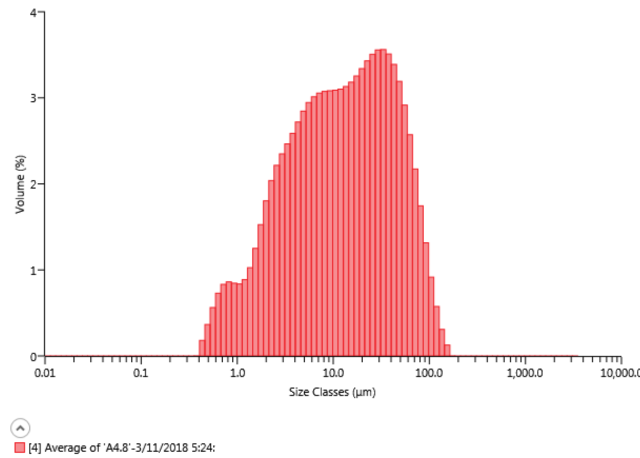
4
3
2
1
0
Volume (%)
0.01
0.1
1.0
10.0
100.0
1,000.0
10,000.0
Size Classes (μm)
[4] Average of 'A4.8'-3/11/2018 5:24:

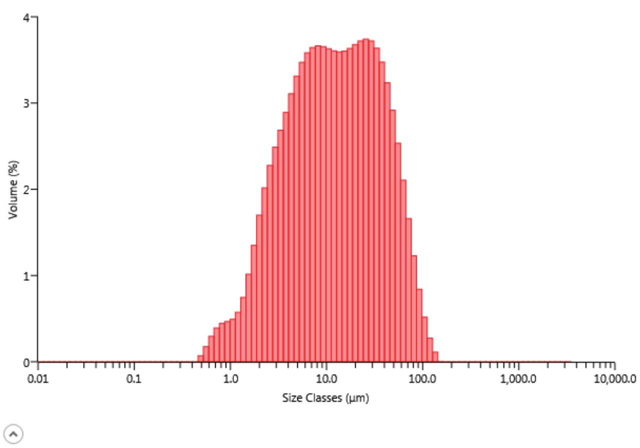
4
3
2
1
0
Volume (%)
0.01
0.1
1.0
10.0
100.0
1,000.0
10,000.0
Size Classes (μm)
[4] Average of 'A4.4'-3/11/2018 4:45:

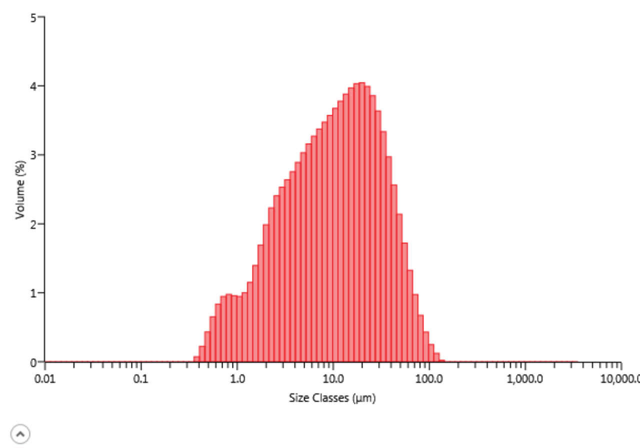
5
4
3
2
1
0
Volume (%)
0.01
0.1
1.0
10.0
100.0
1,000.0
10,000.0
Size Classes (μm)
[4] Average of 'A5.0'-3/11/2018 5:30:

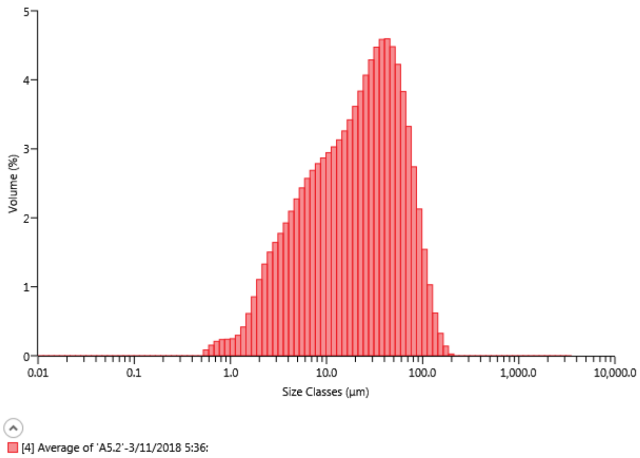
Volume (%)
Size Classes (µm)
0.01 0.1 1.0 10.0 100.0 1,000.0 10,000.0
[4] Average of 'A5.2'-3/11/2018 5:36:

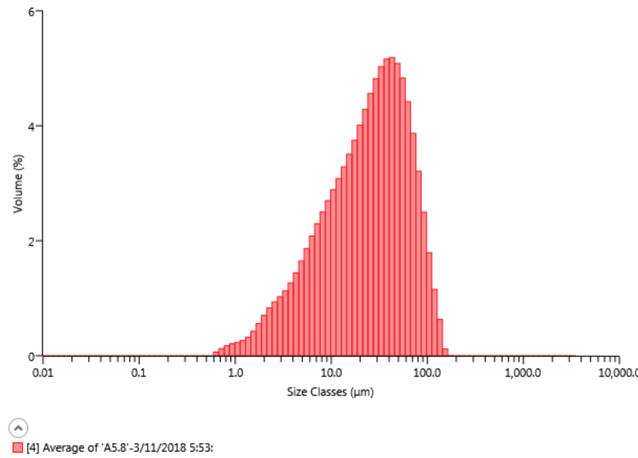
Volume (%)
Size Classes (µm)
0.01 0.1 1.0 10.0 100.0 1,000.0 10,000.0
[4] Average of 'A5.8'-3/11/2018 5:53:

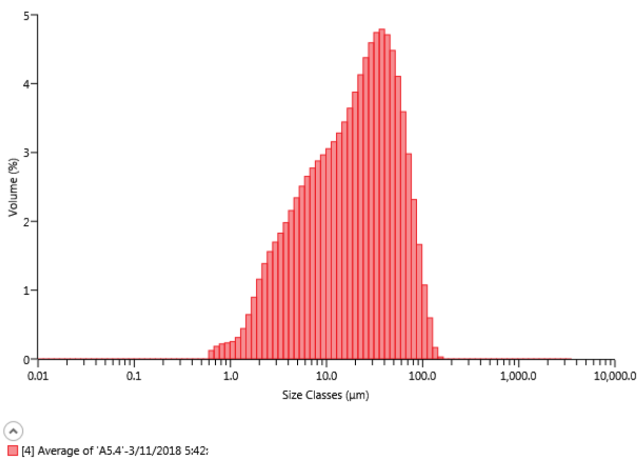
Volume (%)
Size Classes (µm)
0.01 0.1 1.0 10.0 100.0 1,000.0 10,000.0
[4] Average of 'A5.4'-3/11/2018 5:42:

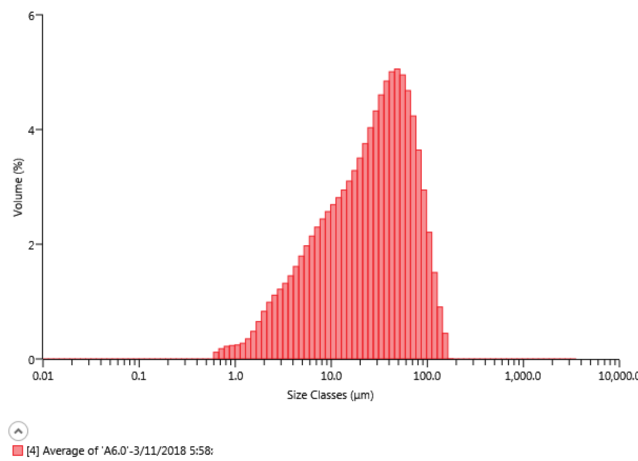
Volume (%)
Size Classes (µm)
0.01 0.1 1.0 10.0 100.0 1,000.0 10,000.0
[4] Average of 'A6.0'-3/11/2018 5:58:

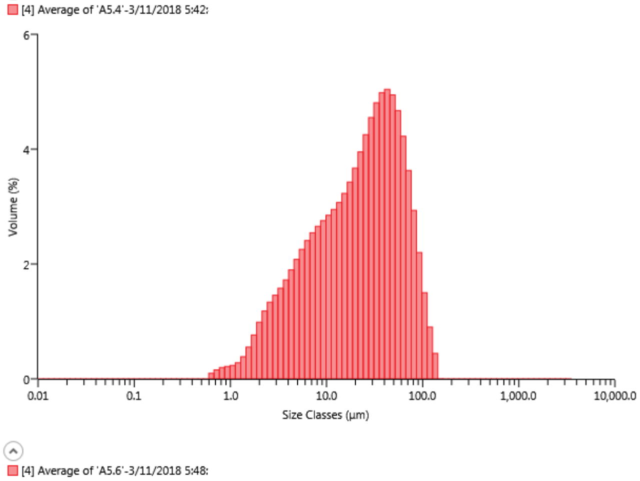
Volume (%)
Size Classes (µm)
0.01 0.1 1.0 10.0 100.0 1,000.0 10,000.0
[4] Average of 'A5.6'-3/11/2018 5:48:

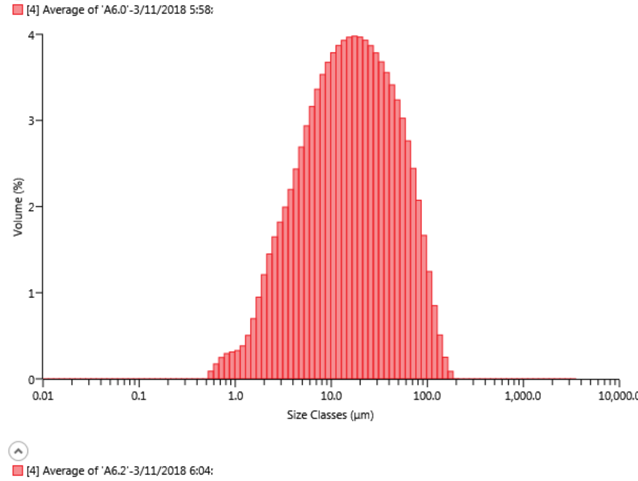
Volume (%)
Size Classes (µm)
0.01 0.1 1.0 10.0 100.0 1,000.0 10,000.0
[4] Average of 'A6.2'-3/11/2018 6:04:

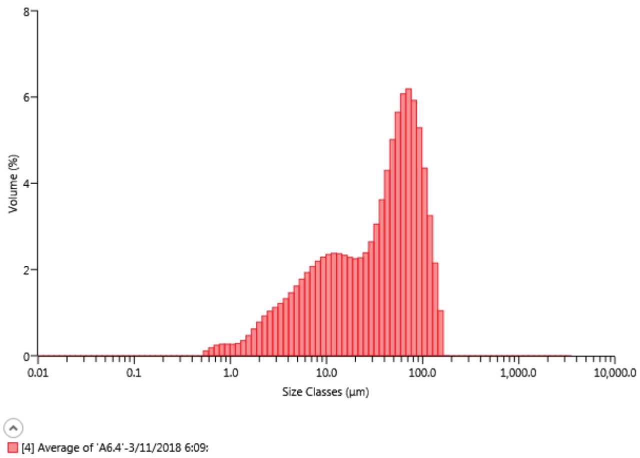
Volume (%)
Size Classes (µm)
0.01
0.1
1.0
10.0
100.0
1,000.0
10,000.0
[4] Average of 'A6.4'-3/11/2018 6:09:

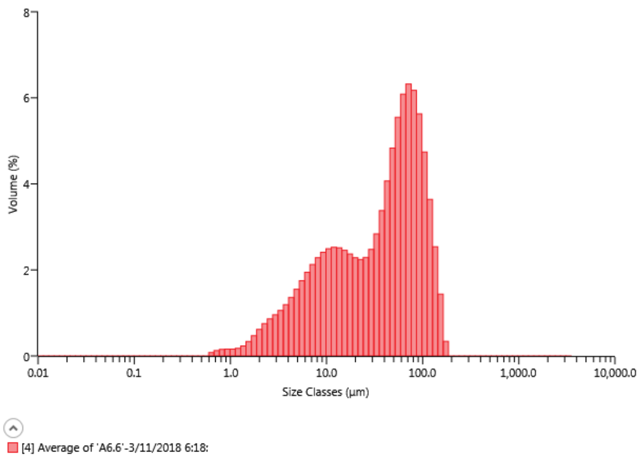
Volume (%)
Size Classes (µm)
0.01
0.1
1.0
10.0
100.0
1,000.0
10,000.0
[4] Average of 'A6.6'-3/11/2018 6:18:

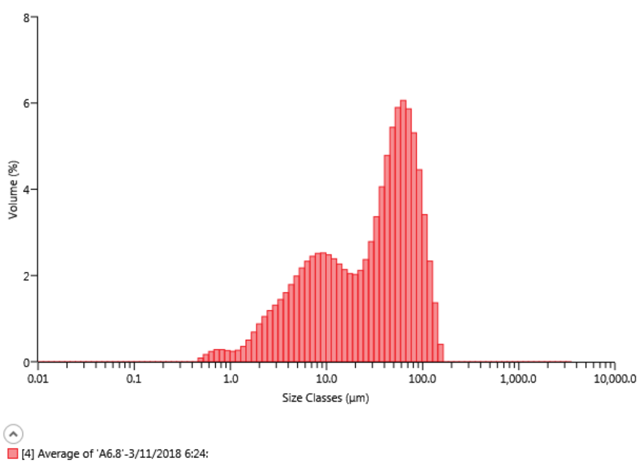
Volume (%)
Size Classes (µm)
0.01
0.1
1.0
10.0
100.0
1,000.0
10,000.0
[4] Average of 'A6.8'-3/11/2018 6:24:

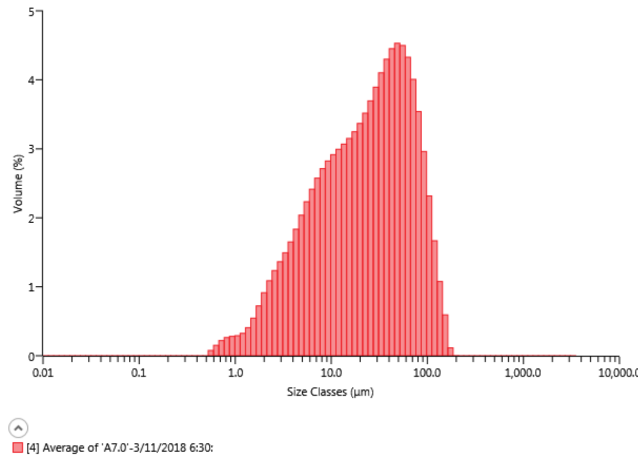
Volume (%)
Size Classes (µm)
0.01
0.1
1.0
10.0
100.0
1,000.0
10,000.0
[4] Average of 'A7.0'-3/11/2018 6:30:

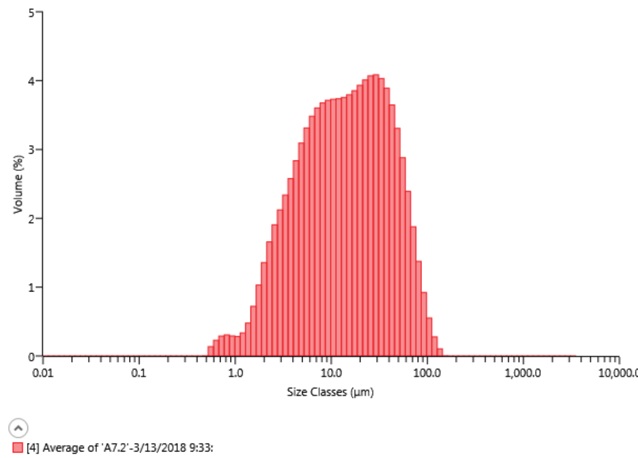
Volume (%)
Size Classes (µm)
0.01
0.1
1.0
10.0
100.0
1,000.0
10,000.0
[4] Average of 'A7.2'-3/13/2018 9:33:

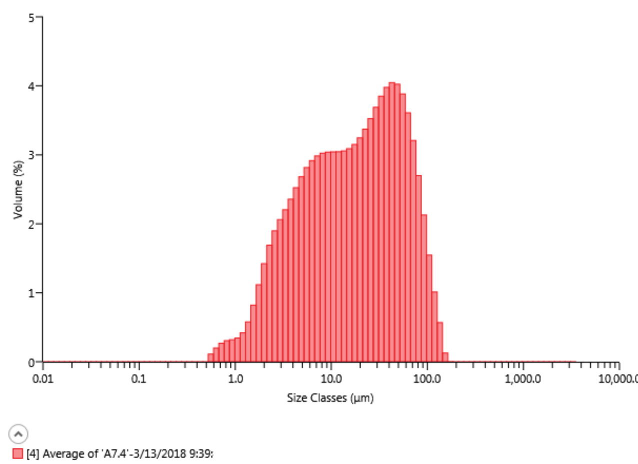
Volume (%)
Size Classes (µm)
0.01
0.1
1.0
10.0
100.0
1,000.0
10,000.0
[4] Average of 'A7.4'-3/13/2018 9:39:

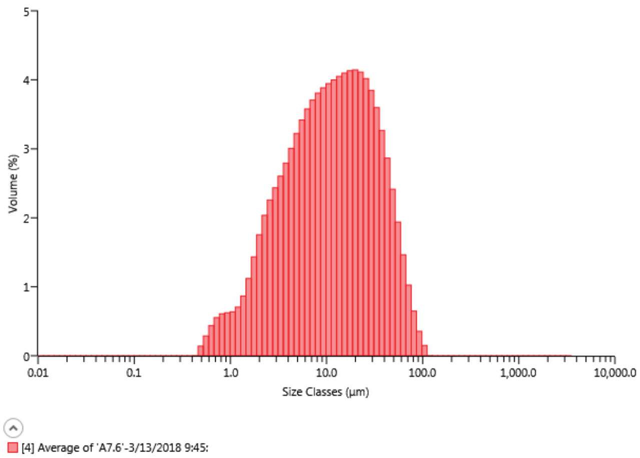
Volume (%)
0 1 2 3 4 5
0.01 0.1 1.0 10.0 100.0 1,000.0 10,000.0
Size Classes (µm)
[4] Average of 'A7.6'-3/13/2018 9:45:

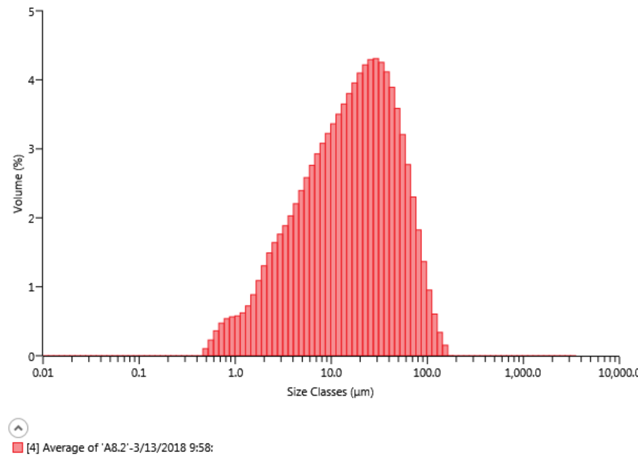
Volume (%)
0 1 2 3 4 5
0.01 0.1 1.0 10.0 100.0 1,000.0 10,000.0
Size Classes (µm)
[4] Average of 'A8.2'-3/13/2018 9:58:

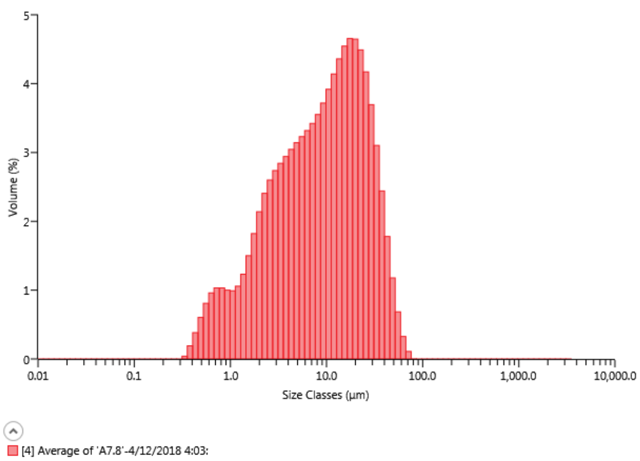
Volume (%)
0 1 2 3 4 5
0.01 0.1 1.0 10.0 100.0 1,000.0 10,000.0
Size Classes (µm)
[4] Average of 'A7.8'-4/12/2018 4:03:

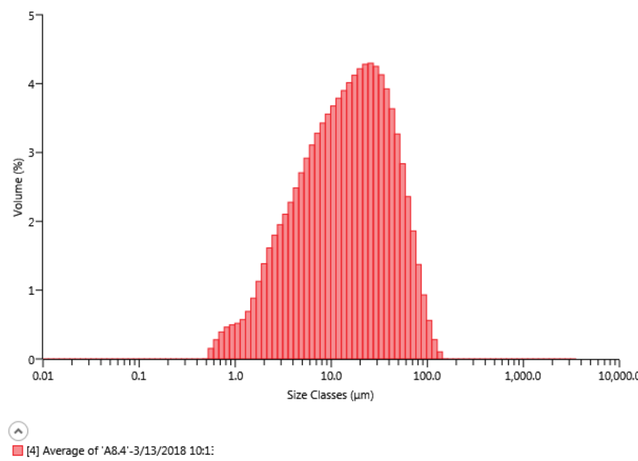
Volume (%)
0 1 2 3 4 5
0.01 0.1 1.0 10.0 100.0 1,000.0 10,000.0
Size Classes (µm)
[4] Average of 'A8.4'-3/13/2018 10:1:

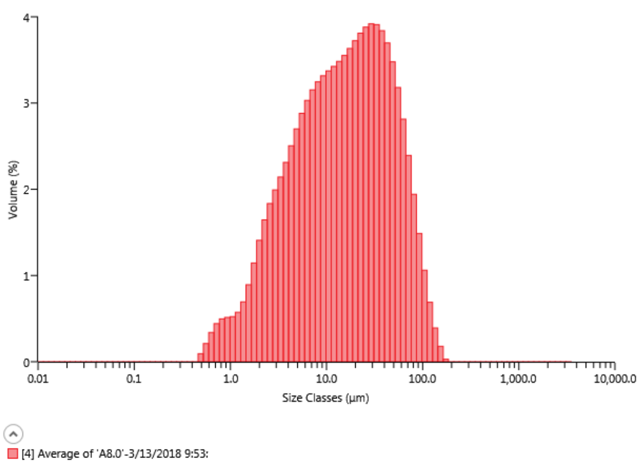
Volume (%)
0 1 2 3 4
0.01 0.1 1.0 10.0 100.0 1,000.0 10,000.0
Size Classes (µm)
[4] Average of 'A8.0'-3/13/2018 9:53:

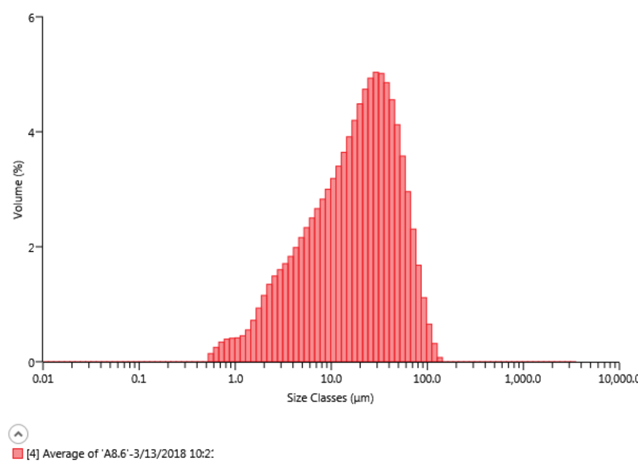
Volume (%)
0 2 4 6
0.01 0.1 1.0 10.0 100.0 1,000.0 10,000.0
Size Classes (µm)
[4] Average of 'A8.6'-3/13/2018 10:2:

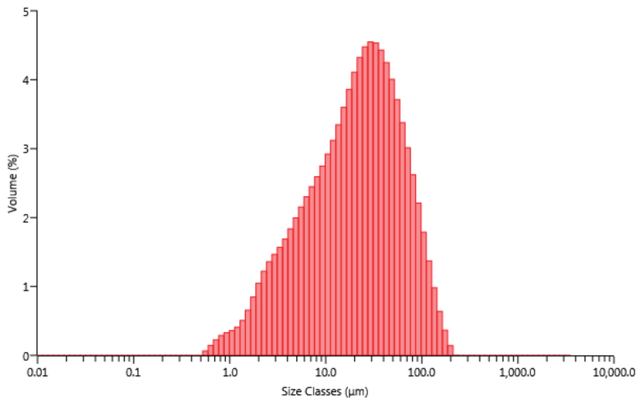

[4] Average of 'A8.8'-3/13/2018 10:2(

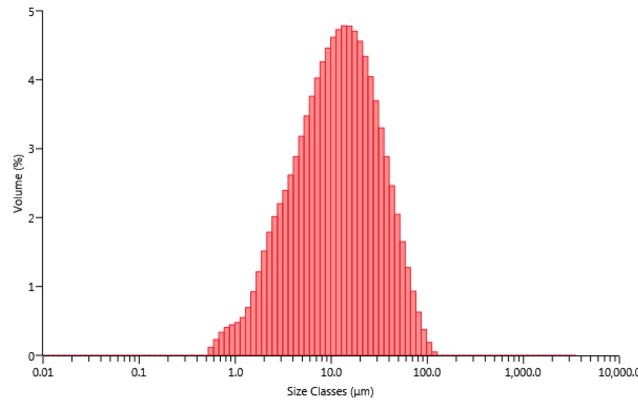

[4] Average of 'A9.4'-3/13/2018 10:4

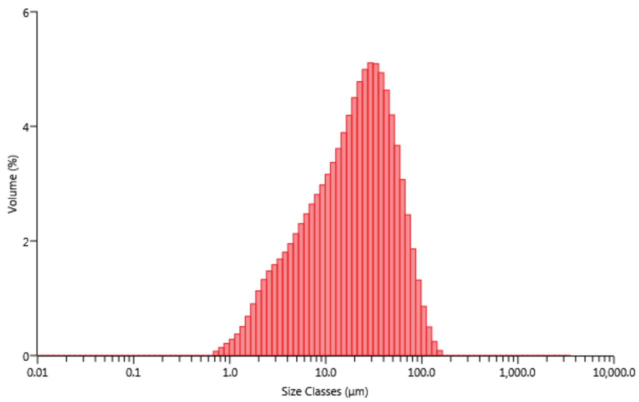

[4] Average of 'A9.0'-3/13/2018 10:3

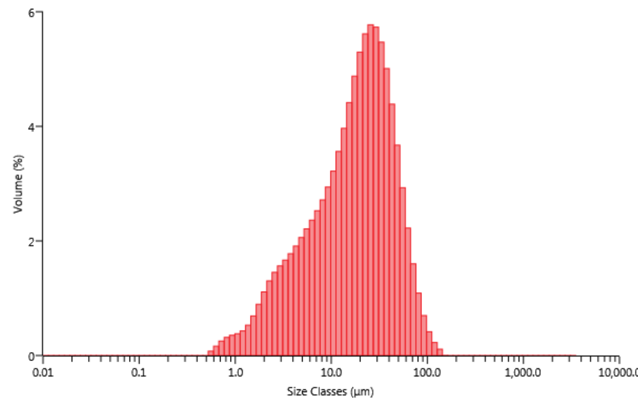

[4] Average of 'A9.6'-3/13/2018 10:5

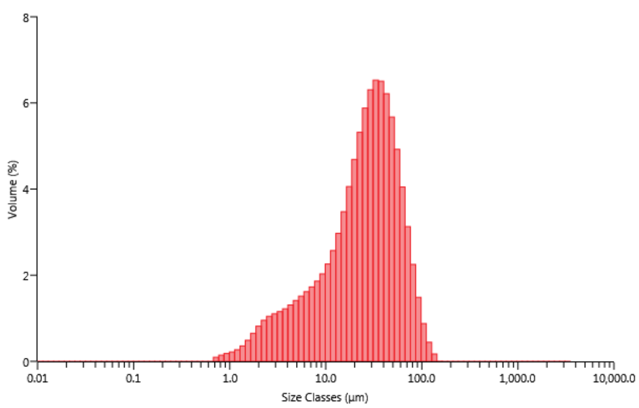

[4] Average of 'A9.2'-3/13/2018 10:3

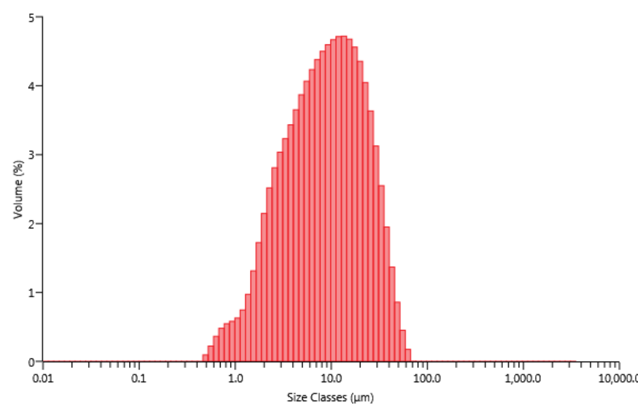

[4] Average of 'A9.8'-3/13/2018 11:0

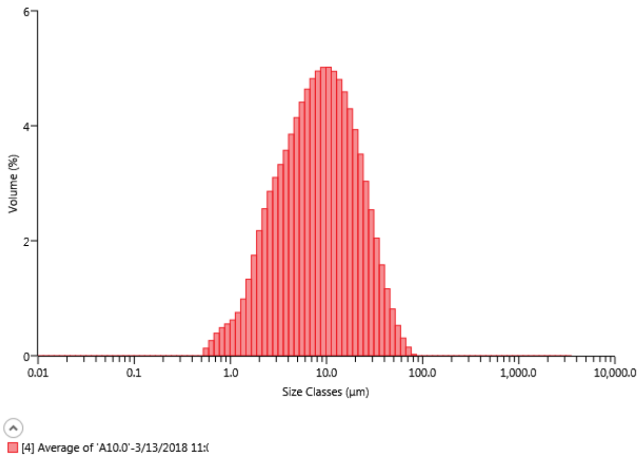
Volume (%)
0.01 0.1 1.0 10.0 100.0 1,000.0 10,000.0
Size Classes (µm)
[4] Average of 'A10.0'-3/13/2018 11:

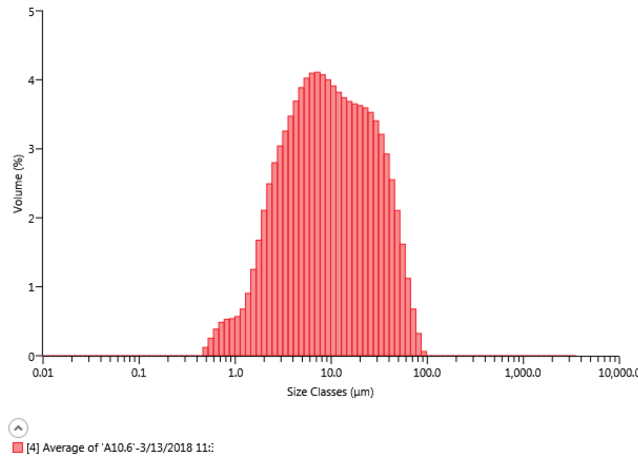
Volume (%)
0.01 0.1 1.0 10.0 100.0 1,000.0 10,000.0
Size Classes (µm)
[4] Average of 'A10.6'-3/13/2018 11:

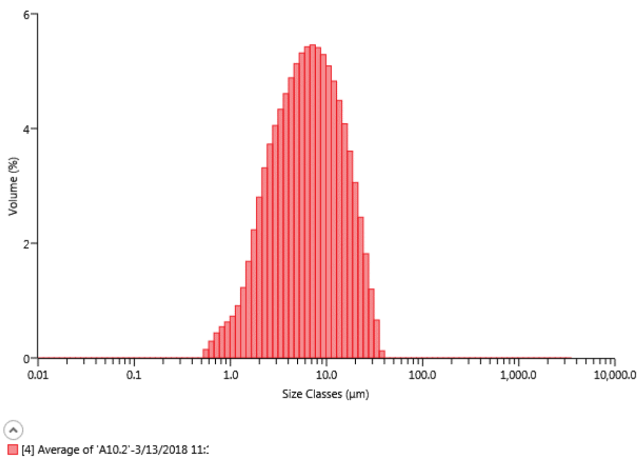
Volume (%)
0.01 0.1 1.0 10.0 100.0 1,000.0 10,000.0
Size Classes (µm)
[4] Average of 'A10.2'-3/13/2018 11:

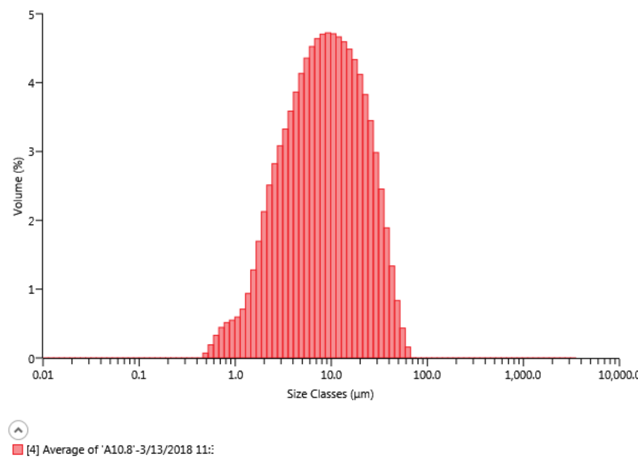
Volume (%)
0.01 0.1 1.0 10.0 100.0 1,000.0 10,000.0
Size Classes (µm)
[4] Average of 'A10.8'-3/13/2018 11:

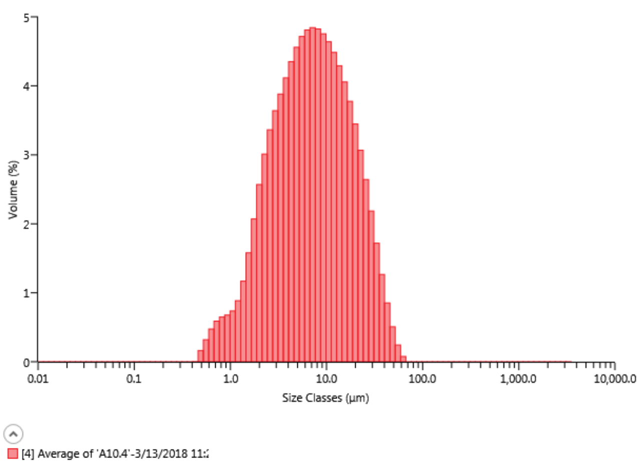
Volume (%)
0.01 0.1 1.0 10.0 100.0 1,000.0 10,000.0
Size Classes (µm)
[4] Average of 'A10.4'-3/13/2018 11:

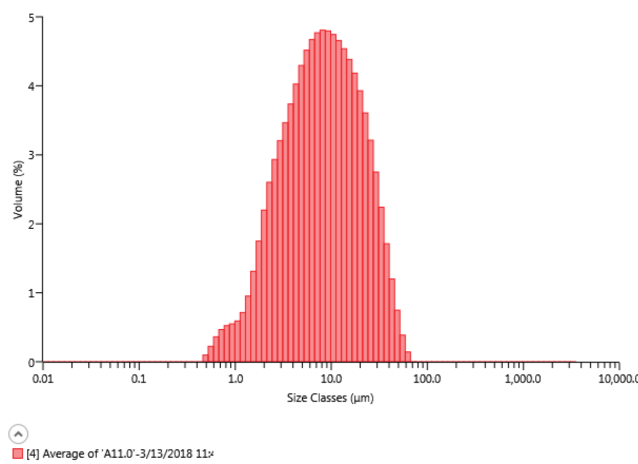
Volume (%)
0.01 0.1 1.0 10.0 100.0 1,000.0 10,000.0
Size Classes (µm)
[4] Average of 'A11.0'-3/13/2018 11:

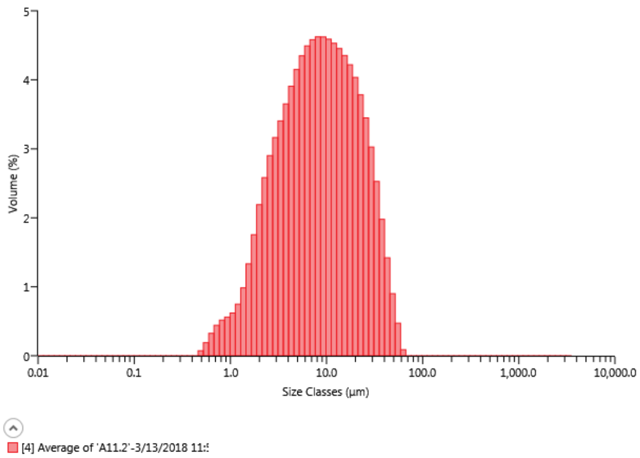
Volume (%)
Size Classes (μm)
[4] Average of 'A11.2'-3/13/2018 11:

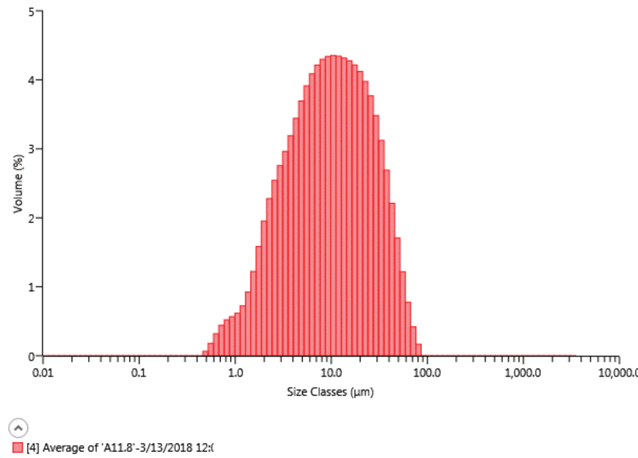
Volume (%)
Size Classes (μm)
[4] Average of 'A11.8'-3/13/2018 12:

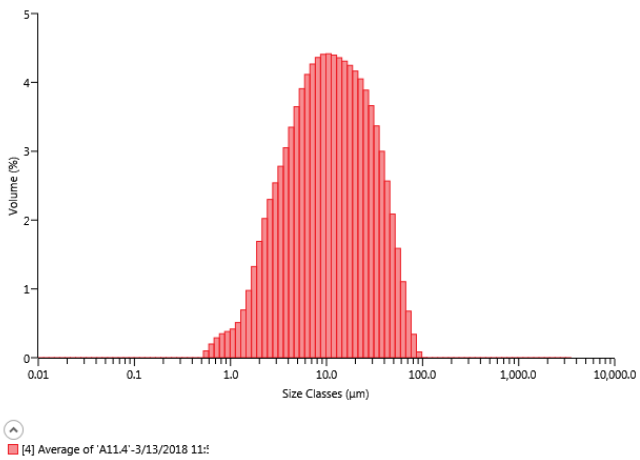
Volume (%)
Size Classes (μm)
[4] Average of 'A11.4'-3/13/2018 11:

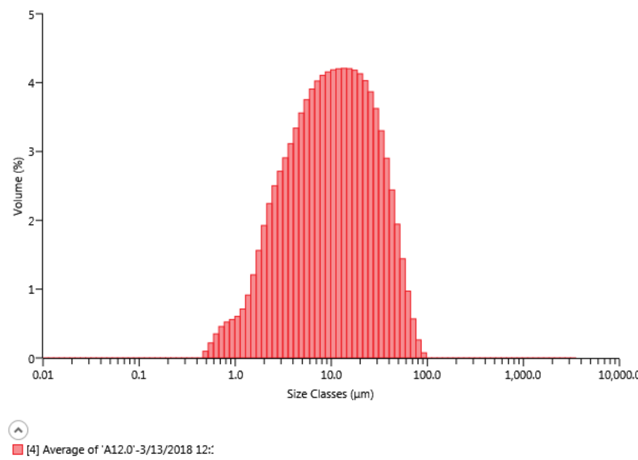
Volume (%)
Size Classes (μm)
[4] Average of 'A12.0'-3/13/2018 12:

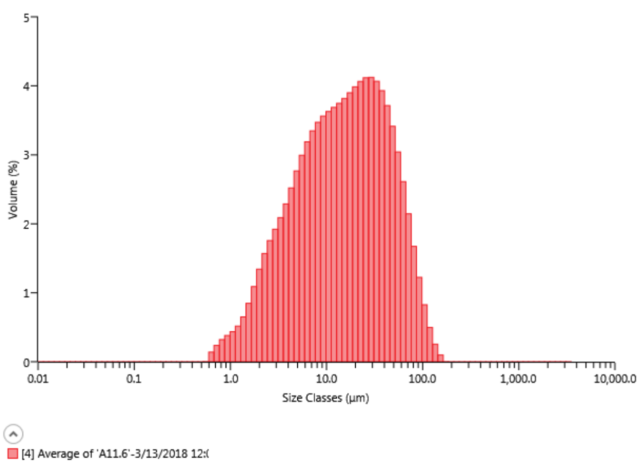
Volume (%)
Size Classes (μm)
[4] Average of 'A11.6'-3/13/2018 12:

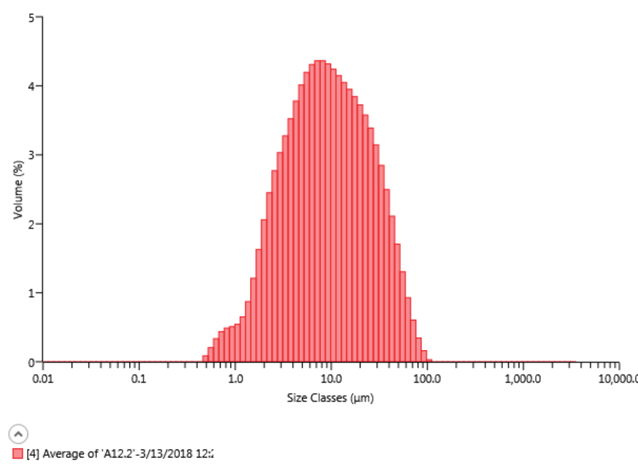
Volume (%)
Size Classes (μm)
[4] Average of 'A12.2'-3/13/2018 12:

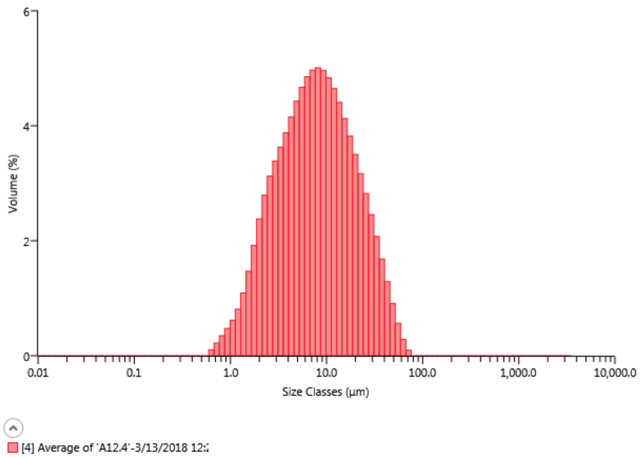
6
4
2
0
Volume (%)
0.01
0.1
1.0
10.0
100.0
1,000.0
10,000.0
Size Classes (µm)
[4] Average of 'A12.4'-3/13/2018 12

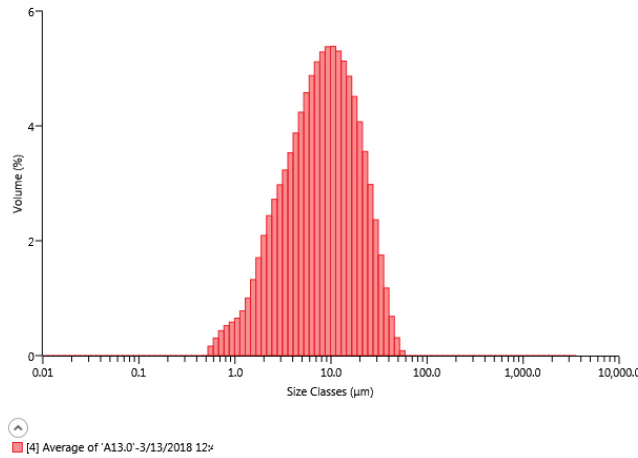
6
4
2
0
Volume (%)
0.01
0.1
1.0
10.0
100.0
1,000.0
10,000.0
Size Classes (µm)
[4] Average of 'A13.0'-3/13/2018 12

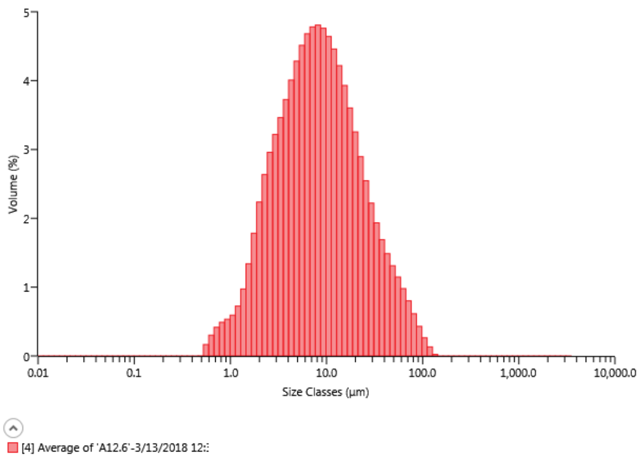
5
4
3
2
1
0
Volume (%)
0.01
0.1
1.0
10.0
100.0
1,000.0
10,000.0
Size Classes (µm)
[4] Average of 'A12.6'-3/13/2018 12

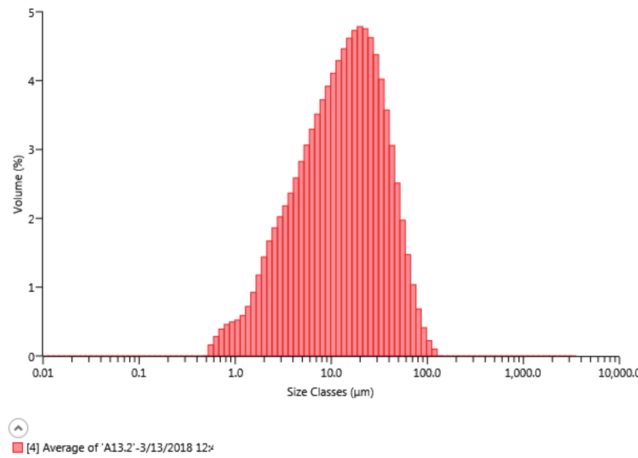
5
4
3
2
1
0
Volume (%)
0.01
0.1
1.0
10.0
100.0
1,000.0
10,000.0
Size Classes (µm)
[4] Average of 'A13.2'-3/13/2018 12

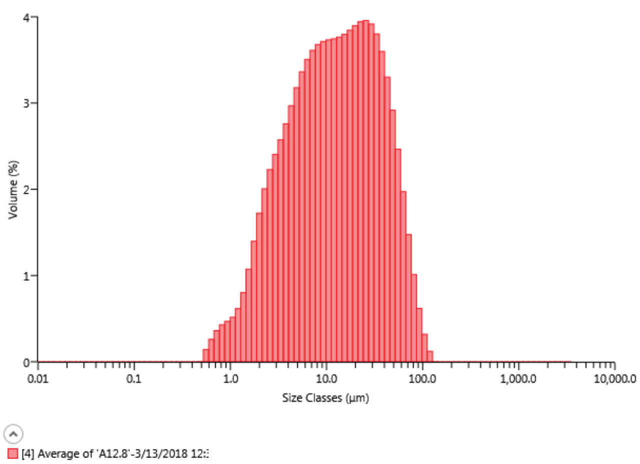
4
3
2
1
0
Volume (%)
0.01
0.1
1.0
10.0
100.0
1,000.0
10,000.0
Size Classes (µm)
[4] Average of 'A12.8'-3/13/2018 12

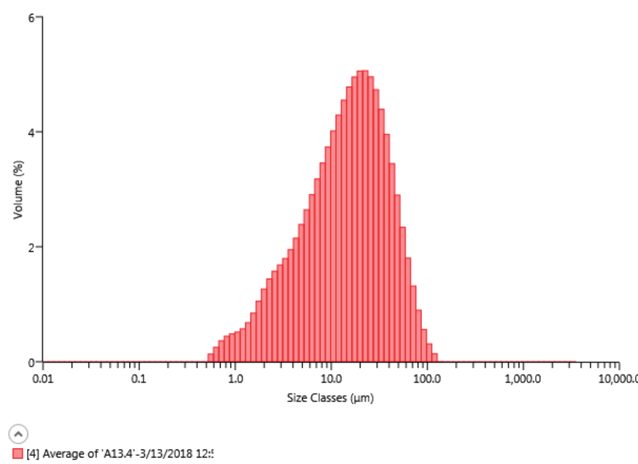
6
4
2
0
Volume (%)
0.01
0.1
1.0
10.0
100.0
1,000.0
10,000.0
Size Classes (µm)
[4] Average of 'A13.4'-3/13/2018 12

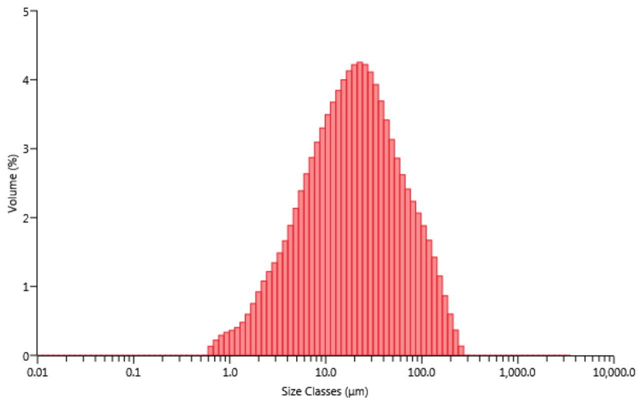

[4] Average of 'A13.6'-3/13/2018 12:

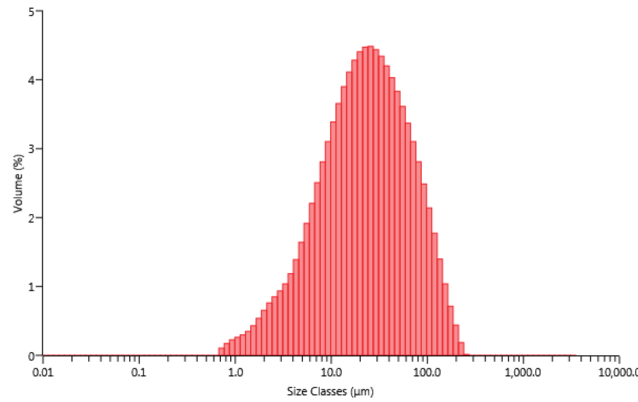

[4] Average of 'A14.4A'-3/13/2018 1:

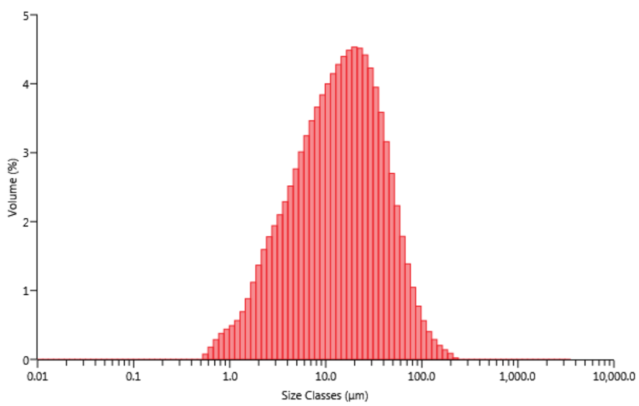

[4] Average of 'A13.8'-3/13/2018 1:0

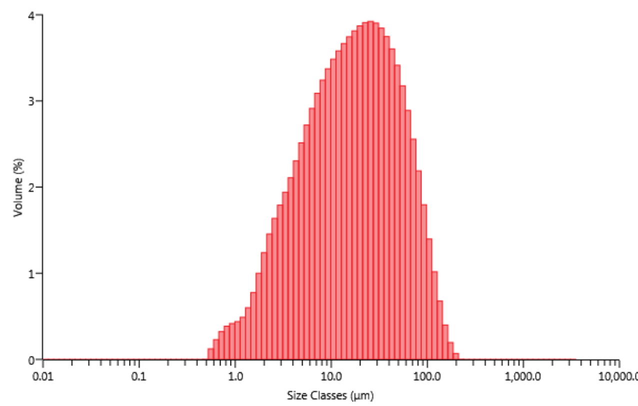

[4] Average of 'A14.6'-3/13/2018 2:1

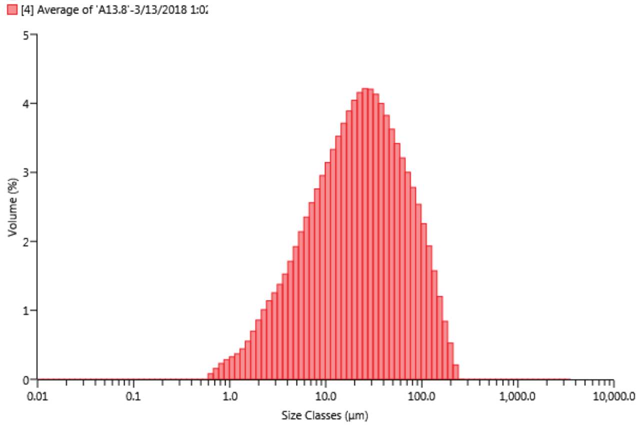

[4] Average of 'A14.0'-3/13/2018 1:0

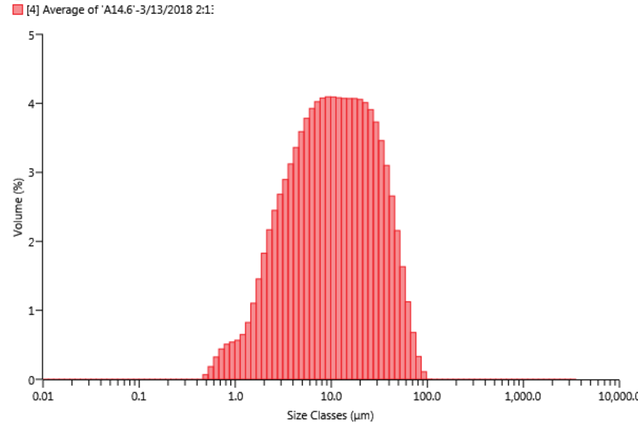

[4] Average of 'A15.0'-3/13/2018 2:1

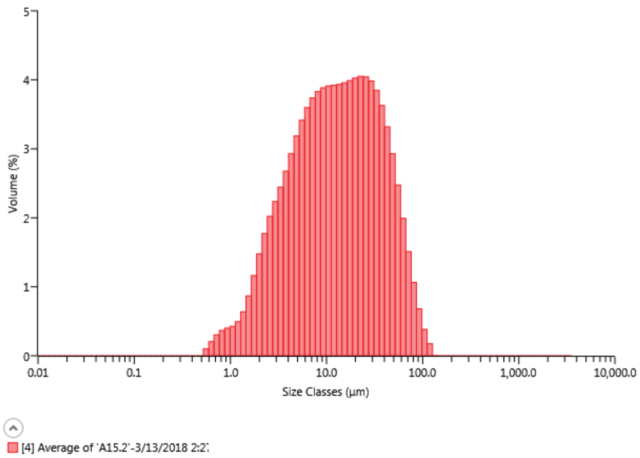
Volume (%)
0.01 0.1 1.0 10.0 100.0 1,000.0 10,000.0
Size Classes (µm)
[4] Average of 'A15.2'-3/13/2018 2:2

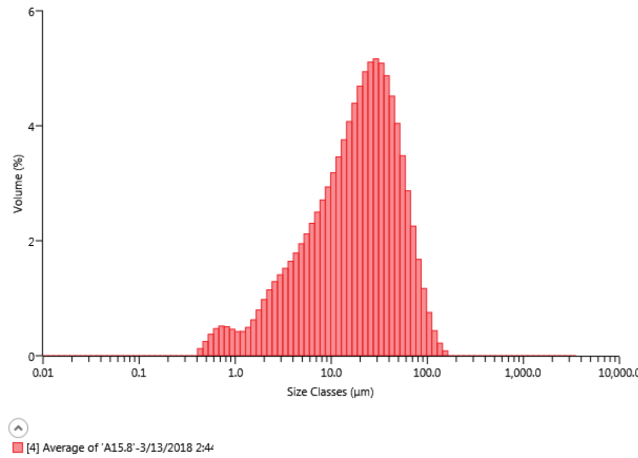
Volume (%)
0.01 0.1 1.0 10.0 100.0 1,000.0 10,000.0
Size Classes (µm)
[4] Average of 'A15.8'-3/13/2018 2:4

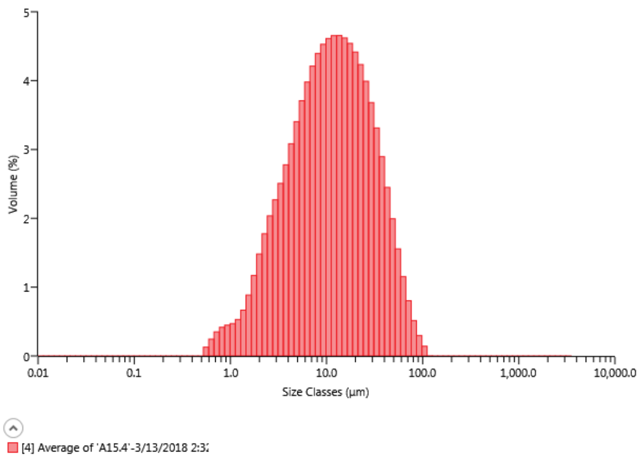
Volume (%)
0.01 0.1 1.0 10.0 100.0 1,000.0 10,000.0
Size Classes (µm)
[4] Average of 'A15.4'-3/13/2018 2:3

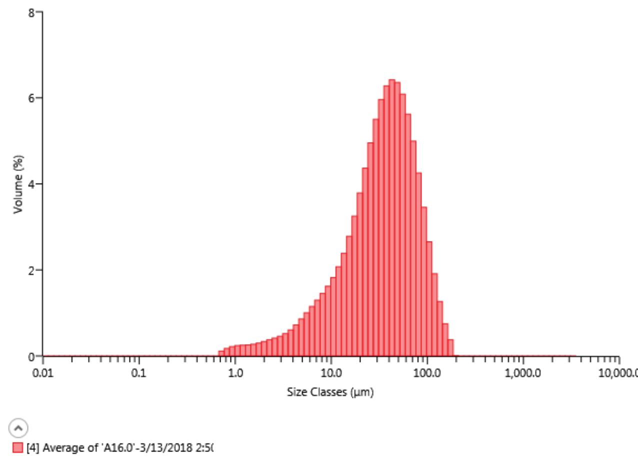
Volume (%)
0.01 0.1 1.0 10.0 100.0 1,000.0 10,000.0
Size Classes (µm)
[4] Average of 'A16.0'-3/13/2018 2:5

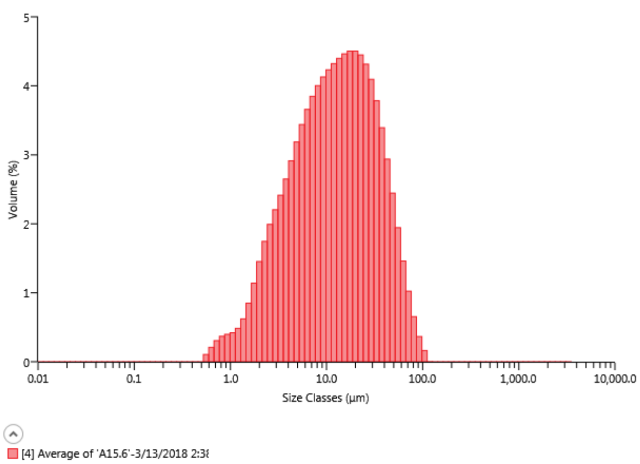
Volume (%)
0.01 0.1 1.0 10.0 100.0 1,000.0 10,000.0
Size Classes (µm)
[4] Average of 'A15.6'-3/13/2018 2:3

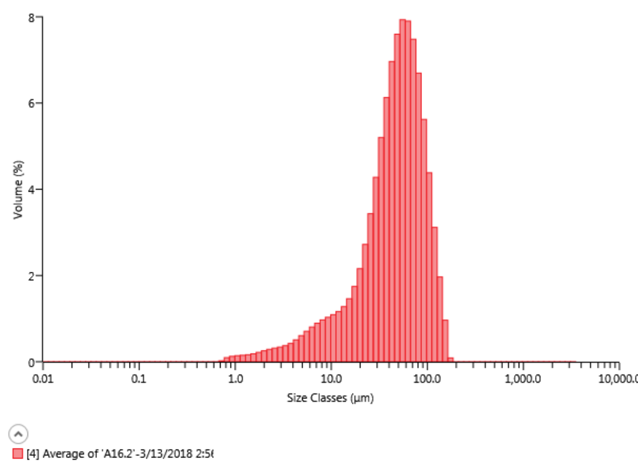
Volume (%)
0.01 0.1 1.0 10.0 100.0 1,000.0 10,000.0
Size Classes (µm)
[4] Average of 'A16.2'-3/13/2018 2:5

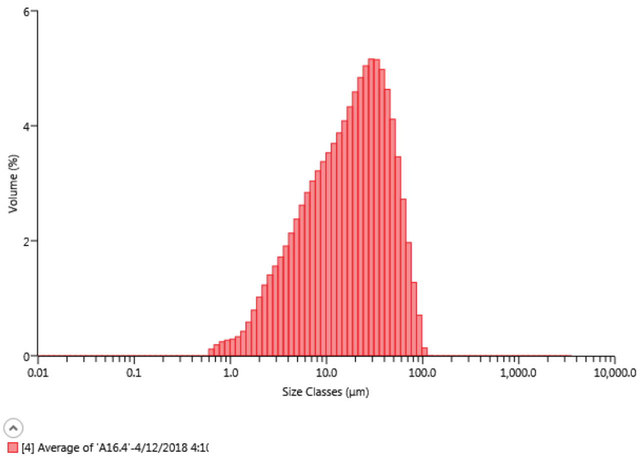
Volume (%)
Size Classes (µm)
0.01 0.1 1.0 10.0 100.0 1,000.0 10,000.0
[4] Average of 'A16.4'-4/12/2018 4:1

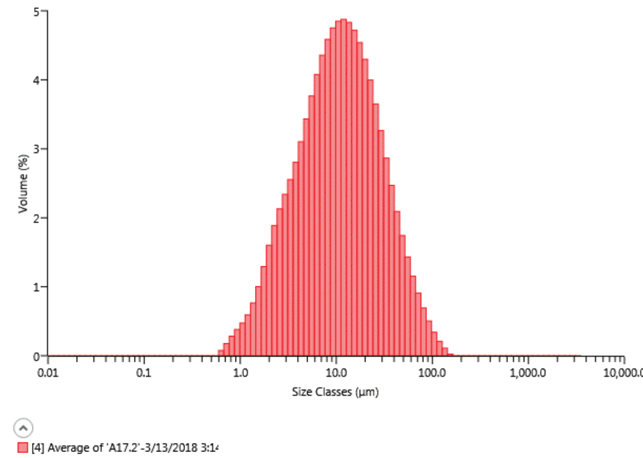
Volume (%)
Size Classes (µm)
0.01 0.1 1.0 10.0 100.0 1,000.0 10,000.0
[4] Average of 'A17.2'-3/13/2018 3:1

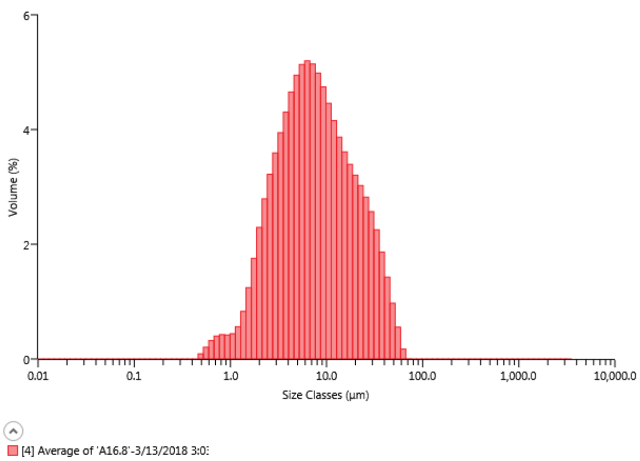
Volume (%)
Size Classes (µm)
0.01 0.1 1.0 10.0 100.0 1,000.0 10,000.0
[4] Average of 'A16.8'-3/13/2018 3:0

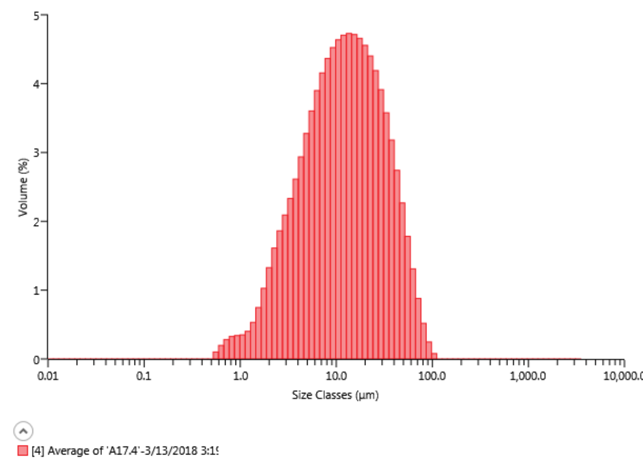
Volume (%)
Size Classes (µm)
0.01 0.1 1.0 10.0 100.0 1,000.0 10,000.0
[4] Average of 'A17.4'-3/13/2018 3:1

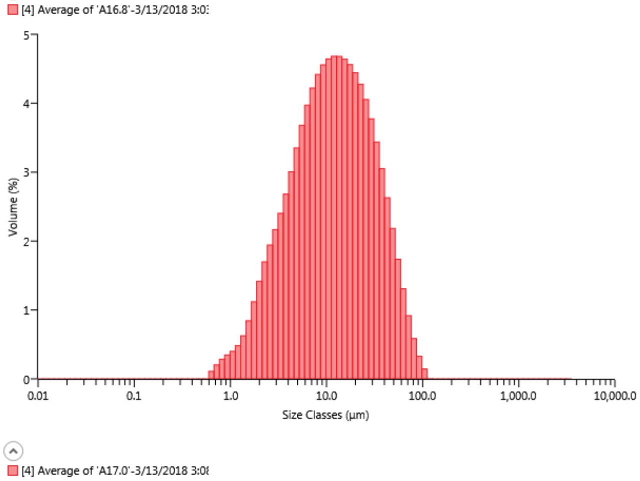
Volume (%)
Size Classes (µm)
0.01 0.1 1.0 10.0 100.0 1,000.0 10,000.0
[4] Average of 'A17.0'-3/13/2018 3:0

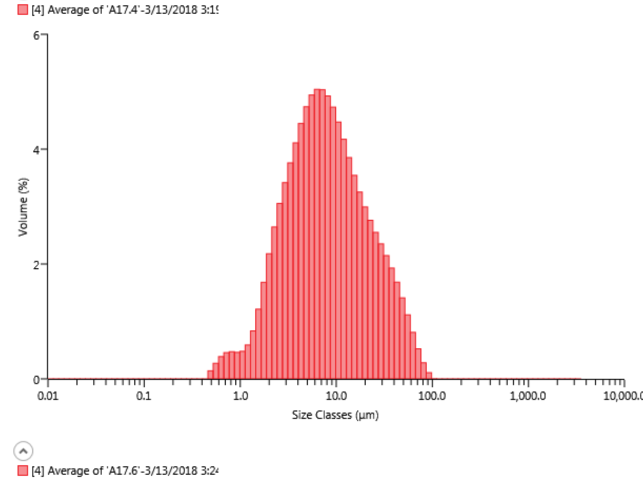
Volume (%)
Size Classes (µm)
0.01 0.1 1.0 10.0 100.0 1,000.0 10,000.0
[4] Average of 'A17.6'-3/13/2018 3:2

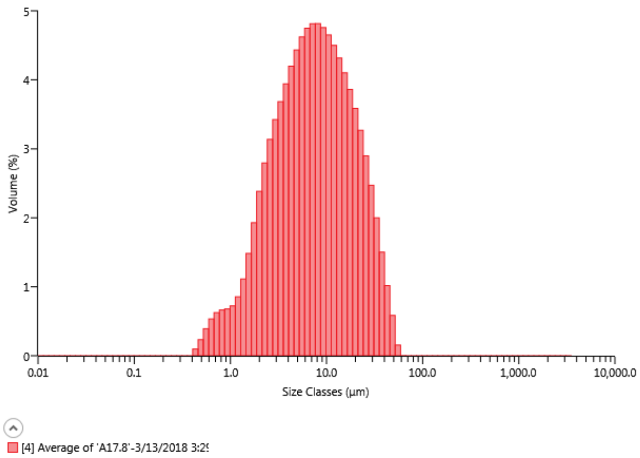
Volume (%)
Size Classes (µm)
0.01 0.1 1.0 10.0 100.0 1,000.0 10,000.0
[4] Average of 'A17.8'-3/13/2018 3:2

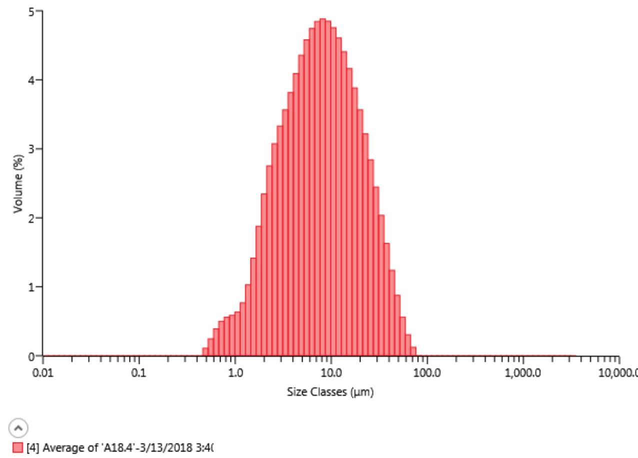
Volume (%)
Size Classes (µm)
0.01 0.1 1.0 10.0 100.0 1,000.0 10,000.0
[4] Average of 'A18.4'-3/13/2018 3:4

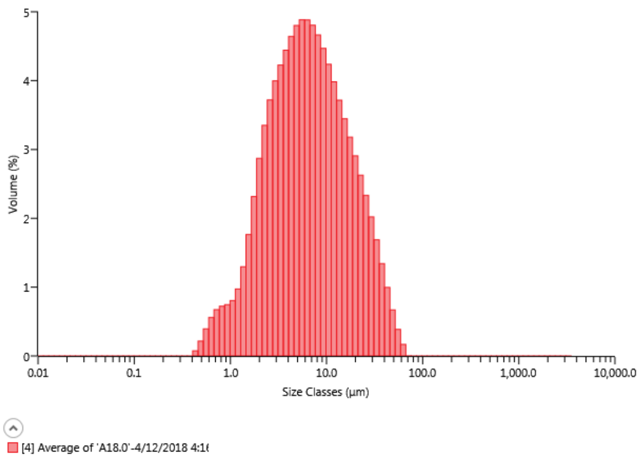
Volume (%)
Size Classes (µm)
0.01 0.1 1.0 10.0 100.0 1,000.0 10,000.0
[4] Average of 'A18.0'-4/12/2018 4:1

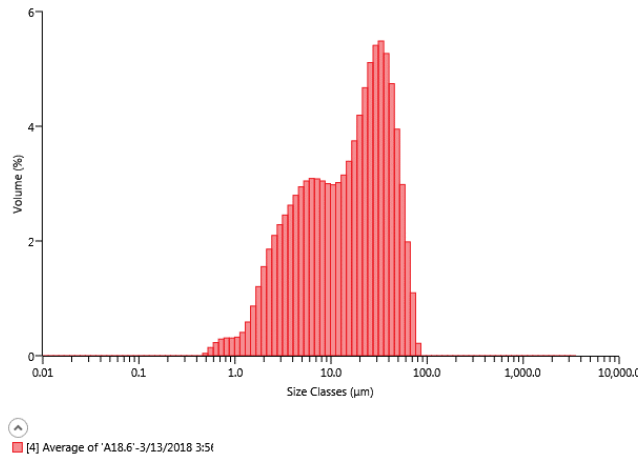
Volume (%)
Size Classes (µm)
0.01 0.1 1.0 10.0 100.0 1,000.0 10,000.0
[4] Average of 'A18.6'-3/13/2018 3:5

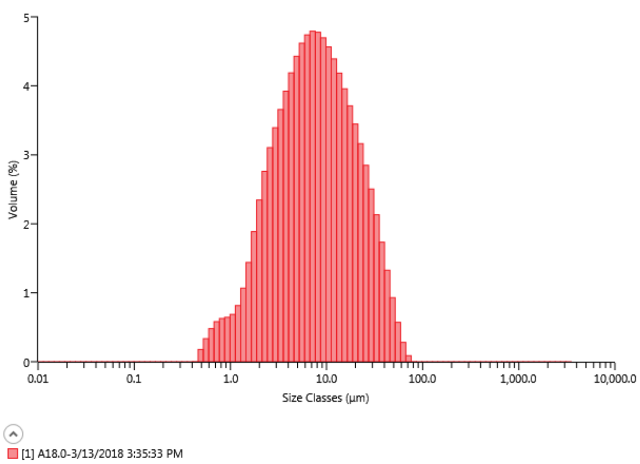
Volume (%)
Size Classes (µm)
0.01 0.1 1.0 10.0 100.0 1,000.0 10,000.0
[1] A18.0-3/13/2018 3:35:33 PM

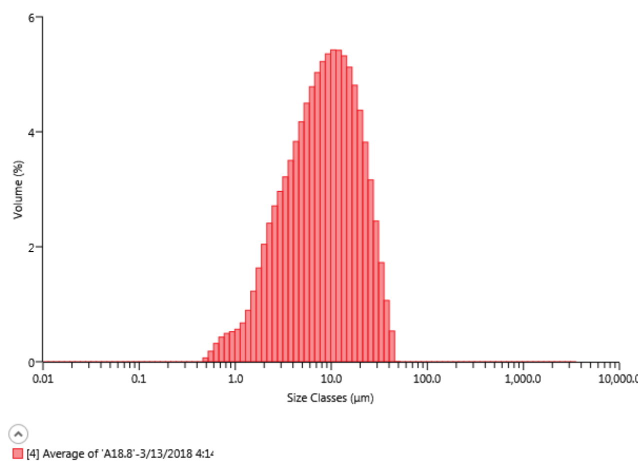
Volume (%)
Size Classes (µm)
0.01 0.1 1.0 10.0 100.0 1,000.0 10,000.0
[4] Average of 'A18.8'-3/13/2018 4:1

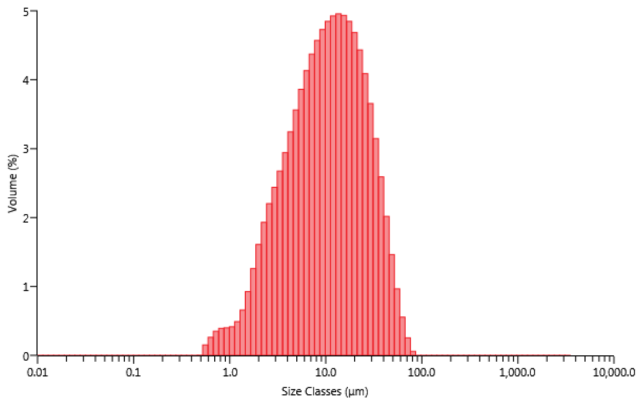

[4] Average of 'A19.0'-3/13/2018 4:3

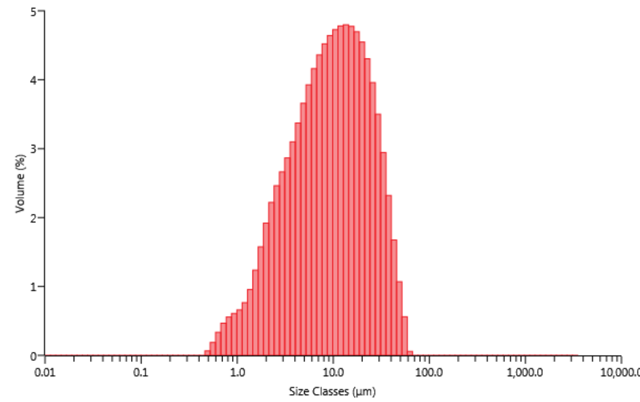

[4] Average of 'A19.6'-3/13/2018 5:1

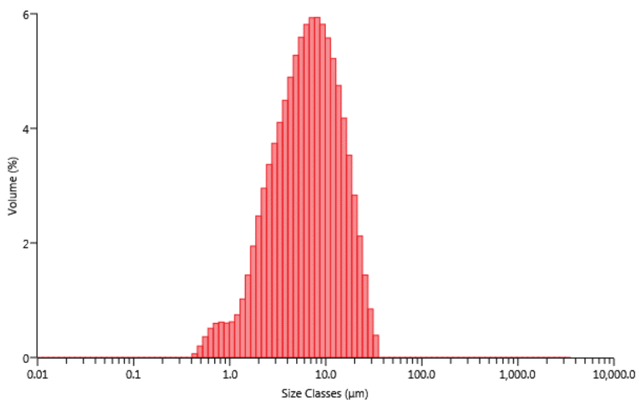

[4] Average of 'A19.2'-3/13/2018 4:3

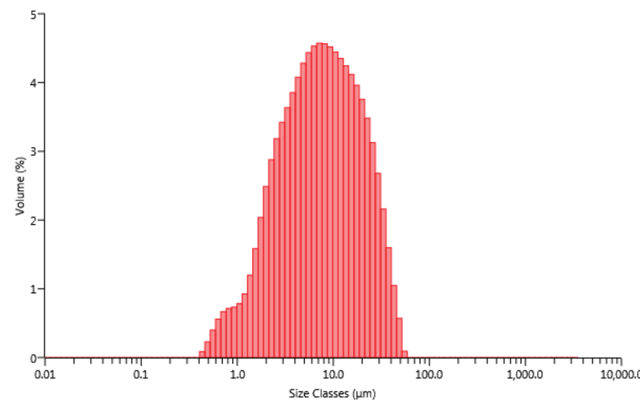

[4] Average of 'A19.8'-3/13/2018 5:1

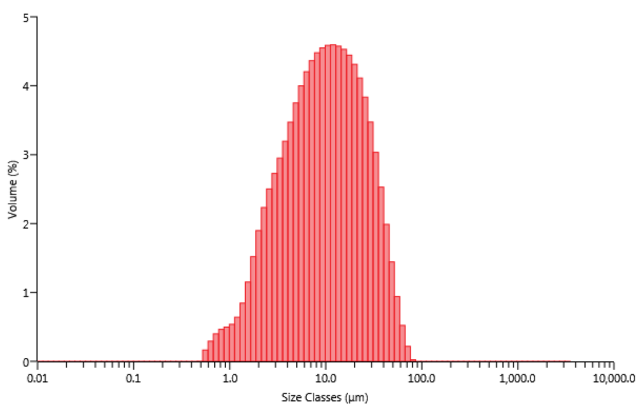

[4] Average of 'A19.4'-3/13/2018 4:5

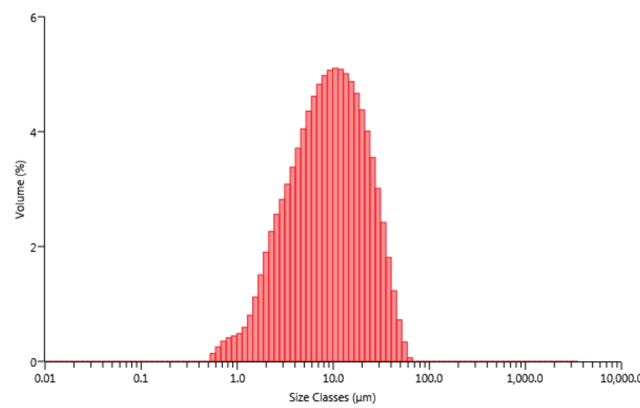

[4] Average of 'A20.0'-3/13/2018 5:2

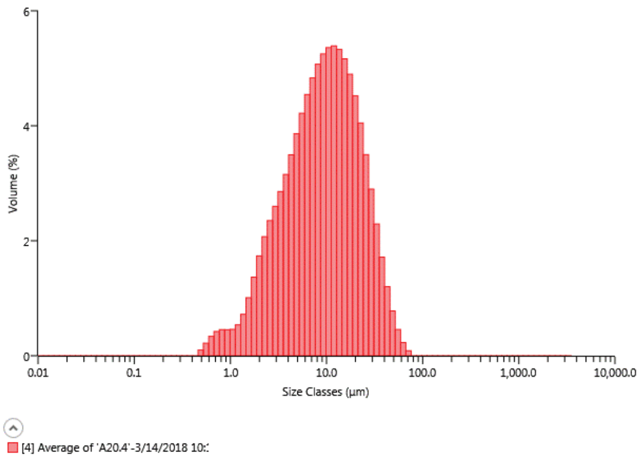
6
4
2
0
Volume (%)
0.01
0.1
1.0
10.0
100.0
1,000.0
10,000.0
Size Classes (µm)
[4] Average of 'A20.4'-3/14/2018 10:

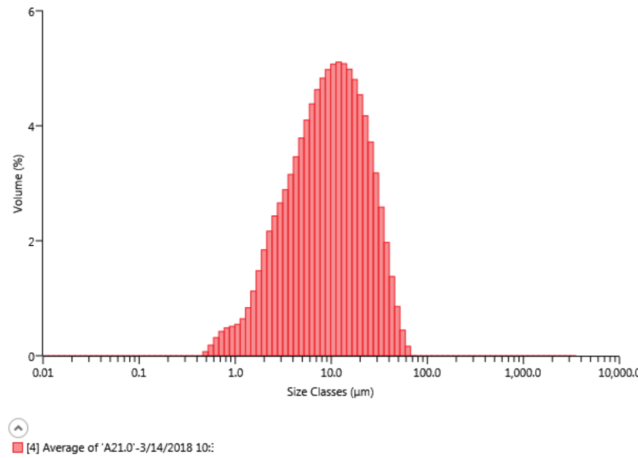
6
4
2
0
Volume (%)
0.01
0.1
1.0
10.0
100.0
1,000.0
10,000.0
Size Classes (µm)
[4] Average of 'A21.0'-3/14/2018 10:

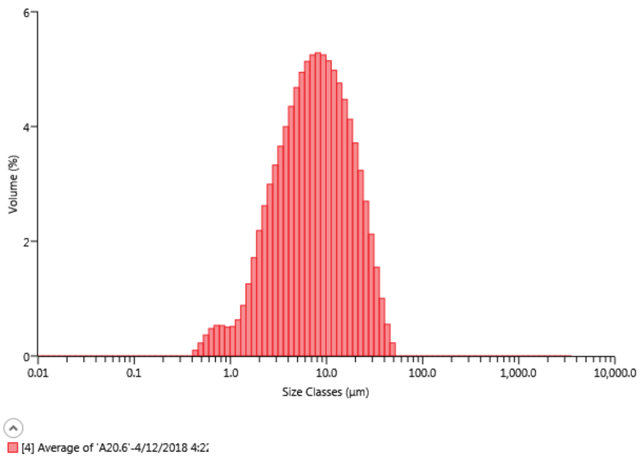
6
4
2
0
Volume (%)
0.01
0.1
1.0
10.0
100.0
1,000.0
10,000.0
Size Classes (µm)
[4] Average of 'A20.6'-4/12/2018 4:2

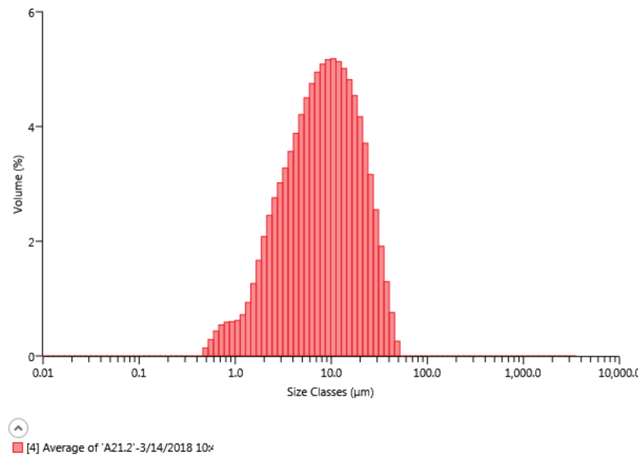
6
4
2
0
Volume (%)
0.01
0.1
1.0
10.0
100.0
1,000.0
10,000.0
Size Classes (µm)
[4] Average of 'A21.2'-3/14/2018 10:

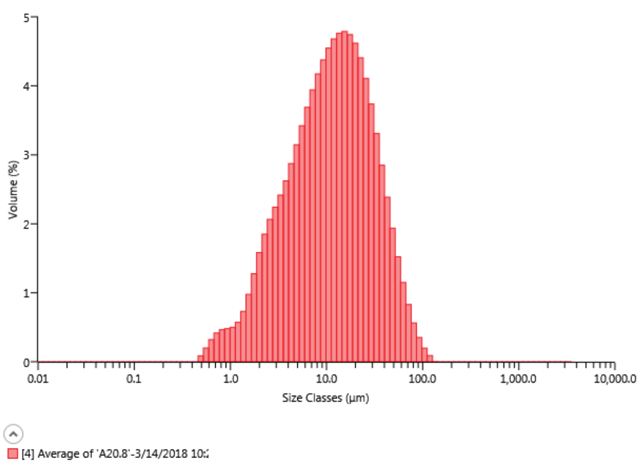
5
4
3
2
1
0
Volume (%)
0.01
0.1
1.0
10.0
100.0
1,000.0
10,000.0
Size Classes (µm)
[4] Average of 'A20.8'-3/14/2018 10:

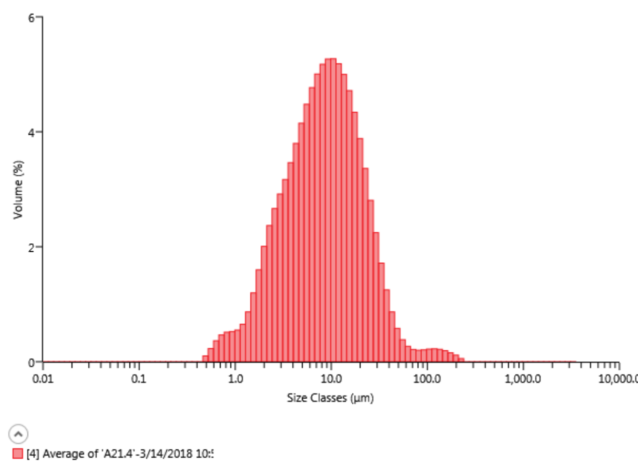
6
4
2
0
Volume (%)
0.01
0.1
1.0
10.0
100.0
1,000.0
10,000.0
Size Classes (µm)
[4] Average of 'A21.4'-3/14/2018 10:

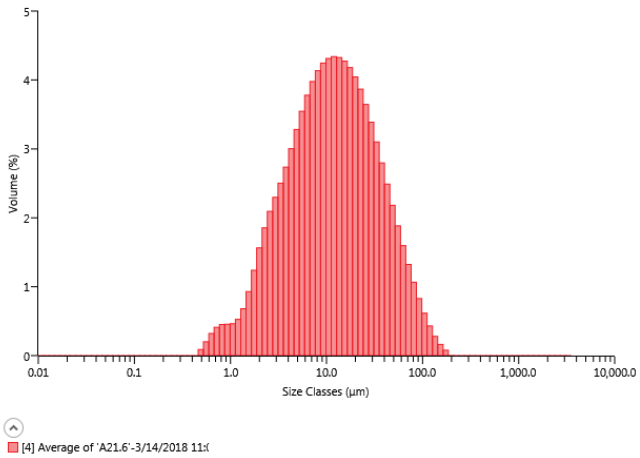
Volume (%)
Size Classes (µm)
[4] Average of 'A21.6'-3/14/2018 11:(

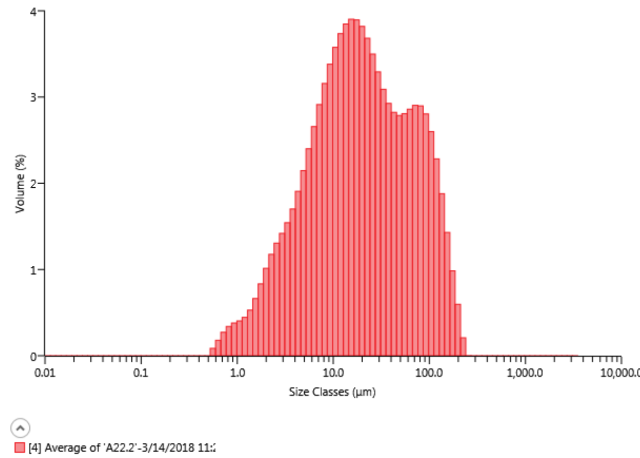
Volume (%)
Size Classes (µm)
[4] Average of 'A22.2'-3/14/2018 11:

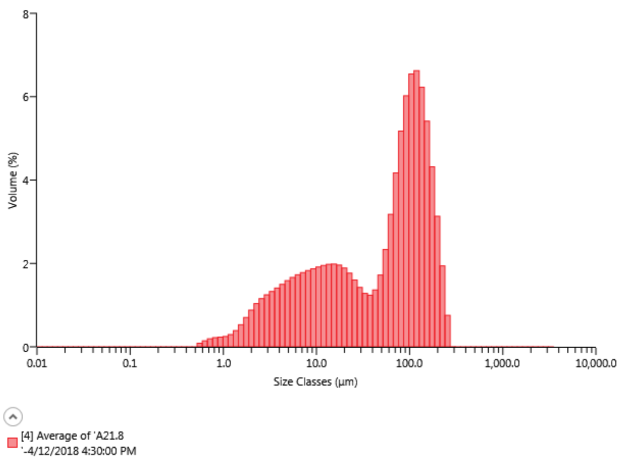
Volume (%)
Size Classes (µm)
[4] Average of 'A21.8
'-4/12/2018 4:30:00 PM

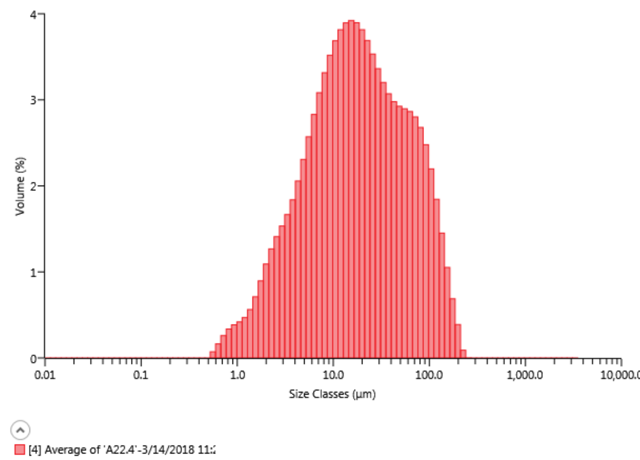
Volume (%)
Size Classes (µm)
[4] Average of 'A22.4'-3/14/2018 11:

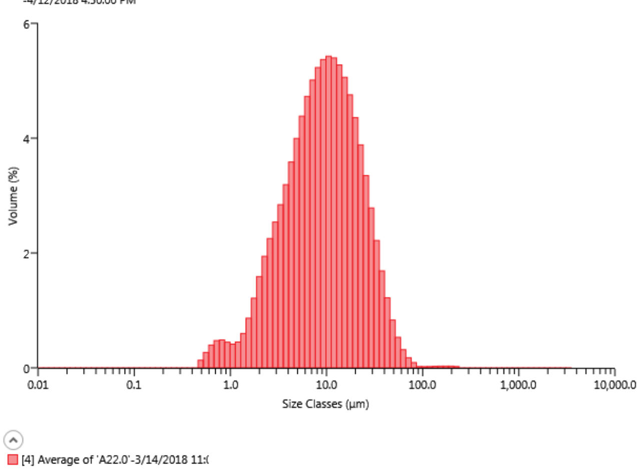
Volume (%)
Size Classes (µm)
[4] Average of 'A22.0'-3/14/2018 11:(

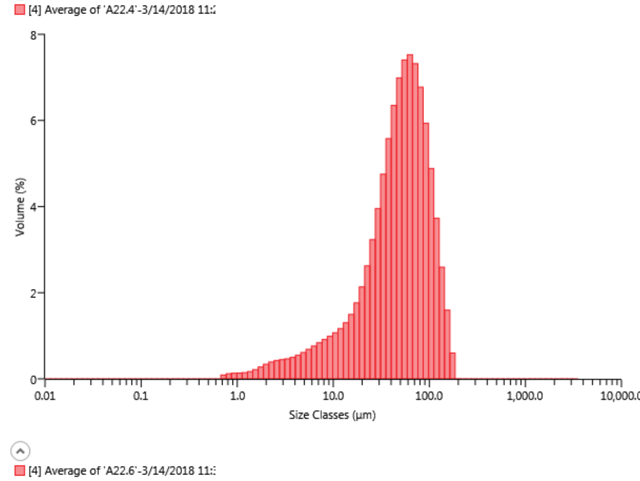
Volume (%)
Size Classes (µm)
[4] Average of 'A22.6'-3/14/2018 11:

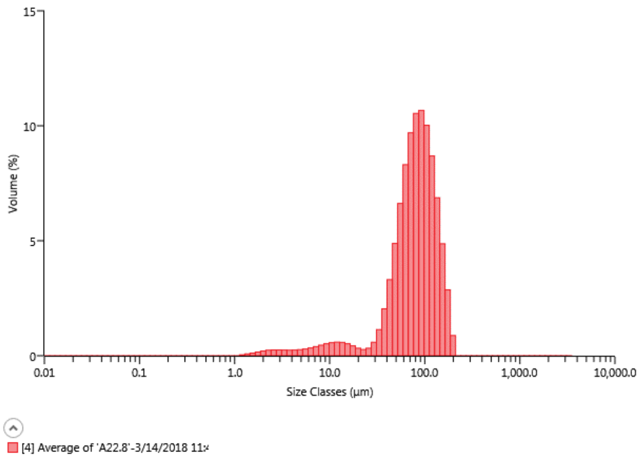
15
10
5
0
Volume (%)
0.01
0.1
1.0
10.0
100.0
1,000.0
10,000.0
Size Classes (μm)
[4] Average of 'A22.8'-3/14/2018 11:

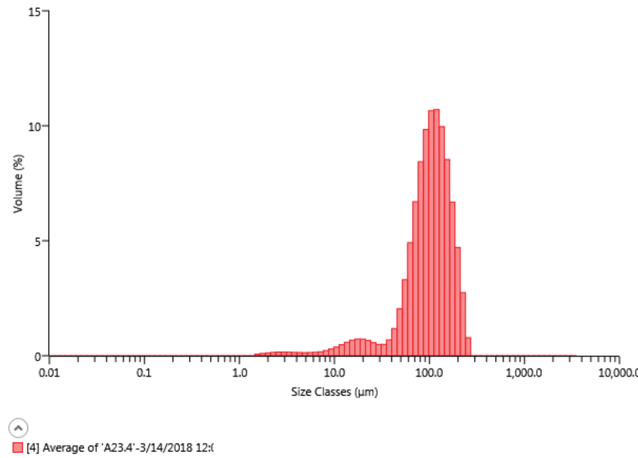
15
10
5
0
Volume (%)
0.01
0.1
1.0
10.0
100.0
1,000.0
10,000.0
Size Classes (μm)
[4] Average of 'A23.4'-3/14/2018 12:

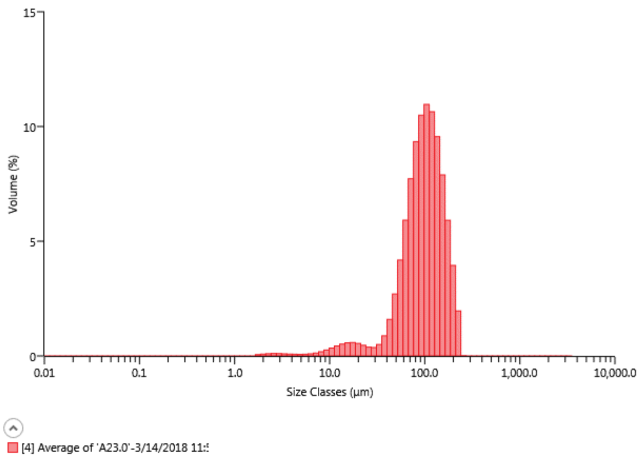
15
10
5
0
Volume (%)
0.01
0.1
1.0
10.0
100.0
1,000.0
10,000.0
Size Classes (μm)
[4] Average of 'A23.0'-3/14/2018 11:

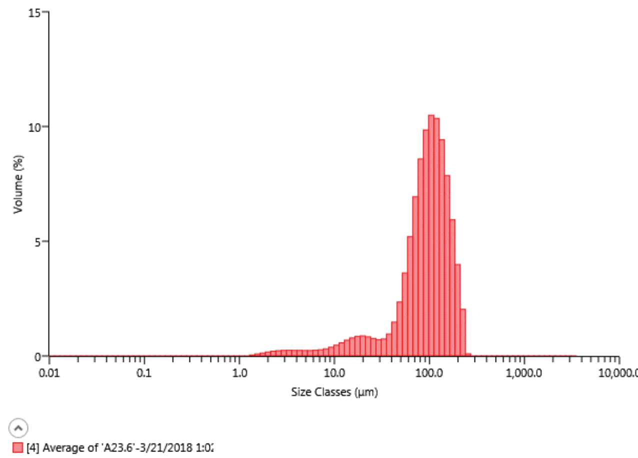
15
10
5
0
Volume (%)
0.01
0.1
1.0
10.0
100.0
1,000.0
10,000.0
Size Classes (μm)
[4] Average of 'A23.6'-3/21/2018 1:

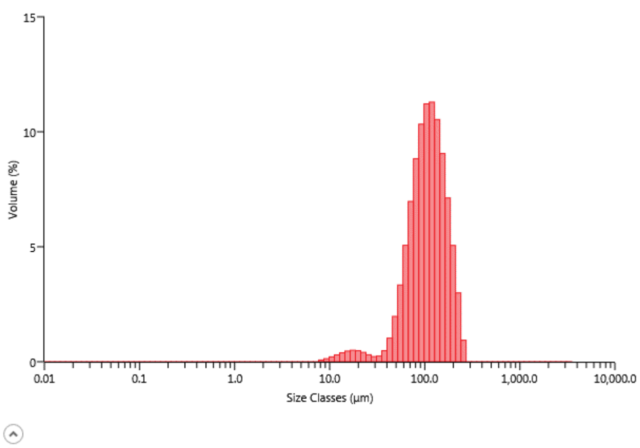
15
10
5
0
Volume (%)
0.01
0.1
1.0
10.0
100.0
1,000.0
10,000.0
Size Classes (μm)
[4] Average of 'A23.2'-3/14/2018 11:

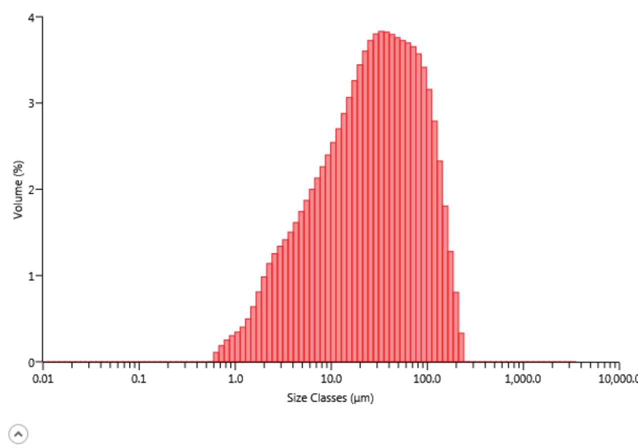
4
3
2
1
0
Volume (%)
0.01
0.1
1.0
10.0
100.0
1,000.0
10,000.0
Size Classes (μm)
[4] Average of 'A23.8'-3/21/2018 1:

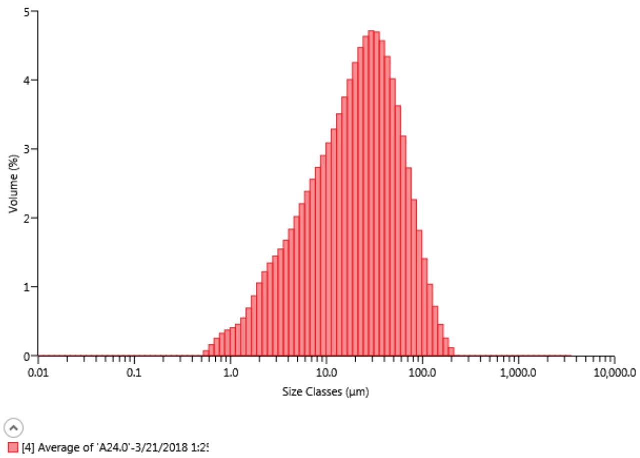
Volume (%)
Size Classes (µm)
0.01 0.1 1.0 10.0 100.0 1,000.0 10,000.0
[4] Average of 'A24.0'-3/21/2018 1:2

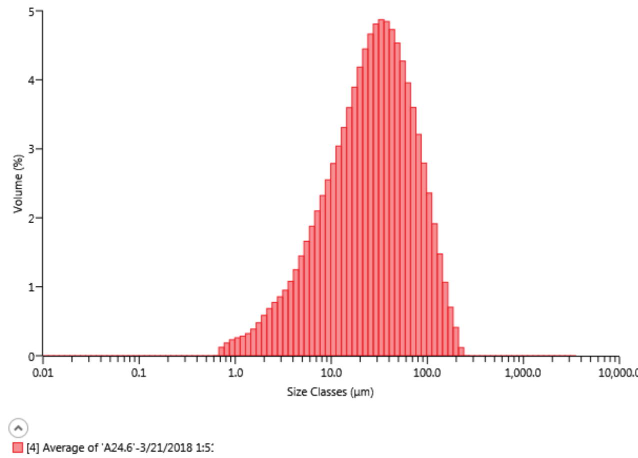
Volume (%)
Size Classes (µm)
0.01 0.1 1.0 10.0 100.0 1,000.0 10,000.0
[4] Average of 'A24.6'-3/21/2018 1:5

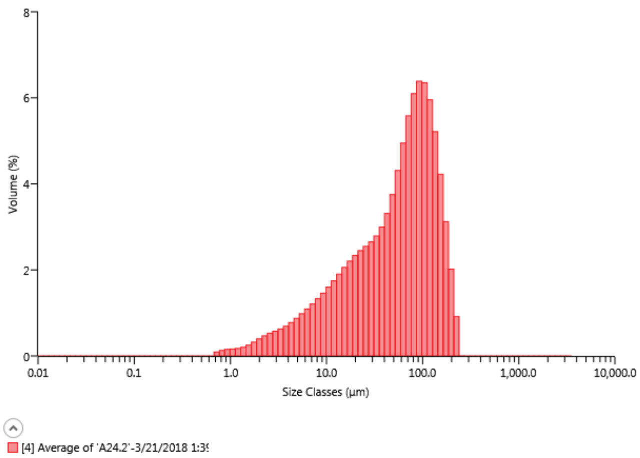
Volume (%)
Size Classes (µm)
0.01 0.1 1.0 10.0 100.0 1,000.0 10,000.0
[4] Average of 'A24.2'-3/21/2018 1:3

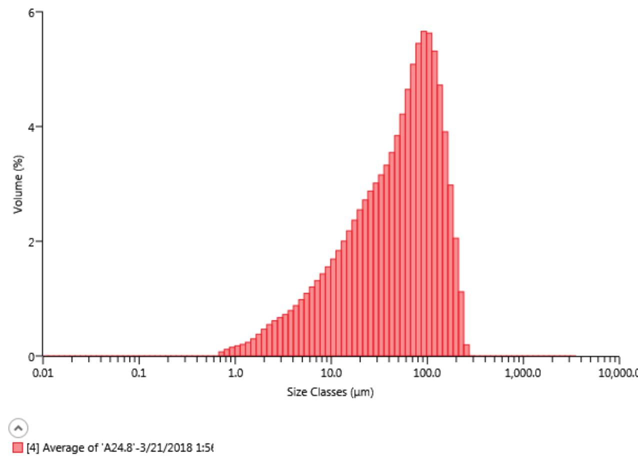
Volume (%)
Size Classes (µm)
0.01 0.1 1.0 10.0 100.0 1,000.0 10,000.0
[4] Average of 'A24.8'-3/21/2018 1:5

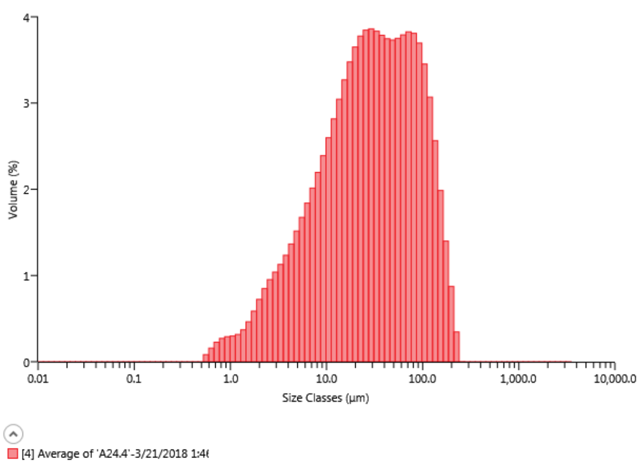
Volume (%)
Size Classes (µm)
0.01 0.1 1.0 10.0 100.0 1,000.0 10,000.0
[4] Average of 'A24.4'-3/21/2018 1:4

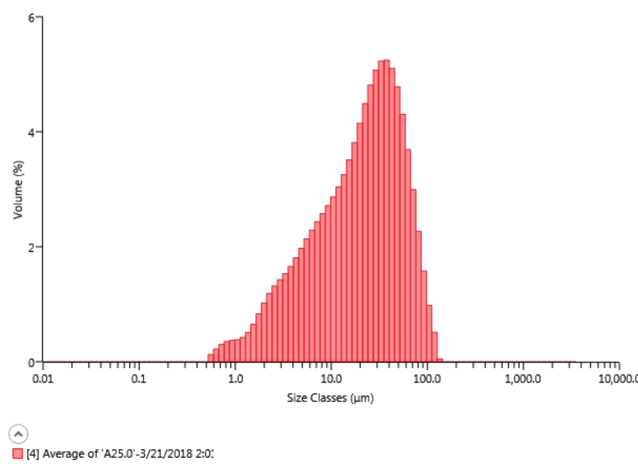
Volume (%)
Size Classes (µm)
0.01 0.1 1.0 10.0 100.0 1,000.0 10,000.0
[4] Average of 'A25.0'-3/21/2018 2:0

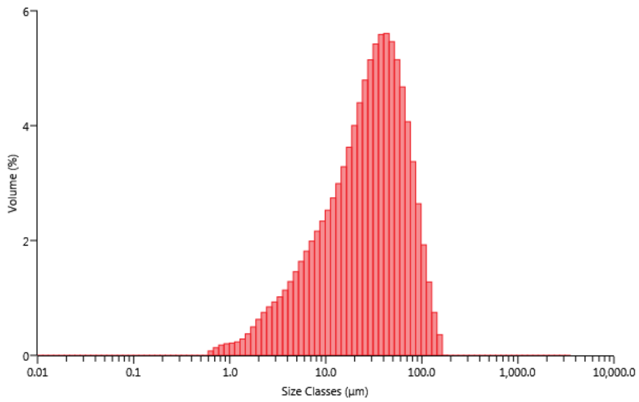

[4] Average of 'A25.2'-3/21/2018 2:0

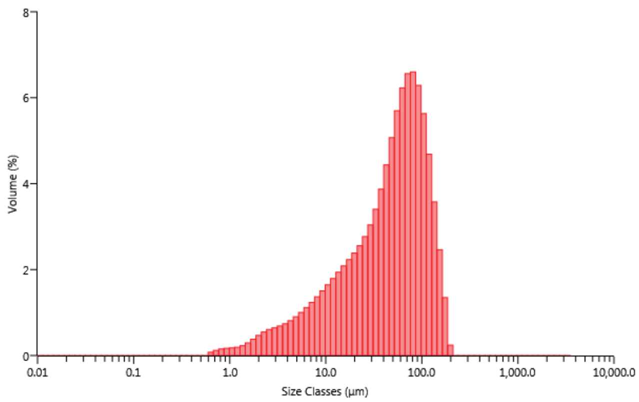

[4] Average of 'A25.4'-3/21/2018 2:1

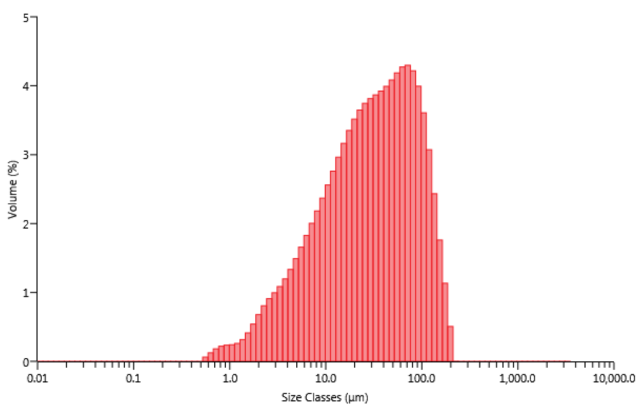

[4] Average of 'A25.6'-3/21/2018 2:2

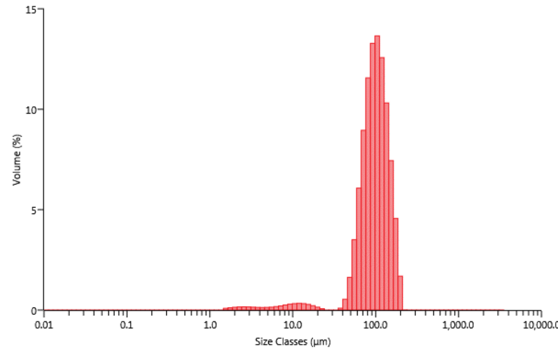

[4] Average of 'A26.2'-3/21/2018 2:5

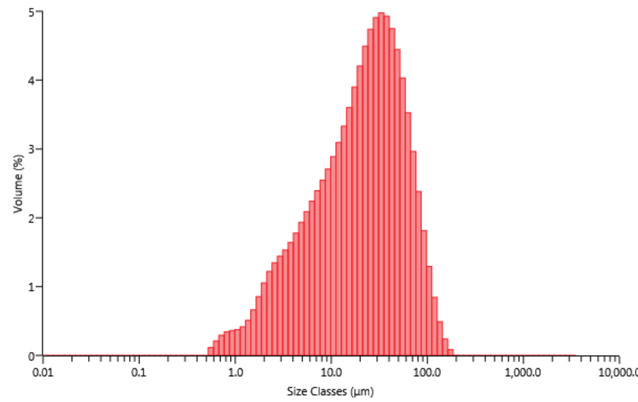

[4] Average of 'A25.8'-3/21/2018 2:3

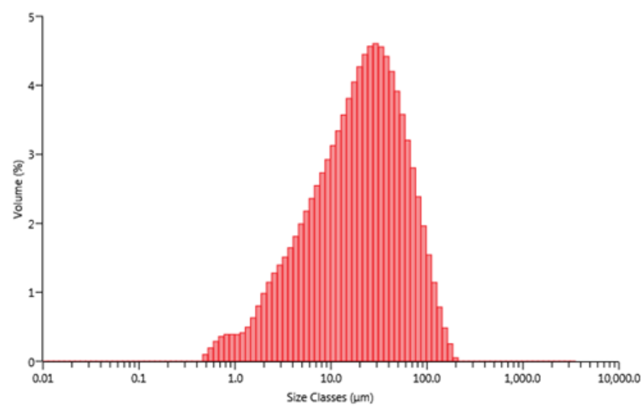

[4] Average of 'A26.0'-3/21/2018 2:3

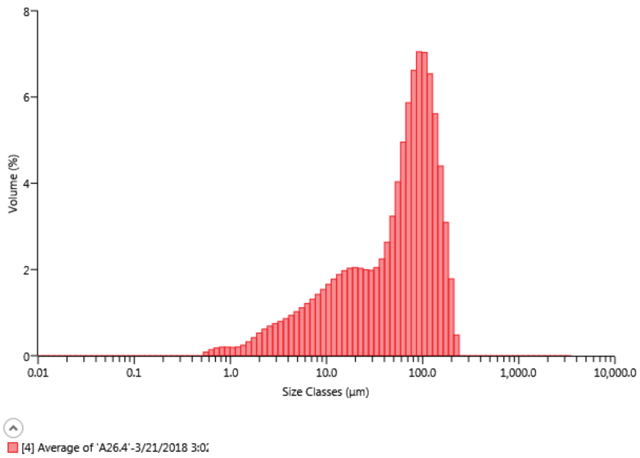
8
6
4
2
0
Volume (%)
0.01
0.1
1.0
10.0
100.0
1,000.0
10,000.0
Size Classes (μm)
[4] Average of 'A26.4'-3/21/2018 3:0